Generating and Interrogating Crystallographic Data to Predict Solid-State Properties

Lygia Silva de Moraes

A thesis presented in fulfilment of the requirements for the degree of Doctor of Philosophy in the Faculty of Science of the University of Strathclyde

July 2019

Abstract

A bespoke database of crystalline structures of salt forms of active pharmaceutical ingredients has been expanded to 300 structures, by the addition of 75 new crystal structures of salt forms of four bases that were all derivatives of phenylethylamine. These structures, with the addition of salt forms obtained from the CCDC database were analysed in detail according to features of the crystal structure such as cation conformation, presence of multiple crystallographically independent cations in the asymmetric unit and crystal packing similarity.

General trends of hydrate formation were observed for these bases. Halides, aliphatic sulfonates, benzoates and monocarboxylate counterions can be classified as predominantly anhydrous while dicarboxylates, inorganic salts with tetrahedral anions and aryl-sulfonates are likely to be hydrates, depending on synthesis and crystallisation conditions.

This work also studied the physicochemical properties of these salt forms, such as hardness, solubility and melting point. A new method for analysis of nanoindentation data was presented and used in this work showing a linear relationship between hardness and Young's Modulus. This linearity is characterised by the gradient of the trendline, the elasticity index. It was observed that salt forms of racemic methylephedrine will have higher elasticity index compared to the other salts. There is also a relationship between the hardness / Young's Modulus of the compounds and the size of the anion, clearly observed for halides but also observed in benzoates with different substitutions on the aromatic ring.

There is a linear relationship between solubility and melting point when comparing salt forms according to the type of active pharmaceutical ingredient used. Five counterions had interesting results when plotting solubility versus melting point, and these counterion groups can behave in three different ways according to the analysis of the trendlines: (1) when solubility tends to zero the value of x axis tends to the molecular weight of the free acid; (2) when solubility tends to zero the x axis, when corrected by the density of the free acid, also tends to the molecular weight of the free acids; and (3) the samples have solubility increasing with melting point - the inverse behaviour to normal expectation.

Acknowledgements

Table of Contents

Table of Figures

Table of Tables

xxiii

1. INTRODUCTION

A new pharmaceutical treatment must be designed to maximise the desirable pharmacological effects of the active substance inside or on the body. The development of a successful treatment must consider the dosage form to protect the active pharmaceutical ingredient (API) from the environment and to enable delivery of the ideal amount and concentration of the active substance to the site of action [1].

There are thought to be approximately 10000 known drug-like compounds, substances with acceptable pharmacokinetic properties: i.e. absorption, distribution, metabolism, and excretion (ADME), and of course low-toxicity. Due to the vast range of accessible chemistry space in the human body, the distribution of the APIs through the human body can be done in several different ways [2] and this wide distribution can decrease the expected activity of the drug. The generalised pharmacokinetic process involved in the administration of a drug to the human body is shown in Figure 1.1.
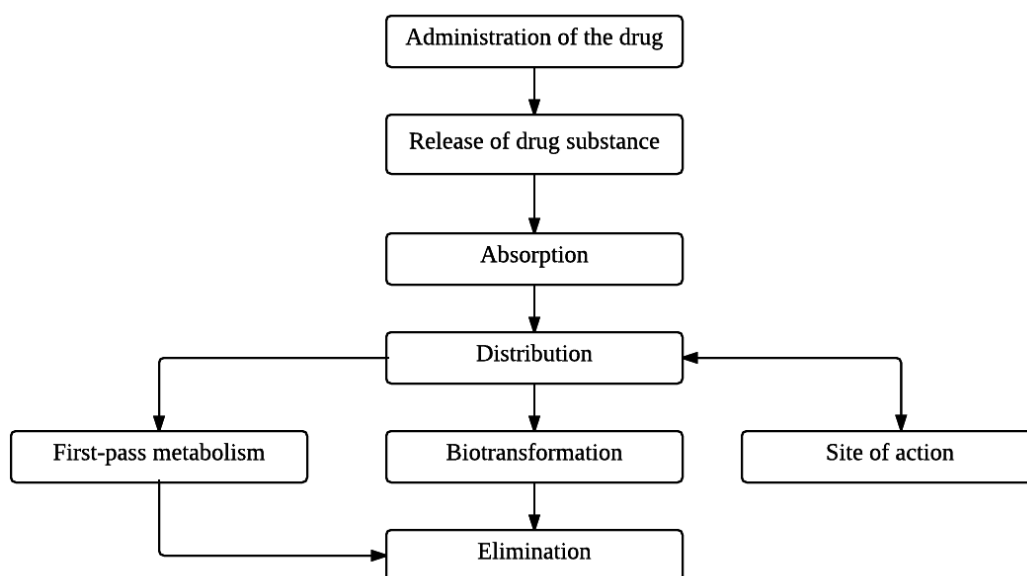
Figure 1. 1. Pharmacokinetics profile for the administration of a drug (adapted from Pfannkuch *et al.*, 2002) [2].

The preference of the pharmaceutical industry is to use the API in a solid-state form, such as tablets or capsules. This is a result of the usually higher stability and design flexibility of the solid drug forms; also, a solid dosage is easier to process and to administer to a patient. To produce a satisfactory new solid-state dosage form, the development of the API must consider the physical and chemical properties and the compatibility of the active ingredient, the excipients and the package.

The following physical properties of the API and excipients are prerequisites that must be considered before the production of a potential drug; the aim is stability during the manufacturing and formulation processes. To keep the substance from degrading or melting during the processing of the sample it is necessary for the API to have a relatively high melting point. As processing the solid depends on the particle size and shape, is important to have a sufficiently hard API and excipients to be able to grind and crush them into uniform and homogeneous samples. A related property to particle size is the surface area of the sample, which can be correlated to the aqueous solubility of the drug. High solubility and the related high rate of dissolution are generally desirable to increase the bioavailability of the API as it must be soluble enough to be absorbed by the human body. Any chemical reaction of, or structural change in, the API may result in variation of its physical properties which can in turn lead to an unsatisfactory pharmaceutical performance [1,3,4].

1.1. SALT FORMATION AND ITS IMPORTANCE IN THE PHARMACEUTICAL INDUSTRY

According to Brønsted-Lowry theory, acids are defined as proton donors and bases as proton acceptors, and salt formation is the reaction that occurs between an acid and a base involving either neutralization or the transfer of a proton [5]. The reactions given below show examples of types of reaction used to produce salt forms where reaction 1.1 represents the neutralization an organic acid (RCOOH) by an alkali metal base (MOH), while reaction 1.2 represents the proton transfer reaction between an organic acid (RCOOH) and an organic base (NH_2R').

$$RCOOH + MOH \rightarrow RCOO^- M^+ + H_2O$$

<div align="right">**Reaction 1. 1**</div>

$$RCOOH + NH_2R' \rightarrow RCOO^- {}^+NH_3R'$$
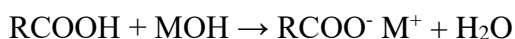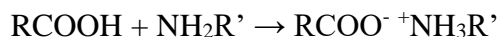
<div align="right">**Reaction 1. 2**</div>

The pharmaceutical salt will be the stoichiometric product of the reaction between an active pharmaceutical ingredient (API) and an acid or base that provides a counter-ion [6]. Salt-formers can be classified primarily according to their safety with some consideration given to the possible beneficial activity that the administration of the drug can cause. The first class of ions are generally taken to be those that have a natural occurrence in the body or are present in foods or beverages, so their use is unrestricted; the second class salt-formers are those low in toxicity and with a good tolerability but which do not occur naturally; the third class ions are those used to achieve a specific property of the salt or route of administration, with limited application because of possible undesirable effects in the body; and the fourth class salt-formers are those prohibited because of their toxicity and safety problems [2,7].

As many free organic acids and bases are only slightly soluble in water, generation of salt forms of APIs is important in pharmaceutical industries as a method to improve the solubility of the API in water and to increase the drug dissolution rate in aqueous solution [8]. The salt form also modifies other important physicochemical properties in comparison with the solid form of the parent compound, including typically increasing the melting point and altering hygroscopicity, taste, stability, mechanical hardness, bioavailability and toxicity [9,10]. However, improving solubility of the active pharmaceutical ingredient does not always imply a better and safer drug form. For example, the relative toxicity of the pharmaceutical drug can increase with increased bioavailability, generating unwanted effects [2].

1.2. PROPERTIES OF THE SOLID STATE

Most pharmaceutical dosage forms are in the solid state in the form of tablets or capsules [1]. Crystalline solids are typically chosen as they are usually more stable and have well-established solubility and dissolution rate as compared to alternatives. These physicochemical properties and many other physical properties depend on the crystal structure [4, 11]. For that reason, pharmaceutical companies must comprehend what changes can affect variations in solid state forms. To aid understanding, solid structures are classified as crystalline or amorphous solids and crystalline structures of an API can be further categorised as polymorphs, salt forms, solvates and cocrystals. Table 1.1 shows a brief difference in the structure of the product when polymorphism, amorphous solid, solvate and co-crystal occurs. Note that when making salts, slight variation of the experimental procedure can generate products with the same cation and anion composition but with different crystal structures (polymorphs of salt forms) or the products may differ by the presence or absence of water molecules (hydrates of salt forms); or the acid and base can crystallize as neutral forms rather than the expected salt form of the product (a co-crystalline form) [12].

Table 1. 1. Difference between possible solid-state forms (Adapted from Morrison, 2012) [12].

FORM	REPRESENATION	SYMBOL	KEY
Crystalline Polymorphs			active molecule
Amorphous			
Crystalline Solvate			solvent molecule
Crystalline Co-crystal			inactive molecule

1.2.1. CRYSTALLINE FORM

A crystalline solid can be defined as a material with a regular, long range and three-dimensional fixed and rigid pattern (known as a lattice). This can be composed of atoms, ions or molecules, with the basic repeating unit of the lattice called the unit cell. The unit cell is defined by the lengths of three axes a, b and c, and by the angles α (angle between b and c), β (angle between a and c) and γ (angle between a and b). Crystals can be categorised by the symmetry that describes their repeating patterns. There are seven crystal systems observed in nature and fourteen possible Bravais lattices (primitive and centred versions of the seven crystal systems). Figure 1.2 is a representation of the unit cell, with axis and angles described (a) and shows the propagation of the crystal structure by translational displacement in direction x (b), directions x and y (c) and directions x, y and z (d). Table 1.2 describes the axes and angles of the crystal systems with a representation of the Bravais lattices, which describes all the possible cell morphologies of real crystals [4, 13-15].
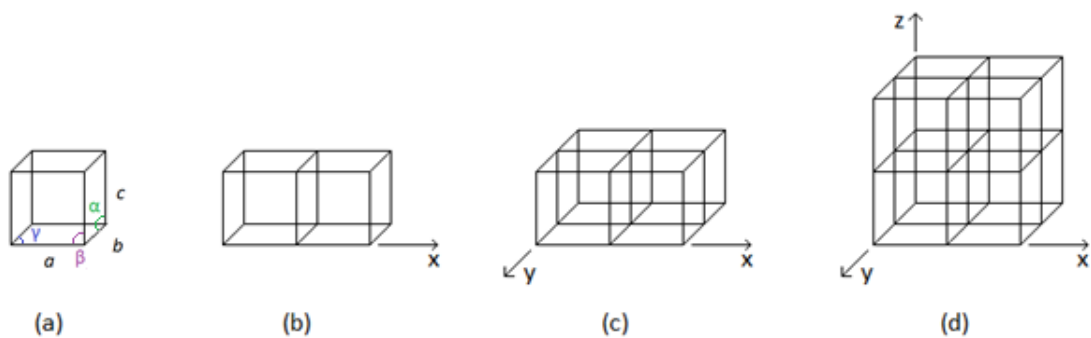
Figure 1. 2. Unit cell and crystal growth (adapted from Florence and Kennedy, 2010) [4].

In external form, the ideal solid crystal has well defined shape and angles, and flat faces; with physical properties potentially changing through different directions in the crystal and on different crystal faces. Another fundamental characteristic of the crystalline solid state is the ability to diffract X-rays [4].
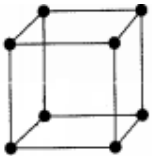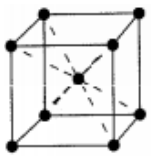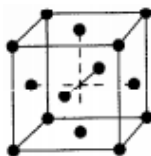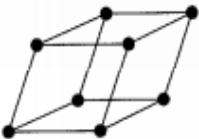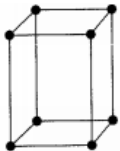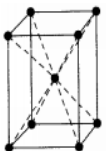
1.2.2. AMORPHOUS FORMS
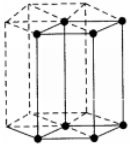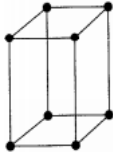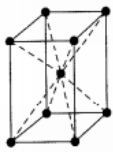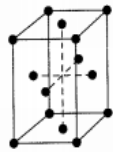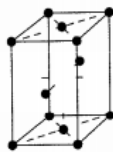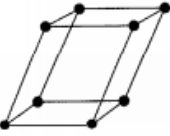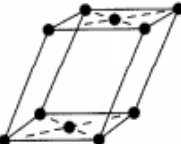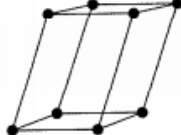
Amorphous forms occur when no long-range order appears in the solid. The random structure of the amorphous solid is like the liquid state, except that the molecules of the solid form have less mobility and more permanent intermolecular interactions [1,13]. In contrast with the crystalline state, amorphous solids have irregular shapes and their physical properties are identical in all directions [4].

1.2.3. POLYMORPHISM

With respect to crystalline solids the term *form* is used to refer to the internal crystal structure, while the term *habit* is used to describe the external shape of the crystal [16]. Polymorphism occurs when identical compounds are organized in more than one repeating pattern of the solid form [11, 16]. This can be done either by changing the molecular conformation or by the molecules maintaining the conformation but arranging themselves differently in a new unit cell. Both imply changes in intermolecular interactions, such as π-π interactions, van der Waals forces and hydrogen bonds [17,33]. As changing the crystalline form of the solid results in a new unit cell with different interactions between the atoms, the physical and chemical properties of the polymorphs will be different from each other [13]. Being able to design and control the polymorph formation of the pharmaceutical active ingredient and of any excipients is thus of vital importance to pharmaceutical companies as they attempt to select suitable physicochemical properties and develop a new drug [18].

Table 1. 2. System, axis, angles and Bravais lattices present in nature (adapted from Miessler and Tarr, 2004 [15]). The outward geometry of the units is a consequence of their symmetry and strictly it is this symmetry that defines the different crystal systems rather than their shapes. (E.g. a monoclinic crystal must display 2/m symmetry and a hexagonal crystal must display symmetry with a 6-fold rotation).

SYSTEM	AXIS (Å)	ANGLES (º)	BRAVAIS LATTICES			
			PRIMITIVE (P)	BODY-CENTERD (I)	FACE-CENTERED (F)	END-CENTERED (C)
Cubic	a = b = c	$\alpha = \beta = \gamma$ = 90				
Trigonal	a = b = c	$\alpha = \beta = \gamma$				
Tetragonal	a = b ≠ c	$\alpha = \beta = \gamma$ = 90				

7

Hexagonal	$a = b \neq c$	$\alpha = \beta = 90;$ $\gamma = 120$	
Orthorhombic	$a \neq b \neq c$	$\alpha = \beta = \gamma$ $= 90$	
Monoclinic	$a \neq b \neq c$	$\alpha = \gamma = 90;$ $\beta \neq 90$	
Triclinic	$a \neq b \neq c$	$\alpha \neq \gamma \neq \beta$	

An example of polymorphism is the three known polymorphs of the hormone estrone (Figure 1.3). While form I and form II crystallize as orthorhombic crystals with different unit cell dimensions, form III is a monoclinic crystal. This result in different hydrogen-bonds occurring between the molecules: Forms I and III have stronger hydrogen-bonds between the layers of parallel molecules while form II has weaker hydrogen-bonds between molecules in a herringbone arrangement [19].
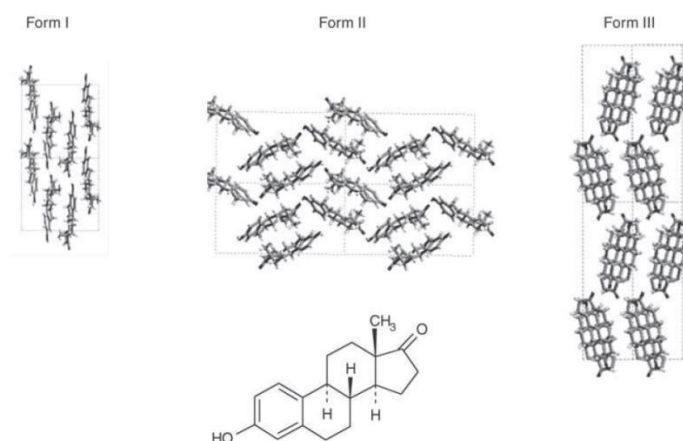
Figure 1. 3. Three possible polymorphs of estrone (from Steele and Austin, 2009) [7].

1.2.4. CO-CRYSTALS, SOLVATES AND HYDRATES

Co-crystals occur when neutral molecules of more than one material, all of which are solids at room temperature, generate a homogeneous crystal structure. Solvates occur when solvent molecules are present inside the crystalline structure. Solvates of salts or co-crystals are possible. If the solvate is water, the crystal form is denominated a hydrate. In the case of pharmaceutical co-crystals, the component which crystallizes with the API is referred as the co-crystal former or co-former [6]. Co-crystalline and solvate crystals are thus similar solid-state forms and are differentiated not by what they are but by physical differences between their constituent parts. The formal definition can be easily confused, e.g. by creating co-crystals above and below the formal melting point of solvents or simply by co-crystallising a liquid API [20].

Generating co-crystals can modify the physical and chemical properties without change to the molecular structure of the active pharmaceutical ingredient and can extend the product life of the drug [17]. For example, generating the co-crystal form of carbamazepine (an anti-epileptic agent that is water insoluble) and saccharin (Figure 1.4) gives a viable alternative that avoids the complicated polymorphism of carbamazepine, whilst maintaining the stability and bioavailability of the drug when compared with the marketed product [21].
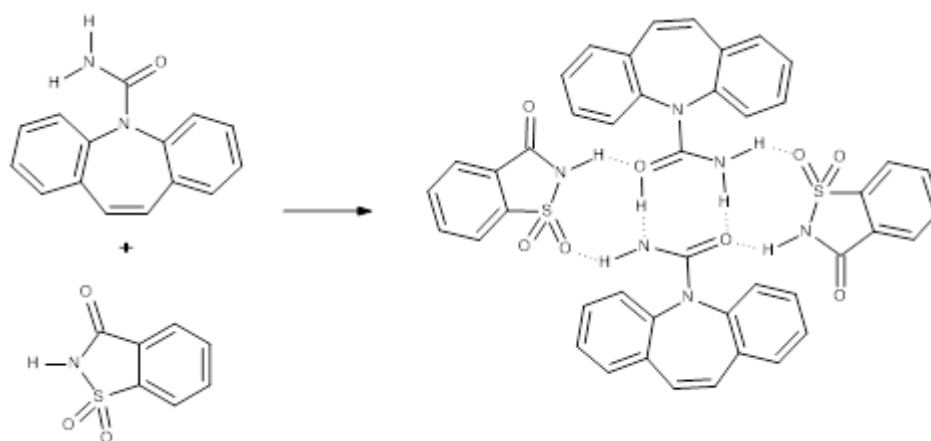
Figure 1. 4. Structures of carbamazepine, saccharin and the 1:1 generated co-crystal (adapted from Reference 21)

1.3. SALT SELECTION

For pharmaceutical companies it is often not practical to create many structures of salt forms of an API and analyse each crystal structure; to save time and money a salt screening is done. The idea is to produce small amounts of various salt forms and to quickly identify desirable/undesirable physical properties. An unsuccessful drug form may lack an essential desirable property (for instance a high dissolution rate) or it may be unstable and present unacceptable changes in the salt form during the process of manufacturing or under storage and use. Another factor is cost, hence any form that adds additional costs in the development of a new drug will be disfavoured. Preformulation studies, including chemical and physical analysis, are made of both the

API and of excipients in their raw forms to examine their physicochemical properties and to optimize the formulation of the product [4, 22, 34].

Salt screening begins with the identification and selection of the ionisable functional group of the API and appropriated counter ion to synthetize various salt forms [23]. For a successful and stable salt formation, the difference between the pK_a value of the weak base and the pK_a of the weak acid must be positive and greater than 2 [31,32]. The composition of the final salt must not alter with time or changes in storage conditions. Unacceptable changes include changes in the state of hydration and chemical stability [22]. Also, it is generally desirable that the salt form has a higher aqueous solubility and dissolution rate in the physiologic pH then the free API [8].

The solid formed must be stable and this usually is associated with it having a good crystallinity. In the case of the solid having a low crystallinity, the amorphous solid may still be used to create the drug (for instance if it has a high solubility and this is a useful property change). In case of polymorphs in the salt formation, the most stable and applicable form must be identified and typically used [13, 23]. The suitable drug must have a good compatibility with excipient to deliver the drug. After finding the most desirable salt form, regulatory and patent aspects are applicable. Figure 1.5 shows a flowchart to select the best salt form.
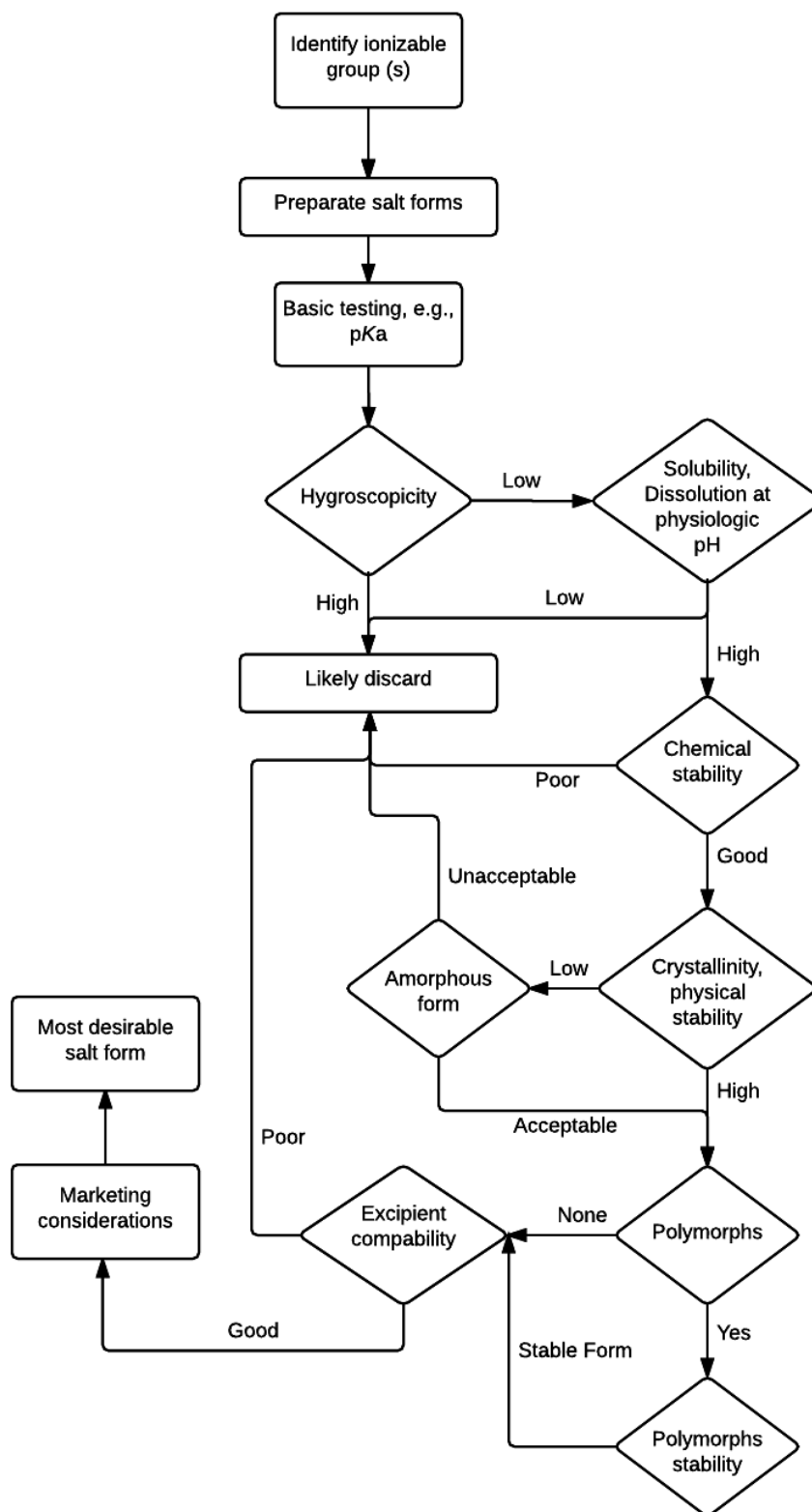
Figure 1. 5. Process diagram to select the best salt form (adapted from Niazi, 2007) [13].

1.4. MEASURING MECHANICAL PROPERTIES OF PHARMACEUTICAL COMPOUNDS

For pharmaceutical companies, measurement and undertstanding of mechanical properties of active APIs can be a challenging subject. However, understanding is required as mechanical properties influence aspects of manufacturability – especially grinding processes and tableting. Hardness is defined by Small (1960) [24] as the "property of solids and very viscous liquids which is indicated by their solidity and firmness. The quality of a mineral, the degree of which is determined by its power to scratch, or be scratched by other minerals, as arranged on an arbitrary scale; difficult to affect injuriously; resistant; hardness has no relation to density, or the number of particles within a given space, but depends only on the nature of the particles, the mutual arrangement, and cohesion." The last part of this definition implies that stronger intermolecular interactions will give harder materials.

There are many ways to measure the hardness of a material such as penetration, scratching, resilience, machinability and yield point [25]. An example of the behaviour of a sample can be observed in Figure 1.6 (a) where the sample is in its natural size, with no force applied to the rectangular surface, A. When force starts to be applied to the surface, the surface compresses and if there is no breakage in the sample, the maximum compression is directly related to the maximum force applied (Figure 1.6-b). Once the force is removed from the surface, three different things can occur:

1. The sample may recover completely which indicates that this sample is perfectly elastic;

2. The sample may stay with the position where the maximum load was applied, with no recovery from the sample, which indicates this sample is perfectly plastic; or

3. Part of the sample may recover from the maximum compression however, a partial permanent compression is left in the sample, smaller than the maximum compression. This type of intermediate sample is illustrated in Figure 1.6-c

where part of the sample recovers to its original state but there is still have a permanent compression.

This recovery of the sample described in item 3 is related to the elasticity of the sample, Young's Modulus, which is a relationship defined by Hook's Law between the stress applied to the sample (stress: $\sigma = P/A$) and the percentage of deformation in the surface after the stress is removed (strain: $\varepsilon = (l - l_0)/l_0$) [26-27].
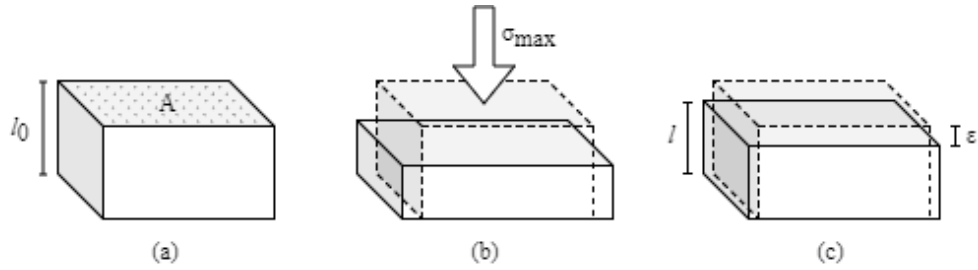
Figure 1. 6. (a) No stress applied to the sample, (b) maximum stress applied to the sample. Maximum compression occurs and (c) sample after stress removed with permanent damage on the surface.

Stress (σ) and hardness (H) have the same relationship involving the force applied and the area indented or compressed, as it can be observed in Equations 1.1 and 1.2. In this work an approximation between hardness and stress can be made for plots of hardness versus Young's Modulus (E), Figure 1.7. If a relationship of stress and hardness can be approximated, this relationship between Hardness and Young's modulus will be approximate to the strain (ε) of the sample, which is a characteristic particular to each material. In this work, this approximation will be called elasticity index (I_E) [35].

$$E = \frac{\sigma}{\varepsilon}$$

Equation 1. 1

$$\varepsilon \cdot E = \sigma \cong H$$

Equation 1. 2
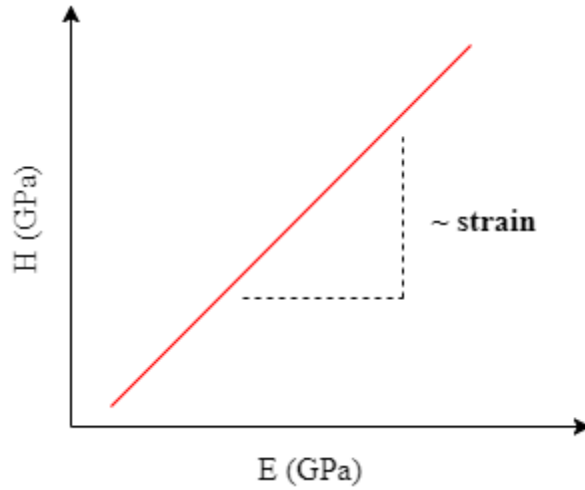
Figure 1. 7. Example of the approximation used in this work when plotting hardness versus Young's Modulus.

1.4.1. SCRATCH HARDNESS MEASUREMENT

Scratch hardness determinates the resistance of a material when it is submitted to a scratch from a sharp object. This resistance can be denominated friction. The basic procedure is a diamond stylus scratches the surface of the material with a constant speed [28]. The scratch hardness number (HSp) is calculated measuring the average width of the scratch (x) created by the applied force (P) by Equation 1.3:

$$\text{HSp} = \frac{8P}{\pi x^2}$$

Equation 1. 3

1.4.2. REBOUND HARDNESS

This type of hardness measurement is related to the energy absorption of the material after the impact of a compresser and the material. The compresser collides with the object surface at an initial constant speed and after collision the reduced speed of the indenter is measured [28]. The relationship between the speed before the collision (A)

and after the collision (B) is known as Leeb hardness value (HL) and can be calculated by Equation 1.4:

$$HL \ = \ 1000 \cdot \frac{B}{A}$$

Equation 1. 4

1.4.3. INDENTATION METHODS

Indentation hardness describes the size of the impression made by an indenter of specific size and shape under a known load [25]. The value obtained of the hardness measurement will depend on the type of indenter used in the experimental procedures. In all cases that will be described below F is the specific applied load for a determinate period, D is the diameter of the indenter and d the diameter of the indentation as measured after the force has been removed.

Two types of hardness measurement use a ball indenter (Figure 1.8 - a) to make permanent impressions in the sample: Brinell Hardness (HBW) is a number related to the size of the permanent impression made by the indenter pressed into the surface of the material; while in Rockwell Hardness (HR), the indenter is pressed into the surface of the test piece in a preliminary test force, where the force is applied in a short period of time; then an additional and higher test force is applied, maintained for a longer period, and returned to the minimum load generating a permanent increase in penetration depth at a preliminary test force (h). Hardness can also be obtained using pyramidal indenters and the hardness value will vary according to the type of indenter used. For example, hardness can be obtained using a three-sided pyramid (Berkovich hardness, Figure 1.8-b), a square-based pyramid diamond indenter (Vickers hardness, Figure 1.8 - c) and by a rhombic-based diamond indenter (Knoop hardness, Figure 1.8 - d) [28]. The value related to the hardness measurements can be obtained by the equations below: Brinell hardness - equation 1.5; Rockwell hardness - equation 1.6

(where N and S are constants); Vickers hardness - equation 1.7 (where α = 136 °); and Knoop Hardness – equation 1.8 (where α = 172.5 ° and β =130 °):

(a) Spherical
(Brinell)

(b) Trigonal Pyramid
(Berkovich)

(c) Square Pyramid
(Vickers)

(d) Elongated Pyramid
(Knoop)
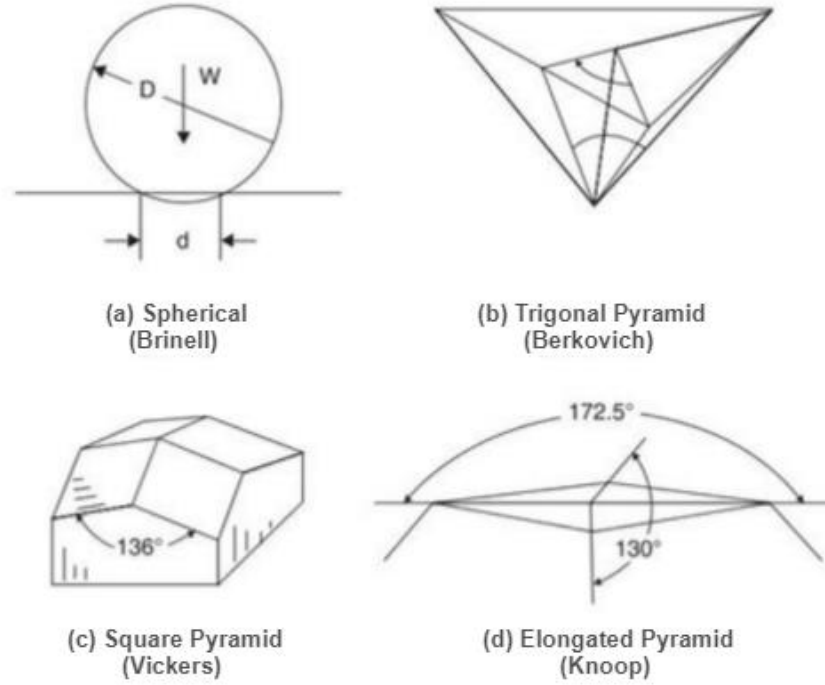
Figure 1. 8. Types of hardness indenters (from Gilman, 2009) [26].

$$HBW \ = \ 0.102 \cdot \frac{2F}{\pi D \left(D - \sqrt{D^2 - d^2}\right)}$$

Equation 1. 5

$$HR \ = \ N - \frac{h}{S}$$

Equation 1. 6

$$HV \ = \ 0.102 \cdot \frac{2F \cdot sen\left(\frac{\alpha}{2}\right)}{d^2}; \text{and } d = \frac{d1 + d2}{2}$$

Equation 1. 7

$$HK = 0.102 \cdot \frac{2F}{c \cdot d^2}; \text{ and } c = \frac{\tan(\frac{\beta}{2})}{\tan(\frac{\alpha}{2})}$$

<div align="right">**Equation 1. 8**</div>

1.4.4. INSTRUMENTAL INDENTATION

A Vickers or a Berkovich indenter is pressed into the surface of the material under an applied force (F), measuring the maximum indenter penetration (h) and the penetration profile after the load is removed (Figure 1.9). This procedure is capable of measuring both the plastic and elastic deformation of the material under testing. The unloading contact compliance (C) and the contact depth (h_c) can be calculated [29].
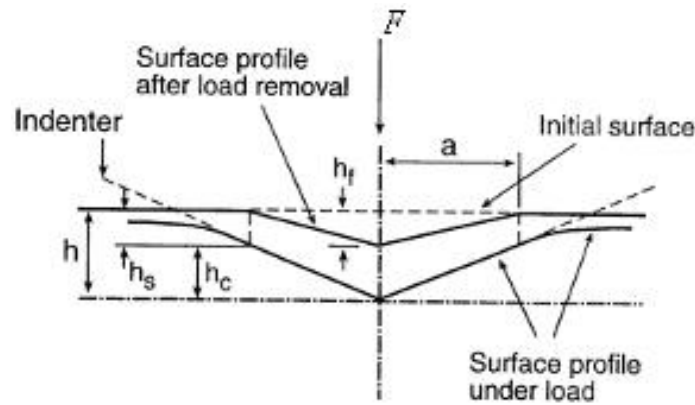
Figure 1. 9. Profile of the surfaces before and after the load is removed (from Oliver and Pharra, 2004) [29].

The stiffness on the contact can be determined and thus the indentation modulus (E_{IT}), the indentation hardness (H_{IT}) and the Martens hardness (HM) of a material. Martens hardness is the total hardness calculated by the division of the test force by the original (deepest) surface area [As(h)] for both indenters. The difference in the equation to obtain Martens hardness value for the two indenters is minimal, in the constant C. For Vickers indenter the value of C is 26.43 while for Berkovich indenter, the value of C

is 26.44. The relationship between Martens hardness, the force and the maximum indenter penetration is given by the equation 1.9:

$$HM = \frac{F}{As(h)} = \frac{F}{C \cdot h^2}$$

The indentation hardness (H_{IT}) is calculated from the test force divided by difference between the projected area of the surface in maximum load and the surface after load removed ($A(h_c)$). H_{IT} can be calculated using equation 1.10:

$$H_{IT} = \frac{F}{A(h_c)}$$

The Young's modulus (E*) is calculated from the gradient of the top 1/3 of the unloading curve, S (figure 1.10); and v_{st} and $v_{indenter}$ which are the Poisson's ratio of the test piece and the indenter. Poisson's ratio is the ratio of the transverse contraction strain (ε) to longitudinal extension strain in the direction of the stretching force through the length of the extension (L). Young's modulus and can be determined using equations 1.11 and 1.12, respectively.

$$E^* = \frac{(1 - v_{st}{}^2)}{\frac{2}{\sqrt{\pi}} \cdot \frac{\sqrt{A(h_c)}}{S} - \frac{1 - v_{indenter}{}^2}{E_{indenter}}}$$

$$v = \frac{-\varepsilon_{transversal}}{\varepsilon_{longitudinal}} \; ; \text{ and } \varepsilon = \frac{\Delta L}{L}$$

<div align="right">**Equation 1. 12**</div>

Figure 1. 10. Load profile as a function of the displacement relative to the initial underformed surface (from Oliver and Pharra, 2004) [29].

1.4.5. NANOINDENTATION

The methodology used in nanoindentation involves the analysis of load-depth curves as described in Chapter 1.4.4, that result from loading and unloading the probe onto the surfaces of the materials using different forces. During the nanoindentation process, the tip indents the surface of the material until a pre-determined value of load (P_{max}) is achieved. When the indenter ceases to increase force, the tip is found in the maximum depth of penetration (h_{max}). When the material is completely plastic, the permanent depth left in the sample is the same as h_{max}. However, due to the sample's elasticity part of the surface can recover to the original shape of the surface [29, 36, 37]. The depth recovered from the sample to the initial shape after the maximum force was achieved is shown in Figure 1.9 as h_c and the permanent depth after recovery of part of the sample is shown in Figure 1.9 as h_s.

The procedure described generates a compliance curve, such as the one observed in Figure 1.10 for experimental results obtained using thin films [38], which shows the behaviour of the sample when the force is increasing (loading, in blue) and when the

force ceased (unloading, in red). Important information can be obtained from the compliance curve such as P_{max} and h_{max}. Another important information is the elastic unloading stiffness, $S = dP/dh$, defined as the gradient of the top 1/3 portion of the unloading curve.

The procedure to calculate hardness (H) in this experiment considers the elasticity of the samples which involves relationships between the maximum depth (h_{max}), the depth recovered from the sample to the initial shape after the maximum force was achieved (h_c) and the permanent depth on the sample (h_s), which is described by calculated models [39-43] as $h_s = \varepsilon(P_{max}/S)$, where ε is the intercept factor, a constant equal to 0.75 for pyramidal indenters.

$$h_{max} = h_c + h_s$$

<div align="right">**Equation 1. 13**</div>

$$h_c = h_{max} - \varepsilon(P_{max}/S)$$

<div align="right">**Equation 1. 14**</div>

The indentation area is a function of indentation depth and the geometry of the probe, as described by Equation 1.15. The constant B corrects the indent area according to the geometry of the indenter. For a cube corner indenter, as used in this work, $B = 3\sqrt{3} \cdot \tan^2 \theta$, where θ is the back angle of the tip, equal to 35.26° [36].

$$A = F(h) \ \therefore \ A = B \cdot h^2$$

<div align="right">**Equation 1. 15**</div>

Hardness (H) is measured by the applied force divided by the indentation area, Equation 1.16. The general equation for hardness using a cube corner indenter can be obtained by combining Equations 1.13 to 1.16 and is observed below as Equation 1.17.

$$H = \frac{P_{max}}{A_c}$$

$$H = \frac{P_{max}}{\left[2.598 \cdot \left(h_{max} - 0.75 \cdot \left(\frac{P_{max}}{S}\right)\right)^2\right]}$$

1.4.6. MEYER'S HARDNESS

Meyer's hardness describes the depth-dependence of the force-penetration in the measurement of hardness [30]. Meyes's hardness can be measured by the combination of two equations: The Meyer's hardness number equation (HMe) which correlates the applied force (F) with the indentation diameter (d) (equation 1.18), and the relationship between force (F) and indentation diameter and the ball intender diameter (D), considering the constants that characterizing material parameters of the hardness properties, K and n (equation 1.19).

$$\text{HMe} = \frac{4F}{\pi \cdot d^2}$$

$$F = K\left(\frac{d}{D}\right)^{n}$$

The general form of Meyer's hardness (H) is described by equation 1.20:

$$H = \frac{4K}{\pi \cdot D^2} \cdot \left(\frac{F}{K}\right)^{1-2/n}$$

In general, using ball indenters the value of n is bigger than or equal to 2, while the value of n is smaller than 2 for square-based pyramid indenter. Vickers hardness number depends on the indentation load applied and the effect the indentation size (ISE) will have in the sample is divided in two types: normal ISE, which usually involves a decrease in microhardness with increasing indentation load; and reverse ISE, where microhardness increases with increasing indentation load [30].

1.5. REFERENCES

[1]   Giron, D. & Grant, D. J. W. (2002). Evaluation of solid-state properties of salts. In: Stahl, P.H. & Wermuth, C.G., eds. Handbook of Pharmaceutical Salts. Zurich: Wiley-VCH, 2002.

[2]   Pfannkuch, F., Rettig, H. & Stahl, P. H. (2002). Biological effects of the drug salt form. In: Stahl, P.H. & Wermuth, C.G., eds. Handbook of Pharmaceutical Salts. Zurich: Wiley-VCH.

[3]   Lipinski, C. A. (2000). Journal of Pharmacological and Toxicological Methods, 44, 235-249.

[4]   Florence, A.T. & Kennedy, A.R. (2010). Background notes for practical crystallisation course – Handout to accompany course.

[5]   Atkins, P., Overton, T., Rourke, J., Weller, M., Amstrong, F. & Hagerman, M. (2010). Inorganic chemistry. W. H. Freeman and Company, New York. 5th edition

[6]   Bond, A. D. (2012). Fundamental aspects of salts and co-crystals. In: Woulters, J., Quéré, L. Pharmaceutical salts and co-crystals, RSC.

[7]   Steele, G. & Austin, T. (2009). Preformulation Investigations using Small Amounts of Compound as an Aid to Candidate Drug Selection and Early Development. In: Gibson, M. Pharmaceutical Preformulation and Formulation - A Practical Guide from Candidate Drug Selection to Commercial Dosage Form. Informa Healthcare USA.

[8]   Pudipeddi, M., Serajuddin, A. T. M., Grant, D. J. W. & Stahl, P.H. (2002). Solubility and dissolution of weak acids, bases, and salts. In: Stahl, P.H. & Wermuth, C.G., eds. Handbook of Pharmaceutical Salts. Zurich: Wiley-VCH.

[9]   Gibson, M. (2009). Pharmaceutical Preformulation and Formulation - A Practical Guide from Candidate Drug Selection to Commercial Dosage Form. 2nd ed. Informa Healthcare USA, Inc.

[10]   Berge, S. M., Bighley, L. D. & Monkhouse, D. C. (1977). Pharmaceutical Salts. Journal of Pharmaceutical Sciences. Vol. 66, No. 1.

[11]   Bauer, J. F. (2008).. Journal of Validation Technology, p 15-24

[12]   Morrison, C.A. (2012). Salt selection for pharmaceutical use University of Strathclyde. Dept. of Pure and Applied Chemistry. Thesis [Ph. D] - University of Strathclyde.

[13]   Niazi, S. K. (2007). Handbook of Preformulation - Chemical, Biological, and Botanical Drugs. Informa Healthcare USA, Inc.

[14]   Mullin, J. W. (2001). Crystallization, 4th Ed., Butterworth-Heinemann

[15]   Miessler, G.L., Tarr, D.A. (2004), Inorganic Chemistry, 3nd. Ed., Person Educaton, Inc., New Jersey.

[16]   Borka, L. & Haleblian, J. K. (1990). Acta Pharm. Jugosl. 40,71-94.

[17]   Sarma. B., Chen, J., His. H. & Myerson, A. S. (2011). Korean J. Chem. Eng., 28(2), 315-322.

[18]   Bernstein, J. (2002). Polymorphism in Molecular Crystals (Vol. 9780199236565). Oxford: Oxford University Press USA - OSO.

[19]   Busetta, B., Courseille C. & Hospital M.(1973). Acta Cryst. B29, 298-313.

[20]   McKellar, S. C., Kennedy, A. R., McCloy, N. C., McBride, E. & Florence, A. J. (2014). Cryst. Growth Des. 14, 2422−2430

[21]   Hickey, M.B., Peterson, M. L., Scoppettuolo, L. A., Morrisette S. L., Vetter, A., Guzman, H., Remenar, J. F., Zhang, Z., Tawa M. D., Haley, S., Zaworotko M. J. & Almarsson, O. (2007). European Journal of Pharmaceutics and Biopharmaceutics 67 112–119

[22]   Stahl, P. H. & Nakano, M. (2002). Pharmaceutical Aspects of the Drug Salt Form. In: Stahl, P.H. & Wermuth, C.G., eds. Handbook of Pharmaceutical Salts. Zurich: Wiley-VCH.

[23]   Serajuddin, A. T. M. & Pudipeddi, M. (2002). Salt selection strategies. In: Stahl, P.H. & Wermuth, C.G., eds. Handbook of Pharmaceutical Salts. Zurich: Wiley-VCH.

[24]   Small, L. (1960) 'Hardness: theory and practice, part 1: practice'. Voyager.

[25]   Williams, S. R. (1942). 'Hardness and hardness measurements'. Voyager.

[26]   Gilman, J. J. (2009). Chemistry and Physics of Mechanical Hardness. John Wiley & Sons, Inc.

[27]   Young, W. & Budynas, R. (2002). Roark's Formulas for Stress and Strain. McGraw-Hill Publishing. Retrieved 10 March 2016, from <http://www.myilibrary.com?ID=91331>

[28]   NPL, National Physics Laboratory (2010) 'Hardness methods and sensitivity coefficients'. Available at: http://www.npl.co.uk/science-technology/mass-and-force/hardness/ (Accessed: 15 October 2015).

[29]   Oliver, W.C. and Pharra, G.M. (2004). J. Mater. Res., 19 (1), pp. 3-20.

[30]   Berg, G and Grau, P. (1997). Cryst. Res. Technol, 32 (1), pp. 149-154.

[31]   Anderson, B. D. & Flora, K. P. (1996). The Practice of Medicinal Chemistry. Ed. C. G. Wermuth, Academic Press, London, pp. 739 – 754

[32]   Remington, J. P. (2013). The science and practice of pharmacy. 22nd ed. / editor-in-chief, Loyd V. Allen Jr. London : Pharmaceutical

[33]   Olovsson, I. & Jönsson, P.-G. (1976). The Hydrogen Bond. Recent Developments in Theory and Experiments, edited by P. Schuster, G. Zundel & C. Sandorfy, pp. 393-455. Amsterdam: North-Holland.

[34]   Morissette, S. L., Almarsson, O., Peterson M. L., Remenar, J. F., Read, M. J., Lemmo, A. V., Ellis, S., Cima, M. J. & Gardner, C. R. (2004). Advanced Drug Delivery Reviews, 56 275–300

[35]   Cheng, Yang-Tse, & Cheng, Che-Min. (1998). Applied Physics Letters, 73(5), 614-616.

[36]   Fischer-Cripps, A., & Springerlink. (2011). Nanoindentation [internet resource] (3rd ed., Mechanical engineering series ; 1). New York: Springer.

[37]   Egart, M., Janković, B., & Srčič, S. (2016). Acta Pharmaceutica (Zagreb, Croatia), 66(3), 303-330.

[38]   Doerner, M. & Nix, W. (1986). Journal of Materials Research, 1(4), 601-609

[39]   Sneddon, I. N. (1965). Int. J. Engng. Sci., 3, 47-57.

[40]   Love, A.E.H., (1939). Q.J. Math. 10, 161.

[41]   Love, A.E.H., (1929). Philos. Trans. A 228, 377.

[42]   Harding, J.W. & Sneddon, I.N (1945). Proc. Cambridge Phil. Soc. 41, 16.

[43]   Sneddon, I.N. (1951). Fourier Transforms (McGraw-Hill, New York), pp. 450–467

2. METHODS, MATERIALS AND EXPERIMENTAL PROCEDURES

2.1. ACTIVE PHARMACEUTICAL INGREDIENT SELECTION

Four organic bases were initially selected and used as models of active pharmaceutical ingredients (APIs) to generate a database of systematically related crystal structures of API salt forms. These bases were: *p*-hydroxyphenylethylamine (normally called tyramine (TYR), enantiopure (1*R*,2*S*)-(−)-N-methylephedrine (MEPD), racemic (+/-) methylephedrine (RMEPD) and enantiopure (1*R*,2*S*)-(−)-N-ephedrine (EPD). The group of bases was chosen to include primary, secondary and tertiary amines (Figure 2.1). All the bases used in this work are slightly soluble in water at room temperature and have the physical form of plate or needle crystals according to the crystallisation solvent [1]. All the bases were obtained from Sigma-Aldrich or Alfa Aesar.

Tyramine
(TYR)

(1*R*,2*S*)-N-methylephedrine
(MEPD)

(+/-)-methylephedrine
(RMEPD)

(1*R*,2*S*)-N-ephedrine
(EPD)
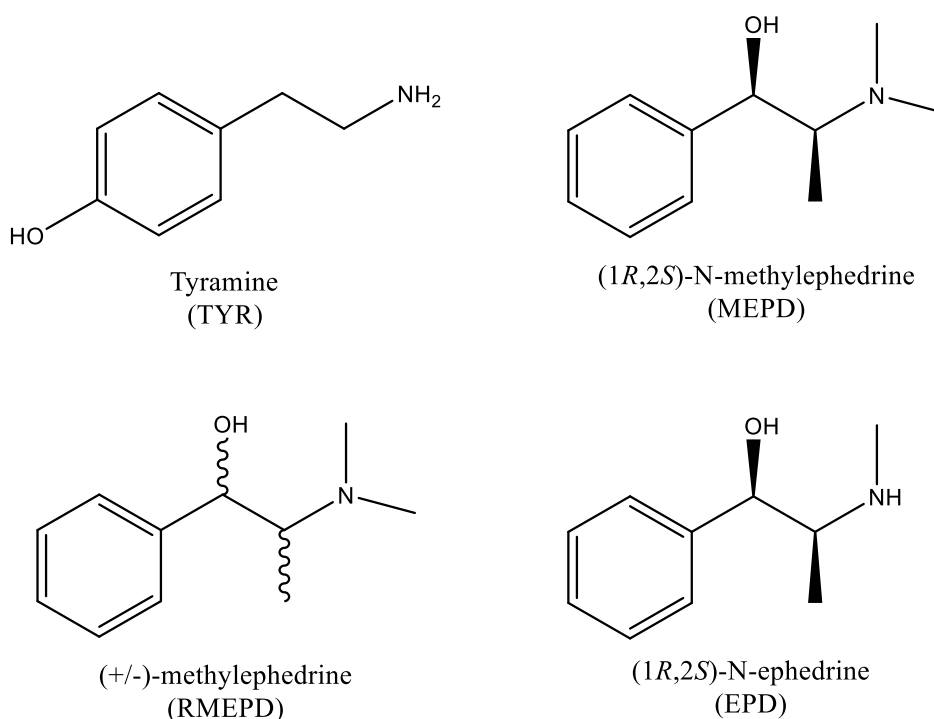
Figure 2. 1. Structures and abbreviated name of the selected bases.

2.2. COUNTERION SELECTION

The selection of the counterions was made to complement, and to avoid repetition of, literature results and previous samples prepared within the local group. According to the literature, of the eighty-two acids selected, at least twenty-seven are widely used as first- and second-class pharmaceutical counter-ions. These classes are defined as acids with unrestricted to good tolerability by the human body, but which may not occur naturally [2], and include sulfonic acids and mono and di-carboxylic acids. Some acids in the counterion selection were chosen simply for structural comparison, even though they are not commonly pharmaceutically acceptable. For example, anions of several mono-sulfonated azo dyes were included although they are not usually used as counter ions. However, they do offer a structural contrast to anions such as benzenesulfonate that are pharmaceutically acceptable. All the acids were obtained from Sigma-Aldrich, Fluka or BDH or were previously prepared locally by students. The acid selection includes mostly carboxylic acids and sulfonic acids with variations in the size of the aliphatic chain or of the substituent groups of the aromatic compounds. A summary of the distribution of acid selection for all the attempts of synthesis, according to the base used, can be observed in Figure 2.2.
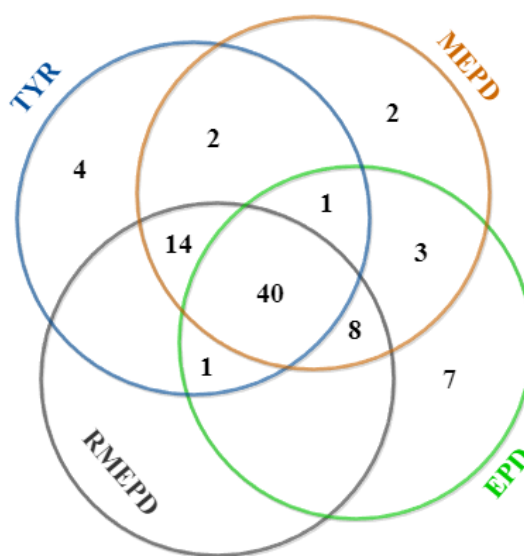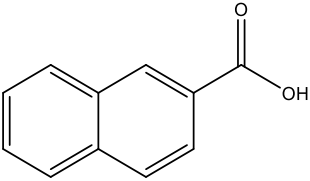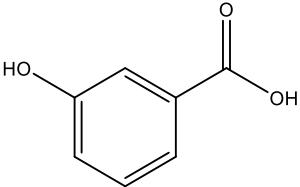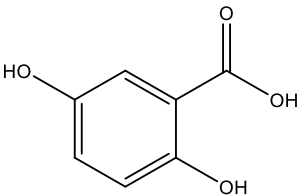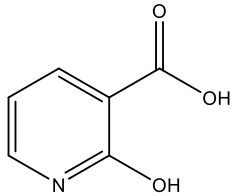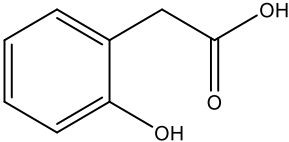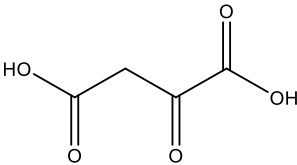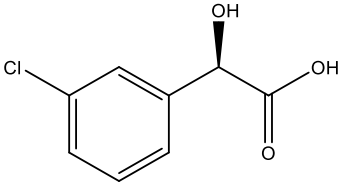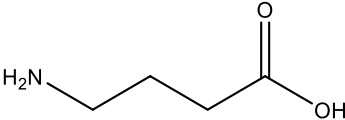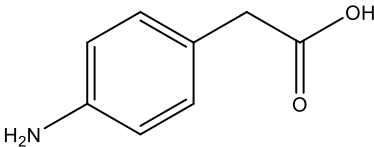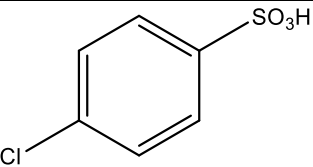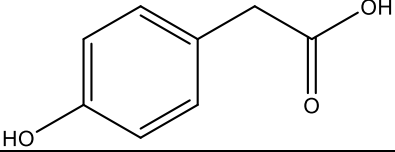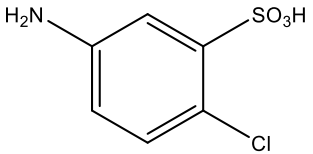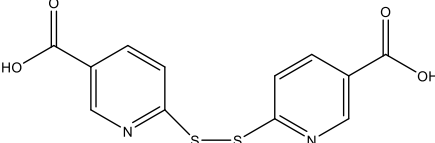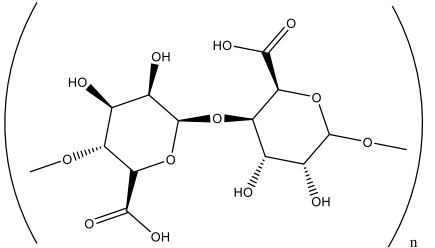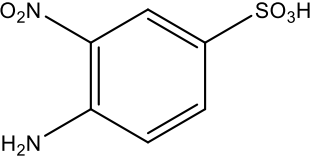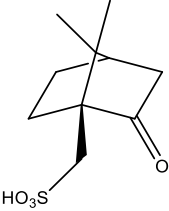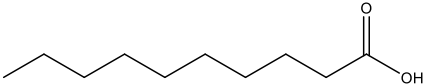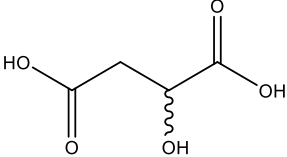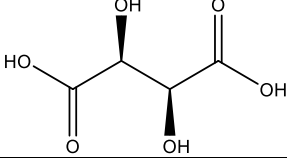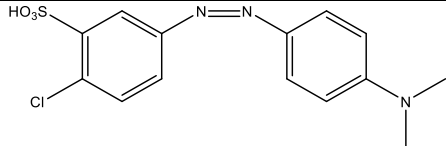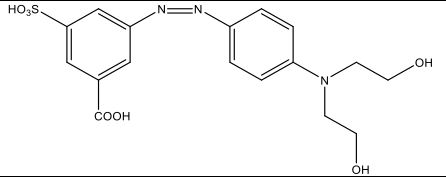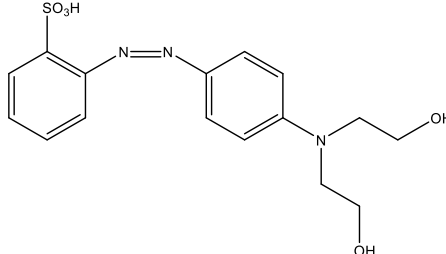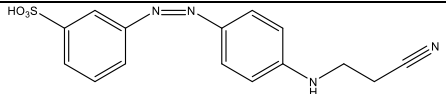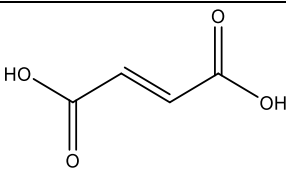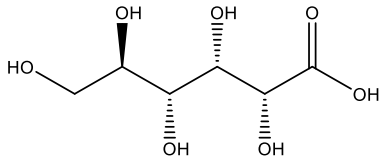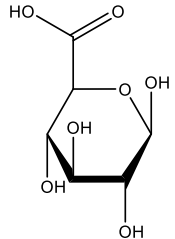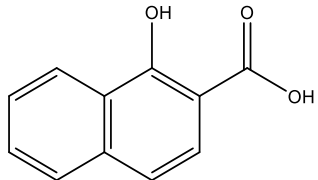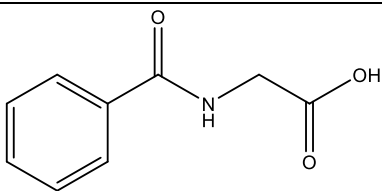
Figure 2. 2. Distribution of acid selection for each base. The circle in blue represents attempts of syntheses with the tyramine base, the circle in orange represents attempts of syntheses with enantiopure methylephedrine, in grey attempts of syntheses with racemic methylephedrine and the circle in green represents attempts of syntheses with enantiopure ephedrine.
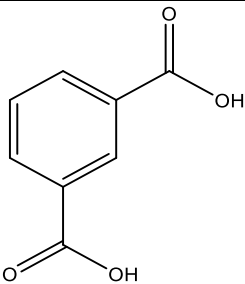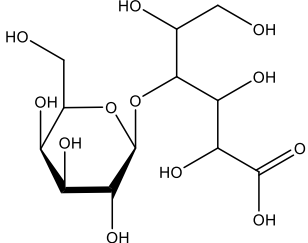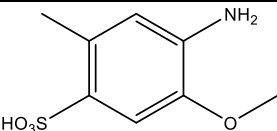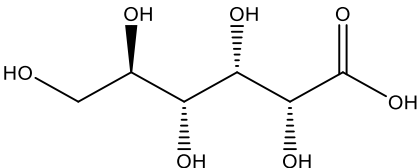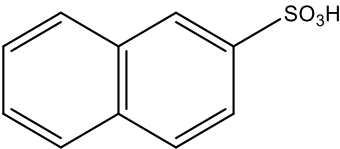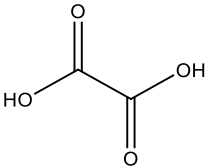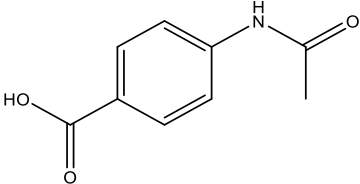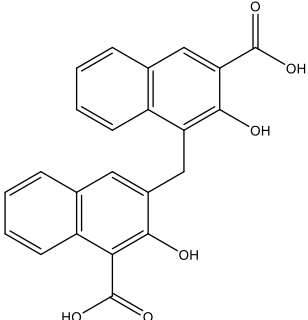
The selected acids can be separated into 10 groups divided according to the bases they were used with. The acids of these groups are illustrated in the following tables: Group 1 includes a selection of forty acids common to all bases (Table 2.1); Group 2 includes a selection of fourteen acids common to tyramine (TYR), enantiopure methylephedrine (MEPD) and racemic methylephedrine (RMEPD) (Table 2.2); Group 3, includes a selection of eight acids common to enantiopure methylephedrine (MEPD), racemic methylephedrine (RMEPD) and enantiopure ephedrine (EPD) (Table 2.3); Group 4 contains one acid common to tyramine (TYR), enantiopure methylephedrine (MEPD) and enantiopure ephedrine (EPD) (Table 2.4); Group 5 contains one acid common to tyramine (TYR), racemic methylephedrine (RMEPD) and enantiopure ephedrine (EPD) (Table 2.5); Group 6 includes a selection of two acids common to tyramine (TYR) and enantiopure methylephedrine (MEPD) (Table 2.6); Group 7 includes a selection of three acids common to enantiopure methylephedrine (MEPD) and enantiopure ephedrine (EPD) (Table 2.7); Group 8 includes a selection of four acids used only in tyramine (TYR) experiments (Table 2.8); Group 9 includes a selection of two acids used only in enantiopure methylephedrine (MEPD) experiments (Table 2.9) and Group 10 includes a selection of seven acids used only in enantiopure (EPD) ephedrine experiments (Table 2.10).

Table 2. 1. Group 1: Selection of forty acids common to all bases

Acid	Abbreviated Name	Molecular Structure
2-naphthoic acid	2NAPH	
2-hydroxybenzoic acid	2HB	
2,5-dihydroxybenzoic	25HB	
2-hydroxypyridine-3-carboxylic acid	2HP3C	
2-hydroxyphenylacetic acid	2HPA	
2-ketoglutaric	2KG	
3-chloromandelic acid	3CMD	
4-aminobutyric acid	4ABUT	
4-aminophenylacetic acid	4APA	

4-chlorobenzenesulfonic acid	4CBS	
4-hydroxyphenylacetic acid	4HPA	
5-chloro-2-nitrobenzoic acid	5C2NB	
6,6′-dithiodinicotinic acid	66TN	
Alginic acid	ALG	
4-amino-3-nitrobenzene-1-sulfonic acid	ANBS	
D-camphor-10-sulfonic acid	CAMPH	
Decanoic acid (Capric acid)	CAP	
DL-malic acid	DLMAL	
D-tartaric acid	DTAR	

Dye A	DYEA	
Dye B	DYEB	
Dye C	DYEC	
Dye E	DYEE	
Fumaric acid	FUM	
D-Gluconic acid 50% aqueous solution	GLUCON	
D-glucuronic acid	GLUCUR	
Hydroxy-2-napthoic	H2NAPH	
Hippuric acid	HIP	

Isophthalic acid	IPH	
Lactobionic acid	LACB	
4-amino-5-methoxy-2-methylbenzenesulfonic acid	MMBS	
Mucic acid	MUC	
Naphthalene-2-sulfonic acid	N2S	
Oxalic acid dihydrate	OXA	
p-acetamidobenzoic acid	PAAB	
Pamoic acid	PAM	
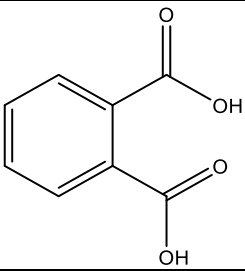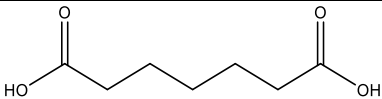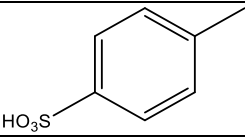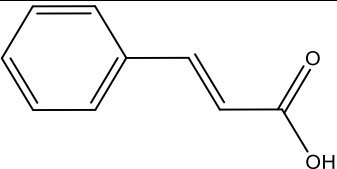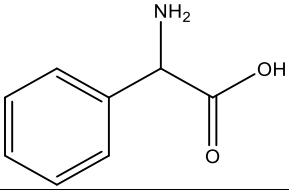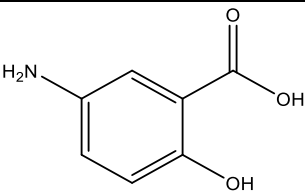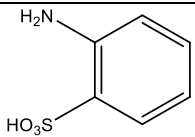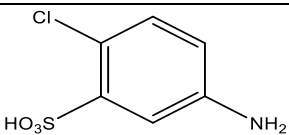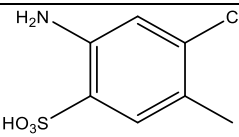
Phthalic acid	PH	
Pimelic acid	PIM	
p-Toluenesulfonic	PTS	
trans-Cinnamic acid	TCIN	

Table 2. 2 Group 2: Selection of fourteen acids common to tyramine (TYR), enantiopure methylephedrine (MEPD) and racemic methylephedrine (RMEPD).

Acid	Abbreviated Name	Molecular Structure
2-phenylglycine	2PG	
5-aminosalicylic acid	5AMS	
Aniline-2-sulfonic acid	A2S	
5-amino-2-chlorobenzene-1-sulfonic acid	ACLBS	
2-amino-4-chloro-5-methylbenzene-1-sulfonic acid	ACLMBS	
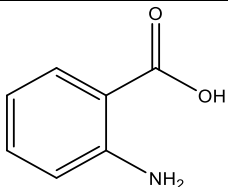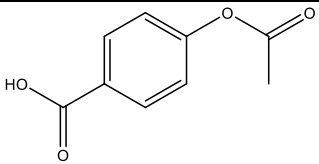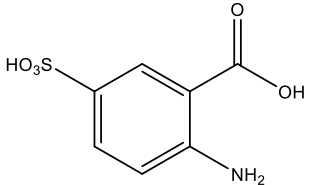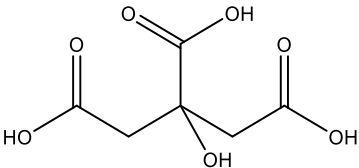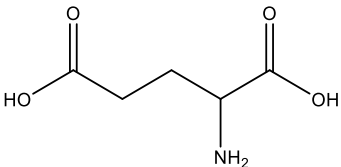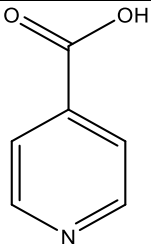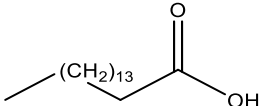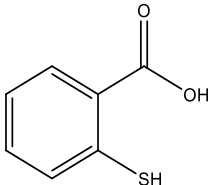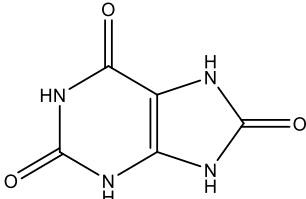
Anthranilic acid	ANT	
Acetylsalicilic acid	AS	
2-Amino-5-sulfobenzoic acid	ASB	
Citric acid	CIT	
Glutamic acid	GLU	
Isonicotinic acid	IN	
Palmitic acid	PAL	
Thiosalicylic acid	TIOSA	
Uric acid	UR	

Table 2. 3 Group 3: Selection of eight acids common to enantiopure methylephedrine (MEPD), racemic methylephedrine (RMEPD) and enantiopure ephedrine (EPD).
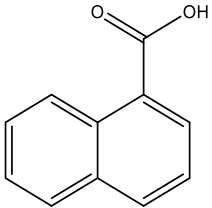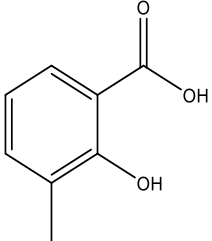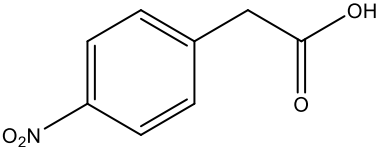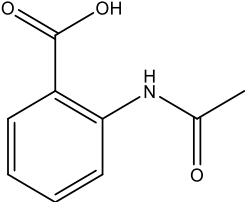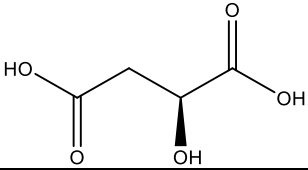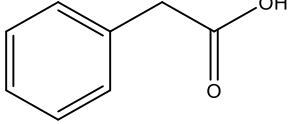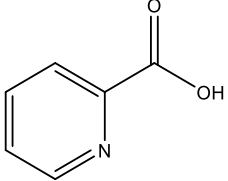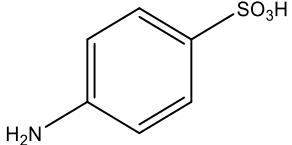
Acid	Abbreviated Name	Molecular Structure
1-naphthoic acid	1NAPH	
3-methylsalicylic acid	3MS	
4-nitrophenylacetic acid	4NPA	
Acetylanthranilic acid	AA	
L-malic acid	LMAL	
Phenylacetic acid	PA	
Picolinic acid	PICO	
Sulfanilic acid	SULFA	

Table 2. 4 Group 4: Selection of one acid common to tyramine (TYR), enantiopure methylephedrine (MEPD) and enantiopure ephedrine (EPD).
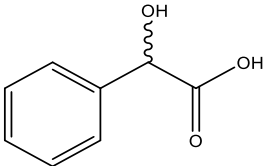
Acid	Abbreviated Name	Molecular Structure
(+/-)Mandelic acid	RMD	

Table 2. 5 Group 5: Selection of one acid common to tyramine (TYR), racemic methylephedrine (RMEPD) and enantiopure ephedrine (EPD).
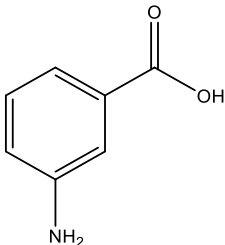
Acid	Abbreviated Name	Molecular Structure
3-aminobenzoic acid	3AB	

Table 2. 6 Group 6: Selection of two acids common to tyramine (TYR) and enantiopure methylephedrine (MEPD).
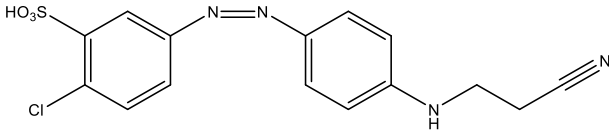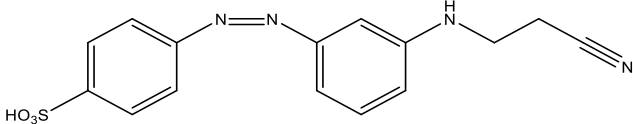
Acid	Abbreviated Name	Molecular Structure
Dye 1	CLDIA	
Dye 2	4CNDIA	

Table 2. 7 Group 7: Selection of three acids common to enantiopure methylephedrine (MEPD) and enantiopure ephedrine (EPD).
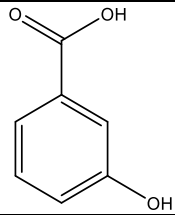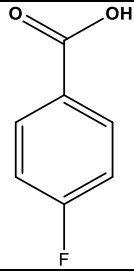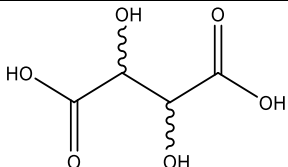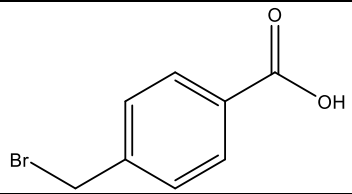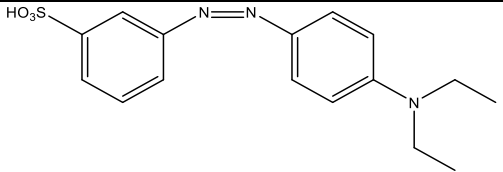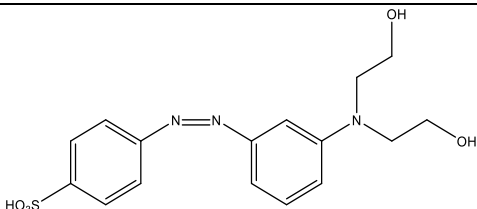
Acid	Abbreviated Name	Molecular Structure
3-hydroxybenzoic acid	3HB	
4-fuorobenzoic acid	4FB	
DL-tartaric acid	RTAR	

Table 2. 8 Group 8: Selection of four acids used only in tyramine (TYR) experiments.

Acid	Abbreviated Name	Molecular Structure
α-Bromo-p-toluic acid	BRTOL	
Dye D	DYED	
Dye 3	HEDIA	

| Mercaptosuccinic acid | MERCA | |

Table 2. 9 Group 9: Selection of two acids used only in enantiopure methylephedrine (MEPD) experiments.
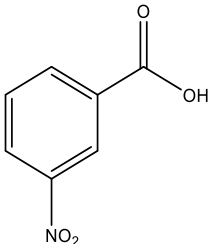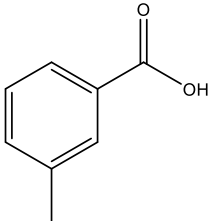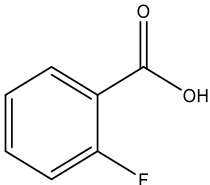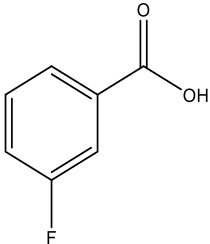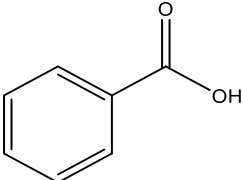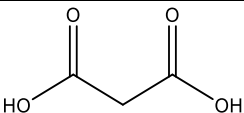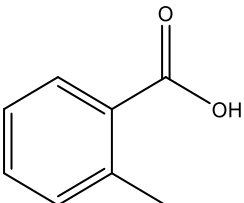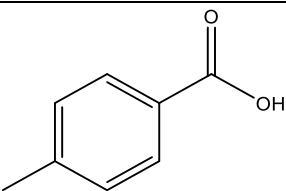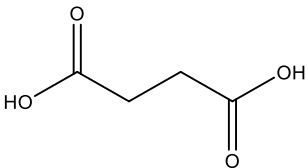
Acid	Abbreviated Name	Molecular Structure
3-nitrobenzoic acid	3NB	
m-toluic acid	MTOL	

Table 2. 10 Group 10: Selection of seven acids used only in enantiopure (EPD) ephedrine experiments.

Acid	Abbreviated Name	Molecular Structure
2-fuorobenzoic acid	2FB	
3-fuorobenzoic acid	3FB	
Benzoic acid	BZ	

Malonic acid	MALON	
o-toluic acid	OTOL	
p-toluic acid	PTOL	
Succinic acid	SUC	

2.3. PREPARATION OF REACTANTS

2.3.1. PREPARATION OF (+/-)METHYLEPHEDRINE

Racemic (+/-)methylephedrine was prepared by mixing and grinding a 50:50 proportion of (1R,2S)-(−)-N-methylephedrine and (1S,2R)-(+)-N-methylephedrine. The final product was stored in the fridge.

2.3.2. PREPARATION OF STOCK SOLUTION

The sodium hydroxide stock solution was prepared by dissolution of 1.04 g of sodium hydroxide pellets in 0.05 dm³ of distilled water. The final concentration of the solution was 0.52 M.

2.4. SYNTHESIS METHODS AND CRYSTALLISATION

2.4.1. SALT FORMS WITH STOICHIOMETRY 1:1

All the salt form syntheses designed to result in a salt stoichiometry of 1:1 for cation:anion typically involved adding a slight molar excess of the acid in an aqueous solution to a partially dissolved aqueous slurry of the base. Scale was typically 1.12 mmol of methylephedrine, 1.21 mmol of ephedrine and 1.46 mmol of tyramine (approximate 0.20 g of the base). The base and the acid were both dissolved in approximately 5 cm³ of deionised water. The resulting solution was stirred at 50 °C for 30 minutes and filtered. The solution was then put into a test tube and left to slowly evaporate and to cool to room temperature. Where no precipitate appeared after 14 days, the solution was transferred to watch glasses to speed the rate of evaporation. After crystal formation, the solution was filtered, and the crystals stored in the fridge. This method was designed to give quality single crystal products and not to maximise yield, which was not recorded. The results for all the synthesis attempts can be observed in Table 2.11 for tyrammonium salt forms, Table 2.12 for enantiopure methylephedrinium salt forms, Table 2.13 for racemic methylephedrinium salt forms and Table 2.14 for enantiopure ephedrinium salt forms.

Table 2. 11. Synthesis results for tyrammonium (TYR) salt forms

Counterion	Quantity (in g)		Quantity (in mmol)		Outcome
	Base	Acid	Base	Acid	
25HB	0.210	0.290	1.53	1.88	crystals of free acid
2HB	0.199	0.230	1.45	1.67	crystals of TYR 2HB
2HP3C	0.199	0.250	1.45	1.80	crystals of free acid
2HPA	0.216	0.250	1.57	1.64	crystals of TYR 2HPA
2KG	0.200	0.250	1.46	1.71	crystals of free acid
2NAPH	0.200	0.280	1.46	1.63	crystals of TYR 2NAPH.3H2O
2PG	0.200	0.300	1.46	1.98	crystals of free acid
3AB	0.200	0.490	1.46	3.57	poor crystal

3CMD	0.200	0.300	1.46	1.61	oil
4ABUT	0.196	0.190	1.43	1.84	oil
4APA	0.205	0.250	1.49	1.65	degradation of acid
4CBS	0.218	0.640	1.59	1.75	crystals of TYR 4CBS
4CNDIA	0.039	0.110	0.29	0.33	crystals of TYR 4CNDIA
4HPA	0.220	0.280	1.60	1.84	crystals of TYR 4HPA
5AMS	0.204	0.280	1.49	1.83	crystals of free acid
5C2NB	0.199	0.340	1.45	1.69	crystals of TYR 5C2NB
66TN	0.199	0.510	1.45	1.65	crystals of free acid
A2S	0.195	0.300	1.42	1.73	degradation of acid
ACLBS	0.191	0.360	1.40	1.73	crystals of TYR ACLBS
ACLMBS	0.202	0.360	1.48	1.62	crystals of TYR ACLMBS
ALG	0.200	0.220	1.46	1.83	oil
ANBS	0.210	0.460	1.53	2.11	crystals of free acid
ANT	0.191	0.230	1.39	1.68	degradation of acid
AS	0.194	0.330	1.42	1.83	crystal of free acid
ASB	0.214	0.370	1.56	1.70	crystals of TYR ASB
BRTOL	0.200	0.400	1.46	1.86	oil
CAMPH	0.210	0.400	1.53	1.72	poor crystal
CAP	0.230	0.300	1.68	1.74	crystals of TYR CAP
CIT	0.196	0.330	1.43	1.72	crystals of free acid
CLDIA	0.196	0.620	1.43	1.70	poor crystal
DLMAL	0.200	0.250	1.46	1.86	crystals of TYR DLMAL
DTAR	0.200	0.230	1.46	1.53	poor crystal
DYEA	0.097	0.272	0.71	0.80	poor crystal
DYEB	0.109	0.354	0.80	0.86	poor crystal
DYEC	0.100	0.297	0.73	0.81	crystals of TYR DYEC
DYED	0.035	0.070	0.25	0.21	poor crystal
DYEE	0.102	0.262	0.74	0.79	crystals of TYR DYEE
FUM	0.200	0.210	1.46	1.81	crystals of TYR FUMS
GLU	0.207	0.270	1.51	1.84	crystals of free acid
GLUCON	0.210	0.530	1.53	2.70	crystals of TYR GLUCON
GLUCUR	0.210	0.340	1.53	1.75	amorphous solid
H2NAPH	0.200	0.360	1.46	1.91	crystals of TYR H2NAPH
HEDIA	0.029	0.110	0.21	0.30	amorphous solid
HIP	0.210	0.300	1.53	1.67	crystals of TYR HIP
IN	0.220	0.200	1.60	1.62	amorphous solid
IPH	0.200	0.280	1.46	1.69	crystals of TYR IPH
LACB	0.200	0.620	1.46	1.73	amorphous solid
MERCA	0.200	0.400	1.46	2.66	degradation of acid
MMBS	0.210	0.360	1.53	1.78	crystals of TYR MMBS

MUC	0.200	0.340	1.46	1.62	crystals of TYR MUC
N2S	0.200	0.340	1.46	1.63	crystals of TYR N2S
OXA	0.196	0.250	1.43	1.98	crystals of TYR OXA
PAAB	0.197	0.300	1.44	1.67	crystals of TYR PAAB
PAL	0.220	0.500	1.60	1.95	degradation of acid
PAM	0.200	0.680	1.46	1.75	oil
PH	0.219	0.310	1.60	1.87	crystals of TYR PH
PIM	0.220	0.290	1.60	1.81	crystals of free acid
PTS	0.210	0.330	1.53	1.92	crystals of TYR PTS
RMD	0.190	0.250	1.39	1.64	oil
TCIN	0.270	0.300	1.97	2.02	crystals of TYR TCIN.2H2O
TIOSA	0.180	0.250	1.31	1.62	crystals of TYR TIOSA
UR	0.200	0.270	1.46	1.61	crystals of TYR UR

Table 2. 12 Synthesis results for enantiopure methylephedrinium (MEPD) salt forms.

Counterion	Quantity (in g)		Quantity (in mmol)		Outcome
	Base	Acid	Base	Acid	
1NAPH	0.210	0.220	1.17	1.28	crystals of RMEPD 1NAPH
25HB	0.200	0.200	1.12	1.30	oil
2HB	0.210	0.190	1.17	1.38	crystals of MEPD 2HB (VAVHUI)
2HP3C	0.190	0.180	1.06	1.29	poor crystal
2HPA	0.210	0.220	1.17	1.45	crystals of MEPD 2HPA
2KG	0.200	0.190	1.12	1.30	oil
2NAPH	0.210	0.220	1.17	1.28	crystals of MEPD 2NAPH
2PG	0.210	0.150	1.17	1.24	degradation of acid
3CMD	0.190	0.220	1.06	1.18	oil
3CNDIA	0.040	0.090	0.22	0.27	amorphous solid
3HB	0.200	0.210	1.12	1.52	crystals of free acid
3MS	0.200	0.190	1.12	1.25	crystals of free acid
3NB	0.220	0.270	1.23	1.62	crystals of free acid
4ABUT	0.210	0.280	1.17	2.72	poor crystal
4APA	0.200	0.190	1.12	1.26	poor crystal
4CBS	0.200	0.450	1.12	1.23	crystals of MEPD 4CBS
4CNDia	0.040	0.080	0.22	0.24	crystals of MEPD 4CNDIA
4FB	0.200	0.180	1.12	1.28	crystals of MEPD 4FB
4HPA	0.190	0.210	1.06	1.38	crystals of MEPD 4HPA
4NPA	0.180	0.230	1.00	1.27	crystals of MEPD 4NPA
5AMS	0.200	0.190	1.12	1.24	degradation of acid
5C2NB	0.200	0.250	1.12	1.24	oil

66TN	0.200	0.410	1.12	1.33	oil
A2S	0.210	0.230	1.17	1.33	oil
AA	0.200	0.240	1.12	1.34	oil
ACLBS	0.200	0.280	1.12	1.35	amorphous solid
ACLMBS	0.200	0.300	1.12	1.35	crystals of MEPD ACLMBS
ALG	0.200	0.170	1.12	1.42	oil
ANBS	0.190	0.290	1.06	1.33	amorphous solid
ANT	0.200	0.190	1.12	1.39	degradation of acid
AS	0.200	0.270	1.12	1.50	crystals of free acid
ASB	0.230	0.300	1.28	1.38	oil
CAMPH	0.180	0.320	1.00	1.38	crystals of MEPD CAMPH
CAP	0.200	0.210	1.12	1.22	poor crystal
CIT	0.200	0.240	1.12	1.25	crystals of free acid
CLDIA	0.230	0.460	1.28	1.26	amorphous solid
DLMAL	0.210	0.210	1.17	1.57	oil
DTAR	0.190	0.190	1.06	1.27	oil
DYEA	0.108	0.216	0.60	0.64	poor crystal
DYEB	0.102	0.501	0.57	1.22	poor crystal
DYEC	0.107	0.227	0.60	0.62	poor crystal
DYEE	0.105	0.201	0.59	0.61	poor crystal
FUM	0.200	0.150	1.12	1.29	crystals of MEPD FUM
GLU	0.190	0.190	1.06	1.29	crystals of free acid
GLUCON	0.200	0.610	1.12	3.11	oil
GLUCUR	0.200	0.250	1.12	1.29	oil
H2NAPH	0.210	0.290	1.17	1.54	crystals of MEPD H2NAPH
HIP	0.200	0.240	1.12	1.34	crystals of free acid
IN	0.220	0.230	1.23	1.87	crystals of free acid
IPH	0.200	0.210	1.12	1.26	crystals of free acid
LACB	0.200	0.470	1.12	1.31	amorphous solid
LMAL	0.200	0.210	1.12	1.57	oil
MMBS	0.210	0.280	1.17	1.38	crystals of MEPD MMBS
MTOL	0.210	0.210	1.17	1.54	crystals of free acid
Muc	0.210	0.280	1.17	1.33	crystals of MEPD MUC
N2S	0.200	0.200	1.12	0.96	crystals of MEPD N2S
OXA	0.190	0.180	1.06	1.43	crystals of MEPD OXA
PA	0.200	0.170	1.12	1.25	crystals of MEPD PA
PAAB	0.200	0.250	1.12	1.28	crystals of free acid
PAL	0.190	0.340	1.06	1.33	degradation of acid
PAM	0.220	0.210	1.23	0.54	oil
PH	0.220	0.210	1.23	1.26	crystals of free acid
PICO	0.190	0.170	1.06	1.38	oil

PIM	0.200	0.220	1.12	1.37	poor crystal
PTS	0.190	0.200	1.06	1.16	crystals of free acid
RMD	0.220	0.200	1.23	1.31	crystals of RMEPD RMD
RTAR	0.200	0.190	1.12	1.27	oil
SULFA	0.210	0.220	1.17	1.27	oil
TCIN	0.190	0.190	1.06	1.28	crystals of free acid
TIOSA	0.200	0.220	1.12	1.43	oil
UR	0.190	0.230	1.06	1.37	oil

Table 2. 13 Synthesis results for racemic methylephedrinium (RMEPD) salt forms.

Counterion	Quantity (in g)		Quantity (in mmol)		Outcome
	Base	**Acid**	**Base**	**Acid**	
1NAPH	0.200	0.210	1.12	1.22	crystals of free acid
25HB	0.200	0.220	1.12	1.43	oil
2HB	0.210	0.200	1.17	1.45	crystals of RMEPD 2HB
2HP3C	0.200	0.180	1.12	1.29	oil
2HPA	0.180	0.150	1.00	0.99	crystals of free acid
2KG	0.200	0.200	1.12	1.37	oil
2NAPH	0.200	0.220	1.12	1.28	crystals of MEPD 2NAPH
2PG	0.210	0.160	1.17	1.32	poor crystal
3AB	0.200	0.200	1.12	1.46	crystals of RMEPD 3AB
3CMD	0.190	0.250	1.06	1.34	oil
3MS	0.190	0.210	1.06	1.38	oil
4ABUT	0.200	0.130	1.12	1.26	amorphous solid
4APA	0.200	0.200	1.12	1.32	oil
4CBS	0.200	0.470	1.12	1.29	crystals of RMEPD 4CBS
4HPA	0.200	0.220	1.12	1.45	crystals of MEPD 4HPA
4NPA	0.190	0.240	1.06	1.32	crystals of RMEPD 4NPA
5AMS	0.200	0.240	1.12	1.57	crystals of free acid
5C2NB	0.200	0.270	1.12	1.34	crystals of RMEPD 5C2NB
66TN	0.190	0.410	1.06	1.33	oil
A2S	0.200	0.220	1.12	1.27	oil
AA	0.190	0.250	1.06	1.40	crystals of RMEPD AA
ACLBS	0.190	0.270	1.06	1.30	amorphous solid
ACLMBS	0.200	0.280	1.12	1.26	amorphous solid
ALG	0.190	0.180	1.06	1.50	oil
ANBS	0.200	0.280	1.12	1.28	poor crystal
ANT	0.200	0.200	1.12	1.46	oil
AS	0.200	0.230	1.12	1.28	oil

ASB	0.220	0.210	1.23	0.97	amorphous solid
CAMPH	0.210	0.310	1.17	1.33	crystals of MEPD CAMPH
CAP	0.210	0.200	1.17	1.16	crystals of free acid
CIT	0.210	0.270	1.17	1.41	crystals of free acid
DLMAL	0.200	0.200	1.12	1.49	oil
DYEA	0.100	0.202	0.56	0.60	poor crystal
DYEB	0.111	0.231	0.62	0.56	poor crystal
DYEC	0.093	0.237	0.52	0.65	crystals of RMEPD DYEC
DYEE	0.111	0.197	0.62	0.60	poor crystal
FUM	0.190	0.270	1.06	2.33	crystals of RMEPD FUM
GLU	0.220	0.190	1.23	1.29	oil
GLUCON	0.200	0.510	1.12	2.60	amorphous solid
GLUCUR	0.200	0.250	1.12	1.29	amorphous solid
H2NAPH	0.200	0.240	1.12	1.28	crystals of MEPD H2NAPH
HIP	0.200	0.240	1.12	1.34	oil
IN	0.200	0.230	1.12	1.87	amorphous solid
IPH	0.200	0.240	1.12	1.44	crystals of free acid
LACB	0.200	0.470	1.12	1.31	oil
LMAL	0.200	0.220	1.12	1.64	crystals of free acid
LTAR	0.200	0.190	1.12	1.27	crystals of free acid
MMBS	0.190	0.280	1.06	1.38	amorphous solid
MUC	0.190	0.280	1.06	1.33	crystals of RMEPD MUC
N2S	0.200	0.350	1.12	1.68	crystals of MEPD N2S
OXA	0.200	0.232	1.12	1.84	crystals of free acid
PA	0.200	0.170	1.12	1.25	oil
PAAB	0.210	0.230	1.17	1.28	crystals of RMEPD PAAB
PAL	0.190	0.330	1.06	1.29	crystals of free acid
PAM	0.210	0.510	1.17	1.31	oil
PH	0.190	0.270	1.06	1.63	crystals of free acid
PICO	0.200	0.200	1.12	1.62	oil
PIM	0.210	0.230	1.17	1.44	oil
PTS	0.200	0.250	1.12	1.45	crystals of MEPD PTS
SULFA	0.210	0.290	1.17	1.67	oil
TCIN	0.200	0.270	1.12	1.82	amorphous solid
TIOSA	0.200	0.200	1.12	1.30	poor crystal
UR	0.200	0.220	1.12	1.31	crystals of free acid

Table 2. 14 Synthesis results for enantiopure ephedrinium (EPD) salt forms.

Counterion	Quantity (in g)		Quantity (in mmol)		Outcome
	Base	**Acid**	**Base**	**Acid**	
1NAPH	0.190	0.230	1.15	1.34	crystals of free acid
25HB	0.207	0.240	1.16	1.56	crystals of free acid
2FB	0.194	0.240	1.18	1.71	oil
2HP3C	0.229	0.220	1.39	1.27	poor crystal
2HPA	0.223	0.260	1.35	1.35	crystals of free acid
2KG	0.190	0.210	1.06	1.44	poor crystal
2NAPH	0.224	0.254	1.36	1.47	crystals of free acid
3AB	0.211	0.200	1.28	1.49	poor crystal
3AB	0.201	0.250	1.22	1.82	amorphous solid
3CMD	0.207	0.259	1.25	1.89	poor crystal
3FB	0.216	0.230	1.31	1.64	poor crystal
3HB	0.216	0.240	1.31	1.74	oil
3MS	0.190	0.200	1.15	1.31	oil
4ABUT	0.181	0.147	1.09	1.43	oil
4APA	0.206	0.200	1.24	1.32	crystal of EPD 4APA
4CBS	0.219	0.499	1.33	1.37	crystal of EPD 4CBS
4FB	0.192	0.290	1.16	2.07	oil
4HPA	0.211	0.248	1.27	1.33	crystal of EPD 4HPA
4NPA	0.191	0.250	1.16	1.38	oil
5C2NB	0.201	0.290	1.22	1.92	crystal of EPD 5C2NB
66TN	0.215	0.420	1.30	2.85	crystals of free acid
AA	0.196	0.270	1.19	1.51	crystal of EPD AA
ALG	0.203	0.300	1.13	2.50	crystals of free acid
ANBS	0.199	0.320	1.21	2.13	oil
BZ	0.188	0.240	1.14	1.97	oil
CAMPH	0.215	0.320	1.30	2.00	oil
CAP	0.215	0.250	1.30	1.50	crystals of free acid
DLMAL	0.201	0.190	1.22	0.94	oil
DTAR	0.185	0.240	1.12	1.57	amorphous solid
DYEA	0.107	0.219	0.60	0.64	poor crystal
DYEB	0.097	0.258	0.54	0.63	poor crystal
DYEC	0.092	0.020	0.51	0.05	poor crystal
DYEE	0.104	0.231	0.58	0.70	poor crystal
FUM	0.221	0.190	1.34	1.64	poor crystal
GLUCON	0.197	0.450	1.10	2.29	oil
GLUCUR	0.202	0.270	1.13	1.39	oil
H2NAPH	0.201	0.270	1.12	1.43	poor crystal
HIP	0.202	0.250	1.13	1.40	oil

IPH	0.196	0.230	1.19	1.37	amorphous solid
LACB	0.216	0.510	1.21	1.42	poor crystal
LMAL	0.194	0.240	1.18	1.79	crystals of free acid
MALON	0.226	0.180	1.37	1.73	poor crystal
MMBS	0.181	0.300	1.10	2.02	crystal of EPD MMBS
MUC	0.210	0.300	1.17	1.43	oil
N2S	0.199	0.300	1.11	1.44	crystal of EPD N2S
OTOL	0.209	0.260	1.27	1.91	oil
OXA	0.218	0.260	1.32	2.06	poor crystal
PA	0.208	0.200	1.26	1.47	oil
PAAB	0.186	0.240	1.13	1.58	crystals of free acid
PAM	0.200	0.590	1.12	1.52	poor crystal
PH	0.205	0.273	1.24	1.52	oil
PICO	0.225	0.180	1.36	1.46	crystals of free acid
PIM	0.199	0.260	1.20	1.71	oil
PTOL	0.195	0.220	1.18	1.62	poor crystal
PTS	0.200	0.250	1.11	1.45	poor crystal
RMAL	0.196	0.240	1.19	1.79	crystals of free acid
RMD	0.199	0.210	1.20	0.82	crystal of EPD LMD
RTAR	0.189	0.250	1.14	1.67	crystals of free acid
2HB	0.187	0.203	1.13	1.47	poor crystal
SUC	0.192	0.210	1.16	1.78	oil
SULFA	0.192	0.240	1.16	1.39	amorphous solid
TCIN	0.187	0.230	1.13	1.87	poor crystal
TIOSA	0.201	0.243	1.21	1.57	oil
UR	0.209	0.261	1.26	1.88	poor crystal

2.4.2. LARGER SCALE SALT FORMATION EXPERIMENTS THAT GAVE DIFFERENT STRUCTURES

There were 52 salt forms that were also synthesised on a larger scale, with a slight excess of base, but with an otherwise similar route of synthesis as described in Chapter 2.4.1. Of those, only two were found to have different crystal structures when compared to the first synthesis attempt. Both were salt forms of tyramine that produced anhydrous crystals (TYR2NAPH and TYRTCIN) instead of the hydrated forms

previously shown. Details of the quantity of reactants used in these syntheses can be observed in Table 2.15.

Table 2. 15 Synthesis results for new tyramine salts formed in other synthesis.

	Counterion	Quantity (in g)		Quantity (in mmol)		Outcome
		Base	**Acid**	**Base**	**Acid**	
TYR	2NAPH	5.260	6.230	38.34	36.18	crystals of TYR 2NAPH
	TCIN	1.080	1.080	7.87	7.29	crystals of TYR TCIN

2.4.3. SALT FORMS WITH STOICHIOMETRY 2:1

Of the eighty-two acids used in the 1:1 stoichiometry synthesis, fourteen acids had more than one acidic site. For these acids attempts were also made to synthetize organic salts with stochiometric proportion of 2:1 of cations to dicarboxylate anions / sulfonate-carboxylate anions. The acids were: Oxalic acid (OXA), citric acid (CIT), glutamic acid (GLU), L-malic acid (LMAL), R-tartaric acid (RTAR), 6,6′-dithiodinicotinic acid (66TN), phthalic acid (PH), uric acid (UR), fumaric acid (FUM), L-tartaric acid (LTAR), D-tartaric acid (DTAR), DL-malic acid (DLMAL), pimelic acid (PIM) and isophthalic acid (IPH).

The synthesis was carried out by adding a slurry of 1.12 mmol of methylephedrine, 1.21 mmol of ephedrine or 1.46 mmol of tyramine (approximate 0.20 g of the base) to a 15% molar excess of acid. Both acid and base were in approximately 5 cm³ of deionised water. The resulting solutions were stirred at 50 °C for 30 minutes and filtered. To the resultant solution was added an approximate 1 mmol of a metal alkali hydroxide pellets or the previously prepared aqueous solution of sodium hydroxide (Chapter 2.3.2). In all the cases, the resulting solution was put into a test tube and left to slowly cool to room temperature and to evaporate. Where no precipitate appeared after 14 days, the solutions were transferred to watch glasses to speed the rate of evaporation. After crystal formation, the solution was filtered, and the crystals stored

in the fridge. The general route of synthesis used in all experiments is summarized in Figure 2.3.
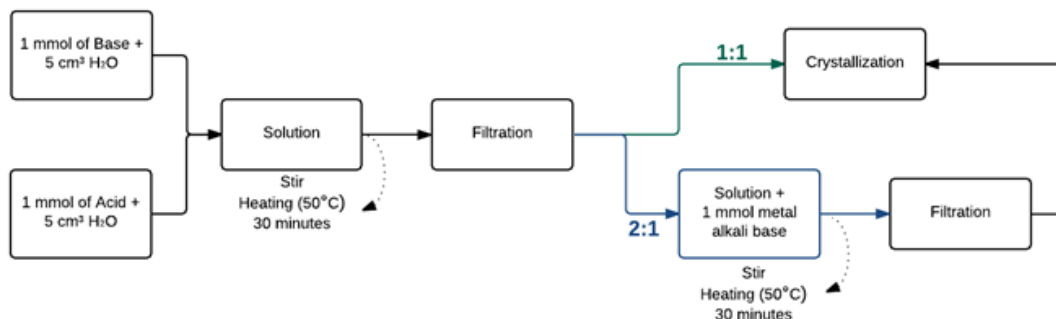
Figure 2. 3 General method used in the synthesis of the salt forms.

Attempts of synthesis with stoichiometry 2:1 were made for all the bases: tyramine, enantiopure methylephedrine, racemic methylephedrine and enantiopure ephedrine. Using this method, crystals of nine salt forms of tyramine and two salt forms of ephedrine were formed with different compositions to those previously described in Chapter 2.4.1. Details of these compounds can be observed in Table 2.16. Compound labels with a "2" after the base label gave the desired 2:1 products.

Table 2. 16 Results for synthesis with stoichiometry 2:1 of API and counterion.

| Counterion | | Quantity | | | Outcome |
		Base	Acid	NaOH	
TYR	DTAR	0.210 g	0.260 g	3.20 mL	crystal of TYR(H).TYR.CL.H2O
	LMAL	0.220 g	0.210 g	3.00 mL	crystal of TYR.H2O
	LTAR	0.210 g	0.280 g	3.10 mL	crystal of TYR LTAR.NA.2H2O
	MALON	0.200 g	0.350 g	3.20 mL	crystal of TYR 2MALON
	OXA	0.230 g	0.220 g	0.090 g	crystal of TYR 2OXA
	PH	0.210 g	0.270 g	3.00 mL	crystal of TYR 2PH
	RMAL	0.200 g	0.230 g	3.40 mL	crystal of TYR 2RMAL
	RTAR	0.200 g	0.400 g	3.20 mL	crystal of TYR 2RTAR.wc
	RTAR	0.210 g	0.390 g	0.060 g	crystal of TYR 2RTAR.4H2O
EPD	DTAR	0.203 g	0.240 g	3.00 mL	crystal of EPD 2TAR.H2O
	MUC	0.204 g	0.330 g	3.00 mL	crystal of EPD 2MUC

2.5. SINGLE CRYSTAL X-RAY DIFFRACTION

2.5.1. DATA COLLECTION AND REFINEMENT

The crystals produced were measured at the University of Strathclyde using Gemini or Xcalibur Oxford Diffraction instruments, typically at 123K, with Mo Kα (λ = 0.7107 Å) or Cu Kα (λ = 1.5418 Å) radiation. Measurements of some poor-quality or weakly diffracting crystals were performed by the National Crystallography Service (NCS) at University of Southampton, at low temperature, using a Bruker-Nonius CCD diffractometer with radiation of wavelength Mo Kα (λ = 0.7107 Å). The data collected at Strathclyde was processed with the software CrysAlis Pro [3]. The atoms, except hydrogen, had atomic coordinates and anisotropic thermal parameters refined to convergence using full-matrix least-square methods on F^2. Programs used for structure solution were SHELXS [4] or SIR92 [5]. Refinement used SHELXL-2014 [4]. All were implemented within the WinGX suite [6]. Most H atoms bound to C were placed in geometric positions and refined with riding modes. Where possible H atoms bound to

O or N were found by difference syntheses and refined with isotropic displacement parameters. Where this refinement was not possible, they were added in geometrically sensible positions and refined in riding modes. Brief details of symmetry and unit cells are given in Tables 2.17 to 2.20, with full crystallographic data in .cif format available in the electronic Appendix in the folder CIF.

2.5.2. SINGLE CRYSTAL X-RAY DIFFRACTION RESULTS FOR ALL SALT FORMS

This work generated seventy-five new crystal structures of salt forms of tyramine, enantiopure methylephedrine, racemic methylephedrine and ephedrine. Of the thirty-eight salt forms of tyramine (Table 2.17), eighteen were hydrated forms, five were disordered structures, two disordered structures contained a water chain, one was a double salt of tyramine and sodium with l-tartarate as a counter ion and one was a cocrystal/salt form of tyramine chloride. Of the new seventeen salt forms of enantiopure methylephedrine that were elucidated (Table 2.18) there were three hydrated salts and two disordered structures. Of the twelve new salt forms of racemic methylephedrine described (Table 2.19) there were three normal and one disordered hydrate, and another three disordered anhydrous salt forms. Finally, this work presents eight new structures of enantiopure ephedrine (Table 2.20), all anhydrous salts forms. There is also the presence of one disordered structure of enantiopure ephedrine and naphthalene-2-sulfonate (EPD N2S).

In addition, several new crystal structures are presented and used in this work that involved the work of other students of the group. These are listed in Table 2.21. Most were samples found to have phase changed over time, since their initial synthesis and characterisation by Catriona Morrison for her PhD thesis [7]. An exception is sample D (TYR HBR.TYR) which was synthesised and solved by the final year student Charlie Logan for his MChem thesis [8].

Table 2. 17 Crystal lattice parameters and space group for all new tyramine salt structures.

	Sample	Space Group	Lattice parameters							Notes
			a (Å)	b (Å)	c (Å)	α (°)	β (°)	γ (°)	V (Å³)	
1	TYR 2DLMAL.H2O	P 2$_1$/c	11.853	7.860	11.937	90	100.61	90	1093.0	disorder in anion
2	TYR 2HB	P b c a	13.664	8.288	24.799	90	90	90	2808.2	
3	TYR 2HPA	P 2$_1$ 2$_1$ 2$_1$	5.896	7.796	30.222	90	90	90	1389.2	
4	TYR 2MALON.H2O [α]	P -1	8.019	11.943	12.572	63.65	72.375	85.66	1025.92	
5	TYR 2NAPH [α]	P 2$_1$/c	25.552	10.690	12.449	90	102.82	90	3315.6	
6	TYR 2NAPH.3H2O	P n n a	8.070	42.499	11.071	90	90	90	3796.9	
7	TYR 2OXA	P 2$_1$/c	7.648	11.247	42.319	90	93.63	90	3633.0	
8	TYR 2PH [α]	P 2$_1$/c	7.928	22.443	12.790	90	93.15	90	2272.3	
9	TYR 4CBS	P b c a	19.773	19.782	7.588	90	90	90	2967.9	disorder in anion
10	TYR 4HPA.H2O	P 2$_1$	8.959	6.116	14.684	90	104.48	90	779.1	disorder in cation
11	TYR 5C2NB [α]	P n a 2$_1$	25.476	4.939	25.414	90	90	90	3197.8	
12	TYR ACLBS	P 2$_1$/n	10.534	9.079	16.763	90	105.48	90	1545.1	
13	TYR ACLMBS.H2O	P 2$_1$/a	11.468	8.660	18.336	90	100.98	90	1787.7	
14	TYR ASB.3H2O [α]	P -1	8.774	11.201	18.355	93.41	100.47	90.60	1770.3	
15	TYR CAP	P 2/c	30.200	5.756	21.651	90	99.16	90	3715.8	
16	TYR DLMAL.H2O *	P -1	9.202	11.055	13.550	87.42	87.83	89.80	1376.0	disorder in cation
17	TYR DYEB.H2O	P -1	9.049	9.084	17.100	102.58	104.98	95.18	1309.1	
18	TYR DYEC.2H2O	P -1	8.302	9.005	18.313	96.93	101.18	97.58	1316.2	disorder in water
19	TYR DYEE.H2O	P b c a	8.171	10.747	52.750	90	90	90	4632.1	

20	TYR GLUCON	P 2_1 2_1 2_1	5.097	8.811	33.128	90	90	90	1487.8	
21	TYR H2NAPH [a]	P 2_1	10.120	8.386	18.985	90	104.03	90	1563.2	
22	TYR HIP [a]	P -1	9.933	12.019	13.878	97.02	100.01	90.29	1618.8	
23	TYR IPH	P c	7.314	8.921	11.442	90	102.08	90	730.0	
24	TYR LTAR.NA.2H2O	P 2_1	8.117	6.191	15.872	90	93.01	90	796.4	
25	TYR MMBS.H2O	P 2_1/c	9.808	8.597	20.863	90	95.96	90	1749.6	
26	TYR MUC	P 2_1/c	13.303	7.261	13.365	90	117.13	90	1148.9	
27	TYR N2S.H2O	P 2_1/n	11.036	7.721	20.610	90	94.78	90	1750.2	
28	TYR OXA	P 2_1	5.640	7.549	12.364	90	90.78	90	526.3	
29	TYR PAAB	P b c a	7.361	17.597	23.804	90	90	90	3083.3	
30	TYR PH	P 2_1 2_1 2_1	6.747	12.283	17.244	90	90	90	1429.1	
31	TYR PTS.H2O	P b c a	11.305	7.851	36.450	90	90	90	3234.8	
32	TYR RTAR.4H2O [b]	P n 2_1 a	16.449	10.113	26.596	90	90	90	4424.4	
33	TYR RTAR.wc [b]	P -1	10.046	13.580	18.390	74.60	83.90	82.88	2393.1	disorder in cation
34	TYR TCIN	P 2_1	11.102	5.876	11.836	90	100.50	90	759.2	
35	TYR TCIN.H2O *	P 2_1/n	14.710	6.112	26.023	90	98.69	90	2312.9	
36	TYR TIOSA.wc	P 4_2/n	26.686	26.686	8.932	90	90	90	6360.7	disorder in cation
37	TYR.TYR.CL.H2O	P c a 2_1	10.999	18.981	8.033	90	90	90	1677.0	
38	TYR UR.3H2O [a]	P -1	10.770	11.272	14.117	79.14	73.88	63.96	1474.8	

Table 2. 18 Crystal lattice parameters and space group for all enantiopure methylephedrine salts formed.

	Sample	Space Group	Lattice parameters							Notes
			a (Å)	b (Å)	c (Å)	α (°)	β (°)	γ (°)	V (Å^3)	
1	MEPD 2HB	P 2$_1$ 2$_1$ 2$_1$	9.443	11.644	15.068	90	90	90	1656.8	(VAVHUI)
2	MEPD 2HPA	P 2$_1$ 2$_1$ 2$_1$	7.519	9.717	24.033	90	90	90	1755.9	
3	MEPD 2NAPH	P 2$_1$	5.798	15.310	10.572	90	100.03	90	924.1	
4	MEPD 4CBS	P 2$_1$ 2$_1$ 2$_1$	8.199	10.245	20.368	90	90	90	1710.8	
5	MEPD 4CNDIA [a]	P 2$_1$	11.908	7.522	28.844	90	101.57	90	2531.3	
6	MEPD 4FB	P 2$_1$	5.706	14.817	9.798	90	96.05	90	823.8	
7	MEPD 4HPA	P 2$_1$ 2$_1$ 2$_1$	5.937	14.734	19.765	90	90	90	1728.7	
8	MEPD 4NPA [a]	P 1	5.984	12.508	12.523	85.07	77.64	89.49	912.2	
9	MEPD ACLMBS.2H2O [a]	P 2$_1$	11.067	10.501	18.847	90	104.45	90	2121.0	
10	MEPD CAMPH	P 2$_1$	7.500	10.970	13.258	90	101.05	90	1070.7	
11	MEPD FUM [a]	P 1	5.942	9.991	12.880	87.709	88.47	89.052	763.6	disorder in anion
12	MEPD H2NAPH	P 2$_1$	6.097	14.264	11.152	90	102.36	90	947.5	
13	MEPD MMBS	P 2$_1$	10.385	7.909	12.998	90	107.42	90	1018.7	
14	MEPD MUC.2H2O [a]	C 2	26.524	5.918	19.172	90	90.72	90	3008.9	
15	MEPD N2S.3H2O [a]	P 2$_1$ 2$_1$ 2$_1$	6.045	20.900	32.402	90	90	90	4093.4	disorder in water
16	MEPD OXA	P 2 2$_1$ 2$_1$	5.712	8.240	28.706	90	90	90	1351.0	
17	MEPD PA	P 2$_1$ 2$_1$ 2$_1$	7.498	9.936	23.009	90	90	90	1714.1	
18	MEPD PTS	P 2$_1$ 2$_1$ 2$_1$	7.076	11.081	22.744	90	90	90	1783.2	

Table 2. 19 Crystal lattice parameters and space group for all racemic methylephedrine salts formed.

	Sample	Space Group	Lattice parameters							Notes
			a (Å)	b (Å)	c (Å)	α (°)	β (°)	γ (°)	V (Å^3)	
1	RMEPD 1NAPH	P 2$_1$/c	23.832	8.084	9.680	90	90.09	90	1864.9	
2	RMEPD 2HB	P 2$_1$/n	9.272	11.808	15.256	90	98.77	90	1650.7	
3	RMEPD 3AB	P b c a	8.035	10.142	42.022	90	90	90	3424.5	
4	RMEPD 4CBS.H2O	P 2$_1$/c	5.943	32.653	10.133	90	105.75	90	1892.7	
5	RMEPD 4NPA *	P -1	5.906	11.776	18.819	98.97	92.22	92.51	1290.2	disorder in anion
6	RMEPD 5C2NB	P 2$_1$/c	12.512	16.230	9.495	90	107.19	90	1842.0	
7	RMEPD AA	P -1	5.971	10.139	16.160	76.24	88.97	84.80	946.4	disorder in anion
8	RMEPD DYEC.H2O	P 2$_1$/c	15.503	20.182	9.381	90	105.08	90	2834.2	
9	RMEPD FUM	P 2$_1$/c	16.069	8.033	9.808	90	92.01	90	1265.2	
10	RMEPD MUC.H2O	C 2/c	40.498	7.440	10.057	90	93.88	90	3023.3	disorder in water
11	RMEPD PAAB.H2O	P -1	6.464	9.792	16.492	97.70	96.62	104.52	989.3	
12	RMEPD RMD	P 2$_1$/c	13.065	9.547	13.901	90	91.57	90	1733.3	disorder in anion

Table 2. 20 Crystal lattice parameters and space group for all ephedrine salts formed.

	Sample	Space Group	Lattice parameters							Notes
			a (Å)	b (Å)	c (Å)	α (°)	β (°)	γ (°)	V (Å³)	
1	EPD 2MUC	P 2_1	9.638	7.630	18.954	90	103.75	90	1353.9	
2	EPD 2TAR.H2O	P 2_1	6.057	32.885	7.142	90	114.04	90	1299.1	(FIRJAU)
3	EPD 4APA	P 2_1 2_1 2_1	5.947	13.907	20.273	90	90	90	1676.8	
4	EPD 4CBS	P 2_1 2_1 2_1	5.639	7.047	42.599	90	90	90	1692.9	
5	EPD 4HPA	P 2_1 2_1 2_1	5.872	14.090	20.168	90	90	90	1668.7	
6	EPD 5C2NB	P 2_1 2_1 2_1	7.259	9.310	25.431	90	90	90	1718.5	
7	EPD AA	P 2_1 2_1 2_1	6.022	13.526	22.562	90	90	90	1837.5	
8	EPD LMD	C 2	18.005	6.497	13.753	90	92.72	90	1607.0	(DINLAN02)
9	EPD MMBS [a]	P 2_1	6.789	27.703	10.143	90	103.71	90	1853.2	
10	EPD N2S [b]	P 1	8.583	8.916	26.271	97.833	97.594	99.430	1940.0	disorder in anion

Table 2. 21 Crystal lattice parameters and space group for structures synthesise by others and solved / refined for this work. PEPD is pseudoephedrine, PEA is phenylethylamine, MPEA is methylphenylethylamine.

| | Sample | Space Group | Lattice parameters | | | | | | | Notes |
			a (Å)	b (Å)	c (Å)	α (°)	β (°)	γ (°)	V (Å^3)	
A	TYR 3HB.2	P 2$_1$ 2$_1$ 2$_1$	6.011	13.498	16.396	90	90	90	1330.3	
B	TYR 4CB.2	P 2$_1$/c	12.027	11.435	11.415	90.00	109.15	90.00	1483.1	
C	TYR FUMS.H2O	P 2$_1$/c	11.605	7.574	12.338	90	99.61	90	1069.3	
D	TYR HBR.TYR	P c a 2$_1$	18.395	10.338	8.487	90	90	90	1613.9	
F	MEPD BS.H2O	P 2$_1$ 2$_1$ 2$_1$	6.006	9.630	30.892	90	90	90	1786.8	
G	EPD SO4.H2O.2	P 2$_1$ 2$_1$ 2$_1$	5.661	12.711	18.072	90	90	90	1300.3	
E	PEPD 3NB.2	P 2$_1$ 2$_1$ 2$_1$	12.199	37.504	7.212	90	90	90	3299.3	
F	PEPD I	P 2$_1$ 2$_1$ 2$_1$	6.760	11.246	15.711	90	90	90	1194.3	
G	PEA TAR	P -1	7.322	7.807	12.602	99.04	96.79	98.52	696.2	
H	PEA ETSO3	P b c n	45.783	7.277	7.349	90	90	90	2448.3	
I	PEA MALE	P -1	5.544	9.954	12.53	111.67	93.09	98.20	631.7	
K	PEA SIF6	P 2$_1$/c	18.091	10.225	10.158	90	100.97	90	1844.7	
L	MPEA 2HB	C 2/c	16.003	7.589	24.662	90	93.733	90	2988.7	
M	MPEA 4NB	P -1	8.371	13.130	30.586	86.07	85.23	71.92	3181.5	

2.6. STRUCTURAL ANALYSIS

All structural analyses were made using Mercury CSD v4.1.0 software [9, 10] from data presented in this work or obtained from Cambridge Crystallographic Data Centre (CCDC) [11] database using the search engine ConQuest v2.0.1. Details of the methodology used in each case can be observed in the following sub-chapters.

2.6.1. TORSION ANGLE COLLECTION

Torsion angles were collected using the 'Search for any feature from a crystal structure' module on CSD-Materials tool. First, all molecules of one cation were selected from a non-disordered crystal structure. Contrains were added to the number of hydrogens and bonds, and all torsion angles from the aliphatic chain were selected in the cation molecule. All the crystal structures presented in this work, in addition to structures obtained from the ConQuest search were added and the software provided all torsion angles for selected for the cation. When more than one cation was present in the structure, torsion angles for those cations were analysed manually.

2.6.2. WATER ENVIRONMENT

Water environment in hydrates were analysed using the 'Hydrate Analyser' tool [14]. This tool helps visualise hydrogen bonding between water molecules and other molecules. The representation that will be used in this work can be observed in Table 2.22. This representation illustrates the hydrogen bonding environment of the water molecule, where the water molecule can be acting as a proton donor (D) or a proton acceptor (A). The other molecules sharing or receiving the proton are represented as Don and Acc, respectively.

Table 2. 22. Water environment according to the "Hydrate Analyser" tool, where D represents the proton donor water molecule, A represents the proton acceptor water molecule, Don is the other molecule donating a proton to the water molecule and Acc is the other molecule receiving a proton from the water molecule.

	Water Hydrogen Bonding	Representation	Molecular arrangement
1	Zero	0	
2	One_D	1(D)	
3	Two_DD	2(DD)	
4	Three_A	3(A)	
5	Four_AA	4(AA)	
6	Five_DDA	5(DDA)	
7	Six_DDAA	6(DDAA)	
8	Seven_DA	7(DA)	
9	Eight_DAA	8(DAA)	
10	Nine_DDAAA	9(DDAAA)	

2.6.3. CRYSTAL PACKING SIMILARITY

To create the tree diagrams shown in subsequent chapters, the 'Crystal Packing Similarity' tool of Mercury was used [15]. This tool compares the three-dimensional geometry of the reference molecule in the crystal structure within a range of molecules,

comparing the packing of molecules with similar geometric features. The tree diagram is created comparing different sizes of the cluster, ranging from two to fifteen molecules in the packing. For this work, default parameters were used. For all size of clusters, the analyses were made filtering the comparison that do not have all molecules in common, with distance tolerance of 20 % and angle tolerance of 20 °. The work was carried out ignoring hydrogen positions and bond types and allowing structure inversion when comparing crystals. It also ignored the smallest molecular component when comparing multi-component crystals and it was chosen to show only the highest similarity result when comparing crystals with more than one reference compound in the unit cell ($Z' > 1$).

2.7. HARDNESS AND YOUNG'S MODULUS MEASUREMENTS

Nanoindentation measurements were performed on salt forms of eight different API bases. These were phenylethylamine (PEA) and its derivatives tyramine (TYR), enantiopure and racemic methylephedrine (MEPD and RMEPD), enantiopure ephedrine (EPD), enantiopure pseudoephedrine (PEPD), 2-methylphenylethylamine (MPEA) and 2-dimethylphenylethylamine (DMPEA), as it can be observed in Figure 2.4. All syntheses of the salt forms used in nanoindentation are reported in Chapter 2.4 or performed and published by Morrison *et al.* [16 - 18]. The identity of the salt forms measured was dependant on the crystals having suitable size and morphology but included a selection of halides, carboxylates, substituted benzoates and sulfonates.
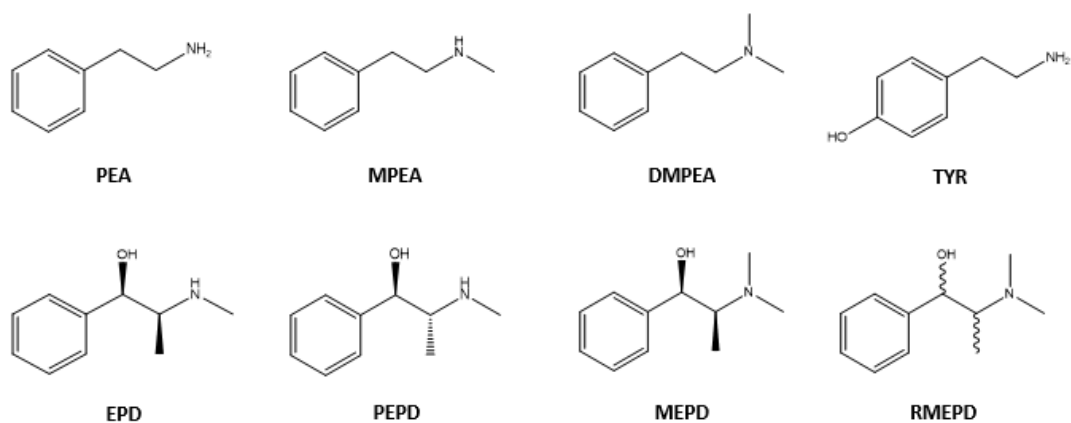
Figure 2. 4 Structure of PEA and related APIs used for nanoindentation measurements.

2.7.1. INDEXING CRYSTAL STRUCTURES

Sample crystals of all the salt forms used in the nanoindentation experiments were indexed by single crystal X-ray diffraction. In each case the data pre-experiment routine of the program CrysAliPro [19] was used. Collecting approximately 6 frames of diffraction data confirmed known unit cell parameters and allowed face indexing to be completed. At least two single crystals of each salt were indexed.

2.7.2. NANOINDENTATION USING ATOMIC FORCE MICROSCOPY

Imaging and indentation were performed on the smoothest surface of the sample at room temperature and atmosphere. As an example, the chosen surface of the crystal PEPD 4AB can be observed in Figure 2.5 where the red cross represents where the probe will engage with the surface.
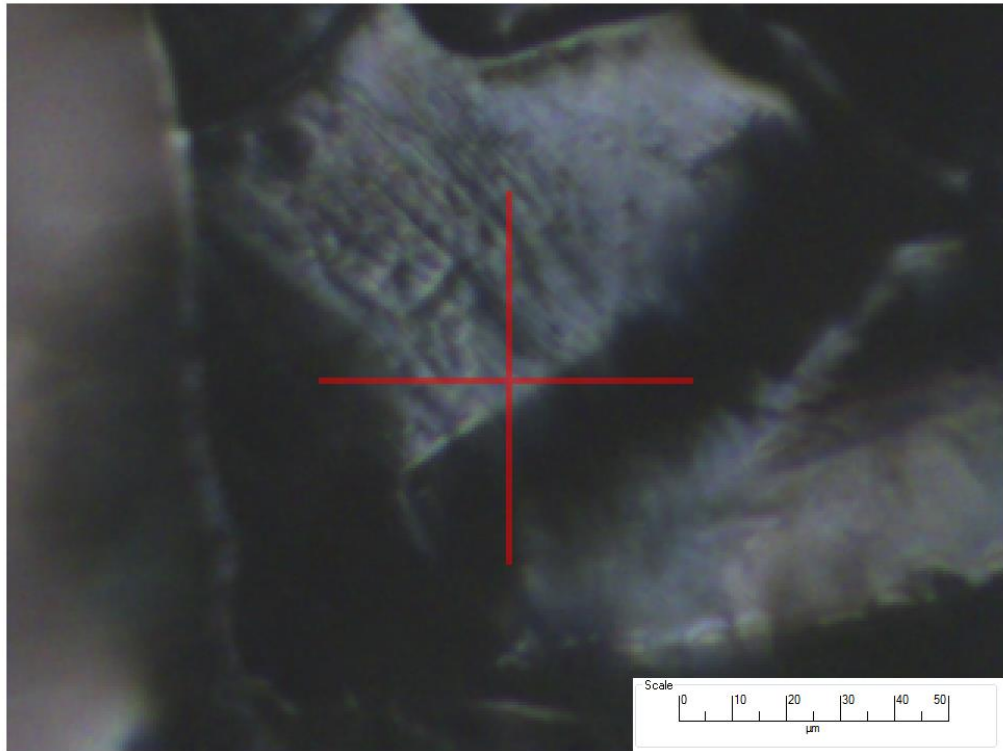
Figure 2. 5. Area chosen on the surface of PEPD 4AB crystal for nanoindentation experiments.The face indented was (1 0 0).

Imaging was made in tapping mode using a Bruker Dimension ICON AFM [20] with a calibrated cube corner diamond probe, type DNISP [21], with length of 50 µm, radius of 40 nm, defection sensitivity of 156.7 nm/V, average spring constant of 272.98 N/m and resonance frequency of 62.9 kHz attached. At the start of each day of measurements, the probe was calibrated in a gold-chromium standard sample and checked with respect to compliance curves and Young's Modulus values within the literature. All the images were collected with the diamond tip in the tapping mode, before and after the indentation with a resolution of 256 x 256 pixels, scan area of 2.0 µm x 2.0 µm and scan rate varying according to the sample. Continuing with the example PEPD 4AB, the area mapped before nanoindentation experiments for this sample can be observed in Figure 2.6, with hills in the surface with maximum size of approximate 20 nm.
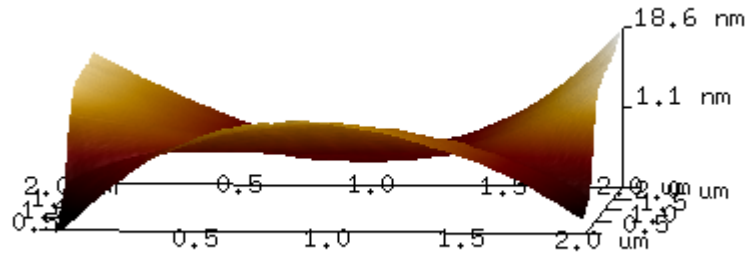
Figure 2. 6 Three-Dimensional view of the surface of PEPD 4AB sample before indentation.

In nanoindentation experiments each sample was measured with trigger thresholds and threshold steps varying according to the sample, in 3 x 3 (columns x rows) matrix with column and row steps of 0.5 µm. When more than one indentation attempt was performed in the sample, different locations on the sample were chosen. Both imaging and nanoindentation results were analysed with the software Nanoscope Analysis v1.40 or Nanoscope Analysis v1.90 [22] for samples with a permanent indent in the surface. Returning to example PEPD 4AB, after nanoindentation experiments the surface had nine resultant indents with well-defined penetration depth (observed in the bottom view of the surface, Figure 2.7-a and significant piling up material (observed in the top view of the surface, Figure 2.7-b [23].

(a)   **(b)**
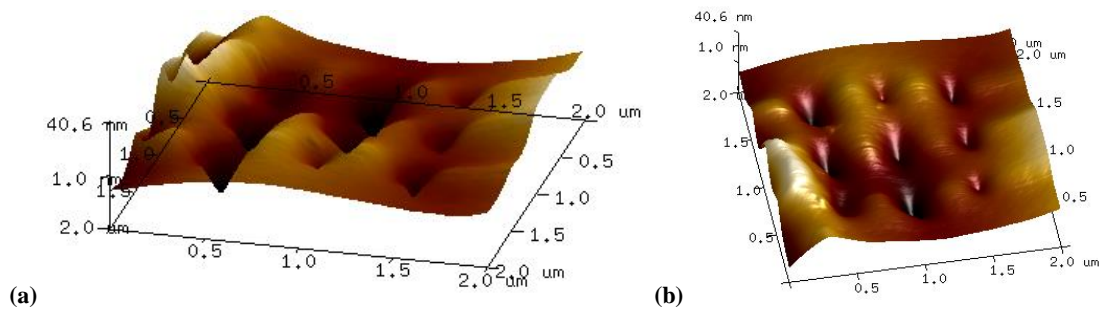
Figure 2. 7 Three-Dimensional view of the surface of PEPD 4AB sample after indentation (a) bottom view of the surface and (b) top view of the surface.

Compliance curves were recorded for each load applied to the sample. An example of data collection can be observed below for the sample PEPD 4AB. There were, in total,

nine compliance curves collected for this sample, three force curves for each of three different maximum applied forces, as shown in Figure 2.8. Baseline correction for each force curve was applied and the values were obtained of the Force versus Separation force curves in Z.
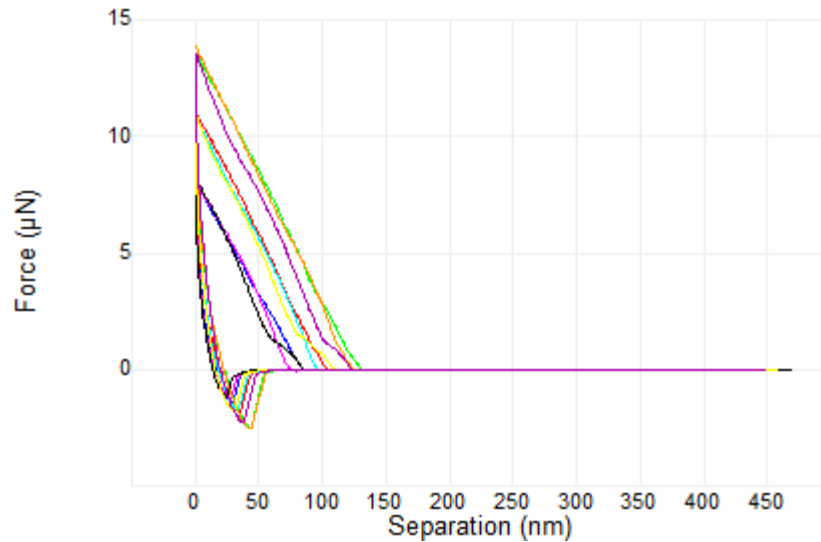
Figure 2. 8 Force versus separation curves for PEPD 4AB in 3 different maximum applied forces. Each coloured curve represents a different force applied to the sample

2.7.3. DATA ANALYSIS – INTERPRETING FORCE CURVES TO OBTAIN HARDNESS VALUES

Regarding data collection, various research groups prefer to collect punctual values of hardness, measuring only one compliance curve per sample or collecting various force curves with the same maximum force applied [33-35]. Instead of this we adopted a method that collects more than one compliance curve with different values of maximum force applied to the same sample [36, 37]. An example of hardness calculated for each compliance curve obtained for the sample PEPD 4AB is given in Table 2.23. In this case, values of maximum depth (h_{max}), maximum force (P_{max}) and the gradient of the elastic unloading stiffness (S) were collected as described in Chapter 1.4.5 and

punctual hardness (H_p) for each force curve was calculated using Equation 1.17. As it can be observed in Table 2.23, the data ranges from 0.38 GPa in force curve number 3 to 0.64 GPa in force curve number 4, giving an average value of punctual hardness equals to $H_p = (0.48 \pm 0.08)$ GPa.

Table 2. 23 Calculated values of hardness for the 9 force curves obtained for PEPD 4AB, where n is the curve label, h_{max} is the maximum depth, P_{max} is the maximum load, S is the elastic unloading stiffness, h_c is the contact depth, A_c is the contact area and H_p is the punctual hardness of the sample.

	n	h_{max} (m)	P_{max} (N)	S (nN/nm)	h_c (m)	A_c (m²)	H_p (GPa)
	1	8.52E-08	7.93E-06	918.90	7.9E-08	1.6E-14	0.49
	2	1.01E-07	1.08E-05	957.90	9.3E-08	2.2E-14	0.48
	3	1.26E-07	1.32E-05	997.30	1.2E-07	3.5E-14	0.38
	4	7.61E-08	8.02E-06	887.10	6.9E-08	1.2E-14	0.64
PEPD 4AB	5	9.48E-08	1.06E-05	954.00	8.6E-08	1.9E-14	0.55
	6	1.24E-07	1.37E-05	990.80	1.1E-07	3.3E-14	0.41
	7	8.14E-08	7.91E-06	1104.40	7.6E-08	1.5E-14	0.53
	8	1.08E-07	1.08E-05	1072.00	1.0E-07	2.6E-14	0.41
	9	1.22E-07	1.35E-05	1211.60	1.1E-07	3.3E-14	0.41

To analyse the behaviour of punctual hardness for this sample, PEPD 4AB, a scatter graph of each value of hardness versus the load applied can be plotted, this graph helps to analyse how much values of punctual hardness scatter for each load applied to the sample. As can be observed in Figure 2.9, each point represents the value of hardness calculated for one compliance curve and the numbers are a reference to **n**, in Table 2.23. For smaller loads applied to the sample, for P_{max} equal to (7.95 ± 0.06) GPa (points 1, 4 and 7) and for P_{max} equal to (10.73 ± 0.08) GPa (points 2, 5 and 8) the values of punctual hardness have a difference between minimum and maximum value for each load of approximate 0.15 GPa. However, when applying a higher load to the sample ($P_{max} = (13.48 \pm 0.24)$ GPa) the difference between minimum and maximum punctal hardness values decreases five times compared to the values observed at smaller loads (approximate 0.03 GPa).
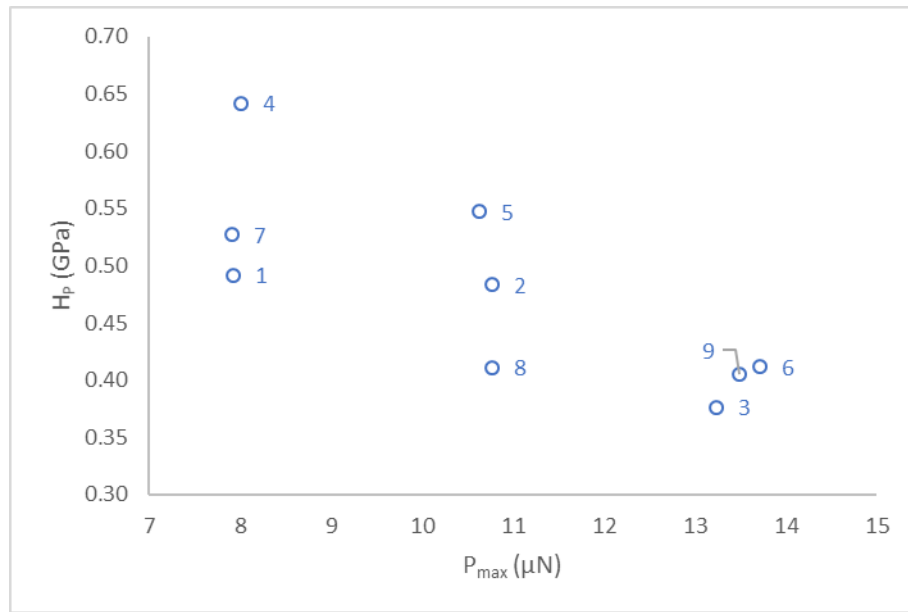
Figure 2. 9 Hardness versus Load scatter plot for the sample PEPD 4AB. Each point represents the value of hardness resultant from one compliance curve and the numbers are a reference to n, in Table 2.23.

For this reason, in this work we propose another methodology to analyse hardness data for variable forces. As observed in Equation 1.16, in Chapter 1.4.5, hardness is a function of the load applied and the indentation area. When variable force is applied, hardness can be calculated by the gradient of the linear variation between force and area as shown in Equations 2.1 and 2.2.

$$P_{max} = f(A_c)$$

Equation 2. 1

$$P_{max} = H \cdot A_c + C$$

Equation 2. 2

Using this method for the same data obtained for the sample PEPD 4AB and calculated in Table 2.23, it is possible to plot a graph of contact area (A_c, in $1000 \cdot nm^2$) versus the maximum load applied (P_{max}, in µN), where the gradient of the curve is a measure of

the hardness of the material (Figure 2.10). The resultant linear equation takes the format of $y = a \cdot x + b$ and, for example for this sample, the linear equation is $P_{max} = 0.2671 \cdot A_c + 4.3889$ with $R^2 = 0.9321$. Thus, the gradient hardness for this sample is $H_G = 0.27 \pm 0.03$ GPa, a difference of 44.04 % when compared with the average punctual hardness ($H_p = 0.48 \pm 0.08$ GPa). The intercept point, C, with the value of 4.4 ± 0.7 μN has no physical meaning and does not affect the value of hardness obtained by the gradient of the line. All errors in the gradient and intercept were calculated using the LINEST function on EXCEL [38]. The advantages of using this method instead of calculating and averaging all punctual hardness values includes the possibility of analysing the quality of the data. For instance, hereafter we only consider any measurements which have coefficient of determination higher than 80 %. This method also minimises calculation errors and indicates outliers in the measurements. In this work, values calculated using the traditional punctual hardness method are available in APPENDICES 8.1 to 8.4 for each compound. However, the following report will only consider gradient hardness as calculated above in the further analysis.
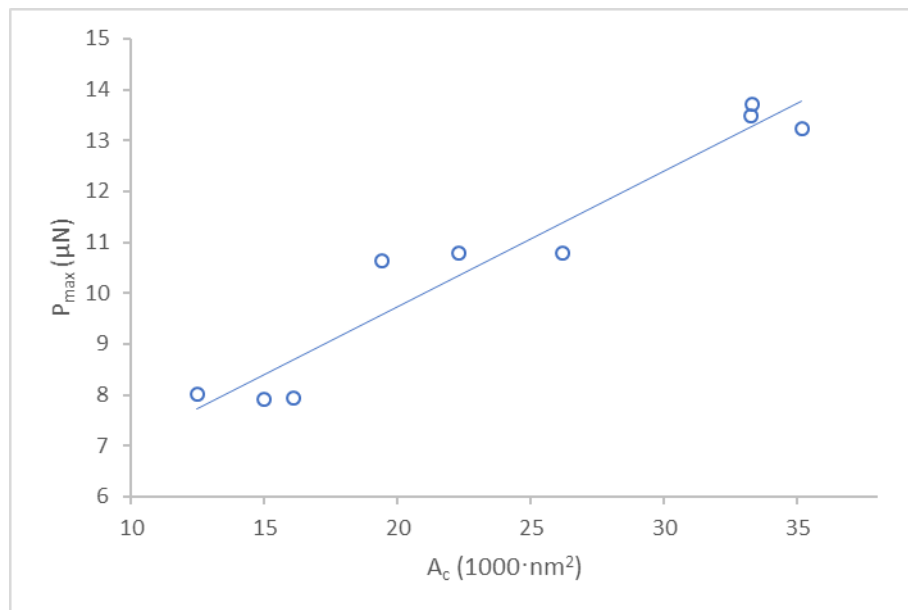
Figure 2. 10 Maximum load applied versus contact area scatter plot and trendline for the sample PEPD 4AB.

2.7.4. DATA ANALYSIS – INTERPRETING FORCE CURVES TO OBTAIN YOUNG'S MODULUS VALUES

As well as the values of hardness, research groups also report punctual values of Young's Modulus, for instance by obtaining values for each force curve from Nanoscope Analysis software [39-41]. Instead of this, we adopted a method that obtains a single value of Young's Modulus per sample from the relationship between force and indentation based on Sneddon models [42-43]. Continuing with the example PEPD 4AB, there were 9 values of Young's (E) and Reduced (E_R) Modulus obtained from the software Nanoscope Analysis. This used the indentation channel from the extend curve, a linearized model, did not consider adhesion forces and used the Sneddon (conical) method. Results can be observed in Table 2.24. The values of punctual Young's Modulus range from 1.64 GPa to 3.47 GPa, giving an average punctual Young's Modulus (E_P) of (2.15 ± 0.54) GPa. The same procedure used to analyse the behaviour of punctual hardness in the previous chapter was used to analyse punctual Young's Modulus for this sample.

Table 2. 24 Values of Young's Modulus obtained from Nanoscope Analysis software for the 9 force curves obtained for PEPD 4AB, where n is the curve label, E_P is the punctual Young's Modulus of the sample and $E_{R,P}$ is the punctual Reduced Modulus of the sample.

	n	E_P (GPa)	$E_{R,P}$ (GPa)
	1	2.23	2.45
	2	2.08	2.28
	3	1.64	1.80
PEPD 4AB	4	2.46	2.70
	5	1.88	2.07
	6	1.66	1.83
	7	3.47	3.82
	8	2.19	2.41
	9	1.71	1.88

A scatter graph of each value of hardness versus the load applied can be plotted, this graph helps to analyse how much values of punctual Young's Modulus scatter for each load applied to the sample. As can be observed in Figure 2.11, each point represents

the value of Young's Modulus obtained for a load in Table 2.24. Again, smaller loads applied to the sample gave values of punctual Young's Modulus have a greater difference between minimum and maximum values than are observed when applying a higher load to the sample.
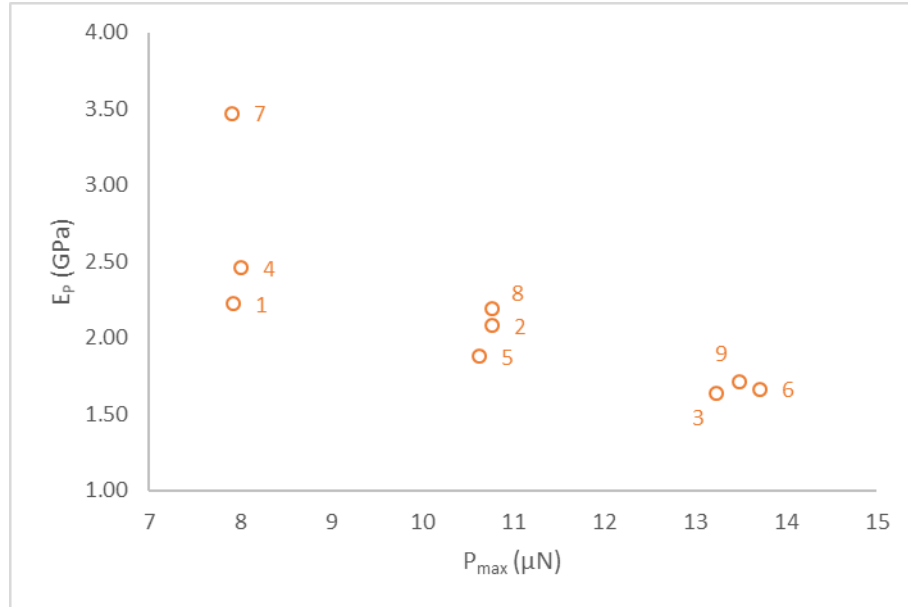
Figure 2. 11 Young's Modulus versus Load scatter plot for the sample PEPD 4AB. Each point represents the value of Young's Modulus resultant from one compliance curve.

In this work we propose another methodology to analyse Young's Modulus data for variable forces. According to Sneddon model [42], the relationship between Young's Modulus, force and indentation can be observed in Equation 2. 3.

$$F = \frac{2}{\pi} \cdot \frac{E}{(1 - v^2)} \cdot \tan \alpha \cdot \delta^2$$

Equation 2. 3

70

Where F is the force applied in the sample, E is the Young's Modulus, α is the half angle of the indenter (for DNISP probe is 18 °), δ is the size of indentation and ν is the Poisson's ratio of the sample, which is variable according to the Young's Modulus of the sample. This is the same method Nanoscope Analysis use to obtain punctual Young's Modulus value for each force curve. When the maximum force is applied, the indentation has the size of the maximum contact depth (h_{max}) and Equation 2.3 becomes a relationship between the area related to the elasticity of the sample, which we will denominate elastic area (A_E) and can be observed in Equation 2.4. Thus, Young's Modulus can be calculated by the gradient of the linear variation between force and elastic area as shown in Equation 2. 5.

$$A_E = \left(\frac{2}{\pi \cdot (1 - \nu^2)} \cdot \tan \alpha \right) \cdot \delta^2$$

Equation 2. 4

$$F = E \cdot A_E$$

Equation 2. 5

Using this method for the same data obtained for the sample PEPD 4AB and calculated in Table 2.24, is possible to plot a graph of maximum load applied (P_{max}, in µN) versus the elastic area (A_E, in 1000·nm²) where the gradient of the curve is a measure of the Young's Modulus of the material (Figure 2.12). The resultant linear equation takes the format of y = a·x + b and, for example for this sample, the linear equation is P_{max} = 2.6281·A_E + 4.3109 with R^2 = 0.9442. Thus, what we will term the gradient Young's Modulus for this sample is E_G = 2.6 ± 0.2 GPa, an increase of 22.2 % over the traditional calculation. This is illustrated in Figure 2.14. All errors in the gradient and intercept were calculated using the LINEST function on EXCEL [38]. All values of traditional punctual Young's Modulus have been calculated and are shown in APPENDIX 8.1 to 8.4 for comparison. However, the following report will only consider gradient Young's Modulus as calculated above in the further analysis.

To compare and verify the data procedures we used in this work with those used in the literature, a case study was performed using data from the paper by Masterson & Cao of Pfizer named "Pharmaceutical nanotechnology evaluating particle hardness of pharmaceutical solids using AFM nanoindentation" [44]. In summary, this paper obtained and compared mechanical measurements of pharmaceutical compounds using nanoindentation. This paper was chosen as the experimental conditions are identical to the ones used in our work, i.e. equipment and probe type are the same. Results for this case study can be observed in APPENDIX 2.7.
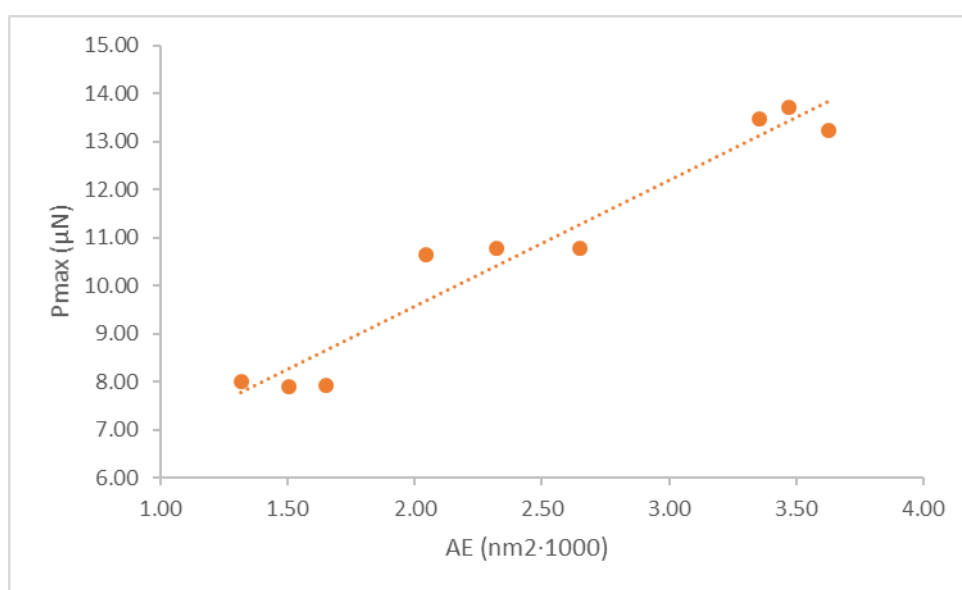
Figure 2. 12 Maximum load applied versus contact area scatter plot and trendline for the sample PEPD 4AB.

2.8.PREDICTION OF HARDNESS

Predictions of values of indentation hardness were made using the method developed by Roberts and Rowe for neutral organic molecules [48] where hardness is obtained from the unit cell as a function of the lattice parameters of the unit cell and the Cohesive Energy Density (CED). This method assumes a relationship between hardness and the weakest plane of the crystal structure. It is detailed in Equation 2. 6 where R_c is the vector described by the lattice parameter of the unit cell, S_r is the slip ratio (equals to 0.707 or 1.000), C_1 and C_2 are the other two lattice parameters, N_A is

the reduced Avogadro's number (0.6) , Z is the number of molecules in the unit cell and F_a is the angular correction which depends on the crystal class: For monoclinic compounds $F_a = \sin\beta$, for orthorhombic compounds $F_a = 1$ and for triclinic compounds $F_a = (1 - \cos^2\alpha - \cos^2\beta - \cos^2\gamma + 2 \cdot \cos\alpha \cdot \cos\beta \cdot \cos\gamma)^{1/2}$.

$$H = \left(\frac{C_1 \cdot C_2 \cdot F_a \cdot 2N_A}{R_c^2 \cdot S_r^2 \cdot Z} \right) \cdot CED$$

Equation 2. 6

2.8.1. CALCULATION OF COHESIVE ENERGY DENSITY

Mechanical properties calculations were made for tyramine, methylephedrine and ephedrine salt samples using Biovia Materials Studio 2017 R2 [49] software with the crystallographic information files (CIF) of non-disordered structures obtained by our group or from the CCDC [50]. Raw CIF files had the cell optimized using geometry optimization task and cohesive energy density was calculated using the geometry optimized cell. All data was obtained using Forcite module, with COMPASSII forcefield, charges forcefield assigned and fine or ultra-fine quality.

The analysis presented in this work was also compared with the predictive method developed by Roberts and Rowe [48] using a case study was performed on the crystal structures of three salt forms of ephedrine published by Collier *et al.* [51]. Details of this case study can be obtained in APPENDIX 2.8.

2.9. REFERENCES

[1]   Lide, D. R. (2009). CRC Handbook of Chemistry and Physics; 89th ed

[2]   Pfannkuch, F., Rettig, H. & Stahl, P. H. (2002). Biological effects of the drug salt form. In: Stahl, P.H. & Wermuth, C.G., eds. Handbook of Pharmaceutical Salts. Zurich: Wiley-VCH.

[3]   Oxford Diffraction (2006). CrysAlis Pro. Oxford Diffraction Ltd, Abingdon, England.

[4]   Sheldrick, G. (2015). Acta Crystallographica Section C-Structural Chem. 71(1), 3-8.

[5]   A. Altomare, F. Cascarano, C. Giacovazzo & A. Gualardi, (1993). Journal of Applied Crystallography, 26, 343-350.

[6]   Farrugia, L. J. (1997). Journal of Applied Crystallography, 30(5), 565.

[7]   Morrison, C.A. (2012). Salt selection for pharmaceutical use University of Strathclyde. Dept. of Pure and Applied Chemistry. Thesis [Ph. D] - University of Strathclyde.

[8]   Logan, C. (2018). Hardness of Pharmaceutical and Organic Crystals. Dept. of Pure and Applied Chemistry. Thesis [MChem] - University of Strathclyde.

[9]   Macrae, C. F., Bruno, I. J., Chisholm, J. A., Edgington, P. R., McCabe, P., Pidcock, E., Rodriguez-Monge, L., Taylor, R., van de Streek, J. & Wood, P. A. (2008). J. Appl. Cryst., 41, 466-470.

[10]   Macrae, C. F., Edgington, P. R., McCabe, P., Pidcock, E., Shields, G. P., Taylor, R., Towler M. & van de Streek, J. (2006). J. Appl. Cryst., 39, 453-457.

[11]   Allen, F. H (2002). Acta Crystallographica Section B-Structural Science, 58, 380.

[12]   Etter, M. C. (1990). Acc. Chem. Res. 23, 120–126.

[13]   Etter, M. C. (1982). J. Am. Chem. Soc., 104, 1095.

[14]   Gillon, A. L., Feeder, N., Davey, R. J., & Storey, R. (2003). Crystal Growth and Design, 3(5), 663-673.

[15]   Macrae, C., Bruno, I., Chisholm, J., Edgington, P., McCabe, P., Pidcock, E., . . . Wood, P. (2008). Journal of Applied Crystallography, 41(2), 466-470.

[16]   Morrison, C.A. (2012). 'Salt selection for pharmaceutical use'. University of Strathclyde. Dept. of Pure and Applied Chemistry. Thesis [Ph. D] – University of Strathclyde.

[17]   Kennedy, A. R., Morrison, C. A., Briggs, N. E., & Arbuckle, W. (2011). Crystal Growth and Design, 11(5), 1821-1834.

[18]   Briggs, N., Kennedy, A., & Morrison, C. (2012). Acta Crystallographica Section B, 68(4), 453-464.

[19]   Oxford Diffraction (2006). CrysAlis Pro. Oxford Diffraction Ltd, Abingdon, England.

[20]   Bruker Corporation. Dimension FastScan - The World's Fastest AFM. Available   at: <https://www.bruker.com/fileadmin/user_upload/8-PDF-Docs/SurfaceAnalysis/AFM/
Brochures/Dimension_FastScan_Atomic_Force_Microscope_brochure.pdf>.
Accessed on 21 June 2017.

[21]   Bruker   AFM   probes.   DNISP.   Details   available   at <http://www.brukerafmprobes.com/p-3253-dnisp.aspx>. Accessed on 21 June 2017.

[22]   The Nanoscale World – Bruker. NanoScope Analysis v1.40 and v1.90. Available   at   <   http://nanoscale   world.bruker-axs.com/nanoscaleworld/media/p/775.aspx>. Accessed on 21 June 2017

[23]   Egart, M., Janković, B., & Srčič, S. (2016). Acta Pharmaceutica (Zagreb, Croatia), 66(3), 303-330.

[24]   Fischer-Cripps, A., & Springerlink. (2011). Nanoindentation [internet resource] (3rd ed., Mechanical engineering series ; 1). New York: Springer.

[25]   Oliver, W.C. & Pharra, G.M. (2004). J. Mater. Res., 19 (10), pp. 3-20.

[26]   Egart, M., Janković, B., & Srčič, S. (2016). Acta Pharmaceutica (Zagreb, Croatia), 66(3), 303-330.

[27]   Doerner, M. & Nix, W. (1986). Journal of Materials Research, 1(4), 601-609.

[28]   Sneddon, I. N. (1965). Int. J. Engng. Sci., 3, 47-57.

[29]   Love, A.E.H., (1939). Q.J. Math. 10, 161.

[30]   Love, A.E.H., (1929). Philos. Trans. A 228, 377.

[31]   Harding, J.W. & Sneddon, I.N (1945). Proc. Cambridge Phil. Soc. 41, 16.

[32]   Sneddon, I.N. (1951). Fourier Transforms (McGraw-Hill, New York), pp. 450–467.

[33]   Zhou, L. & Yao, Y. (2007). Materials Science & Engineering A, 460, 95-100.

[34]   Liao X. & Wiedmann, T.M. (2005). Journal of Pharmaceutical Sciences, Vol. 94, 79–92.

[35]   Mannepalli, S. S., & Mangalampalli, K. (2017). Crystals, 7(11).

[36]   Chen, S., Sheikh, A. & Ho. R. (2014). Journal of Pharmaceutical Sciences, 103(12), 3879-3890.

[37]   Masterson, V.M. & Cao. X. (2008). International Journal of Pharmaceutics, 362(1), 163-171.

[38]   Linest Function. Excel Suport. Available at < https://support.office.com/en-us/article/linest-function-84d7d0d9-6e50-4101-977a-fa7abf772b6d >. Accessed on 15/03/2019.

[39]   Nguyen, Fujinami, & Nakajima. (2016). Polymer, 87, 114-122.

[40]   Radmacher, M. (1997). IEEE Eng. Med. Biol. Mag., 47-57.

[41]   Domke J. & Radmacher, M. (1998). Langmuir 14, 3320-3325

[42]   I. N. Sneddon (1965). Int. J. Engng. Sci., 3, 47-57.

[43] Nanomechanical   Property   Mapping.   Bruker.   Available   at   < http://www.nanophys.kth.se/nanophys/facilities/nfl/afm/icon/bruker-help/Content/ForceVolume/Mechanical%20Property%20Mapping.htm > Accessed on 02/04/2019

[44]   Masterson, V.M. & Cao. X. (2008). International Journal of Pharmaceutics, 362(1), 163-171.

[45]   Ashby, M. F. & Jones, D. R. H., (1980). Endineering Materials: An introduction to their properties and applications (vol, 1), Pergamon.

[46]   Cottrell, A. H., (1964). The Mechanical Properties of Matter, John Wiley.

[47]   Anderson, J. C., Leaver, K. D., Rawlings, R. D. & Alexander, J. M. (1985), Materials Science, Van Nostrand Reinhold, 3rd. ed.

[48]   Roberts, R.J.; Rowe, R.C. & York, P. (1994). J. Mater. Sci. 29, 2289–2296.

[49]   The Cambridge Structural Database (CSD). Available at < https:// www.ccdc.cam.ac.uk/solutions/csd-system/components/csd/   >   Accessed   on 19/01/2018

[50] Biovia   Material   Studio   2017   R2.   Available   at   < http://accelrys.com/products/collaborative-science/biovia-materials-studio/   > Accessed on 19/01/2018

[51]   Collier, E., Davey, R., Black, S., & Roberts, R. (2006). Acta Crystallographica Section B, 62(3), 498-505.

3. GENERAL REMARKS

3.1. TYRAMINE SALT FORMS

Structural analyses were made with the forty-two salt forms of tyramine described in Chapter 2.5 together with the fifty-five tyramine structures available from the CCDC [1-16] on 1st May 2019. The anions present in this group of salt forms can be classified as; benzoates (including disubstituted and poly-substituted benzoates with various groups as substituents); carboxylates (including aliphatic carboxylates and mandelates); inorganic (including halides, sulfates and phosphates and other counterions that do not have carbon atoms); sulfonates (RSO_3 where R = organic); naphthalates (salts of unsubstituted and substituted naphthalic acids); and other (compounds that do not belong to any of the above categories). The percentage distribution of samples used in this work according to the composition of the counterion can be observed in Figure 3.1. A list of all salt forms used in this work with the asymmetric unit contents and literature references can be observed in APPENDIX 3.1.
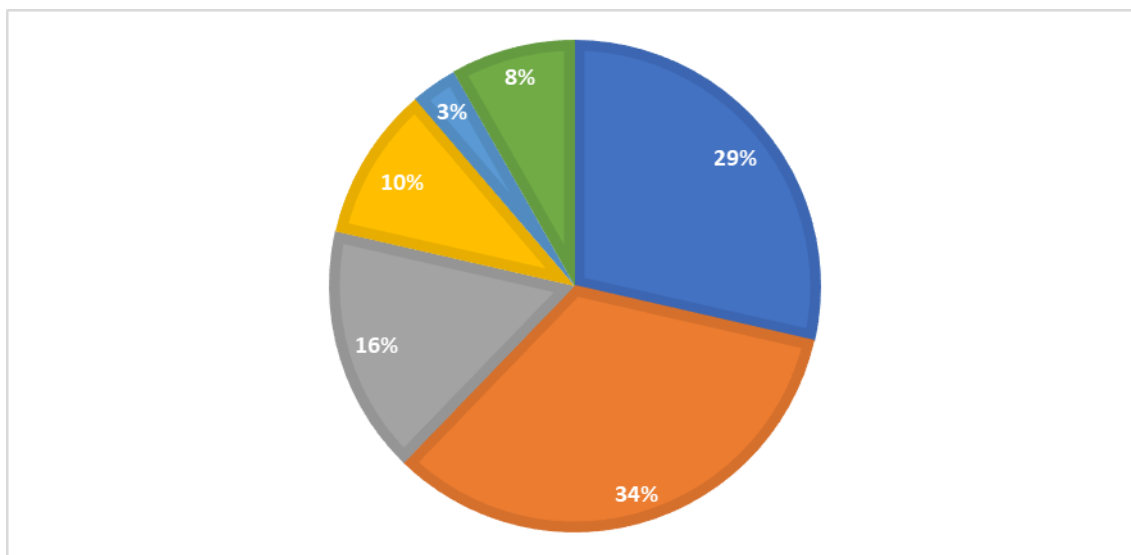
Figure 3. 1. Percentage of salt forms according to the composition of the counterion, where in blue are carboxylates, in orange are benzoates, in grey are sulfonates, in yellow are inorganic counterions, in light blue are naphthalates and in green are compounds characterised as others.

3.2. METHYLEPHEDRINE SALT FORMS

This section will describe the structures that will be used in the following chapters on enantiopure and racemic methylephedrine. There are twenty-nine salt forms of enantiopure and racemic methylephedrine described for the first time in Chapter 2.5 together with two salt forms synthesised by Morrison *et al.* [17] and not published, (1R,2S)-(-)-methylephedrinium ethanesulfonate (*e*ETSO3) and (+/-)-methylephedrinium methanesulfonate (*r*MESO3). These are analysed alongside sixty-one enantiopure and racemic methylephedrine structures available from the CCDC [18-22], on 15th May 2019. In total the compounds analysed in this chapter includes fifty-three salt forms of enantiopure methylephedrine (MEPD) and thirty-eight salt forms of racemic methylephedrine (RMEPD).

The anions present in this group of salt forms are classified similarly to the tyrammonium counterions, that is as benzoates, carboxylates, inorganic, sulfonates, naphthalates and one compound classified as other, a zinc complex with enantiopure methylephedrine, *e*ZN.complex (NAHGUY). The percentage distribution of samples used in this work according to the composition of the counterion can be observed in Figure 3.2 on the left for enantiopure methylephedrine (MEPD) and on the right for racemic methylephedrine. The list of all salt forms used in this work together with the structure of the asymmetric unit and a literature reference can be observed in APPENDIX 3.2 for both enantiopure methylephedrine (represented by a "*e*" before the label) and for racemic methylephedrine (represented by a "*r*" before the label).
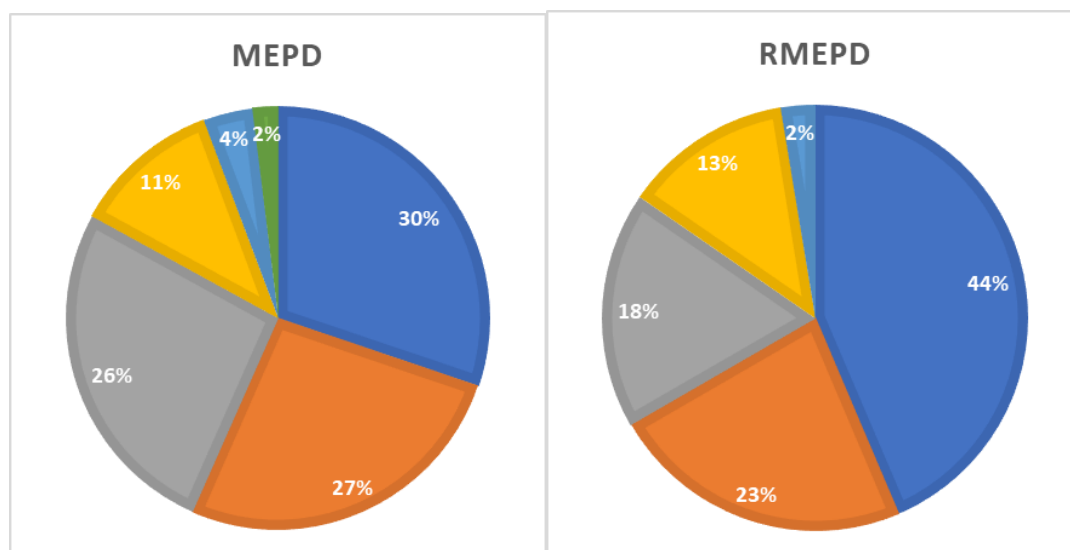
Figure 3. 2. Percentage of salt forms according to the composition of the counterion for enantiopure methylephedrine (MEPD, on the left) and racemic methylephedrine (RMEPD, on the right), where in blue are benzoates, in orange are carboxylates, in grey are sulfonates, in yellow are inorganic counterions, in light blue are naphthalates and in green are compounds characterised as others.

3.2.1. FORMATION OF RACEMIC CONGLOMERATES

An initial result observed from the syntheses of new salt forms of racemic methylephedrine was the formation of racemic conglomerates. This term describes a bulk solid which contains separate crystals of both (1R,2S)-(-)-methylephedrine and (1S,2R)-(+)-methylephedrine in equal amounts, rather than racemic single crystals [57,58]. This spontaneous resolution was found for ten salt forms, namely: 2NAPH, H2N, N2S, CAMPH, 4HB [19], 4CB [19], PTOL [19], PTS, MESO3 and 4HPA. This is a higher (roughly double) occurrence of spontaneous resolution than may be expected [19]. It is interesting to note that certain types of counterion have a much higher likelihood of forming conglomerates with methylephedrine than the approximately 1 in 10 average. The above list contains only carboxylates or sulfonates of naphthalene substituted in the β position (Figure 3.3), *para*-substituted aryl acids (Figure 3.4) and general sulfonates. All three naphthalene-based anions formed conglomerates. However, not all *para*-substituted aryl acids did so. There was the formation of four racemic salt forms of *para*-benzoates: *r*4NB, *r*PAAB.H2O, *r*4AB and *r*4FB, as observed in Table 1, where the formation of racemic conglomerate in this case represents 50.0 % of all successful crystal formation. A similar result can be observed

for the *para*-substituted benzenesulfonates, where only two hydrates crystallised as racemic compounds, *r*4CBS.H2O and *r*4HBS.H2O and the salt form of PTS crystallise as a racemic conglomerate. Of all the sulfonates observed, 33.3 % of the compounds crystallise as conglomerates. Details of the distribution of compounds according to the crystallisation type can be observed in Figure 3.5. Considering all synthesis attempts and results, it seems that composition of the counterion may be related to the formation of racemic conglomerates instead of racemates.
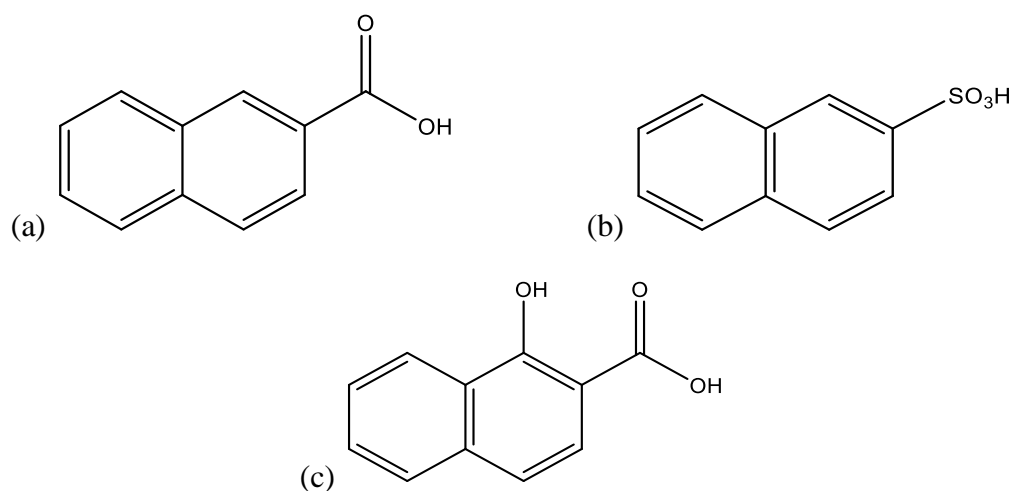
Figure 3. 3. Acid representation for the first group of conglomerates where (a) 2NAPH, (b) N2S and (c) H2N.
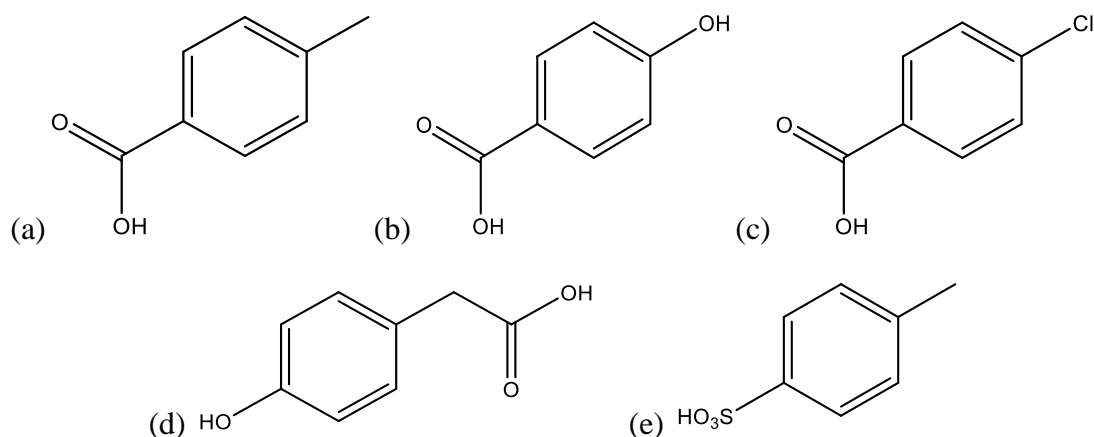
Figure 3. 4. Acid representation for the second group of conglomerates where (a) PTOL, (b) 4HB, (c) 4CB, (d) 4HPA and (e) PTS.
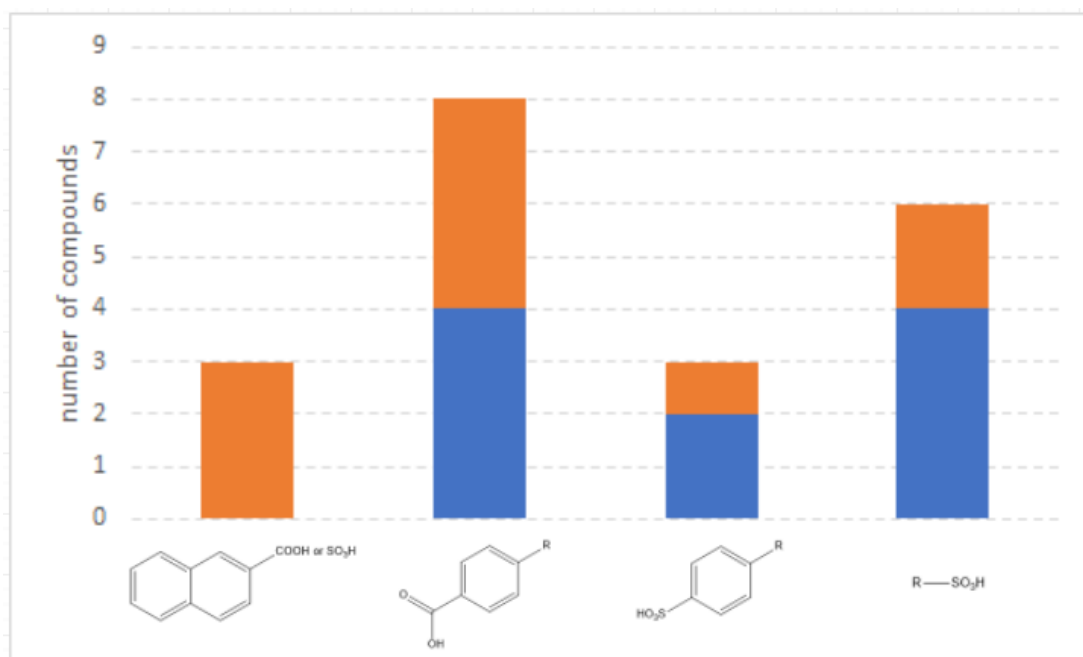
Figure 3. 5. Formation of racemates (in blue) and racemic conglomerates (in orange) for four different types of counterions

.

3.3. EPHEDRINE SALT FORMS

Of the seventy-seven structures of enantiopure ephedrine found in the CSD database [23-54], some were rejected for the following reasons. First, the analysis excluded the samples YITSUS [55], MOXREY [56], MOXRIC [56], MOXROI [56], MOXRUO [56], MOXSAV [56], MOXSEV [56] and MOXSID [56] as these samples were salt forms of ephedrinium chloride co-crystallised with very large organic molecules in the unit cell as it can be observed in Figure 3.6 for the compound MOXSID. Second, the analysis also excluded repeat entries that had the same structure, composition and space group as an accepted structure. This occurred with the counterions chloride, thiocyanate and benzenesulfonate (BS). This left sixty-six structures to be analysed. To these structures were added structures of ten new forms synthesised by Morrison *et al.* [17] and represented as 2CB, 2NB, 3CB, 3NB.H2O, 4AB, 4CB, 4HBS, 4NB (monoclinic), 4NB.2 (orthorhombic) and MTOL. Finally, new nine structures described in Chapter 2.5 were also added to the analysis, giving eighty-seven relevant structures of enantiopure ephedrine.
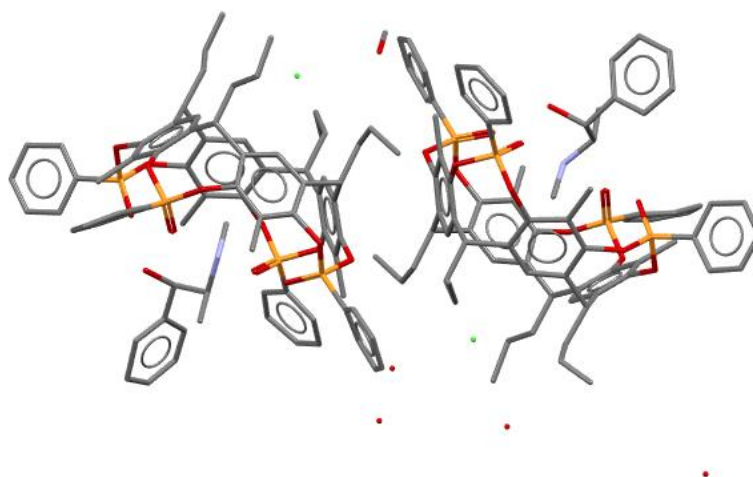
Figure 3. 6. Composition of the asymmetric unit for the sample MOXSID. Hydrogen atoms were omitted for clarity.

The anions present in this group of salt forms were classified as before as benzoates, carboxylates, inorganic (including inorganic complexes with cadmium, gold and palladium as well as the more typical anions seen before), sulfonates and "other". The percentage distribution of samples used in this work according to the composition of the counterion can be observed in Figure 3.7. The list of all salt forms used in this work with the structure of asymmetric unit and reference to the author can be observed in APPENDIX 3.3.
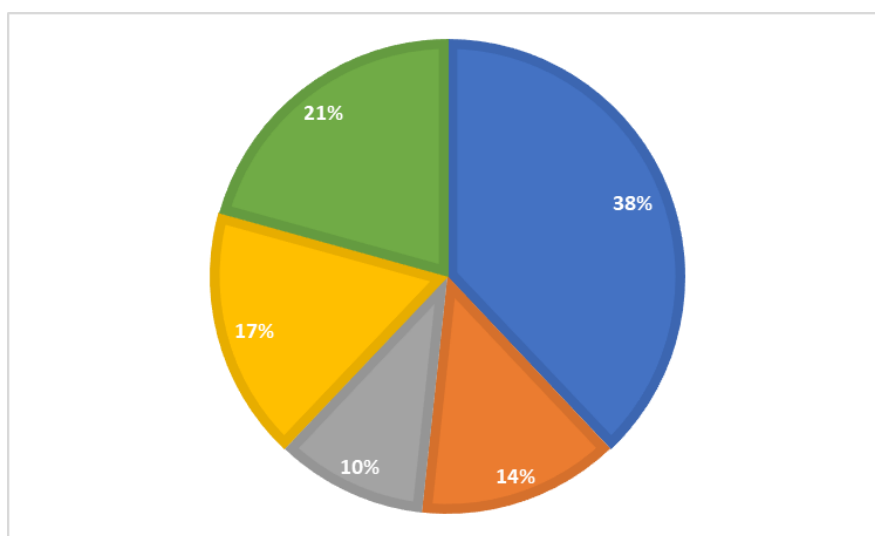
Figure 3. 7 Percentage of salt forms according to the composition of the counterion for enantiopure ephedrine, where in blue are benzoates, in orange are carboxylates, in grey are sulfonates, in yellow are inorganic counterions and in green are compounds characterised as others.

3.4. CONCLUSION

In this work, structural analysis in the following chapters will be done for ninety-seven salt forms of tyramine, fifty-three salt forms of enantiopure methylephedrine, thirty-eight salt forms of racemic methylephedrine and eighty-seven salt forms of enantiopure ephedrine. The structures were previously synthesised in this work or obtained from Morrison *et al.* [17] or the CSD database. Most of the structures are carboxylates, especially benzoates, with smaller numbers of sulfonates, inorganic anions and "other" compounds. Description of the structure and composition are given in APPENDIX 3.1 for tyramine compounds, APPENDIX 3.2 for enantiopure and racemic methylephedrine compounds and APPENDIX 3.3 for ephedrine compounds.

3.5. REFERENCES

[1]   Ivanova, B. & Spiteller, M. (2010). Spectrochimica Acta Part A: Molecular and Biomolecular Spectroscopy, 77(4), 849-855.

[2]   Ivanova, B. & Spiteller, M. (2010). Spectrochim.Acta,Part A, 77, 850.

[3]   Ishida   T.   &   Inoue   M.   (1981).   Acta. Crystallogr.,Sect.B:Struct.Crystallogr.Cryst.Chem. 37, 2117

[4]   Parveen, R., & Dastidar, P. (2016). Chemistry – A European Journal, 22(27), 9257-9266.

[5]   Kolev, T., Koleva, B., Spiteller, M., Sheldrick, W., & Mayer-figge, H. (2009). Amino Acids, 36(2), 185-93.

[6]   Briggs, N., Kennedy, A., & Morrison, C. (2012). Acta Crystallographica Section B, 68(4), 453-464.

[7]   Ohba, S., & Ito, Y. (2002). Acta Crystallographica Section E, 58(5), O584-O585.

[8]   Koleva, B.B., Kolev, T., Seidel, R.W., Spiteller, M., Mayer-Figge, H. & Sheldrick W.S. (2008). Journal of Molecular Structure, 888(1), 138-144.

[9]   Kolev, T., Koleva, B., Seidel, R., Mayer-figge, H., Spiteller, M., & Sheldrick, W. (2009). Amino Acids, 36(1), 29-33.

[10]   Podder, A. Dattagupta, J.K., Saha, N.N. & Saenger, W.(1979). Acta Crystallogr., Sect.B:Struct.Crystallogr.Cryst.Chem., 35, 649.

[11]   Ogawa, K., Tago, K., Ishida, T. & Tomita K.-I. (1980). Acta Crystallogr., Sect.B:Struct.Crystallogr.Cryst.Chem., 36, 2095.

[12]   Prohens, R., Portell, A., Font-Bardia, M., Bauzá, & Frontera. (2014). Crystal Growth and Design, 14(5), 2578-2587.

[13]   Parveen, R., Sravanthi, B. & Dastidar, P. (2017), Chem.Asian J., 12, 792.

[14]   Gryl, M., Rydz, A., Wojnarska, J., Krawczuk, A., Kozieł, M., Seidler, T., . . . Stadnicka, K. (2019). IUCrJ, 6(Pt 2), 226-237.

[15]   Mittapalli, S., Chaitanya Mannava, M., Sahoo, R., & Nangia, A. (2019). Crystal Growth and Design, 19(1), 219-230.

[16]   Rydz, A., Gryl, M., & Stadnicka, K. (2018). Acta Crystallographica Section C, 74(12), 1586-1594.

[17]   Morrison, C.A. (2012). 'Salt selection for pharmaceutical use'. University of Strathclyde. Dept. of Pure and Applied Chemistry. Thesis [Ph. D] – University of Strathclyde

[18]   Yanagi, K., Minobe, M. & Aratani, T. (1986). Acta Crystallogr.,Sect.C: Cryst.Struct.Commun. , 42, 745.

[19]   Kennedy, A. R., Morrison, C. A., Briggs, N. E., & Arbuckle, W. (2011). Crystal Growth and Design, 11(5), 1821-1834.

[20]   Enders, D., Zhu, J., & Raabe, G. (1996). Angewandte Chemie International Edition in English, 35(15), 1725-1728.

[21]   De Moraes, S.L., Edwards, D., Florence, A.J., Johnston, A., Johnston, B.F., Morrison, C.A., & Kennedy, A.R. (2017). Crystal Growth and Design, 17(6), 3277-3286.

[22]   Dan, W., Chen, J., Di, Y., Kong, Y., Wang, Q., Yang, W., & Wang, D. (2010). Chinese Journal of Chemistry, 28(7), 1097-1102.

[23]   Gorman, A., Gould, R.O., Gray, A.M., Taylor, P. & Walkinshaw M.D. (1986). J.Chem.Soc., Perkin Trans.2. 5, 739.

[24]   Kok, A., Wynberg, H., Parthasarathi, V., Smits, J., & Beurskens, P. (1987). Acta Crystallographica Section C, 43(7), 1336-1341.

[25]   García-Granda, S., Beurskens, P., Smits, J., Kok, A., & Wynberg, H. (1988). Acta Crystallographica Section C, 44(12), 2233-2235.

[26]   Ivanova, B. & Spiteller, M. (2010). Spectrochimica Acta Part A: Molecular and Biomolecular Spectroscopy, 77(4), 849-855.

[27]   Ivanova, B., Kolev, T., Lamshöft, M., Mayer-Figge, H., Seidel, R. Sheldrick, W.S. & Spiteller. M. (2010). Journal of Molecular Structure, 971(1), 8-11.

[28]   Li, B.-L., Zhang Z.-G., Wang W., Li, J. & Wang C.-W. (2008). Z.Naturforsch.,B:Chem.Sci. 63, 77.

[29]   Cooke, C. L., Davey, R. J., Black, S. G., Muryn, C., & Pritchard, R. (2010). Crystal Growth and Design, 10(12), 5270-5278.

[30]   Aitken, D., Drouin, L., Goretta, S., Guillot, R., Ollivier, J., & Spiga, M. (2011). Organic & Biomolecular Chemistry, 9(21), 7517-7524.

[31]   Lolya, D.O., Mishnev, A.F., Bleidelis, Ya.Ya., Andrianov, V.I. & Freimanis, Ya.F. (1987). Zh.Org.Khim. 23, 1887.

[32]   Wang, D.-Q., Chen, J.-T., Dan, W.-Y., He, D.-H., Chen, Z.-P. & Di, Y. Y. (2011), J.Chem.Soc.Pak. 33, 333.

[33]   Collier, E., Davey, R., Black, S., & Roberts, R. (2006). Acta Crystallographica Section B, 62(3), 498-505.

[34]   Cheung, E. Y., Harris, K. D., Kang, T. R., Scheffer, J., & Trotter, J. (2006). Journal of the American Chemical Society, 128(49), 15554-15555.

[35]   Moers, F.G., Smits, J.M.M., Beurskens, P.T., Ariaans, G.J.A., Zwanenburg, B., Leusen, F.J.J. & Bruggink, A. (1994).   J.Chem.Cryst. 24, 179.

[36]   Bruins Slot, H., Leusen, F., Van Der Haest, A., & Van Bolhuis, F. (1992). Acta Crystallographica Section C, 48(5), 925-929.

[37]   Gais, H.-J., Lukas, K.L., Ball, W.A., Braun, S. & Lindner, H.J. (1986). Liebigs Ann., 687.

[38]   Wu H., Habgood, M., Parker, J.E., Reeves-McLaren, N., Cockcroft, J.K., Vickers, M., West, A.R. & Jones A.G. (2013). CrystEngComm, 15, 1853.

[39]   Efimenko, I.A., Churakov, A.V., Ivanova, N.A. Erofeeva, O.S. & Demina, L.I. (2017). Zh.Neorg.Khim. 62, 1476.

[40]   Smits, J.M.M., Beurskens, P.T., Parthasarathi, V., Rijk, E.A.V., Kok, A.M.G. & Wynberg, H. (1987). Acta Crystallogr.,Sect.C:Cryst.Struct.Commun. 43, 1334.

[41]   Borszeky, K., Mallat, T., Aeschiman, R., Schweizer, W.B. & Baiker, A.(1996). J.Catalysis, 161, 451.

[42]   Turdybekov, K.M., Lindeman, S.V., Struchkov, Yu.T., Gazaliev, A.M., Fazylov, S.D., Zhurinov, M.Zh. & Zhumazhanova, B.Zh. (1989). Khim.Prir.Soedin, 88.

[43]   Babor M., Nievergelt, P.P., Cejka, J., Zvonicek, V. & Spingler B. (2019) IUCrJ . 6, 145.

[44]   Wood, M.R. & Lalancette, R.A. (2013). Acta Crystallogr.,Sect.C: Cryst.Struct.Commun., 69, 388.

[45]   Zabel, M., Breu, J., Rau, F., Range, K.-J., Krey, V., Uffrecht, A. & Buschauer, A. (2000). Acta Crystallogr.,Sect.C:Cryst.Struct.Commun. 56, 250.

[46]   Charles, N.G.; Rodesiler, P.F., Griffith, E.A.H. & Amma, E.L. (1984) Acta Crystallogr.,Sect.C:Cryst.Struct.Commun. 40, 1676.

[47]   Jones, P.G., Doring, D., Laue, T. & Hopf H. (1993). ActaCrystallogr.,Sect.C:Cryst. Struct.Commun., 49, 1192.

[48]   Nievergelt, P.P., Babor, M., Cejka, J. & Spingler, B. (2018).Chemical Science. 9, 3716

[49]   Hearn, R.A. & Bugg, C.E. (1972). Acta Crystallogr.,Sect.B:Struct.Crystallogr. Cryst.Chem. 28, 3662.

[50]   Hearn, R.A., Freeman, G.R. & Bugg, C.E. (1973). J.Am.Chem.Soc. 95, 7150.

[51]   Banjeree, R., Bhatt, P.M., Ravindra, N.V. & Desiraju, G.R. (2005). Cryst.Growth Des. 5, 2299.

[52]   Garcia-Granda, S., Beurskens, P.T., Smits, J.M.M., Kok, A.M.G. & Wynberg H. (1988). Acta Crystallogr.,Sect.C:Cryst.Struct.Commun. 44, 2233.

[53]   Gauthier, T.J., McLaughlin, M.L. & Fronczek, F.R. (2015). CSD Communication

[54]   Ho, W., Tarhan, O., Kiorpes, T.C., Tutwiler, G.F. & Mohrbacher, R.J. (1987). J.Med.Chem. 30, 1094.

[55]   Danylyuk, O. (2018). CrystEngComm 20, 7642.

[56]   Biavardi, E., Ugozzoli, F. & Massera. C. (2015). Chem.Commun. 51, 3426

[57]   Srisanga & ter Horst, J.H. (2010). Cryst Growth Des, 10, 1808-1812.

[58]   Jacques, J., Collet, A. & Wilen, S.H. (1981).Enantiomers, Racemates, and Resolutions. Wiley: New York.

4. OCCURRENCE OF MORE THAN ONE CATION IN THE UNIT CELL

4.1. TYRAMINE SALT FORMS

There are a variety of fundamental structural features whose occurrence in crystals are not well understood, the classic example being the formation or otherwise of hydrated crystals[1-4]. Another such feature is the occurrence of structures with more than one crystallographically independent molecule (or equivalent) per asymmetric unit. This subject has been reviewed recently [3]. These Z' > 1 structures are of general interest as they raise fundamental problems with our understanding of crystallisation but may also be of specific interest here as some predictions of hardness use an inverse relationship between hardness and Z as will be described in Chapter 8.

Of the ninety-seven salt forms of tyramine analysed, including salt forms synthesised in this work or obtained from the CCDC database [4-6], thirty compounds present more than one cation unit in the unit cell. Table 4.1 lists these compounds. Of these structures, six can be excluded from consideration as they were synthesised with acids with more than one acidic site and are simply 2:1 ratio salt forms. This leaves twenty-two structures that crystallise with two independent cations per asymmetric unit (Z'= 2), two compounds having the presence of four different cations (Z' = 4) and finally the presence of eight different cations (Z' = 8) in the TYR 4CB (MEDDUW) structure. There is thus at least a 23.7 % natural occurrence of Z' > 1 structures for tyramine salts even when some variance in methods of counting unique molecules is considered.

Table 4. 1. Code of the tyramine salt forms with more than one cation per asymmetric unit. Subtitle for the colours: Yellow represents benzoates, green represent carboxylates, blue represents inorganic salt forms, red represents organic sulfonates, pink represents naphthalates and grey represent other salts that does not belong in those categories.

COMPOUND	Z'	COMPOUND	Z'	COMPOUND	Z'
2FB (MEDBII) [4]	2	CAP	2	SO4.2H2O (MOHBUH) [5]	2
2MALON.H2O	2	CLO4.H2O (MECYOK) [4]	2	TIOSA.wc	2
2NAPH	2	DLMAL.H2O	2	TYR.TYR.CL.H2O	2
2NB (MEDCAB) [4]	2	ETSO3 (MECZEB) [4]	2	UR.3H2O	2
2PH	2	H2NAPH	2	2OXA	4
4HBS.H2O (MECZUR) [4]	2	HBR.TYR	2	4HB (MEDFAE) [4]	4
4NB (MEDFIM) [4]	2	HEXA.H2O (MEDGOT) [4]	2	RTAR.4H2O	4
5C2NB	2	HIP	2	RTAR.wc	4
ASB.3H2O	2	LTAR.2H2O	2	TP.CCL4 (VISMOC) [3]	4
BZ (MEDBAA) [4]	2	MTOL (MEDCUV) [4]	2	4CB (MEDDUW) [4]	8

There is no obvious significant trend on formation of Z' > 1 structures according to the composition of the counterion. However, the presence of an extra cation occurs in 17.9 % of the carboxylates, 32.1 % of benzoates and 40.0 % of the inorganic compounds synthesised. Only 3 sulfonates have more than 1 cation per asymmetric unit representing 18.8 % of all sulfonates: ASB, ETSO3 (MECZEB) and 4HBS.H2O (MECZUR). In all cases, the percentage of formation of salt forms with more than one cation per asymmetric unit is greater than that found for general organic structures. A recent review gives an occurrence rate of 9% for general organic compounds and an even lower rate for organic salts [3]. Figure 4.1 illustrates the distribution of compounds with Z' = 1 (in blue), Z' = 2 (in orange), Z' = 4 (in grey) and Z' = 8 (in yellow). It is noted here that 12.5 % of all carboxylates (four compounds) have a free acid present in the structure. Interestingly all these co-crystal of sals are hydrated dicarboxylates: DLMAL.H2O, FUMCC.H2O, HEXA.H2O and TCIN.H2O.
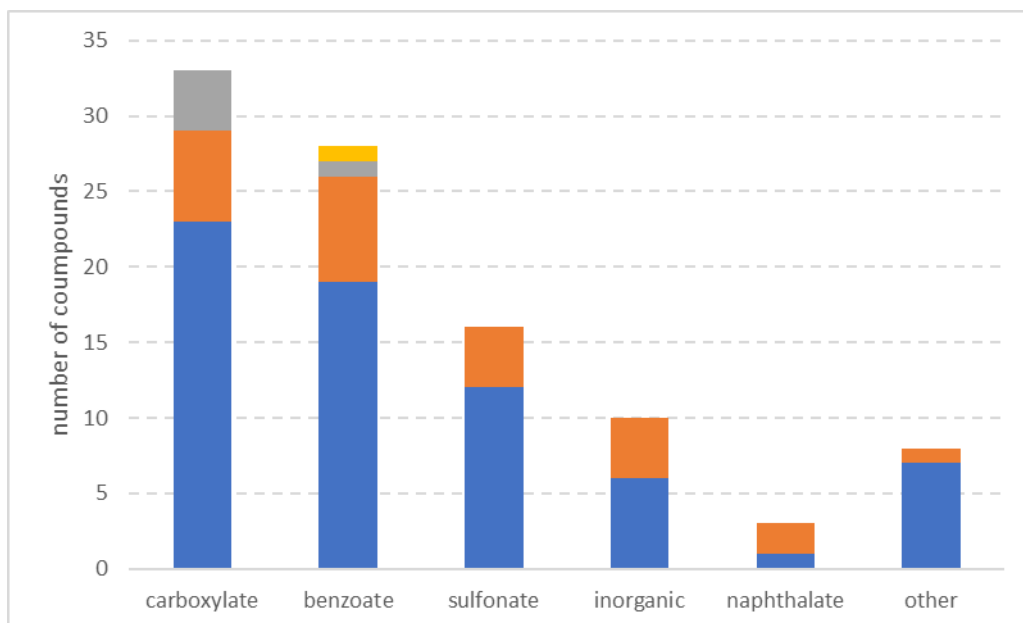
Figure 4. 1. Distribution of number of cations per asymmetric unit in the unit cell according to the composition of the counterion, where the boxes in blue represents Z' = 1, boxes in orange represents Z' = 2, boxes in grey represents Z' = 4 and the box in yellow represents the only compound with Z' = 8, TYR 4CB (MEDDUW). The carboxylate column includes 5 structures that are 2:1 salt forms.

4.2. METHYLEPHEDRINE SALT FORMS

Of all the ninety-two salt forms of enantiopure and racemic methylephedrine, eighteen had more than one independent cation or free base per asymmetric unit (Z' > 1). Of those, seventeen had the presence of two cations (Z'= 2) while one compound had the presence of three different cations (Z' = 3). This last structure was the orthorhombic salt form of enantiopure methylephedrine and methanesulfonate, *e*MESO3 (IVUNET). Of the compounds of enantiopure and racemic methylephedrine, twelve were previously published in the database [7-9]. Excluding the sample eZN.complex (NAHGUY), which have two neutral bases of enantiopure methylephedrine in the unit cell and four bases complexed with zinc, and the complex with dianion $CuCl_4^{2-}$, there is a 17.8 % natural occurrence of an extra cation in the unit cell for enantiopure and racemic salts even when some variance in methods of counting unique molecules is considered. However, when separating enantiopure and racemic compounds, 28.8 % of enantiopure compounds crystallise with an extra cation in the unit cell, while only two compounds of the racemic compounds have an extra cation per asymmetric unit, *r*4HBS.H2O (IVUSAU) and *r*RTAR (VAVMIR) representing 5.1 %. This last value

is in line with that given by the Steed and Steed [3] review for general organic salts. The 28.8 % value for enantiopure compounds is obviously greatly in excess of this.

Table 4. 2. Code of the salt forms with more than one cation per asymmetric unit for enantiopure methylephedrine, represented by "*e*" and racemic methylephedrine, represented by "*r*". Subtitle for the colours: Yellow represents benzoates, green represent carboxylates, blue represents inorganic salt forms, red represents organic sulfonates, pink represents naphthalates and grey represent other salts that does not belong in those categories.

COMPOUND	Z'	COMPOUND	Z'	COMPOUND	Z'
*e*3AB (VAVJAG) [7]	2	*e*CUCL4 (QIHREG) [6]	2	*e*MUC	2
*e*4CNDIA	2	*e*EDS (IVUMUI) [8]	2	*e*N2S.3H2O	2
*e*4HB (IVUSEY) [8]	2	*e*FUM	2	*r*4HBS.H2O (IVUSAU) [8]	2
*e*4NB (IVULOB) [8]	2	*e*I (IVURIB) [8]	2	*r*RTAR (VAVMIR) [7]	2
*e*4NPA	2	*e*MALON (IVUPIZ) [8]	2	*e*ZN_complex (NAHGUY) [7]	2
*e*ACLMBS.2H2O	2	*e*MESO3.2 (IVUNIX) [8]	2	*e*MESO3 (IVUNET) [8]	3

Again, there is no significant trend on formation of structures with more than one cation per asymmetric unit in methylephedrine salt forms according to the composition of the counterion. The presence of an extra cation occurs for enantiopure compounds in 35.7 % of the carboxylates, 18.8 % of benzoates, 20.0 % of inorganic compounds and 40.0 % of the sulfonates. This distribution does not match that found for tyramine salts. Figures 4.2 and 4.3 illustrates the distribution of compounds with Z' = 1 (in blue) and compounds with Z' = 1 (in orange) and Z' = 3 (in grey) according to the composition of the counterion for enantiopure methylephedrine salt forms (Figure 4.2) and racemic methylephedrine salt forms (Figure 4.3). It is important to note that that only one compound of methylephedrine had more than one free acid present in the unit cell, the *para*-nitrobenzoate salt form of racemic methylephedrine, *r*4NB (IVULUH).
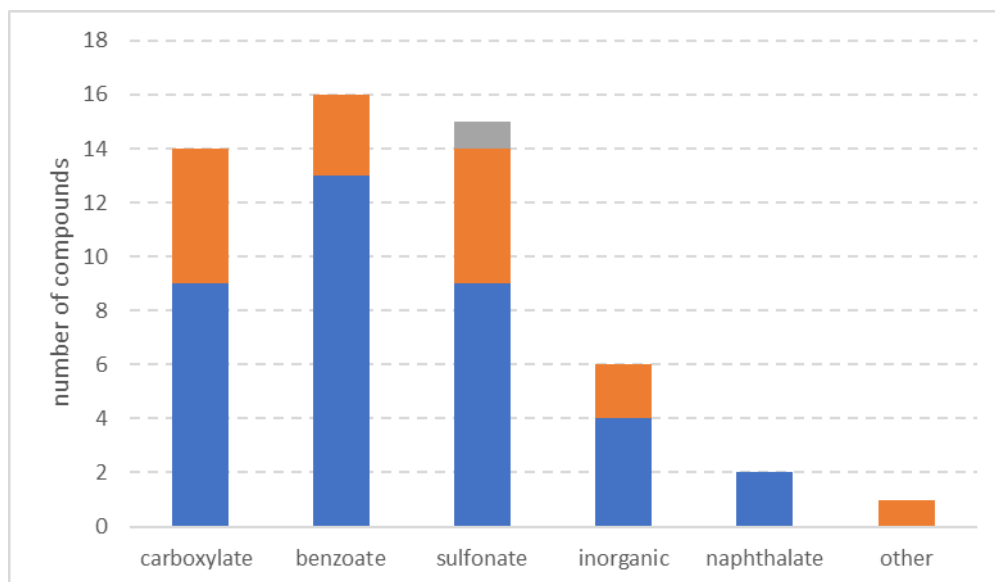
Figure 4. 2. Distribution of number of cations per asymmetric unit in the unit cell for enantiopure methylephedrine compounds according to the composition of the counterion, where the boxes in blue represents Z' = 1, boxes in orange represents Z' = 2, boxes in grey represents the only compound with Z' = 3, *e*MESO3 (IVUNET).
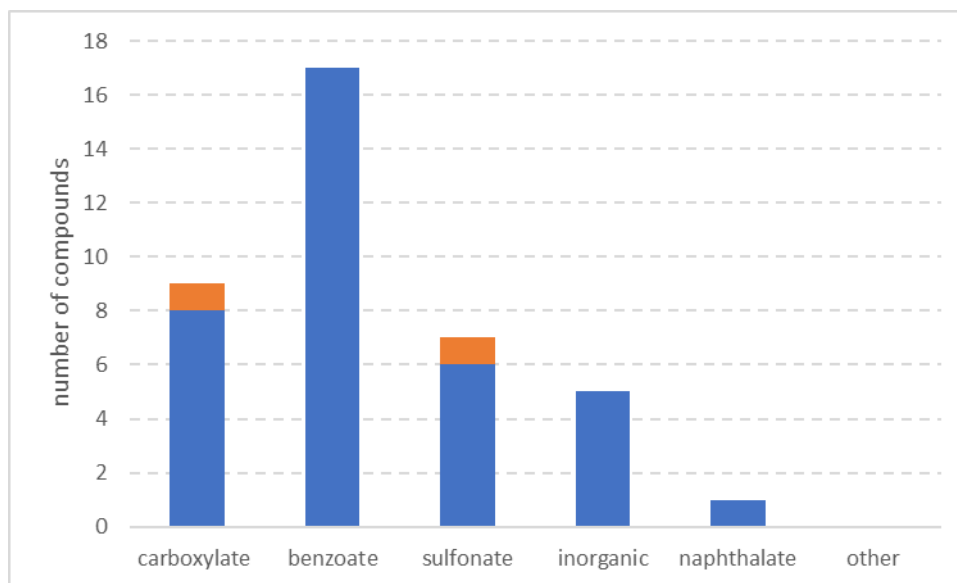
Figure 4. 3. Distribution of number of cations per asymmetric unit in the unit cell for racemic methylephedrine compounds according to the composition of the counterion. The boxes in blue represents Z' = 1 and boxes in orange represents Z' = 2.

4.3. EPHEDRINE SALT FORMS

For ephedrine salt forms, fifteen of the analysed eighty-seven compounds had more than one crystallographically independent cation per asymmetric unit (Z' = 1) present in the unit cell, with thirteen having the presence of two cations (Z'= 2) and two compounds having the presence of three different cations (Z' = 3). There were thirteen structures of ephedrine with Z' > 1 previously published in the database [10-19]. Of these structures, two compounds can be excluded from consideration as they were synthesised with carboxylic acids with more than one acidic site aiming to obtain more than one cation per asymmetric unit. These were EPD MUC and EPD 2TAR. Excluding also the salts with MCl_4^{2-} salt forms for any further calculation, there is a 11.5 % natural occurrence of Z' > 1 structures for ephedrine salts. Table 4.3 lists these compounds. Even when some variance in methods of counting unique molecules is considered, and despite the ephedrine structures being enantiopure, the same extremely high occurrence rate as found for enantiopure methylephedrine is not seen.

Table 4. 3. Code of the salt forms with more than one cation per asymmetric unit. Subtitle for the colours: Yellow represents benzoates, green represent carboxylates, blue represents inorganic salt forms, red represents organic sulfonates, pink represents naphthalates and grey represent other salts that does not belong in those categories.

COMPOUND	Z'	COMPOUND	Z'	COMPOUND	Z'
2MUC	2	HPO4.H2O (EPHEDP) [17]	2	PDCL4 (GEJDUX) [12]	2
ACE (GEHJAF) [12]	2	LTAR.3H2O (GEHLIP) [12]	2	PIN.2 (INEDOV) [16]	2
AHA.H2O (KITLUV) [14]	2	MAL.H2O (FIRHUM) [16]	2	TAR.H2O.3 (FIRJAU) [13]	2
AUCL4 (MEXVOC) [15]	2	MMBS	2	CDCL5.H2O (HUVXON) [18]	3
EDS (GEHJOT) [12]	2	NO3.2 (FIRJEY) [13]	2	I (ZZZSDC01) [12]	3

The presence of an extra cation occurs in 15.1 % of the carboxylates, 40.0 % of inorganic compounds synthesised, and 22.2 % of the sulfonates. Although there was no formation of benzoates with more than one cation per asymmetric unit, one sample

had the presence of a free acid molecule within the unit cell, 3NB.H2O. The other sample with the presence of an extra free acid molecule was the carboxylate MEC.1 (WANKOL). Figure 4.4 illustrates the distribution of compounds with Z' = 1 (in blue) and compounds with Z' =2 (in orange) and the two compounds with Z' = 3 (in grey), according to the composition of the counterion.
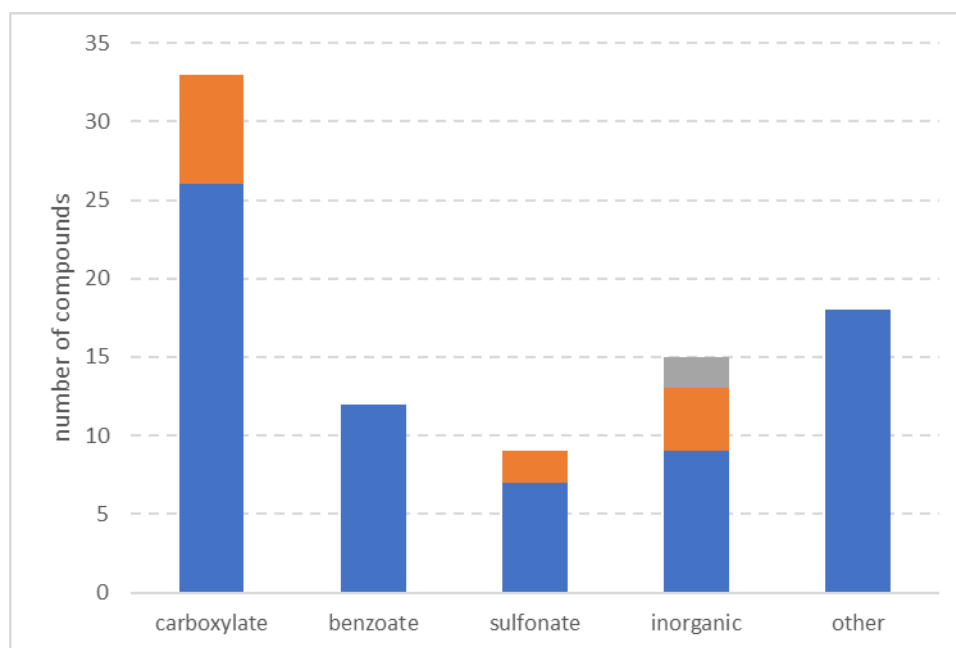
Figure 4. 4. Distribution of number of cations per asymmetric unit in the unit cell for enantiopure ephedrine compounds according to the composition of the counterion, where the boxes in blue represents Z' = 1, boxes in orange represents Z' = 2, boxes in grey represents Z' = 3.

4.4. CONCLUSIONS

This work analysed the presence of multiple cations in the asymmetric unit for two hundred and fifty-one salt forms of tyramine, enantiopure methylephedrine, racemic methylephedrine and ephedrine including compounds synthesised in this work or obtained from the CCDC database. The general formation of salt forms with a presence of an extra cation involves thirty compounds of tyramine, sixteen salt forms of enantiopure methylephedrine, two salt forms of racemic methylephedrine and fifteen salt forms of ephedrine.

There is a natural formation of Z' >1 structures in 20.2 % of the carboxylates, 23.8 % of the benzoates, 27.7 % of the sulfonates, 19.4 % of the inorganic compounds and 33.3 % of the naphthalates. However, these percentages are very variable for each individual base. Formation with two cations in the asymmetric unit (Z' = 2) is the most common formation of compounds with an extra cation, as can be observed in Figure 4.5, in orange, present in fifty-three salt forms. The less common formation of extra cations per asymmetric unit are, Z' = 4 present in five compounds, all of which are salt forms of tyramine: TYR 2OXA, TYR 4HB, TYR RTAR.4H2O, TYR RTAR.wc and TYR TP.CCL4 (Figure 4.5, in yellow), Z' = 3 present in three compounds: MEPD MESO3, EPD CDCL5.H2O and EPD I (Figure 4.5, in grey) and Z' = 8 present in one compound: TYR 4CB (Figure 4.5, in light blue).
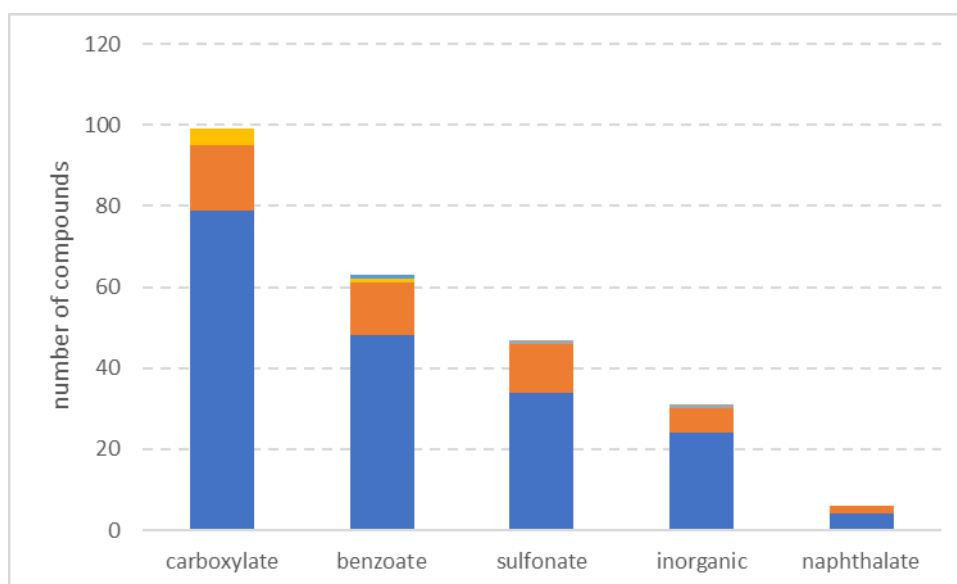
Figure 4. 5. General formation of an extra cation in the asymmetric unit according to the composition of the counterion. In blue are compounds with Z' = 1, in orange compounds with Z' = 2, in grey compounds with Z' = 3, in yellow compounds with Z' = 4 and in in light blue compounds with Z' = 8.

This variance is clearly far greater than that described for general structures by the Steed and Steed review [3] which gives an occurrence rate of 9% for general Z' > 1 structures and a lower occurrence rate of 6.5% for organic salt forms. Only the racemic methylephedrine salts give statistics like this review. Despite the lower occurrence

level given for organic salt forms over general structures in the review, multiple strong directional intermolecular interactions and relatively rigid species are given by Steed and Steed [3] as drivers towards Z' > 1 structures. Both these characteristics are present in tyramine, ephedrine and methylephedrine salt structures. To these drivers we tentatively add an enantiopure nature. Our compounds, especially the methyephedrine salts, show some evidence that enantiopure salts are much more likely to form Z'> 1 structures than their racemic equivalents.

4.5. REFERENCES

[1]   Infantes, L., Fabian, L. & Motherwell, W. D. S. (2007). CrystEng-Comm, 9, 65–71.

[2]   Cruickshank, L., Kennedy, A.R., & Shankland, N. (2013). Journal of Molecular Structure, 1051, 132-136.

[3]   Steed, K.M. & Steed,J.W. (2015). Chem. Rev. 115 (8), 2895–2933

[4]   Briggs, N., Kennedy, A., & Morrison, C. (2012). Acta Crystallographica Section B, 68(4), 453-464.

[5]   Koleva, B.B., Kolev, T., Seidel, R.W., Spiteller, M., Mayer-Figge, H. & Sheldrick W.S. (2008). Journal of Molecular Structure, 888(1), 138-144.

[6]   Rydz, A., Gryl, M., & Stadnicka, K. (2018). Acta Crystallographica Section C, 74(12), 1586-1594.

[7]   De Moraes, S.L., Edwards, D., Florence, A.J., Johnston, A., Johnston, B.F., Morrison, C.A., & Kennedy, A.R. (2017). Crystal Growth and Design, 17(6), 3277-3286.

[8]   Kennedy, A. R., Morrison, C. A., Briggs, N. E., & Arbuckle, W. (2011). Crystal Growth and Design, 11(5), 1821-1834.

[9]   Dan, W., Chen, J., Di, Y., Kong, Y., Wang, Q., Yang, W., & Wang, D. (2010). Chinese Journal of Chemistry, 28(7), 1097-1102.

[10]   Enders, D., Zhu, J., & Raabe, G. (1996). Angewandte Chemie International Edition in English, 35(15), 1725-1728.

[11]   Collier, E., Davey, R., Black, S., & Roberts, R. (2006). Acta Crystallographica Section B, 62(3), 498-505.

[12]   Babor M., Nievergelt, P.P., Cejka, J., Zvonicek, V. & Spingler B. (2019) IUCrJ
. 6, 145.

[13]   Li, B.-L., Zhang Z.-G., Wang W., Li, J. & Wang C.-W. (2008).
Z.Naturforsch.,B:Chem.Sci. 63, 77.

[14]   Wood, M.R. & Lalancette, R.A. (2013). Acta Crystallogr.,Sect.C:
Cryst.Struct.Commun., 69, 388.

[15]   Cooke, C. L., Davey, R. J., Black, S. G., Muryn, C., & Pritchard, R. (2010).
Crystal Growth and Design, 10(12), 5270-5278.

[16]   Hearn, R.A., Freeman, G.R. & Bugg, C.E. (1973). J.Am.Chem.Soc. 95, 7150.

[17]   Wang, D.-Q., Chen, J.-T., Dan, W.-Y., He, D.-H., Chen, Z.-P. & Di, Y. Y.
(2011), J.Chem.Soc.Pak. 33, 333.

[18]   Nievergelt, P.P., Babor, M., Cejka, J. & Spingler, B. (2018).Chemical Science.
9, 3716.

5. CONFORMATION OF THE CATION

5.1. TYRAMINE SALT FORMS

Two different types of cation conformation were previously described for 42 tyramine salt forms [1]. The difference between them involved the aliphatic chain of the cation. The two conformations were, the extended conformation with torsion angle between the C1, C7, C8 and N1 atoms ranging "from 169.2 (2) ° in the iodide salt to 172.3 (9) ° in the *p*-toluate salt", and the folded conformation with torsion angle for the same atoms of ranging "from 61.4 (2) ° for the adipate monohydrate salt to 67.6 (7) ° for one of the crystallographically unique cations in the 4-nitrobenzoate salt" [1]. The relevant torsion angles are illustrated in Fig. 5.1 and the two conformation types in Fig. 5.2. In the current work, the representation of each conformation of tyramine molecule will not be limited to the single torsion angle (C1-C7-C8-N1) but it will also include both torsion angles involving the two methylene carbons and the two subsequent aromatic carbons in the ring (C6-C1-C7-C8 and C2-C1-C7-C8). It will give all torsion angles as positive values, related to a clockwise rotation [2]. An example of the torsion angles used to analyse the cation conformation of the tyramine molecule in the salt PTS is observed in Figure 5.1. In green is highlighted the C1-C7-C8-N1 torsion angle, in orange is highlighted the C6-C1-C7-C8 torsion angle and in blue is highlighted the torsion angle C2-C1-C7-C8.
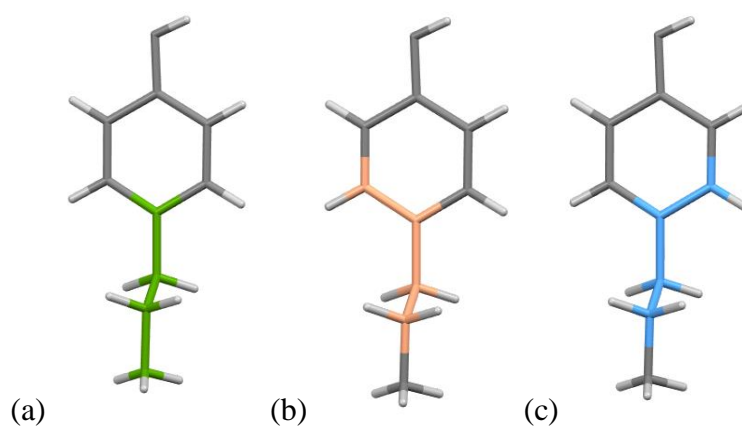
Figure 5. 1. Example of torsion angles used to analyse the cation conformation of the tyramine molecule in the salt PTS. In green is highlighted the C1-C7-C8-N1 torsion angle, in orange is highlighted the C6-C1-C7-C8 torsion angle and in blue is highlighted the torsion angle C2-C1-C7-C8.

In total, there are one hundred and forty-four tyrammonium cations present in the ninety-eight structures analysed in this work. Analysing the three torsion angles related to the aliphatic chain, confirms that the tyrammonium cation can have one of two basic conformations, folded (Figure 5.2-a) and extended (Figure 5.2-b).
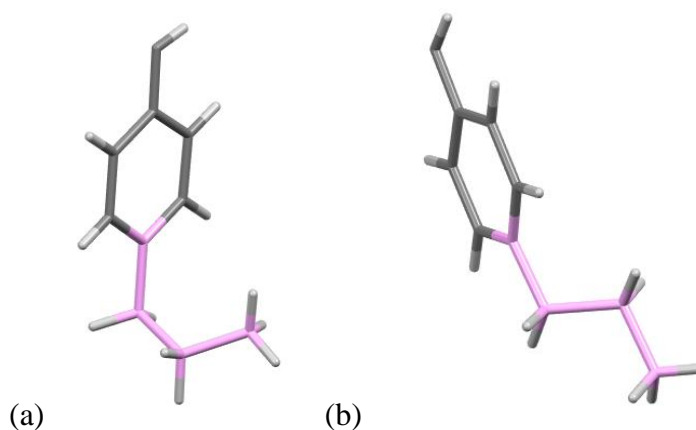
Figure 5. 2. Folded conformation of tyrammonium cations in MMBS salt (a) and extended conformation in 2HB salt (b).

The less common folded conformation was observed in twenty cations. The range of the torsion angle C1-C7-C8-N1 varies, in modulus, between 54.6 (8)° in the salt CNB.2H2O (RUQSOM) to 71.4 (4)° in the salt HOB (XOKSAT). The other two

torsion angles (C2-C1-C7-C8 and C6-C1-C7-C8) in this cation conformation also give relatively tight distributions indicating that the NH_3 group prefers a *gauche* type relationship with the ring plane. Figure 5.3 represents the range of torsion angle for the angles C1-C7-C8-N1 (in blue), C2-C1-C7-C8 (in red) and C6-C1-C7-C8 (in grey).

The extended conformation is the most common conformation for tyrammonium salts being adopted by one hundred and fourteen cations with range of C1-C7-C8-N1 torsion angles, in modulus, between 161.6 (8) ° in one of the cations of the sample 2OXA to 179.9 (2) ° in the disordered cation of the sample ETSO3 (MECZEB). This reflects the original paper's analysis where the extended conformation was also found to be much more common than the folded conformation. Figure 5.4 shows the range of torsion angles for C1-C7-C8-N1 (in blue), C2-C1-C7-C8 (in red) and C6-C1-C7-C8 (in grey).
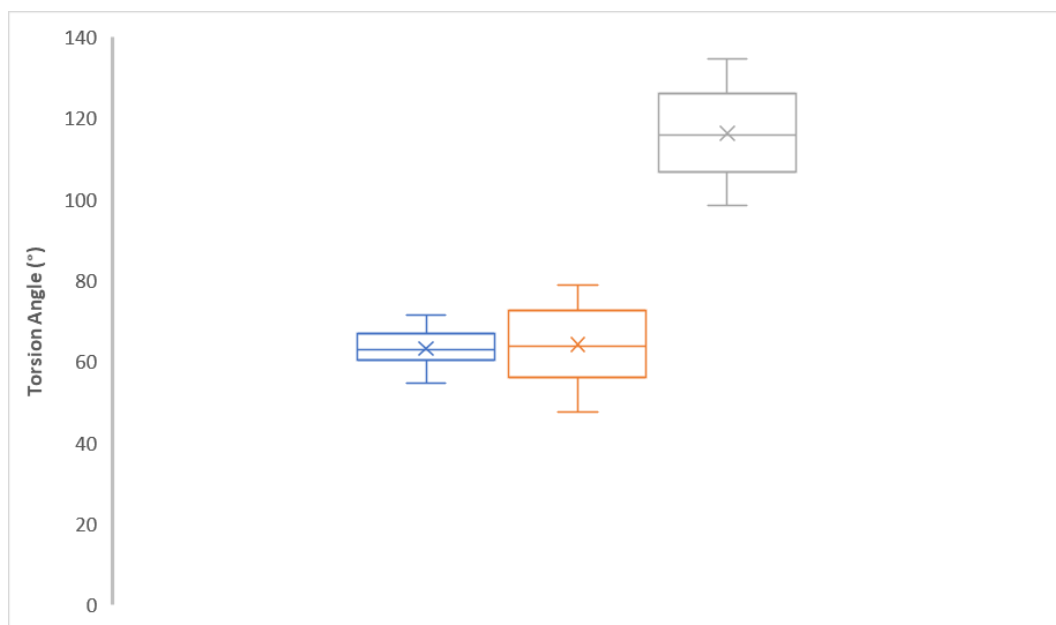
Figure 5. 3. Variation in the torsion angle for the folded conformation. The boxplot in blue represents the torsion angle range for aliphatic chain related to C1-C7-C8-N1 atoms, the boxplot in orange represent the torsion angle between the aromatic carbons C2 and C1, and the aliphatic atoms C7 and C8 and the boxplot in grey represents C6-C1-C7-C8 atoms**.**
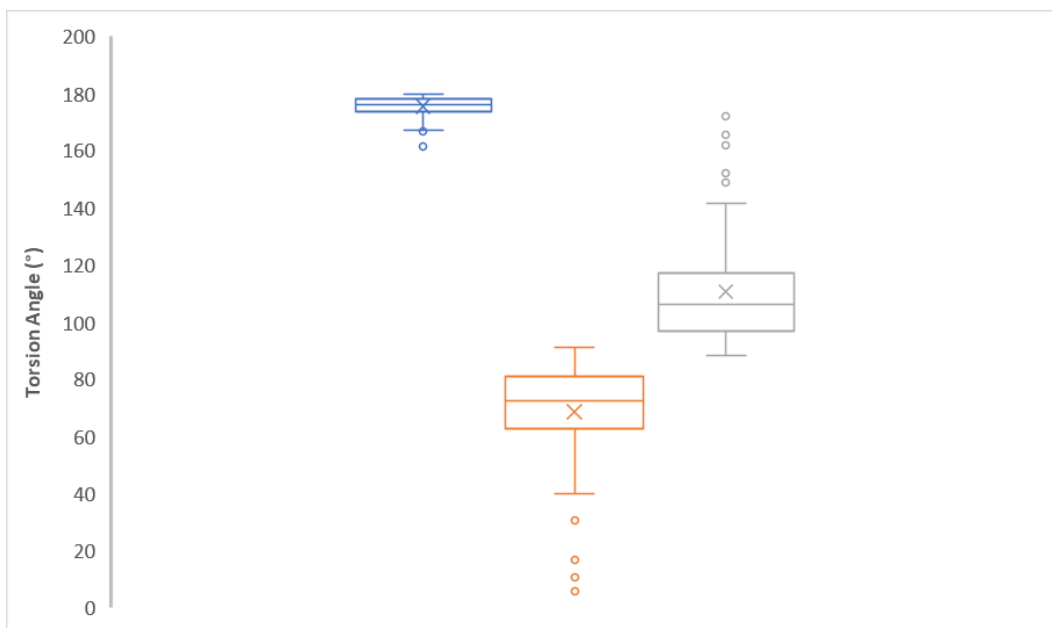
Figure 5. 4. Variation in the torsion angle for the extended conformation. The boxplot in blue represents the torsion angle range for aliphatic chain related to C1-C7-C8-N1 atoms, the boxplot in orange represent the torsion angle between the aromatic carbons C2 and C1, and the aliphatic atoms C7 and C8 and the boxplot in grey represents C6-C1-C7-C8 atoms.

In Figure 5.4 it is easier to observe the presence of outliers in both torsion angles involving the two methylene carbons and two aromatic carbons in the ring. Further analysis of the outliers in Figure 5.4, with torsion angle C2-C1-C7-C8 lower than 35 ° and torsion angle C6-C1-C7-C8 correspondingly higher than 145 °, show that although the aliphatic chain conformation is the same, the aromatic ring can be in one of two different positions. Thus, two sub-classes of the common extended conformation have now been identified. The more common class has gauche type relationships between the NH_3 and the ring plane (labelled α) whilst the outliers form a class with eclipsed or near-eclipsed relationships (labelled β). These can be observed in Fig. 5.5.
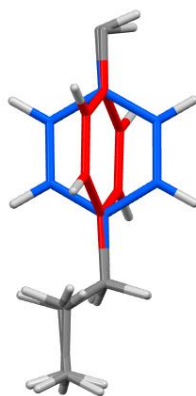
Figure 5. 5. Structure overlay of the sample PH (in blue) with extended conformation α and the sample 4CBS (in red) with extended conformation β

Of the thirty structures with two independent tyramine fragments present in this work only MTOL (MEDCUV) had both extended and folded conformations in the same structure. It is interesting to note that five structures had both α and β extended conformations in the unit cell: two carboxylates [(2OXA and HIP)], two sulfonates [ETSO3 (MECZEB) and 4HBS.H2O (MECZUR)] and one benzoate [4HB (MEDFAE)]. As this last observation might suggest, there is no obvious relationship between conformational type observed and chemical class. A summary of the range of torsion angles can be observed in table 5.1, where n is the number of cations with the conformation, Min is the minimum value of torsion angle and Max is the maximum value of torsion angle. All values of torsion angles for tyramine salt forms can be observed in APPENDIX 5.1.

Table 5. 1. Summary of torsion angles for tyramine salts, where n is the number of cations with the conformation, Min is the minimum value of torsion angle and Max is the maximum value of torsion angle.

	n	Torsion Angle	Min (°)	Max (°)	Average (σ_{TA}) / °
Extended conformation (α)	114	C1-C7-C8-N1	161.6	179.9	175 (3)
		C2-C1-C7-C8	39.8	91.2	73 (12)
		C6-C1-C7-C8	89.4	141.8	107 (13)
Folded conformation	20	C1-C7-C8-N1	54.6	71.4	63 (5)
		C2-C1-C7-C8	47.7	79.0	64 (10)
		C6-C1-C7-C8	98.6	134.7	116 (12)
Extended conformation (β)	10	C1-C7-C8-N1	169.3	179.9	176 (4)
		C2-C1-C7-C8	5.8	32.8	21 (9)
		C6-C1-C7-C8	148.8	172.1	159 (8)

5.2. METHYLEPHEDRINE SALT FORMS

As reported by Kennedy *et al.* [3] three different types of cation conformation were previously observed for thirty-seven methylephedrinium salt forms. In that paper, the difference between them was defined using four different torsion angles involving the aliphatic chain of the cation generating three different conformations: Conformation (a) with a torsion angle C7-C8-N1-H1N range from 26.27 ° in the sample *e*4NB (IVULOB) to 63.75 ° in the sample *r*BR (ZZZFCS02), conformation (b) with torsion angle C7-C8-N1-H1N range from 67.19 ° in the sample *r*BS (IVUMOC) to 91.29 ° in the sample *r*MALE (IVUPEV) and conformation (c) with torsion angle C7-C8-N1-H1N range from 170.62 ° in the sample *e*PTOL (IVUSOI) to 175.65 ° in the sample *e*EDS (IVUMUI). All torsion angle values were kept positive to facilitate analysis and visualisation.

In the current work, the representation of each conformation of methylephedrine molecule will not be limited to the four torsion angles described by Kennedy *et al.* An example of the torsion angles used to analyse the cation conformation of the methylephedrine molecule in the salt *r*MUC is observed in Figure 5.7 where, the torsion angles described by Kennedy *et al.* were: C1-C7-C8-N1 (Figure 5.7 (a), in light green), O1-C7-C8-C9 (Figure 5.7 (g), in light pink), O1-C7-C8-N1 (Figure 5.7 (h), in pink) and C7-C8-N1-H1N (Figure (k), in dark purple); but also include ten other torsion angles in the description of the methylephedrinium cation: C1-C7-C8-C9

(Figure 5.7 (b), in green), C6-C1-C7-C8 (Figure 5.7 (c), in light orange), C6-C1-C7-O1 (Figure 5.7 (d), in orange), C2-C1-C7-C8 (Figure 5.7 (e), in light blue), C2-C1-C7-O1 (Figure 5.7 (f), in blue), C7-C8-N1-C10 (Figure 5.7 (i), in light purple), C7-C8-N1-C11 (Figure 5.7 (j), in purple), C9-C8-N1-C10 (Figure 5.7 (l), in light red), C9-C8-N1-C11 (Figure 5.7 (m), in red) and C9-C8-N1-H1N (Figure 5.7 (n), in dark red).

In total, there are one hundred and nine cations of enantiopure and racemic methylephedrine present in the ninety-two structures analysed in this work. Some considerations were made to analyse equivalents torsion angles of the aliphatic chain of methylephedrine cations:

(i)   For the equivalent pairs of torsion angles involving aromatic carbons and aliphatic carbons [C6-C1-C7-C8 (Figure 5.7 - c) and C2-C1-C7-C8 (Figure 5.7 - e)], higher values of torsion angles were related to the aromatic carbon atom nearest (*syn* to) the hydroxyl group (torsion angle C2-C1-C7-C8). Thus, the values of higher and lower torsion angles were separated according to the position of this aromatic atoms: Lower values of torsion angles related to torsion C6-C1-C7-C8 and higher values of torsion angles related to torsion C2-C1-C7-C8. The same steric effect occurs in another otherwise equivalent pair of torsion angles involving aromatic atoms, [C6-C1-C7-O1 (Figure 5.7 - d) and C2-C1-C7-O1 (Figure 5.7 - f)] where higher values of torsion angle were related to torsion C6-C1-C7-O1 and lower values of torsion angles were related to C2-C1-C7-O1.

(ii)   To avoid mistakes regarding to label of C10 and C11 atoms, the two equivalent torsion angles C7-C8-N1-C11 (Figure 5.7 - i) and C7-C8-N1-C10 (Figure 5.7 - j) were separated where higher values of torsion angles were situated in the torsion C7-C8-N1-C11. The same occur with the equivalent torsion angles C9-C8-N1-C10 (Figure 5.7 - l) and C9-C8-N1-C11 (Figure 5.7 - m).

The torsion angle ranges of (i) above and of several other torsion angles were found to have relatively tight spreads between values of minimum and maximum torsion angle.

These relatively invariant spreads are illustrated in Figure 5.6 but are not considered further.

The six remaining torsion angles involve the aliphatic carbon C7 or methyl carbon C9, the nitrogen atom N1, both methyl atoms bonded with the nitrogen C10 and C11 and the proton bonded to the nitrogen atom H1N, four have a significant variance which confirms the presence of different torsion angle groupings as can be observed in Figure 5.8. C9-C8-N1-C10 (Figure 5.8 – in dark grey) and C7-C8-N1-C10 (Figure 5.8 – in light brown) have limited ranges and again, both torsion angles will be ignored from further analysis. The torsion angles C9-C8-N1-C11 (Figure 5.8 – in petrol blue), C9-C8-N1-H1N (Figure 5.8 – in dark green), C7-C8-N1-C11 (Figure 5.8 – in light purple) and C7-C8-N1-H1N (Figure 5.8 – in light orange) thus define the conformation of the methylephedrine cation.
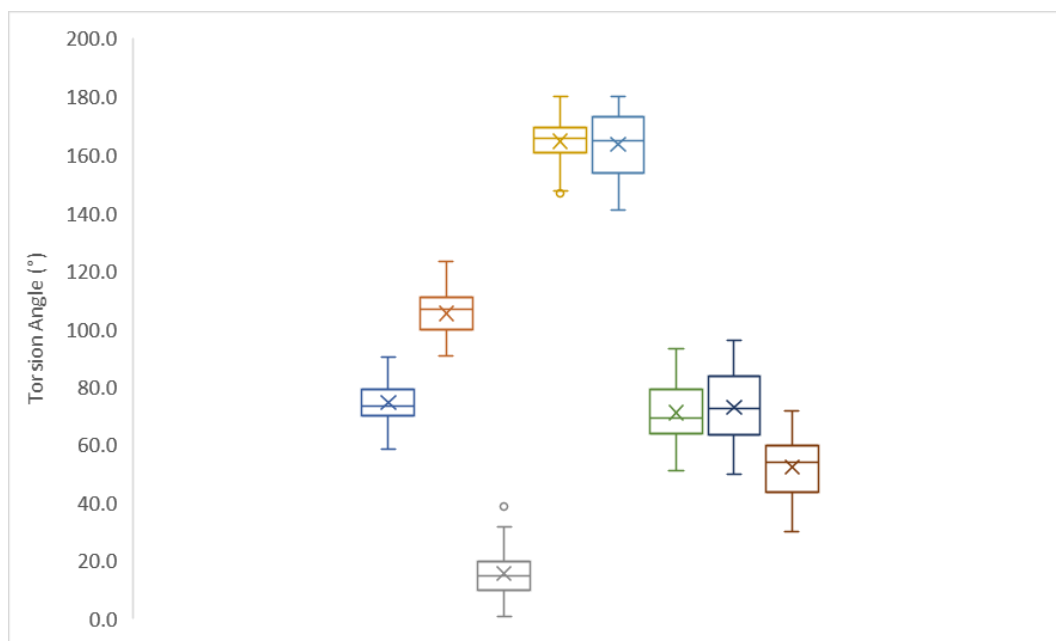
Figure 5. 6. Torsion angles with low variation of the atoms position. In blue is C6-C1-C7-C8, in orange is C2-C1-C7-C8, in grey is C2-C1-C7-O1, in yellow is C6-C1-C7-O1, in light blue is C1-C7-C8-N1, in green is C1-C7-C8-C9, in dark blue is O1-C7-C8-N1 and in brown is O1-C7-C8-C9.
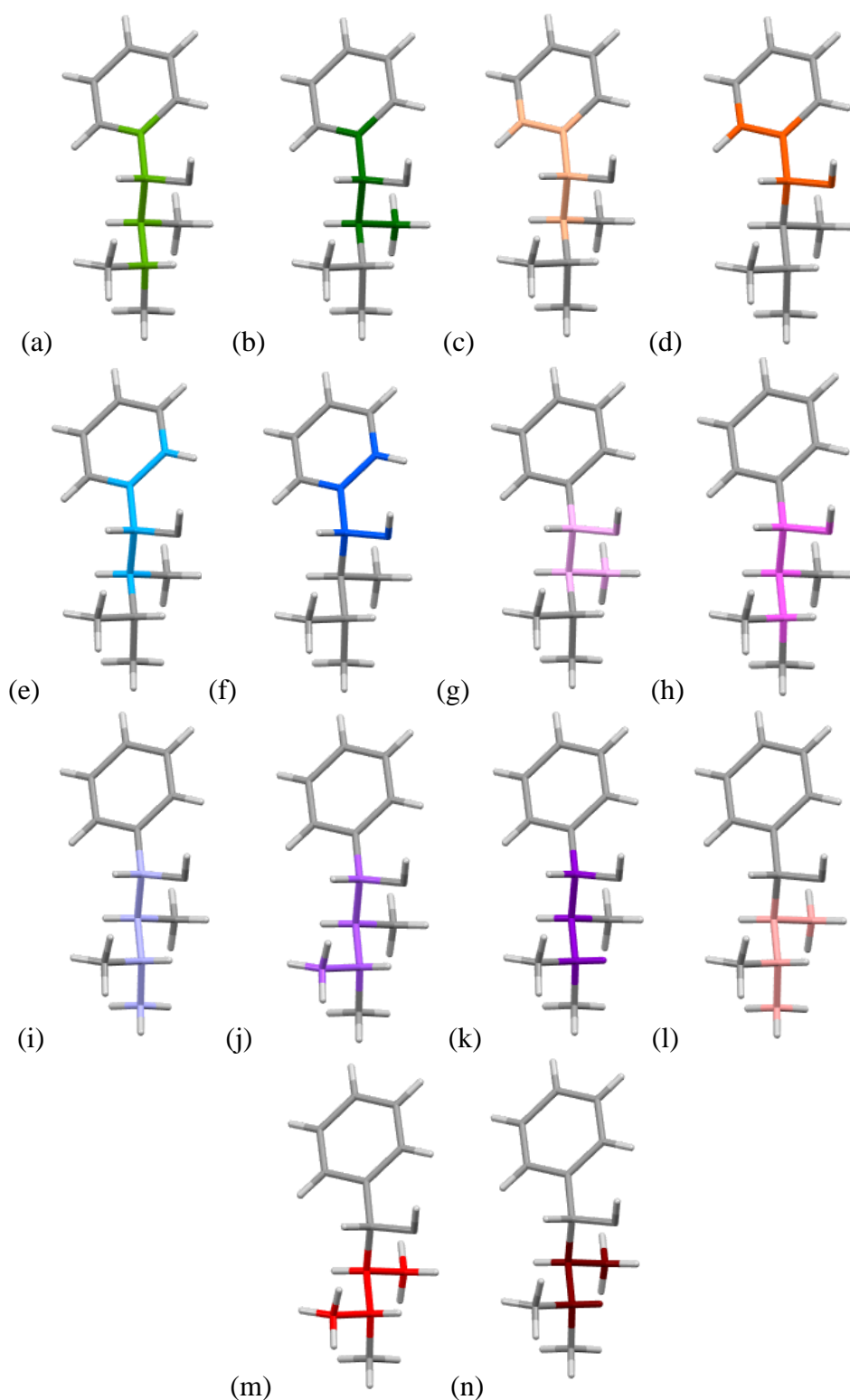
Figure 5. 7. In light green (a) is the C1-C7-C8-N1 torsion angle, in green (b) is the C1-C7-C8-C9 torsion angle, in light orange (c) is the C6-C1-C7-C8 torsion angle, in orange (d) is the C6-C1-C7-O1 torsion angle, in light blue (e) is the torsion angle C2-C1-C7-C8, in blue (f) is the torsion angle C2-C1-C7-O1, in light pink (g) is the torsion angle O1-C7-C8-C9, in pink (h) isthe torsion angle O1-C7-C8-N1, in light purple (i) is the torsion angle C7-C8-N1-C10, in purple (j) is the torsion angle C7-C8-N1-C11, in dark purple (k) is the torsion angle C7-C8-N1-H1N, in light red (l) is the torsion angle C9-C8-N1-C10, in red (m) is the torsion angle C9-C8-N1-C11 and in dark red (n) is the torsion angle C9-C8-N1-H1N.
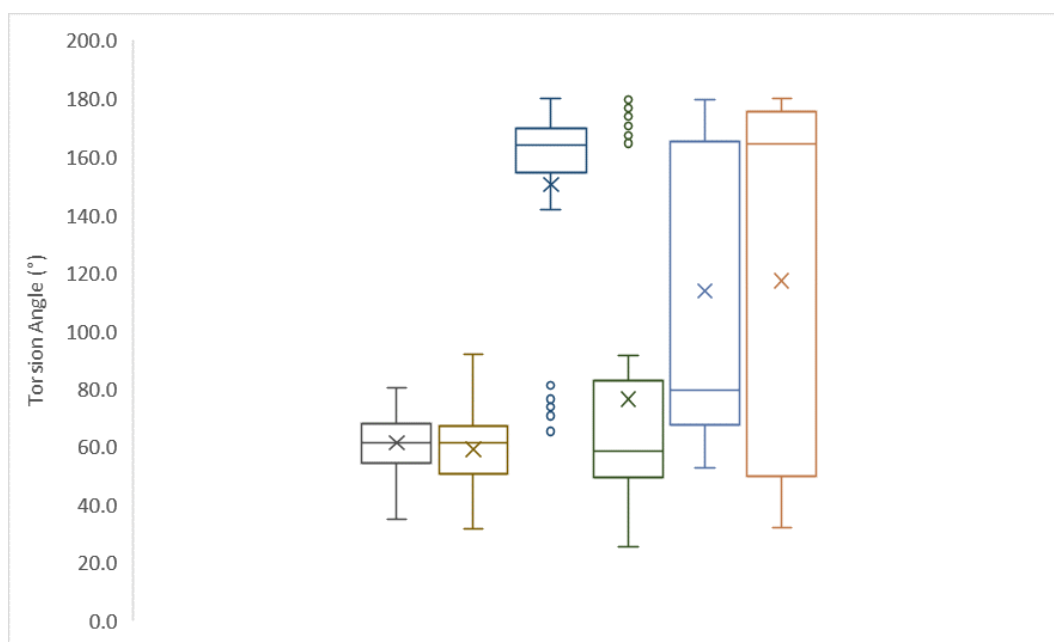
Figure 5. 8. Torsion angles involving the protonated amino group where in dark grey is C9-C8-N1-C10, in light brown is C7-C8-N1-C10, in petrol blue is C9-C8-N1-C11, in dark green is C9-C8-N1-H1N, in light purple is C7-C8-N1-C11 and in light orange is C7-C8-N1-H1N.

Analysing the torsion angles C9-C8-N1-C11, C9-C8-N1-H1N, C7-C8-N1-C11 and C7-C8-N1-H1N there are three possible conformations the methylephedrine cation can obtain: conformation (α), (β) and (γ), as observed in Figure 5.9, in blue. The distribution of conformation (α), conformation (β) and conformation (γ) can be observed in Figures 5.10 to 5.12, respectively. The most common conformation for methylephedrine cations was conformation (γ), present in 55.0 % of the cations analysed, followed by conformation (α), present in 29.4 % of the cations and conformation (β), present in 15.6 % of the cations. As observed by Collier *et al.* [4] for ephedrine cations, conformation (γ) has an intramolecular hydrogen bond between the protonated amino group and the hydroxyl. A summary of the torsion angles involved in these conformations can be observed in Table 5.2. This presents a more detailed and nuanced description than presented previously [3] for enantiopure and racemic methylephedrinium salt forms. Of the seventeen structures with two or more independent methylephedrine cations present in this work, four compounds had two different conformations in the crystal structure. All were salt forms of enantiopure methylephedrine: *e*EDS (IVUMUI) and *e*ACLMBS had both conformations (α) and (β), *e*CUCL4 (QIHREG) had both conformations (β) and (γ) and *e*4HB (IVUSEY) had

both conformations (α) and (γ). As observed for tyramine salt forms, there is no obvious relationship between conformational type observed and chemical class of the counterions. All values of torsion angles for methylephedrine salt forms can be observed in APPENDIX 5.2.

(α)   (β)   (γ)
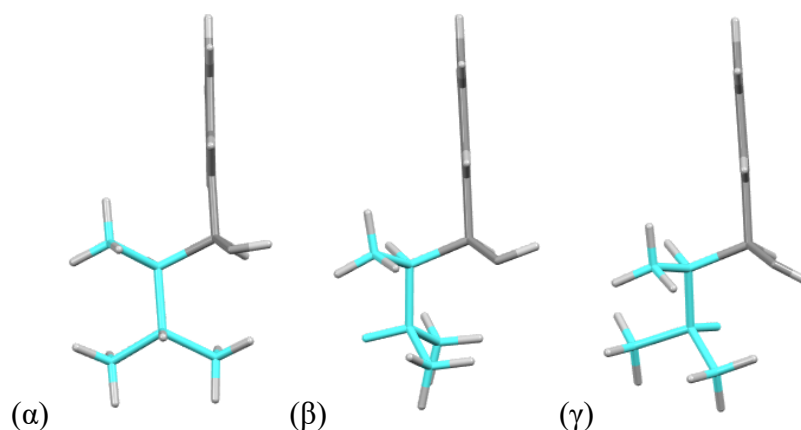
Figure 5. 9. Conformations (α), (β) and (γ) for the methylephedrine salt forms where (α) is the cation for the sample MEPD 4CBS, (β) is the cation of the sample MEPD 4FB and (γ) is the cation of the sample *r*5C2NB.
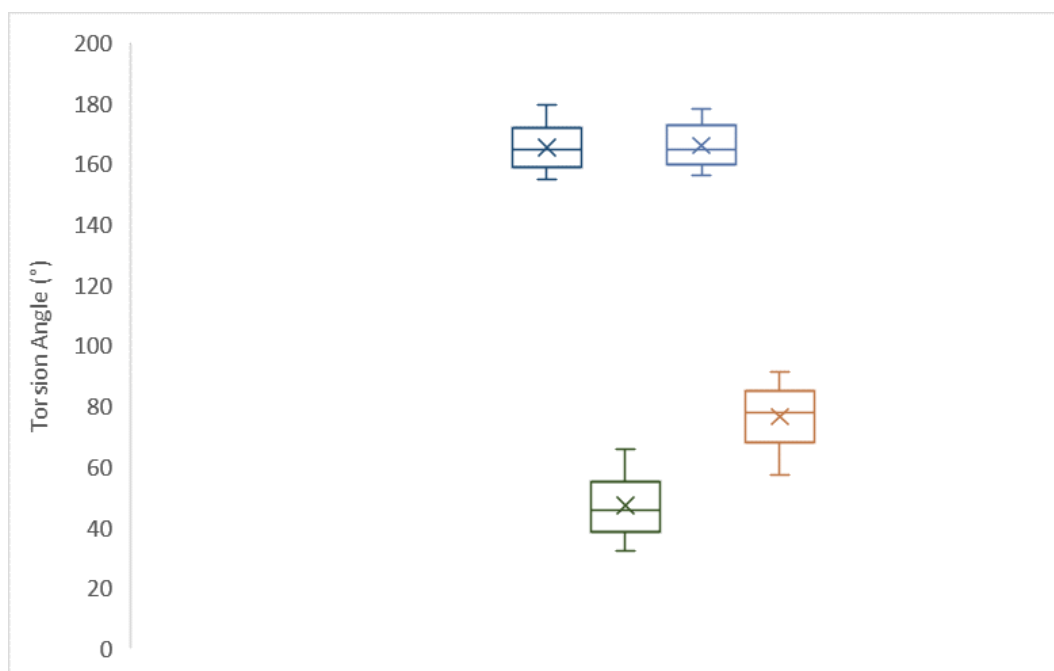
Figure 5. 10. Torsion angles involved in MEPD conformation (α) where in petrol blue is C9-C8-N1-C11, in dark green is C9-C8-N1-H1N, in light purple is C7-C8-N1-C11 and in light orange is C7-C8-N1-H1N.
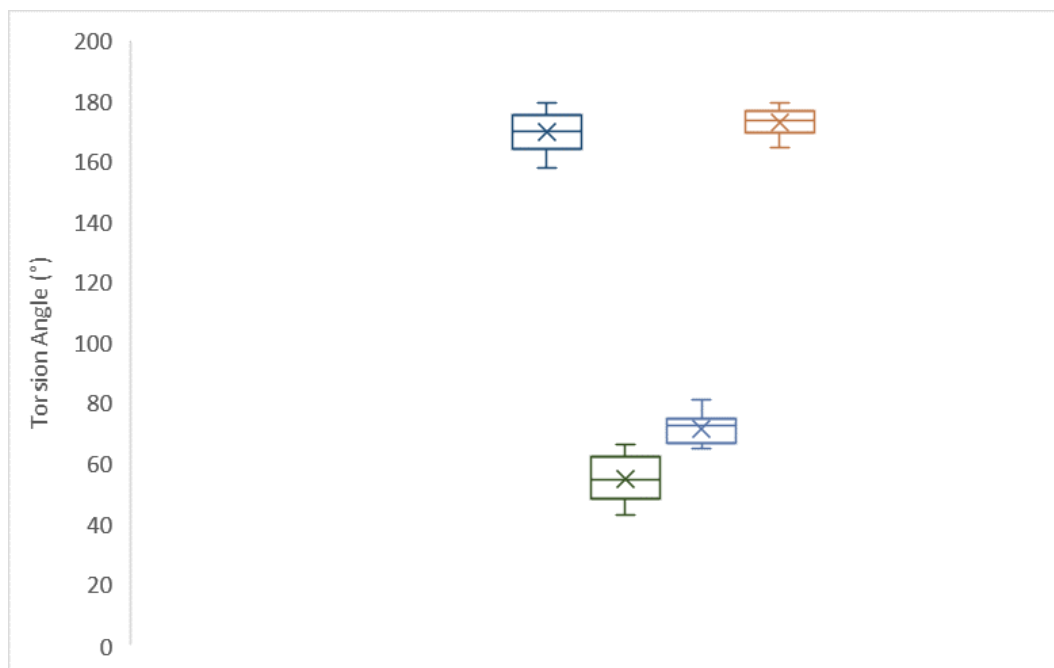
Figure 5. 11. Torsion angles involved in MEPD conformation (β) where in petrol blue is C9-C8-N1-C11, in dark green is C9-C8-N1-H1N, in light purple is C7-C8-N1-C11 and in light orange is C7-C8-N1-H1N.
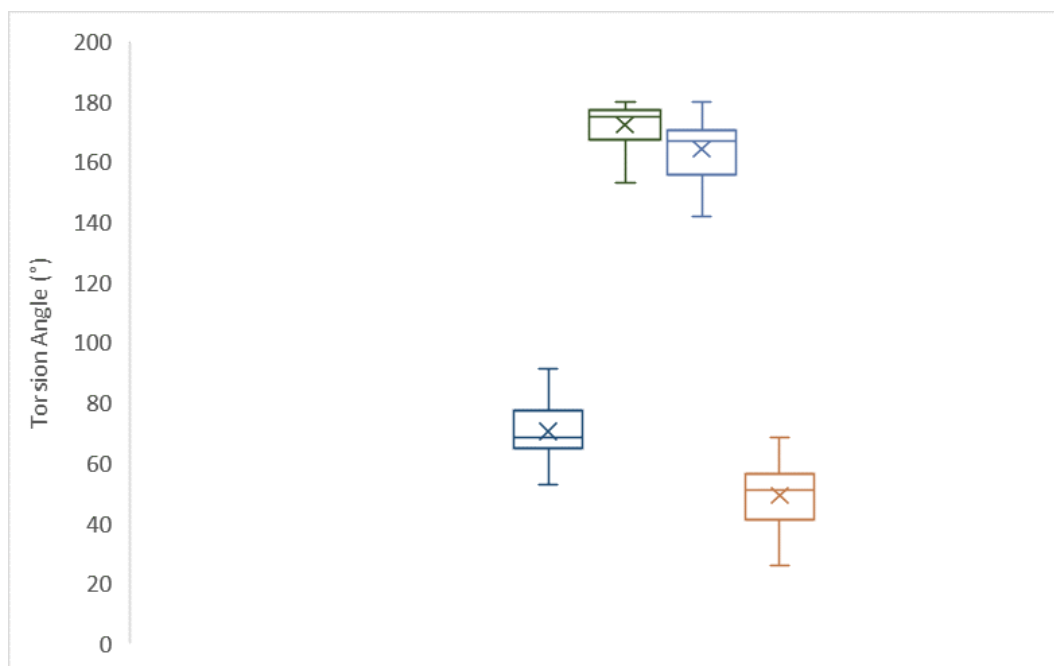
Figure 5. 12. Torsion angles involved in MEPD conformation (γ) where in petrol blue is C9-C8-N1-C11, in dark green is C9-C8-N1-H1N, in light purple is C7-C8-N1-C11 and in light orange is C7-C8-N1-H1N.

Table 5. 2. Summary of torsion angles for methylephedrine salts, where n is the number of cations with the conformation, Min is the minimum value of torsion angle and Max is the maximum value of torsion angle.

	n	Torsion Angle	Min (°)	Max (°)	Average (σ_{TA}) / °
Conformation (α)	32	C9-C8-N1-C11	52.9	91.3	70 (8)
		C9-C8-N1-H1N	153.0	179.8	172 (7)
		C7-C8-N1-C11	141.8	179.9	164 (9)
		C7-C8-N1-H1N	25.6	68.3	49 (10)
Conformation (β)	17	C9-C8-N1-C11	158.1	179.7	170 (7)
		C9-C8-N1-H1N	43.0	66.5	55 (7)
		C7-C8-N1-C11	65.3	81.2	72 (4)
		C7-C8-N1-H1N	164.5	179.6	173 (4)
Conformation (γ)	60	C9-C8-N1-C11	154.9	179.5	165 (7)
		C9-C8-N1-H1N	32.2	65.6	47 (9)
		C7-C8-N1-C11	156.2	178.3	166 (7)
		C7-C8-N1-H1N	57.0	91.3	76 (9)

5.3. EPHEDRINE SALT FORMS

As observed by Collier et al. [4-5] for seventeen salt forms of ephedrine, there are two known conformations for ephedrinium cations involving the atoms illustrated in Figure 5.13. The first torsion angle involved, Figure 5.13 (a) is related to the aromatic carbon, aliphatic carbons and the oxygen atom [C2-C1-C7-O1] and labelled as τ^1, the second torsion angle, labelled as τ^2 (Figure 5.13, b), involves the atoms O1-C7-C8-N1 and the third torsion angle, labelled as τ^3 (Figure 5.13, c), involves the atoms C7-C8-N1-C10. From the work by Collier et al. [4] the two conformations are almost equally likely with the extended conformation present in eight salt forms, while the folded conformation is present in the nine remaining. A summary of the results for torsion angles observed by Collier et al. [4] can be observed in Table 5.3, where all values of torsion angles are in modulus. A similar analysis made for methylephedrine salt forms in Chapter 5.2 will be done in this chapter for ephedrine salt forms. Again, this work will not be limited to the three conformations observed by Collier et al. [4] but for the fourteen torsion angles observed involving the aliphatic atoms in the molecule.

Table 5. 3. Summary of torsion angle observed in the work of Collier *et al.* [4], where n is the number of cations with the conformation, Min is the minimum value of torsion angle and Max is the maximum value of torsion angle.

	n	Torsion Angle	Min (°)	Max (°)
Extended Conformation	8	τ^1 (C2-C1-C7-O1)	5.6	23.7
		τ^2 (O1-C7-C8-N1)	60.0	73.7
		τ^3 (C7-C8-N1-C10)	163.7	178.1
Folded Conformation	9	τ^1 (C2-C1-C7-O1)	16.8	25.8
		τ^2 (O1-C7-C8-N1)	50.0	59.1
		τ^3 (C7-C8-N1-C10)	49.1	72.3

(a)   (b)   (c)
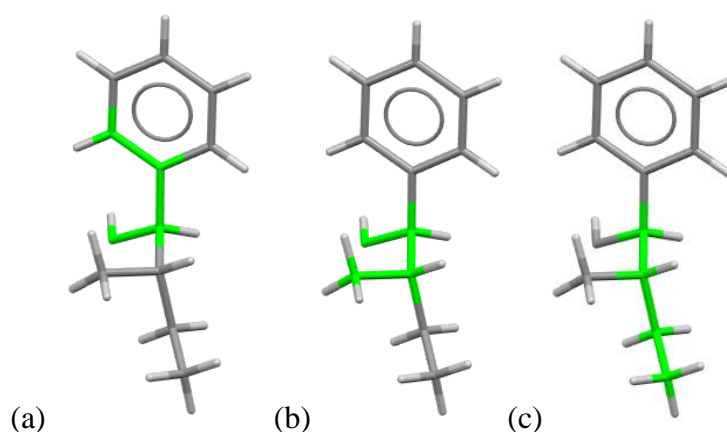
Figure 5. 13. (a) τ^1 involving the atoms C2-C1-C7-O1 (b) τ^2 involving the atoms O1-C7-C8-N1 and (c) τ^3 involving the atoms C7-C8-N1-C10 for the sample OPC.H2O (FIRGUL).

An example of the torsion angles used to analyse the cation conformation of the ephedrine molecule in the salt 4CB is observed in Figure 5.14 where, the torsion angles described by Collier *et al.* [4] were: C2-C1-C7-O1 (Figure 5.14 (b), in pink), O1-C7-C8-N1 (Figure 5.14 (g), in light orange) and C7-C8-N1-C10 (Figure 5.14 (i), in light purple). The remaining eleven torsion angles that will be analysed in this work are described as follows: C6-C1-C7-O1 (Figure 5.14, a - in light pink); C6-C1-C7-C8 (Figure 5.14, c - in light blue); C2-C1-C7-C8 (Figure 5.14, d - in blue); C1-C7-C8-N1 (Figure 5.14, e - in light green); C1-C7-C8-C9 (Figure 5.14, f - in green); O1-C7-C8-C9 (Figure 5.14, h - in orange); C9-C8-N1-C10 (Figure 5.14, j - in purple); C7-C8-N1-H1NA (Figure 5.14, k - in light yellow); C7-C8-N1-H1NB (Figure 5.14, l - in yellow); C9-C8-N1-H1NA (Figure 5.14, m - in light brown); and C9-C8-N1-H1NB (Figure 5.14, n - in brown).
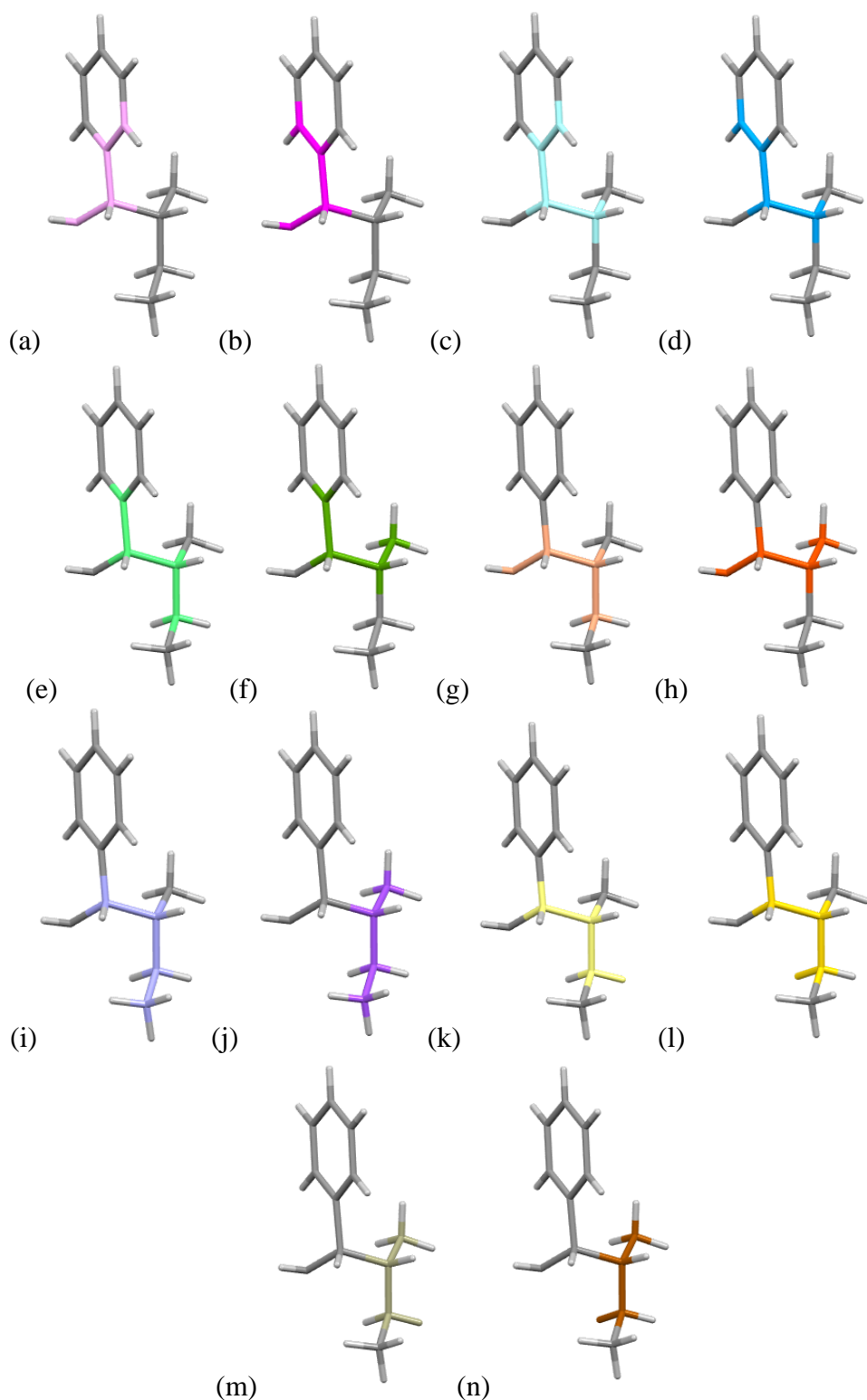
Figure 5. 14. (a) in light pink isthe torsion angle C6-C1-C7-O1; (b) in pink is the torsion angle C2-C1-C7-O1; (c) in light blue is the torsion angle C6-C1-C7-C8; (d) in blue is the torsion angle C2-C1-C7-C8; (e) in light green is the torsion angle C1-C7-C8-N1; (f) in green is the torsion angle C1-C7-C8-C9; (g) in light orange is the torsion angle O1-C7-C8-N1; (h) in orange is the torsion angle O1-C7-C8-C9; (i) in light purple is the torsion angle C7-C8-N1-C10; (j) in purple is the torsion angle C9-C8-N1-C10; (k) in light yellow is the torsion angle C7-C8-N1-H1NA; (l) in yellow is the torsion angle C7-C8-N1-H1NB; (m) in light brown isthe torsion angle C9-C8-N1-H1NA; and (n) in brown is the torsion angle C9-C8-N1-H1NB.

In total, there are one hundred cations of ephedrine present in the eight-seven structures analysed in this work. The same considerations applied in Chapter 5.2 for equivalent pairs of torsion angles were also applied in this chapter for cations of ephedrine. As it can be observed in Figure 5.15, and in contrast to the other bases, there are outliers in all boxplots obtained for the fourteen torsion angles analysed in this work. Thus, all torsion angles will be involved in further analysis of cation conformation.
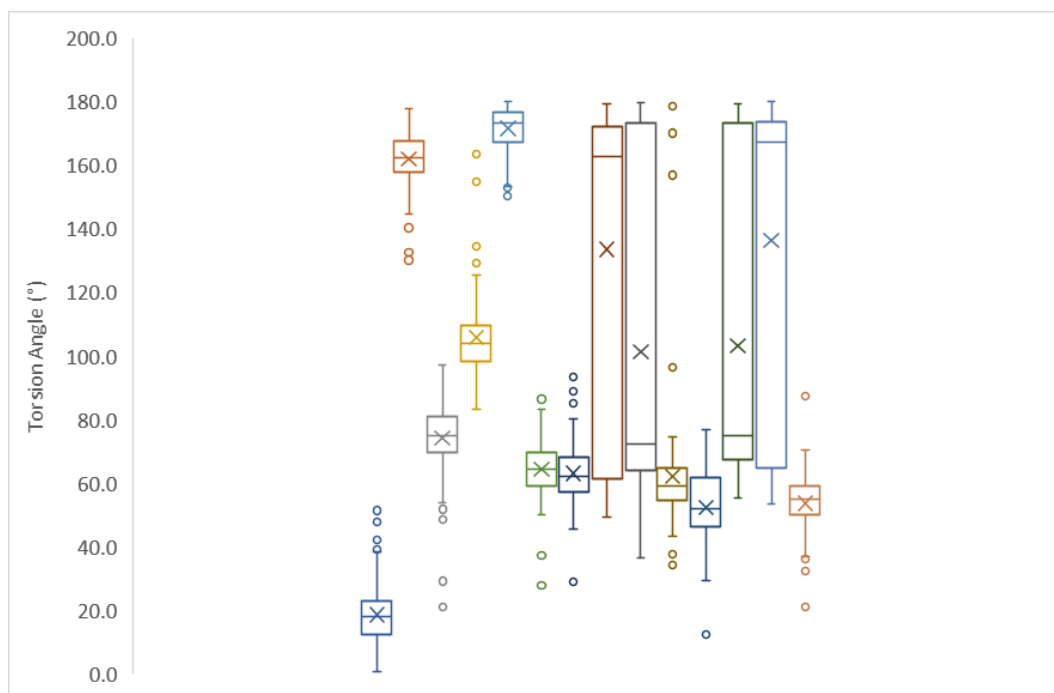
Figure 5. 15. Boxplots for all torsion angles analysed in this work for ephedrine salt forms. In blue is C2-C1-C7-O1, in orange is C6-C1-C7-O1, in grey is C6-C1-C7-C8, in yellow is C2-C1-C7-C8, in light blue is C1-C7-C8-N1, in green is C1-C7-C8-C9, in dark blue is O1-C7-C8-N1, in dark orange is C7-C8-N1-C10, in dark grey is C9-C8-N1-C10, in brown is O1-C7-C8-C9, in petrol blue is C7-C8-N1-H1NB, in dark green is C7-C8-N1-H1NA, in light purple is C9-C8-N1-H1NA and in light brown is C9-C8-N1-H1NB.

As observed by Collier *et al.* [4] there are two basic conformations for the ephedrine cation: The folded conformation is present in thirty-one of the cations analysed (Figure 5.16 – a) and the extended conformation present in the remaining sixty-nine cations (Figure 5.16 – b). Unlike the smaller previous study, the extended conformation can now be identified as being the more common. The distribution of torsion angles

observed for both conformations can be observed in Figure 5.17 for the folded conformation and Figure 5.18 for the extended conformation.

(a)   (b)
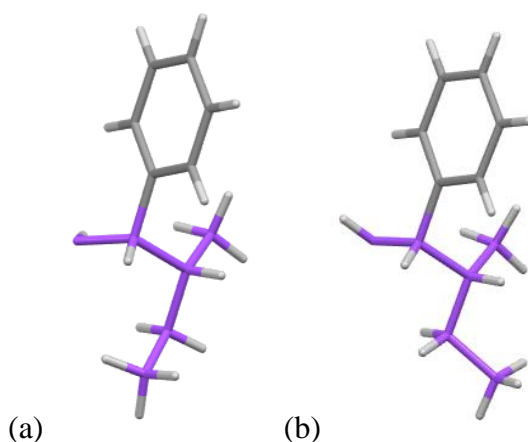
Figure 5. 16. (a) Folded conformation for the sample 4NB, with a (N)-H···O hydrogen bonded distance of 2.660 Å for N···O and (b) Extended conformation for the sample 2NB.
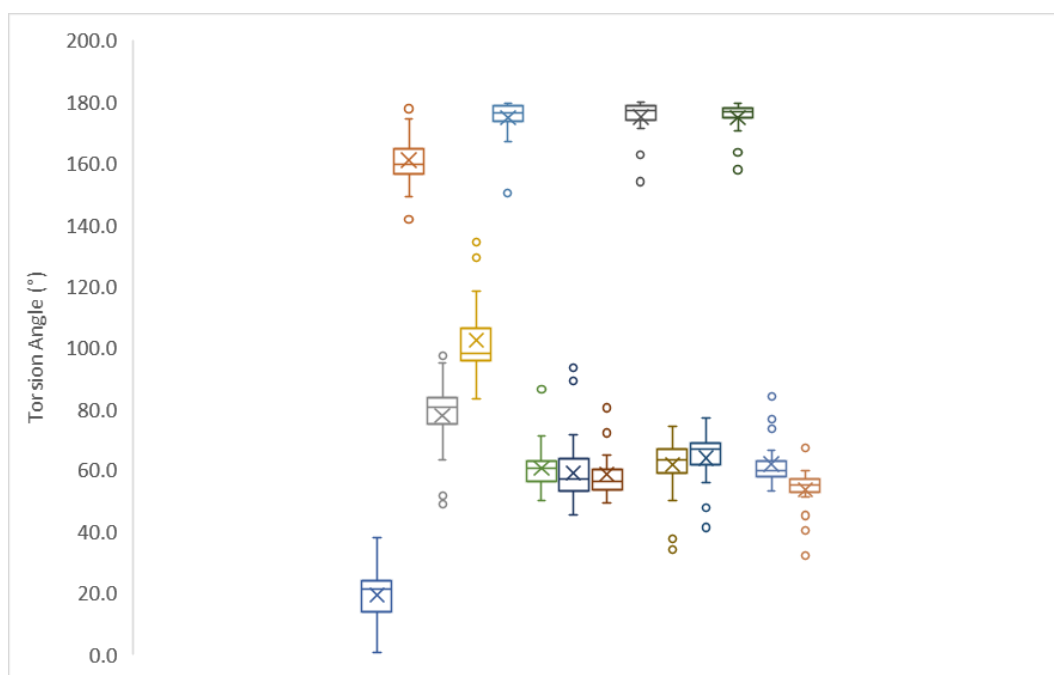
Figure 5. 17. Boxplots for the folded conformation present in 31 cations of ephedrine. In blue is C2-C1-C7-O1, in orange is C6-C1-C7-O1, in grey is C6-C1-C7-C8, in yellow is C2-C1-C7-C8, in light blue is C1-C7-C8-N1, in green is C1-C7-C8-C9, in dark blue is O1-C7-C8-N1, in dark orange is C7-C8-N1-C10, in dark grey is C9-C8-N1-C10, in brown is O1-C7-C8-C9, in petrol blue is C7-C8-N1-H1NB, in dark green is C7-C8-N1-H1NA, in light purple is C9-C8-N1-H1NA and in light brown is C9-C8-N1-H1NB.
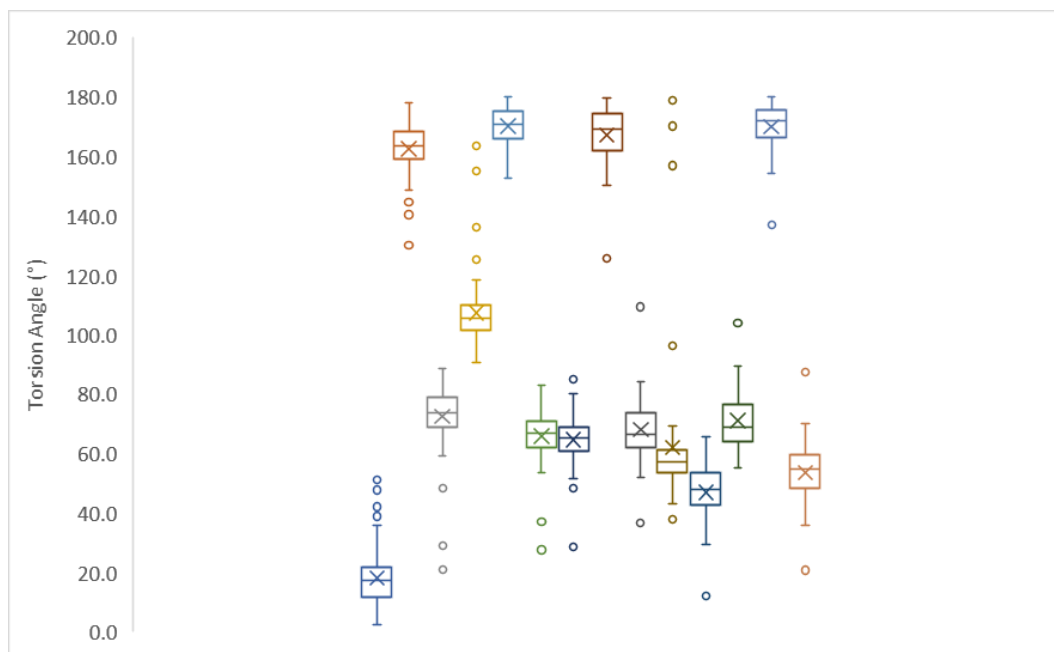
Figure 5. 18. Boxplots for the extended conformation present in 69 cations of ephedrine. In blue is C2-C1-C7-O1, in orange is C6-C1-C7-O1, in grey is C6-C1-C7-C8, in yellow is C2-C1-C7-C8, in light blue is C1-C7-C8-N1, in green is C1-C7-C8-C9, in dark blue is O1-C7-C8-N1, in dark orange is C7-C8-N1-C10, in dark grey is C9-C8-N1-C10, in brown is O1-C7-C8-C9, in petrol blue is C7-C8-N1-H1NB, in dark green is C7-C8-N1-H1NA, in light purple is C9-C8-N1-H1NA and in light brown is C9-C8-N1-H1NB.

First, for the folded conformation, there are five outliers to the torsion angles in Figure 5.17 boxplots: OPH.2 (FIMVAY), LTAR.H2O.2 (GEJMOY), 4HBS, PYR (NAHVUN) and one independent cation of the MUC structure. The structure overlay of these outliers with a compound with a regular folded conformation, PTS (GEHLOV), shows three different cases, as observed in Figure 5.19: (a) three compounds have a small deviation from the folded conformation, OPH.2 (FIMVAY), 4HBS and LTAR.H2O.2 (GEJMOY). These compounds will be labelled with conformation folded α_1. The second case, illustrated in Figure 5.19 (b), is represented by cation 1 of the sample 2MUC, this compound had a similar conformation as the folded α_1 however, the position of the hydroxyl and methyl groups have a torsion angle of around 180 °. This compound will be labelled with conformation folded α_2.

Finally, the structural comparison between PTS (GEHLOV) and PYR (NAHVUN), Figure 5.19 (c), shows the sample PYR (NAHVUN) with a higher O1-C7-C8-N1 torsion angle rotates the molecule from the average of 57 (6) ° for this torsion angle to 93.4 (6) ° and a lower O1-C7-C8-C9 torsion angle, with PYR (NAHVUN) having a

torsion in this case of 37.7 (7) °, a higher discrepancy compared with the average 64 (6) ° for all compounds. This compound will be labelled with conformation folded β.
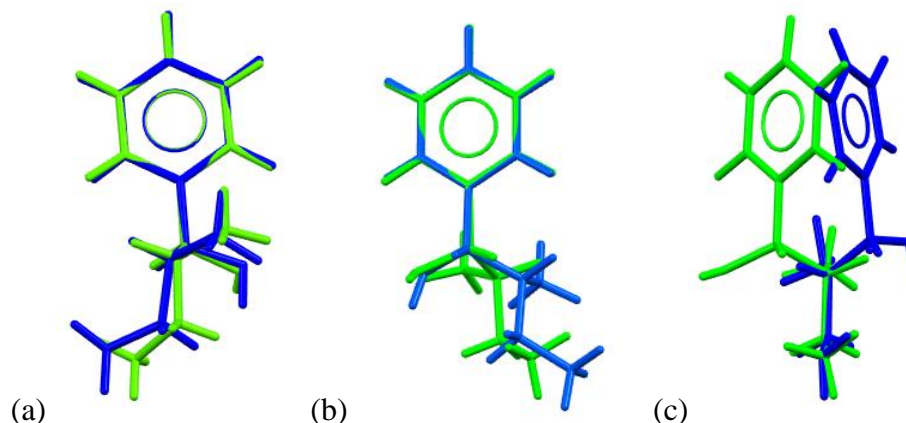
Figure 5. 19. Structural overlay for the outliers (in blue) and a compound with standard EPD folded conformation PTS (GEHLOV), in green): (a) conformation folded α_1 for the sample OPH.2 (FIMVAY), (b) conformation folded α_2 for the cation 1 in the sample 2MUC and (c) conformation folded β for the sample PYR (NAHVUN) .

In the case of the more common extended conformation, there are seven outliers: OHPH (YEYWIJ), cation 2 of the sample AUCL4 (MEXVOC), OBS (VAWPEP), 2CB, 4AB, cation 1 of the sample MMBS and NMC (CURFOM). Interestingly, these outliers can behave in four different ways, three are shown in Figure 5.20. Structural overlay of these outliers with a compound with a regular extended conformation, PIN (INEDIP) (in black) show the differences in the packing of these cations. The first result observed is for two compounds, cation 2 of the sample AUCL4 (MEXVOC) and OBS (VAWPEP) (Figure 20 – a) where these compounds have higher C2-C1-C7-O1 torsion angle, and consequently lower values of C6-C1-C7-O2 torsion angle, which makes the position of the ring deviates from the standard position for the group. This group also has a linear torsion angle O1-C7-C8-C9 (average of 168 (11) °) compared with the other extended group [average of (56 (7) °]. These compounds will be labelled with conformation extension α_1. Interestingly the same occur for the sample NMC (CURFOM) (Figure 20 – b) however, there is also a rotation of the hydroxyl group and the methyl C9 of 180 °. This compound will be labelled with conformation extension α_2. As observed for tyramine salt forms, the extended conformation also has

a rotation of the ring position, which is labelled as extension β. This conformation is present in three cations, of the samples 2CB, 4AB and cation 1 of the sample MMBS.

Finally, there is one sample that does not behave in any of those categories, that have features from both extended and folded conformation as it can be observed in Figure 5.21 (a) for extended conformation and (b) for folded conformation. This sample, OHPH (YEYWIJ), will be labelled as conformation γ. Of the fifteen structures with two or more independent ephedrine cations in the asymmetric unit, six compounds had two different conformations in the crystal structure: PIN.2 (INEDOV), AHA.H2O (KITLUV) and I (ZZZSDC01) had both standard extended and standard folded conformations, AUCL4 (MEXVOC) had the extended α_1 and standard folded conformations, 2MUC had the folded α_2 and standard extended conformation and MMBS have both extended β and standard folded conformations. All values of torsion angles for ephedrine salt forms can be observed in APPENDIX 5.3, however a summary of all torsion angles can be observed in Table 5.4 for extension conformations and Table 5.5 for folded conformations and conformation γ.
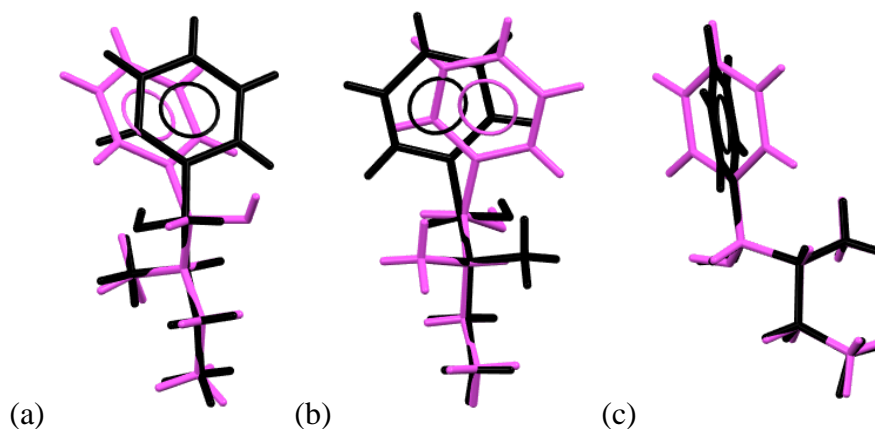
Figure 5. 20. Structural overlay for the outliers (in pink) and a compound with standard extended conformation (INEDIP, in black): (a) conformation extended α_1 for the cation 2 of the sample AUCL4 (MEXVOC), (b) conformation extended α_2 for the sample NMC (CURFOM) and (c) conformation extended β for the sample 2CB where there is a rotation in the ring
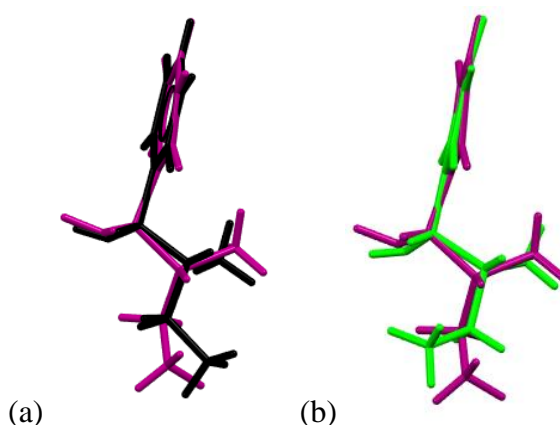
Figure 5. 21. Conformation γ for the sample OHPH (YEYWIJ) (in in purple) and structural packing with the standard extended conformation (a) PIN (INEDIP) (in black) and standard folded conformation (b) PTS (GEHLOV) (in blue).

5.4. CONCLUSIONS

This work analysed the cation conformation of four different active pharmaceutical ingredients: tyramine, enantiopure methylephedrine, racemic methylephedrine and ephedrine. There was found to be no conformational difference between racemic and enantiopure methylephedrine samples and so these are discussed together. Different conformations will have different thermodynamic stabilities, and this could influence bulk properties of interest, e.g. aqueous solubility. Cation conformation was already described for these bases in the literature; however, this work aims to expand the descriptions using significantly greater sample numbers and by analysing all torsion angles involved in the aliphatic chain of the bases. This expanded description analyses three different torsion angles of tyramine and fourteen torsion angles of ephedrine and methylephedrine.

In the case of tyramine, there were two conformations involving the aliphatic chain of the compound, the more common extended conformation and a folded conformation as described by Morrison *et al.* [6]. Further analysis of tyramine's extended conformation identified a new sub-class for ten cations, labelled as conformation extended β, which involved the rotation of the aromatic ring in comparison with the standard extended conformation.

Table 5. 4. Summary of ephedrine torsion angle for the standard extended conformation, extended α*1*, extended α₂ and extended β where n is the number of cations with the conformation, Min is the minimum value of torsion angle and Max is the maximum value of torsion angle

Torsion Angle	Extended (n = 62)			Extended α1 (n = 2)			Extended α2 (n = 1) (°)	Extended β (n = 3)		
	min (°)	max (°)	average (°)	min (°)	max (°)	average (°)		min (°)	max (°)	average (°)
C2-C1-C7-O1	2.4	35.8	16 (6)	39.0	47.8	43 (4)	51.3	15	42	31 (11)
C6-C1-C7-O2	144.6	177.9	164 (6)	132.5	140.4	136 (4)	130.2	142	169	153 (11)
C6-C1-C7-C8	59.2	88.7	74 (6)	71.6	73.7	73 (1)	68.0	21	49	33 (12)
C2-C1-C7-C8	90.7	125.4	105 (7)	106.9	108.0	107.4 (5)	110.5	136	164	152 (11)
C1-C7-C8-N1	152.5	180.0	170 (7)	176.3	177.7	177.0 (7)	171.0	167	175	172 (4)
C1-C7-C8-C9	53.6	83.2	67 (6)	37.1	54.5	46 (9)	67.4	64	70	66 (3)
O1-C7-C8-N1	51.8	86.3	66 (7)	59.4	62.5	61 (2)	48.5	62	69	64 (3)
C7-C8-N1-C10	150.1	179.4	167 (8)	171.9	179.4	176 (6)	170.7	173	179	176 (3)
C9-C8-N1-C10	51.9	84.4	68 (8)	36.6	63.7	50 (14)	66.7	58	63	61 (2)
O1-C7-C8-C9	38.0	69.4	57 (6)	156.9	178.7	168 (11)	170.1	54	60	58 (3)
C7-C8-N1-H1B	29.4	65.6	47 (8)	49.9	55.3	53 (3)	48.9	54	58	56 (2)
C7-C8-N1-H1A	55.2	89.4	71 (8)	59.7	68.4	64 (4)	67.8	60	69	64 (4)
C9-C8-N1-H1A	154.2	179.9	170 (7)	157.6	174.3	166 (8)	171.6	177	178	177.8 (4)
C9-C8-N1-H1B	36.1	70.2	53 (9)	56.0	87.5	72 (16)	54.9	56	64	60 (4)

Table 5. 5. Summary of ephedrine torsion angle for the standard folded conformation, folded α_1, folded α_2, folded β and conformation γ where n is the number of cations with the conformation, Min is the minimum value of torsion angle and Max is the maximum value of torsion angle

	Folded (n = 30)			Folded α1 (n = 3)			Folded α2 (n = 1) (°)	Folded β (n = 1) (°)	Conformation γ (n = 1) (°)
	min (°)	max (°)	average (°)	min (°)	max (°)	average (°)			
C2-C1-C7-O1	0.5	38.3	20 (9)	17.4	22.5	20 (2)	13.4	17.9	18.4
C6-C1-C7-O2	141.8	177.9	161 (9)	155.9	161.6	160 (3)	165.3	164.4	154.1
C6-C1-C7-C8	48.9	94.8	77 (12)	74.9	97.2	83 (10)	72.3	81.2	82.1
C2-C1-C7-C8	83.2	134.4	103 (13)	84.5	106.1	97 (9)	109.0	96.5	105.4
C1-C7-C8-N1	169.4	179.5	176 (2)	167.1	178.9	173 (5)	150.3	168.2	152.9
C1-C7-C8-C9	50.2	67.9	60 (4)	50.2	71.1	60 (9)	86.4	60.7	27.7
O1-C7-C8-N1	45.3	68.0	57 (6)	49.9	71.7	59 (9)	89.0	93.4	28.8
C7-C8-N1-C10	49.4	64.9	56 (4)	72.2	73.3	72.6 (5)	80.4	54.8	125.8
C9-C8-N1-C10	172.5	179.8	177 (2)	162.8	163.7	163.3 (4)	153.9	171.3	109.4
O1-C7-C8-C9	54.8	74.4	64 (5)	50.1	71.9	62 (9)	34.3	37.7	96.5
C7-C8-N1-H1B	56.1	72.6	66 (4)	47.7	49.5	48.9 (8)	41.5	76.9	12.2
C7-C8-N1-H1A	170.7	179.2	176 (2)	163.5	165.7	165 (1)	157.9	179.3	103.9
C9-C8-N1-H1A	53.3	66.5	60 (3)	73.4	76.6	75 (1)	84.2	57.1	137.0
C9-C8-N1-H1B	51.4	67.5	56 (3)	40.5	41.3	40.9 (3)	32.2	45.4	20.8

For methylephedrine salt forms, both enantiopure and racemic, there were three conformations observed, conformation (a), (b) and (c) which, in summary, involves the position of the proton in relationship with the aliphatic carbon C7 in the torsion angle C7-C8-N1-H1N. Conformation (a) have average torsion angle C7-C8-N1-H1N of 49 (10) °, conformation (b) have average torsion angle C7-C8-N1-H1N of 173 (4) ° and conformation (c) have average torsion angle C7-C8-N1-H1N of 76 (9) °. For enantiopure and racemic methylephedrine there were no obvious outliers to analyse in these three torsion angles.

In the case of enantiopure ephedrine, the work of Collier *et al.* [4] was expanded to one hundred cations. The extended conformation was identified as being more common. The two main conformations, extended and folded, were both expanded by the creation of three different sub-classes: Sub-class α_1; sub-class α_2 and sub-class β involving a rotation of the ring regarding the aliphatic chain. There was also the creation of another class, conformation γ, which does not behave similarly to these classifications.

5.5. REFERENCES

[1]   Briggs, N., Kennedy, A., & Morrison, C. (2012). Acta Crystallographica Section B, 68(4), 453-464.

[2]   Klyne, W., & Prelog, V. (1960). Experientia, 16(12), 521-523.

[3]   Kennedy, A. R., Morrison, C. A., Briggs, N. E., & Arbuckle, W. (2011). Crystal Growth and Design, 11(5), 1821-1834.

[4]   Collier, E., Davey, R., Black, S., & Roberts, R. (2006). Acta Crystallographica Section B, 62(3), 498-505.

[5]   Black, S., Collier, E., Davey, R., & Roberts, R. (2007). Journal of Pharmaceutical Sciences, 96(5), 1053-1068.

[6]   Morrison, C.A. (2012). 'Salt selection for pharmaceutical use'. University of Strathclyde. Dept. of Pure and Applied Chemistry. Thesis [Ph. D] – University of Strathclyde

6. PRESENCE OF WATER IN THE CRYSTAL STRUCTURE

6.1. TYRAMINE SALT FORMS

Of the ninety-seven salt forms of tyramine analysed in this work , thirty-nine have one or more water molecules present in the crystal structure. Eighteen of these were from the CSD database [1-6]. Analysis of hydrate environment in salt forms of tyramine was previously described for fourteen salts by Morrison *et al.* [1]. Thus, this expanded work includes twenty-two new hydrated salt forms of tyramine synthesised as described in Chapter 2.4. One water molecule per cation was found in 62.5 % of the hydrates, while 2 water molecules were present in 22.5 % and 3 water molecules in 7.5 %. Only one sample (2.5 %), RTAR.4H2O, had four water molecules in the crystal structure. There were also two samples (5.0 %) with a disordered water channel in the structure, RTAR.wc and TIOSA.wc. This non-stoichiometric structural feature is illustrated for TIOSA.wc in Figure 6.1. Table 6.1 lists all the hydrated tyramine structures.
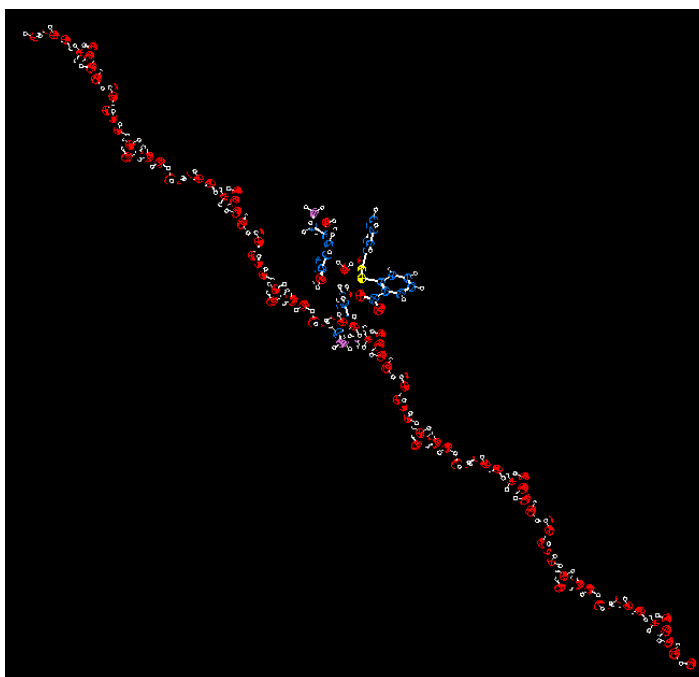
Figure 6. 1. ORTEP view for the water channel present in the sample TYR TIOSA.wc.

Table 6. 1. Code of the tyramine salt forms with water present in the unit cell where * represents the compounds with water channel in the unit cell. Subtitle for the colours: Yellow represents benzoates, green represent carboxylates, blue represents inorganic salt forms, red represents organic sulfonates, pink represents naphthalates and grey represent other salts that does not belong in those categories.

COMPOUND	n H_2O	COMPOUND	n H_2O
2DLMAL.H2O	1	DYEB.H2O	1
2MALON.H2O	1	DYEE.H2O	1
4HBS.H2O (MECZUR) [1]	1	FUM.CC.H2O (MEDGAF) [1]	1
4HPA.H2O	1	FUMS.H2O	1
ACE.H2O (TYRTHM) [4]	1	HEXA.H2O (MEDGOT) [1]	1
ACLMBS.H2O	1	MMBS.H2O	1
ADP.2H2O (MEDGIN) [1]	1	N2S.H2O	1
BF4.H2O (MECYIE) [1]	1	NTO.H2O (KOBNAT) [6]	1
BS.H2O (MECZOL) [1]	1	PTS.H2O	1
DLMAL.H2O	1	LTAR.NA.2H2O	2
RMAL.H2O (MEDHAG) [1]	1	PO4.2H2O (MECYUQ) [1]	2
RTAR.H2O (MEDHIO) [1]	1	SO4.2H2O (MOHBUH) [2]	2
SUC.2H2O (MEDGEJ) [1]	1	TB.H2O (ATOLAX) [3]	2
TCIN.H2O	1	2NAPH.3H2O	3
TYR.TYR.CL.H2O	1	ASB.3H2O	3
CLO4.H2O (MECYOK) [1]	2	UR.3H2O	3
CNB.2H2O (RUQSOM) [5]	2	RTAR.4H2O	4
DYEC.2H2O	2	RTAR.wc	*
HSUC.2H2O (MEDGUZ) [1]	2	TIOSA.wc	*
LTAR.2H2O (MEDHEK) [1]	2		

Figure 6.2 shows the distribution of samples with water present in the unit cell according to the composition of the counterion. When analysing formation of hydrates according to the composition of the counterion, 57.6 % of the carboxylates, 62.5 % of the sulfonates and 50.0 % of the inorganic compounds crystallise as hydrates. It is interesting to note that only two of the benzoate structures, representing 10.7 %, crystallise as hydrate forms: TB.H2O (ATOLAX) and TIOSA. In the case of naphatalates, there was only one structure of the three salt forms crystallising as a hydrate generated, representing 33.3 %. Infantes and Motherwell [19] report that 6.6 % of general organic crystal structures are hydrates, rising to 14% for bioactive

compounds. Of more relevance is a study by Haynes *et al.* [20] who report the higher value of 22% hydrate formation for salt forms of pharmaceutically acceptable protonated amines. It thus appears that tyramine salts are more likely to form as hydrates than literature precedent suggests, and much more likely if the counterion is a carboxylate, sulfonate or inorganic species. One problem though is that the literature reviews do not include only species crystallised from water, as this project's tyramine salts were. Thus, they may be systematically lower for this reason.

Increasing the number of structures analysed by Morrison *et al.* [1], some considerations about hydrate formation according to the composition of the counterion can be updated.

1. Although most benzoates and halides crystallise as anhydrous salt forms, depending on the synthesis route used, benzoates and halides can crystallise as hydrated forms. See for example, the samples TIOSA and TYR.TYR.CL.H2O.

2. All tetrahedral anions formed hydrated salts, as described by Morrison *et al.* [1].

3. All aliphatic sulfonate anions gave anhydrous salts and 83.3 % of the aryl-sulfonates formed hydrated salts, whilst only two samples were anhydrous benzenesulfonates, 4CBS and ACLBS. Regarding the sulfonate dyes: DYEB, DYEC and DYEE, all compounds of these relatively large and functionalised anions crystallised as hydrated salts.

4. 70 % of the dicarboxylate-based anions and 25 % of the monocarboxylate-based anions formed hydrated salts. No trend was found for these samples according to intra-molecular hydrogen bonding in the counterions.
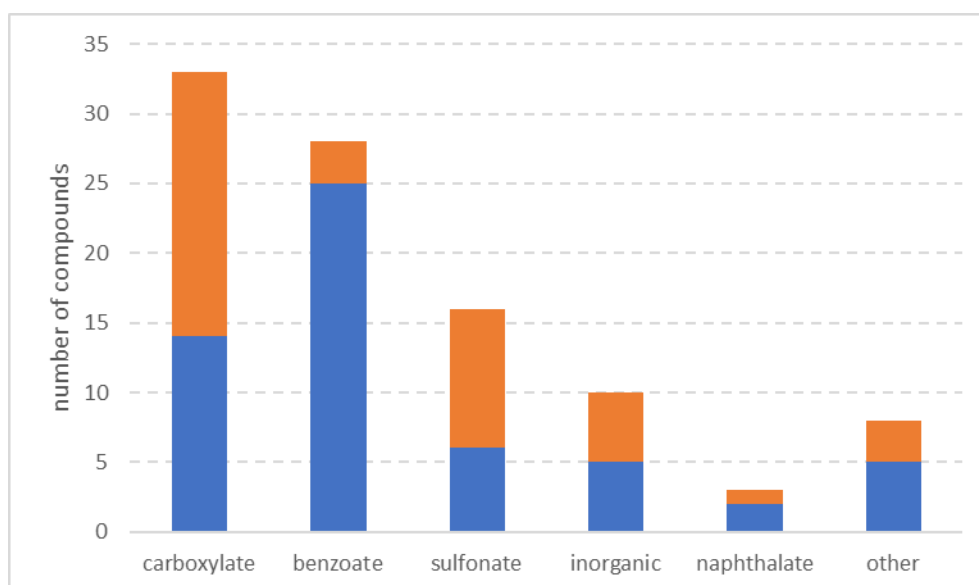
Figure 6. 2. Distribution of water presence in the unit cell according to the composition of the counterion, where the boxes in blue represents anhydrous compounds and the boxes in orange represents hydrated compounds.

As shown in Chapter 2.6.2, there are ten possible hydrogen bonding motifs involving water molecules in the crystal structure of hydrates. Of these ten possible motifs, four were found to be present in the tyramine structures: water molecule acting as a proton donor and sharing both protons to other molecules [2(DD)]; the water molecule acting as a proton donor and acceptor. and sharing two protons with other molecules and receiving one proton from another molecule [5(DDA)]; the water molecule acting as a proton donor and acceptor, and sharing two protons with other molecules and receiving two protons from other molecules [6(DDAA)]; and the water molecule acting as a proton donor and acceptor, and sharing one proton with another molecule and receiving two protons from other molecules [8(DAA)]. Two other motifs, 3(A) and 4(AA), appear to be present in the dataset but the relevant structures TIOSA.wc and TB.2H2O (ATOLAX) have disorder in the water molecule and the water H atoms are missing from the structural model – hence the lack of detection of donor motifs. Details of the water motifs for the thirty-nine hydrates found in this work can be obtained in Table 6.2, where numbers higher than one represent how many such motifs were observed in the structure.

From Table 6.2 and Figure 6.3 it is easy to observe that the 5(DDA) motif is most common, observed forty-four times in twenty-five different structures. The 6(DDAA) motif is also common, observed thirty-six times in seventeen structures. With lower appearances, the other motifs are, 2(DD) present nine times in six different molecules, and 8(DAA) present twice in the same molecule, RTAR.4H2O. Examples of the motifs found for tyramine salts are shown in Figures 6.4-6.7.
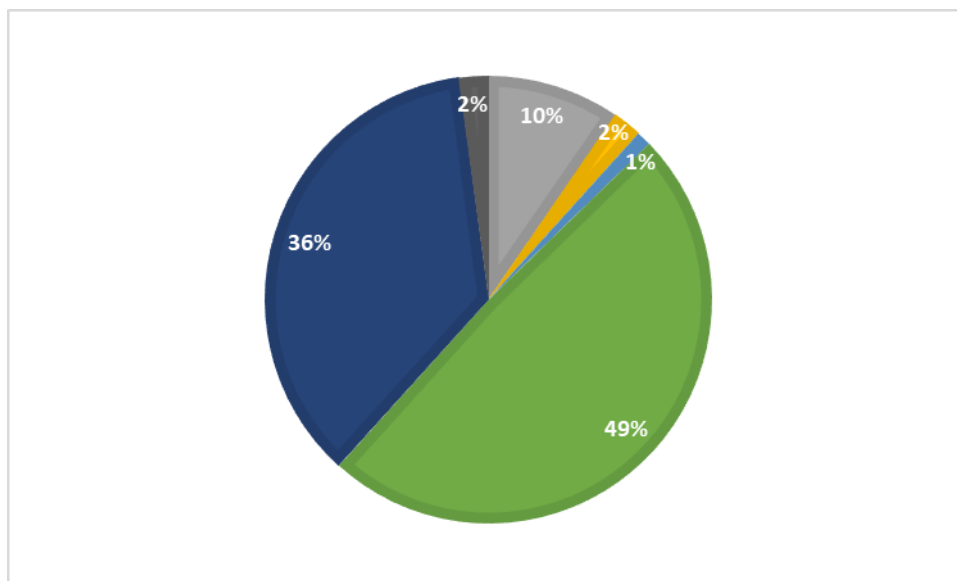
Figure 6. 3. Percentage of water motifs in the unit cell of thirty-nine hydrated forms of tyramine where in green are the percentage of 5(DDA) motifs, in dark blue the percentage of 6(DDAA) motifs, in grey the percentage of 2(DD) motifs, in yellow is the percentage of 3(A) motifs, in light blue is the percentage of 4(AA) motifs, in dark grey is the percentage of 8(DAA) motifs.

Table 6. 2. Number of water motifs found for each hydrate salt form of tyramine.

COMPOUND	number of motifs					
	2(DD)	3(A)	4(AA)	5(DDA)	6(DDAA)	8(DAA)
2DLMAL.H2O					1	
2MALON.H2O					1	
2NAPH.3H2O	1			1	2	
4HBS.H2O					4	
4HPA.H2O				1		
ACE.H2O				1		
ACLMBS.H2O				3		
ADP.2H2O				1		
ASB.3H2O				5	2	

BF4.H2O					2	
BS.H2O				4		
CLO4.H2O					7	
CNB.2H2O				2		
DLMAL.H2O	2					
DYEB.H2O				1		
DYEC.2H2O				2	2	
DYEE.H2O				1		
FUMCC.H2O					1	
FUMS.H2O				1		
HEXA.H2O	1					
HSUC.2H2O				1	1	
LTAR.2H2O				1	1	
LTAR.NA.2H2O	2					
MMBS.H2O	1					
N2S.H2O				2		
NTO.H2O				2		
PO4.2H2O					3	
PTS.H2O				2		
RMAL.H2O					2	
RTAR.4H2O				1	1	2
RTAR.H2O					1	
RTAR.wc				3	2	
SO4.2H2O				4		
SUC.H2O				1		
TB.2H2O		1	1			
TCIN.H2O	2					
TIOSA.wc		1		1	1	
TYR.TYR.CL.H2O				1		
UR.3H2O				3		
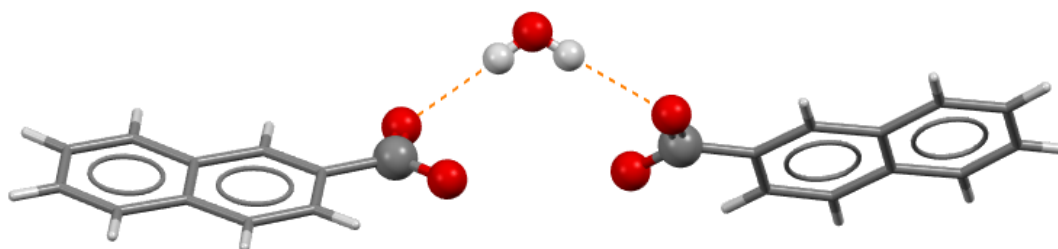
Figure 6. 4. 2(DD) motif for one of the water molecules in the sample 2NAPH.3H2O.
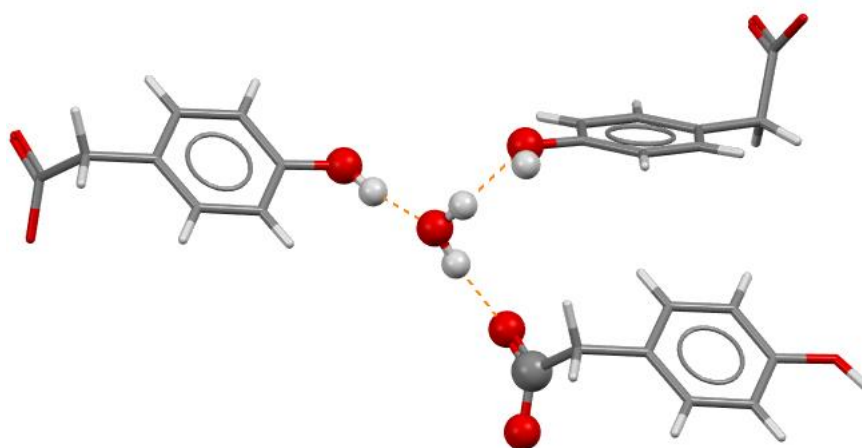
Figure 6. 5. 5(DDA) motifs for the water molecules in the sample 4HPA.H2O.
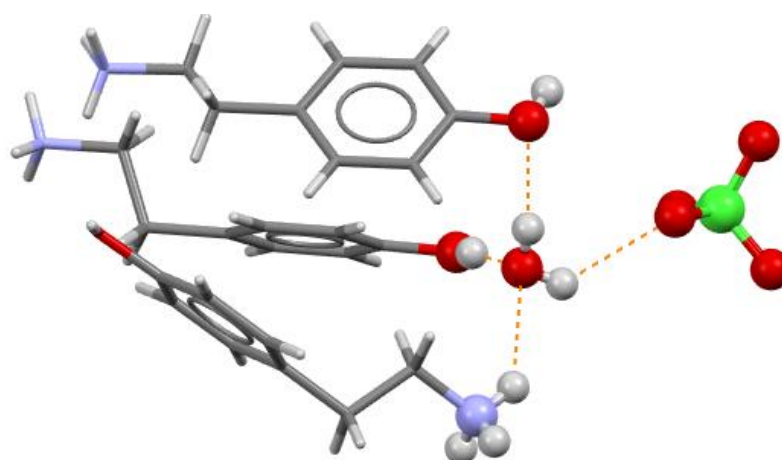
Figure 6. 6. 6(DDAA) motifs for the water molecules in the sample CLO4.2H2O (MECYOK).
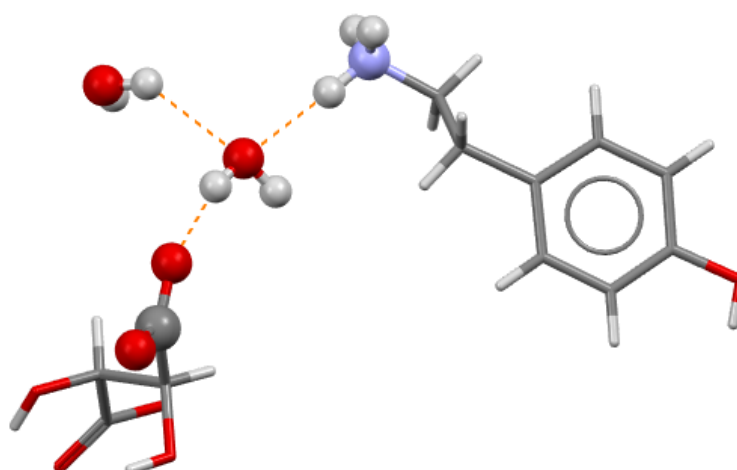
Figure 6. 7. 8(DAA) motifs for one of the water molecules in the sample RTAR.4H2O.

6.2. METHYLEPHEDRINE SALT FORMS

There were ninety-two salt forms of enantiopure (MEPD) and racemic methylephedrine (RMEPD) analysed in this work. Of those, eighteen have the presence of one or more water molecules in the crystal structure, ten hydrates salts of MEPD and eight hydrated salt forms of RMEPD. Of the hydrate structures, thirteen were previously published and found on the CSD database [7,8]. Neither racemic nor enantiopure structures can be said to be more susceptible to hydrate formation. This level of hydrate occurrence is in line with literature suggestions [20] and is much lower than that found above for tyramine salt forms. In the case of both enantiopure and racemic methylephedrine, one water molecule was found in 83.3 % of the hydrates while two water molecules were present in the remaining 16.7 %. Details of the compounds with water molecules present in the unit cell can be observed in Table 6.3 for enantiopure methylephedrine, represented by "*e*" before the label and racemic methylephedrine, represented by "*r*" before the label.

Table 6. 3. Code of the salt forms with water present in the unit cell for enantiopure methylephedrine, represented by "*e*" before the label and racemic methylephedrine, represented by "*r*" before the label. Subtitle for the colours: Yellow represents benzoates, green represent carboxylates, blue represents inorganic salt forms, red represents organic sulfonates, pink represents naphthalates and grey represent other salts that does not belong in those categories.

COMPOUND	n H_2O	COMPOUND	n H_2O
*e*2NB.H2O (IVUKUG) [7]	1	*r*4HBS.H2O (IVUSAU) [7]	1
*e*3CB.H2O (IVUQOG) [7]	1	*r*DYEC.H2O	1
*e*BS.H2O	1	*r*EDS.2.H2O (VAVLIQ) [8]	1
*e*BZ.H2O (IVURAT) [7]	1	*r*MUC.H2O	1
*e*LMD.H2O (VAVKAH) [8]	1	*r*PAAB.H2O	1
*e*LTAR.H2O (VAVJOU) [8]	1	rSO4.H2O (IVUNUJ) [7]	1
*e*SO4.2H2O (IVUNOD) [7]	1	*e*ACLMBS.2H2O	2
*r*2NB.H2O (IVULAN) [7]	1	*e*MUC.2H2O	2
*r*4CBS.H2O	1	*e*N2S.3H2O	2

Figures 6.8 and 6.9 shows the distribution of hydrated samples according to the composition of the counterion. When analysing formation of hydrates according to the composition of the counterion, the only similarity between enantiopure and racemic

salt forms is related to the formation of benzoates, with three salt forms (18.8 %) of enantiopure forming hydrates and two salt forms (11.8 %) of racemic methylephedrine forming hydrates. *Ortho*-nitrobenzoic acid (2NB) formed hydrated forms with both enantiopure and racemic methylephedrine. Another interesting result about hydrate formation is that enantiopure and racemic salt forms of mucic acid (MUC) also formed hydrated structures. The sample *r*MUC.H2O was the only hydrate formed as a racemic salt form of carboxylates, representing 10 % of the total. This may be related to the large number of hydrophilic hydroxyl groups present on mucic acid but see analysis of donor/acceptor ratios below. In the case of enantiopure compounds, 21.4 % of the carboxylates were hydrates. In contrast, for sulfonates, 21.4 % of salt forms of MEPD are hydrates while 57.1 % of the racemic compounds were hydrated salt forms. There were two inorganic salt forms with water in the unit cell, the samples *e*SO4.2H2O (IVUNOD) and *r*SO4.2H2O (IVUNUJ), representing 16.7 % of the enantiopure and 20.0 % of the racemic inorganic compounds. Continuing the analysis following the description for hydrated salt forms according to the composition of the counterion done by Morrison *et al.* [1] for tyramine salt forms, there are some interesting considerations that can be obtained for methylephedrine salt forms.

(i)   Most benzoates and all halides will crystallise as anhydrous salt forms. However, two benzoates of enantiopure methylephedrine and three benzoates of racemic methylephedrine crystallise as hydrates. Interestingly, one sample crystallised as hydrates as enantiopure and racemic salts, the salt form of *ortho*-nitrobenzoate (2NB).

(ii)   Tetrahedral anions of hydrogensulfonate formed hydrated salts however, the only other compound with a tetrahedral counterion, the salt form of enantiopure methylephedrine and tetrachlorocuprate (II), *e*CUCL4 (QIHREG), was anhydrous.

(iii)   85.7 % of the aliphatic sulfonate were anhydrous salt forms salts of enantiopure and racemic methylephedrine. Aryl-sulfonates of racemic methylephedrine formed hydrated salts in 75 % of the cases while aryl-sulfonates of enantiopure methylephedrine formed hydrated salts in only 30 % of the cases. Regarding the sulfonate dyes, the salt form of racemic

methylephedrine and DYEC crystallised as a hydrated salt but the salt form of enantiopure methylephedrine and 4CNDIA formed an anhydrous compound.

(iv)   78.6 % of the dicarboxylate-based anions and 87.5 % of the monocarboxylate-based anions formed anhydrous salts. One counterion gave hydrates of both enantiopure and racemic methylephedrine, that was mucic acid (MUC).
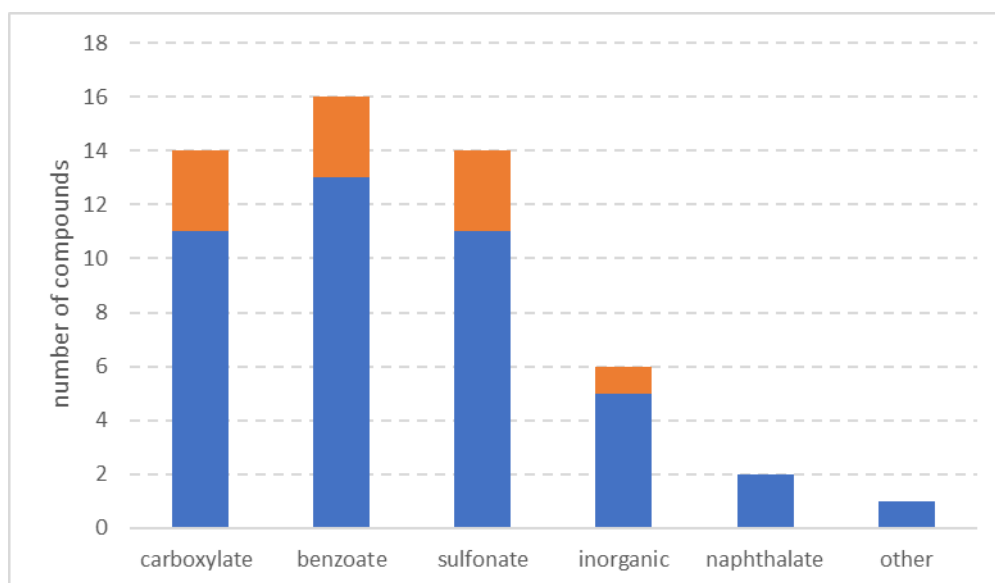
Figure 6. 8 Distribution of water presence in the unit cell for enantiopure methylephedrine according to the composition of the counterion, where the boxes in blue represents anhydrous compounds and the boxes in orange represents hydrated compounds.

Of these ten possible water hydrogen bonding motifs, four were found present in water molecules within enantiopure and racemic methylephedrine unit cells. These are the same four motifs as found for tyramine water and are; molecule acting as a proton donor and sharing both protons to other molecules [2(DD)]; the water molecule acting as a proton donor and acceptor and sharing two protons with other molecules and receiving one proton from another molecule [5(DDA)]; the water molecule acting as a proton donor and acceptor, and sharing two protons with other molecules and receiving two protons from other molecules [6(DDAA)]; and the water molecule acting as a

proton donor and acceptor, and sharing one proton with another molecule and receiving two protons from other molecules [8(DAA)]. The 1(D) motif was also found – but this was in structure eN2S which was highly disordered and is thus likely to be an artefact. Details of the water motifs for the eighteen hydrates found in this work can be obtained in Table 6.4, where numbers higher than one represent how many motifs were observed in the structure, for the same or different water molecules.
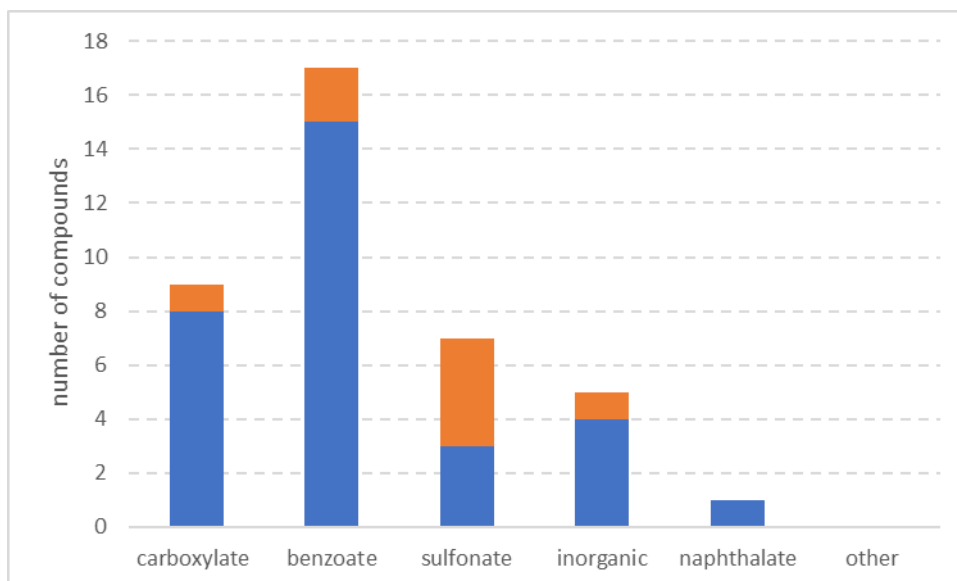
Figure 6. 9. Distribution of water presence in the unit cell for racemic methylephedrine according to the composition of the counterion, where the boxes in blue represents anhydrous compounds and the boxes in orange represents hydrated compounds.

Table 6. 4. Number of water motifs found for each hydrate salt form of enantiopure and racemic methylephedrine.

COMPOUND	number of motifs				
	1(D)	2(DD)	5(DDA)	6(DDAA)	8(DAA)
e2NB.H2O		1			
e3CB.H2O			1		
eACLMBS.2H2O			5		
eBS.H2O			2		
eBZ.H2O		1			
eLMD.H2O			1		
eLTAR.H2O			1		
eMUC.2H2O			1	1	
eN2S.3H2O	1		2		

eSO4.2H2O	2	
r2NB.H2O	3	
r4CBS.H2O	2	
r4HBS.H2O	1	
rDYEC.H2O	1	
rEDS.2.H2O	2	
rMUC.H2O	1	1
rPAAB.H2O	1	
rSO4.2H2O	3	

As observed for tyramine salts, again 5(DDA) motif has a high occurrence, but here it is even more dominant; it is observed twenty-six times in fifteen different compounds. The 6(DDAA) motif which was highly present in tyramine hydrates was only present in one sample of enantiopure methylephedrine, *e*MUC.2H2O. The relative absence of four-fold water nodes is presumably related to a lack of suitable donor H atoms – methylephedrine has a R_3NH cation whilst tyramine is a RNH_3 cation. Of the other motifs, 2(DD) is present five times in three different molecules, and 8(DAA) present once in the sample *r*MUC.H2O. Examples of the motifs found for enantiopure and racemic methylephedrine salts are shown in Figures 6.11 to 6.13.
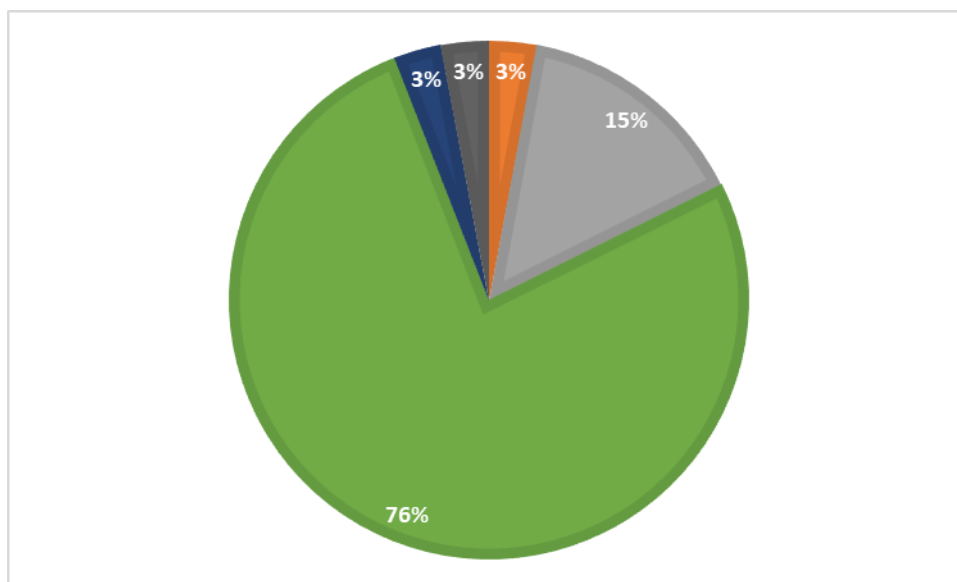
Figure 6. 10. Percentage of water motifs in the unit cell of eighteen hydrated forms of enantiopure and racemic methylephedrine where in dark blue are the percentage of 6(DDAA) motifs, in dark grey the percentage of 8(DAA) motifs, in orange the percentage of 1(D) motif, in grey is the percentage of 2(DD) motifs and in green is the percentage of 5(DDA) motifs.
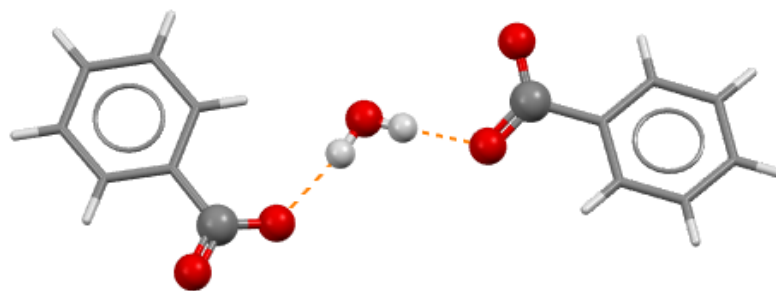
Figure 6. 11. 2(DD) motifs for one of the water molecules in the sample *e*BZ.H2O (IVURAT).
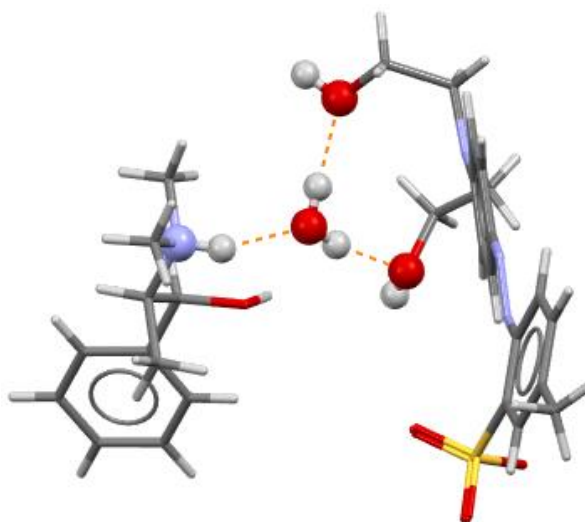
Figure 6. 12. 5(DDA) motifs for one of the water molecules in the sample *r*DYEC.H2O
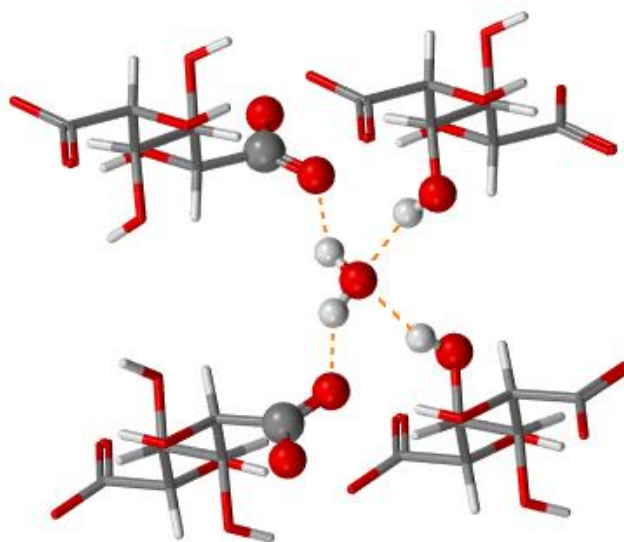
Figure 6. 13. 6(DDAA) motifs for the water molecules in the sample 4HPA.H2O.

6.3. EPHEDRINE SALT FORMS

Of the eighty-seven salt forms of ephedrine synthesise in this work, eighteen crystallise as hydrated forms. Of these hydrated forms, fourteen were previously published [9-18]. For ephedrine salt forms, one water molecule was found in 83.3 % of the hydrates while two water molecules were present in 5.6 % and three water molecules was found in 11.1 % of the hydrated forms. As with methylephedrine, the overall occurrence of hydration is in line with suggested literature values and much less than that found for tyramine salts. There was the formation of 18.5 %, 21.0 % and 42.0 % for methylephedrine (tertiary amine), ephedrine (secondary amine) and tyramine (primary amine) respectively. Details of the hydrated ephedrine compounds can be observed in Table 6.5.

Table 6. 5. Code of the salt forms with water present in the unit cell. Subtitle for the colours: Yellow represents benzoates, green represent carboxylates, blue represents inorganic salt forms, red represents organic sulfonates, pink represents naphthalates and grey represent other salts that does not belong in those categories.

COMPOUND	n H_2O	COMPOUND	n H_2O
2TAR.H2O (FIRJAU) [9]	1	OPC.H2O (FIRGUL) [9]	1
3NB.H2O	1	OPH.4.H2O (GOJJEU) [14]	1
4HBS.H2O	1	OPH.7.H2O (KOSYOG) [15]	1
AHA.H2O (KITLUV) [10]	1	PRC (DINYAA10) [16]	1
CDCL5.H2O (HUVXON) [11]	1	SO4.H2O.2	1
HPO4.H2O (EPHEDP) [12]	1	TAR.H2O.3	1
LTAR.H2O.2 (GEJMOY) [13]	1	CD2CL10.2H2O (COCCEC) [17]	2
MAL.H2O (FIRHUM) [9]	1	BROPH.3H2O (TANXEL) [18]	3
MALE.H2O (GEHKIO) [13]	1	LTAR.3H2O (GEHLIP) [13]	3

When analysing formation of hydrates according to the composition of the counterion, 25.0 % of carboxylates, 7.7 % of benzoates, 11.1 % of sulfonates and 26.7 % of the compounds with inorganic counterion crystallises as hydrates as can be observed in Figure 6.14 where the distribution of hydrated samples according to the composition of the counterion is given. Continuing the analysis following the description for hydrated salt forms according to the composition of the counterion done by Morrison *et al.* [1] for tyramine salt forms and done for enantiopure and racemic methylephedrine salt forms, again, similar results are obtained for ephedrine salt forms:

(i) Most benzoates and all halides of ephedrine crystallise as anhydrous salt forms. However, one benzoate of ephedrine crystallises as a hydrate, the sample 3NB.H2O.

(ii) Tetrahedral anion hydrogenosulfonate formed, again, a hydrated salt with ephedrine. However, there is also the presence of an anhydrous form in the database, the sample SO4 (GEHLEL). The same occur for the tetrahedral anion PO4, where there is in the database both the anhydrous [H2PO4 (EPHDHP)] and hydrated [EPD HPO4.H2O (EPHEDP)] forms. Both square-planar counterions were anhydrous, the samples AUCL4 (MEXVOC) and EPD PDCL4 (GEJDUX).

(iii) All aliphatic sulfonate anions and 80 % of aryl-sulfonates were anhydrous salts.

(iv) In the case of dicarboxylate salt forms of ephedrine, 42.9 % of the compounds were hydrated while 92.9 % of the monocarboxylate salts formed anhydrous salts.
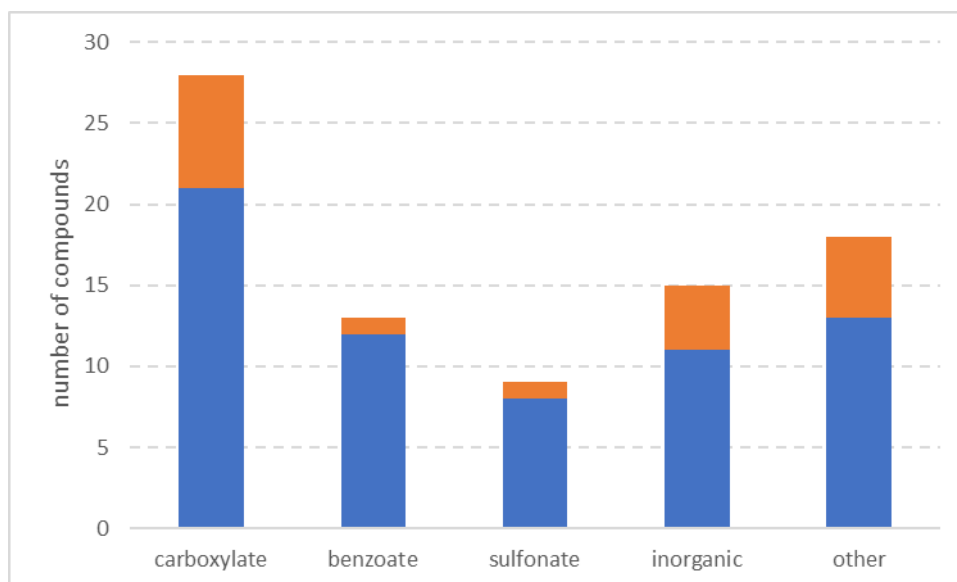
Figure 6. 14. Distribution of water presence in the unit cell for ephedrine salt forms according to the composition of the counterion, where the boxes in blue represents anhydrous compounds and the boxes in orange represents hydrated compounds.

Details of the water motifs for the eighteen hydrates of ephedrine salt forms can be obtained in Table 6.6, where numbers higher than one represent how many motifs were observed in the structure, for the same or different water molecules For ephedrine salt forms, again, 5(DDA) motifs have the highest occurrence, observed twenty-two times in twelve different structures. There was no presence of the 6(DDAA) motif, commonly present in tyramine hydrates. There were lower occurrences of other motifs, 2(DD) present four times in two different molecules and 7(DA) present four times in three different molecules. The two lowest connectivity motifs found were only from the related phosphorinane structures OPH.4.H2O (GOJJEU) and BROPH.3H2O (TANXEL) [14]. The latter has no hydrogen atoms present on its water molecules and so the given motif is an artefact. GOJJEU does have all H atoms present, but careful scrutiny of the structure suggests that at least some are misplaced. The low connectivity motif given here is thus likely to also be an artefact. The distribution of the percentage of motifs for ephedrine salt forms can be observed in Figure 6.15. Examples of the motifs found for hydrated ephedrine salts can be found in Figures 6.16 to 6.18.
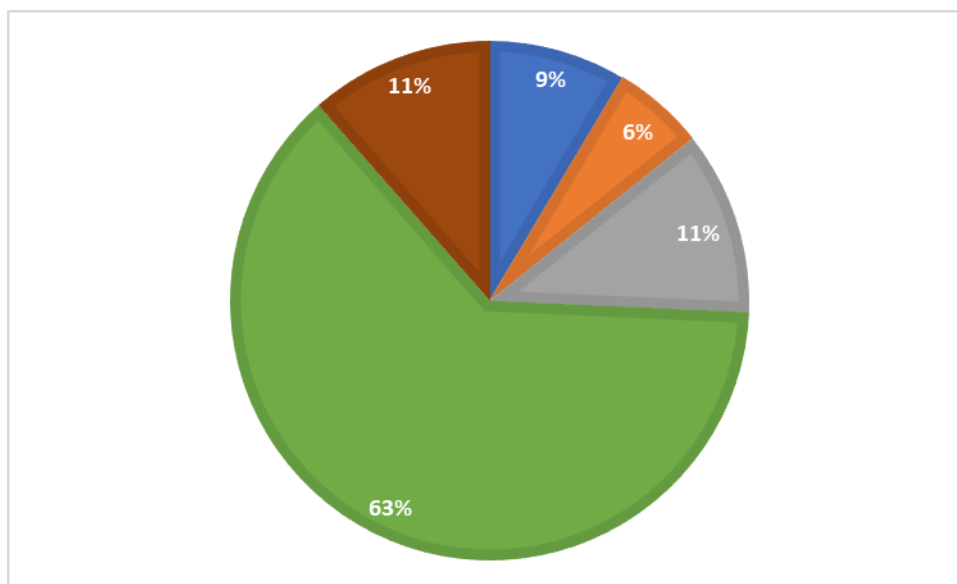
Figure 6. 15. Percentage of water motifs in the unit cell of eighteen hydrated forms of ephedrine. In blue is the zero motif, water molecules that does not hydrogen bond with any compound, in orange is 1(D) motifs, in grey is 2(DD) motif, in green is 5(DDA) motif and in brown is 7(DA) motif.

Table 6. 6. Number of water motifs found for each hydrate salt form of ephedrine.

COMPOUND	number of motifs				
	0	1(D)	2(DD)	5(DDA)	7(DA)
2TAR.H2O (FIRJAU)				1	
3NB.H2O				2	
4HBS.H2O				4	
AHA.H2O (KITLUV)				1	
CDCL5.H2O (HUVXON)				1	
HPO4.H2O (EPHEDP)				1	
LTAR.H2O.2 (GEJMOY)				2	
MAL.H2O (FIRHUM)				2	
MALE.H2O (GEHKIO)				1	
OPC.H2O (FIRGUL)				1	
OPH.4.H2O (GOJJEU)		2			
OPH.7.H2O (KOSYOG)				2	
PRC (DINYAA10)			1		
SO4.H2O.2				4	
TAR.H2O.3					1
CD2CL10.2H2O (COCCEC)					1
BROPH.3H2O (TANXEL)	3				
LTAR.3H2O (GEHLIP)			3		2
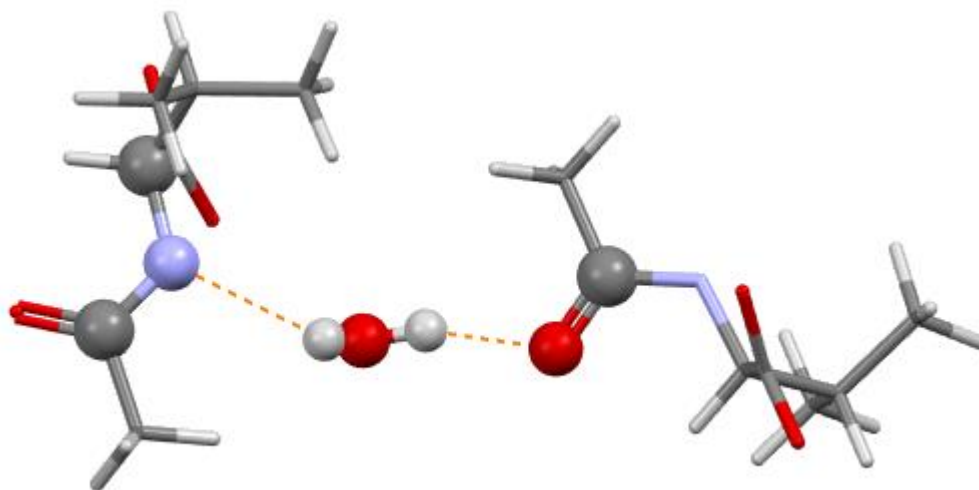
Figure 6. 16. 2(DD) motifs for water molecules in the sample PRC (DINYAA10)
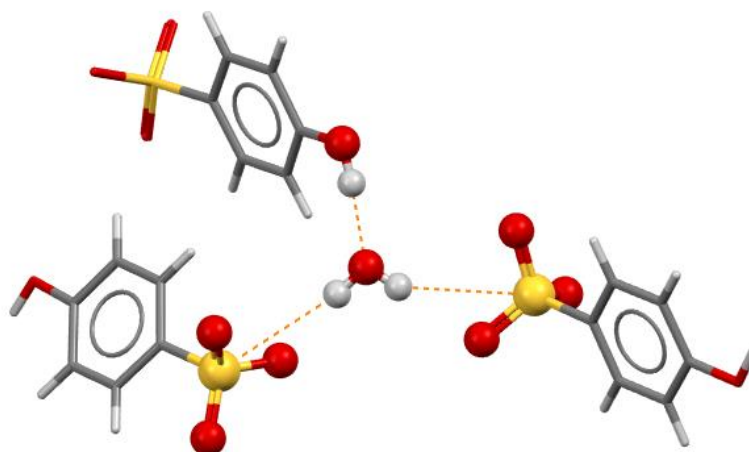
Figure 6. 17. 5(DDA) motifs for water molecules in the sample 4HBS.H2O
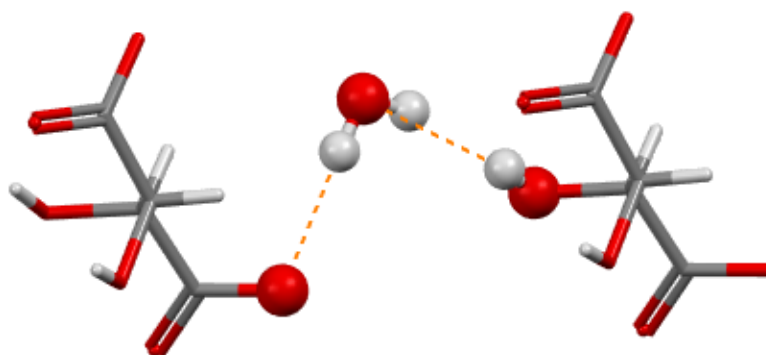
Figure 6. 18. 7(DA) motifs for water molecules in the sample LTAR.3H2O (GEHLIP)

6.4. DONOR ACCEPTOR RATIOS

Two main suggestions have been put forward with respect to using potential hydrogen bond donor and acceptor groups to predict hydrate formation in organic species. To summarise, Desiraju [21] has suggested that donor deficient species are more likely to form hydrates and that the presence of water provides "extra" donor atoms. This allows Etter's [22] rules to be fulfilled as it enables all reliable hydrogen bond acceptors to be utilised in bonding. However, Infantes *et al.* [23] disagree. They state that their CCDC database studies imply no link between donor:acceptor ratios and hydrate formation. They conclude that only the total number of donor and acceptor groups matter, with high totals favouring hydrate formation.

The relatively homogenous set of tyramine, ephedrine and methylephedrine salt structures available herein was used to probe these conflicting statements. Numbers of good hydrogen bond donor atoms and good hydrogen bond acceptor atoms were counted for each salt form. Poor donor or acceptor species (e.g. nitro groups, C-H donors) were ignored. H atoms in position to form intramolecular hydrogen bonds (e.g. the phenol OH of salicylate) were not counted as available donors, in line with Etter's rule to that effect [22]. As this is meant to be a predictive method, no prior knowledge of the actual structure formed was used in donor or acceptor counting. All acid base pairs were assumed to generate 1 to 1 salts. Thus, diacidic species (e.g. oxalic acid, sulfuric acid) were always assumed to lose only one proton and to form part hydrogenated anions with a one minus charge.

Initial analysis split salt forms into three groups for each base, donor deficient (D/A ratio < 1), donor equivalent (D/A = 1) and donor excessive (D/A > 1). For the primary amine tyramine which is noted above to give far more frequent hydrate formation than the other two bases, it was found that 62.0, 63.0 and 14.0 % of the salts formed were hydrates for D/A <1, =1 and > 1 respectively. The equivalent splits for the secondary amine ephedrine and the tertiary amine methylephedrine were 26, 19 and 0 % and 22, 0 and 0 %. This supports Desiraju's [21] claim that donor deficient species are more likely to form hydrates. Though it is a bit contradictory to the initial finding that the tyramine cations form many more hydrates due to their inherently greater number of charged RNH_3 donor atoms. Note that for ephedrine and methylephedrine, hydrates were never formed when the number of potential acceptors was less than the number of donors, indeed for methylephedrine nor were any hydrates formed when D = A.

As for total number of D + A, this was investigated by splitting each base's salt forms in two. For the three bases total D + A ranged from 4 to 8. High DA species were defined as those with D + A > 8. Lower DA species those with D + A ≤ 8. For tyramine, 53 % of high DA salts and 16 % of low DA salts were hydrates. The equivalent figures for ephedrine salts were 33 and 17 % and for methylephedrine salts were 56 and 15 %. Thus, high total numbers of D + A groups also seems to favour hydrate formation but does so without giving any of the absolute predictions as seen for the excess A ratios above. Some species with very high D + A totals are not hydrated (e.g. EPD 2MUC,

total 17). Some salt species with very low D + A totals do form hydrates (e.g. MEPD 2NB, total 5).

6.5. CONCLUSION

This chapter analysed seventy-six hydrated structures of tyramine, ephedrine, enantiopure methylephedrine and racemic methylephedrine which represents 27.4 % of the total of salt forms analysed. There was the formation of thirty-nine hydrated salts of tyramine, ten hydrated salts of enantiopure methylephedrine, eight hydrated salt forms of racemic methylephedrine and eighteen hydrated salts of ephedrine. Thirty-four of these hydrate structures were synthesised as described in Chapter 2.4 and are thus new additions to the structural database. Overall, monohydrate formation was much more common than the formation of higher hydrates, but examples of species with more than one water molecule were found for crystal structures of all four bases. There were also two samples of tyramine with a disordered water channel in the structure, TYR RTAR.wc and TYR TIOSA.wc.

A reasonable estimate for hydrate occurrence in general organic structures is 6.6%, rising to about 22.5% for organic salts with NH groups [19-20]. For most categories of anion, tyramine clearly is much more likely to form hydrated salt forms than the other salts, followed by ephedrine and methylephedrine, respectively. There are two obvious structural differences between the tyrammonium cation and the others. TYR has a charged RNH_3 group that provides more extremely good hydrogen bond donor groups than the other cations (R_2NH_2 and R_3NH respectively) and TYR has a phenol OH substituent rather than the alkyl OH substituent of the ephedrine derivatives. Of these changes, the extra charged donor atoms are perhaps the more likely driver to hydration. Infantes *et al.* [23] have shown that increased numbers of potential hydrogen bonding groups favours hydrate formation. Salt forms with one or more water molecule present in the unit cell were formed with all types of counterions: carboxylates, halides, sulfonates and benzoates.

Analysis of D + A totals and of D/A ratios indicate that higher D + A totals do favour (but far from guarantee) hydrate formation. Low D/A ratios also favour hydrate formation, indicating that water may be included as a source of donor atoms for donor deficient structures. For ephedrine no salt with an excess of D groups formed hydrates. For methylephedrine, no salt with D/A ratios ≥ 1 formed hydrates. The division of hydrates amongst the different anion types for all four APIs is shown in Figure 6. 19. Thus, the analysis made for TYR by Morrison *et al.* [1], can be updated and expanded with all results obtained:

(i)   There is around a 10.0 % occurrence of hydrates in halides (6.3 %), aliphatic sulfonates (7.7 %), benzoates (9.4 %) and monocarboxylates (10.8 %) salt forms of tyramine, enantiopure and racemic methylephedrine and ephedrine. These compounds will predominantly form anhydrous salt forms.

(ii)   There is around a 50 % occurrence of hydrates in dicarboxylates (47.2 %), inorganic salts with tetrahedral anions (50.0 %) and aryl-sulfonates (53.1 %) of tyramine, enantiopure and racemic methylephedrine and ephedrine. Formation of hydrates for these compounds is thus relatively likely given suitable synthesis and crystallisation conditions.

The commonest environment of the water molecules is described by the threefold 5(DDA) motif where the water molecule acts as a proton donor and acceptor, donating two protons with other molecules and receiving one proton from another molecule. The motif 2(DD) is present in at least one salt form of all bases, where the water molecule acts only as a proton donor and shares both protons to other molecules without accepting a classical hydrogen bond. It is interesting to note that although the motif 6(DDAA), where the water molecule acts as a four-fold proton donor and acceptor, is not present in ephedrine and racemic methylephedrine species, and is present in only one sample of enantiopure methylephedrine, it is commonly present in tyramine salt structures. The higher incidence of water molecules accepting hydrogen bonds for TYR must be related to the greater number of charged H donors available from the RNH_3 cation.
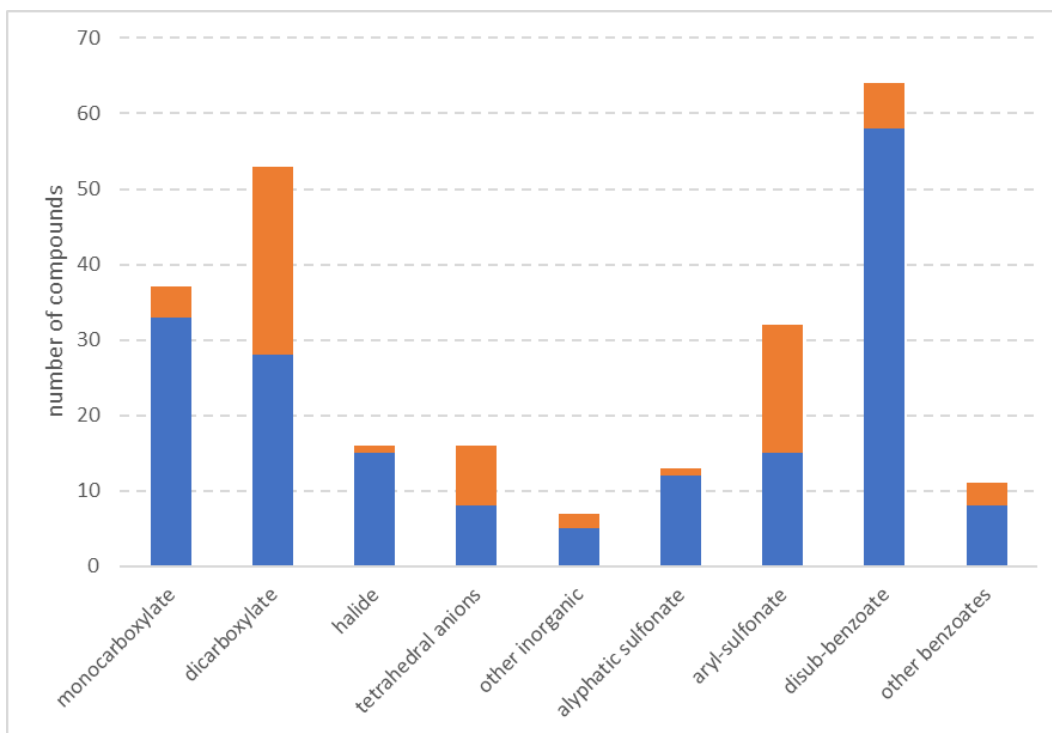
Figure 6. 19. Number of hydrated (in orange) and anhydrous (in blue) compounds for tyramine, enantiopure methylephedrine, racemic methylephedrine and ephedrine according to the composition of the counterion.

6.6. REFERENCES

[1]   Briggs, N., Kennedy, A., & Morrison, C. (2012). Acta Crystallographica Section B, 68(4), 453-464.

[2]   Koleva, B.B., Kolev, T., Seidel, R.W., Spiteller, M., Mayer-Figge, H. & Sheldrick W.S. (2008). Journal of Molecular Structure, 888(1), 138-144.

[3]   Ivanova, B. & Spiteller, M. (2010). Spectrochimica Acta Part A: Molecular and Biomolecular Spectroscopy, 77(4), 849-855.

[4]   Ogawa, K., Tago, K., Ishida, T. & Tomita K.-I. (1980). Acta Crystallogr., Sect.B:Struct.Crystallogr.Cryst.Chem., 36, 2095.

[5]   Kolev, T., Koleva, B., Seidel, R., Mayer-figge, H., Spiteller, M., & Sheldrick, W. (2009). Amino Acids, 36(1), 29-33.

[6]   Gryl, M., Rydz, A., Wojnarska, J., Krawczuk, A., Kozieł, M., Seidler, T., . . . Stadnicka, K. (2019). IUCrJ, 6(Pt 2), 226-237.

[7]   Kennedy, A. R., Morrison, C. A., Briggs, N. E., & Arbuckle, W. (2011). Crystal Growth and Design, 11(5), 1821-1834.

[8]   De Moraes, S.L., Edwards, D., Florence, A.J., Johnston, A., Johnston, B.F., Morrison, C.A., & Kennedy, A.R. (2017). Crystal Growth and Design, 17(6), 3277-3286.

[9]   Babor M., Nievergelt, P.P., Cejka, J., Zvonicek, V. & Spingler B. (2019) IUCrJ . 6, 145.

[10]   Li, B.-L., Zhang Z.-G., Wang W., Li, J. & Wang C.-W. (2008). Z.Naturforsch.,B:Chem.Sci. 63, 77.

[11]   Wang, D.-Q., Chen, J.-T., Dan, W.-Y., He, D.-H., Chen, Z.-P. & Di, Y. Y. (2011), J.Chem.Soc.Pak. 33, 333.

[12]   Hearn, R.A., Freeman, G.R. & Bugg, C.E. (1973). J.Am.Chem.Soc. 95, 7150.

[13]   Collier, E., Davey, R., Black, S., & Roberts, R. (2006). Acta Crystallographica Section B, 62(3), 498-505.

[14]   Kok, A.M.G, Wynberg, H., Garcia-Granda, S., Beurskens, P.T. & Smits, J.M.M. (1988). Acta Crystallogr.,Sect.C:Cryst.Struct.Commun. 44, 2235.

[15]   Bruins Slot, H., Leusen, F., Van Der Haest, A., & Van Bolhuis, F. (1992). Acta Crystallographica Section C, 48(5), 925-929.

[16]   Gorman, A., Gould, R.O., Gray, A.M., Taylor, P. & Walkinshaw M.D. (1986). J.Chem.Soc., Perkin Trans.2. 5, 739.

[17]   Charles, N.G.; Rodesiler, P.F., Griffith, E.A.H. & Amma, E.L. (1984) Acta Crystallogr.,Sect.C:Cryst.Struct.Commun. 40, 1676.

[18]   Bruins Slot, H., Leusen, F., Van Der Haest, A., & Van Bolhuis, F. (1992). Acta Crystallographica Section C, 48(5), 925-929.

[19]   Infantes, L. & Motherwell, W. D. S. (2002). CrystEngComm, 4, 454–461.

[20]   Haynes, D. A., Jones, W. & Motherwell, W. D. S. (2005). CrystEngComm, 7, 342–345.

[21]   Desiraju, G. R. (1991). J. Chem. Soc. Chem. Commun. 426–428.

[22]   Etter, M. C. (1990). Acc. Chem. Res. 23, 120–126.

[23]   Infantes, L., Fabian, L. & Motherwell, W. D. S. (2007). CrystEngComm, 9, 65–71.

7. CRYSTAL PACKING SIMILARITY

7.1. TYRAMINE SALT FORMS

Packing similarity analyses are often displayed as tree diagrams. These show successive increases in the number of neighbouring molecular fragments that can be overlaid for different structures, with 15 out of 15 matching fragments being termed isostructural for the fragment investigated. An example of the crystal packing similarity can be observed for 17 salt forms of ephedrine previously published by Collier *et al.* [3] in a case study published in CCDC website [9] where the author analysed the relationship between the packing similarity and the morphology of the crystal.

This work expands the previously calculated tree diagram for tyramine salt structures of Briggs *et al.* [1] in two ways. Firstly, there is an increase from forty-two analysed structures to ninety-seven structures. Secondly, the new molecular cation conformations identified (above) are included in the analysis. To facilitate visualisation, a tree diagram was developed naming only the counter-ion present in the structure, as can be observed in Figure 7.1, where the compounds in red have extended α conformation, the compounds in blue have folded conformation, the compounds in green have extended β conformation, the single structure in pink features both extended α and folded conformations (the salt form of *m*-toluate MTOL/MEDCUV) and the structures in orange feature both extended α and β conformations.

From the top of the tree diagram to cluster size two are the twenty-nine structures that have no similarity with the others, mostly containing compounds with extended α conformation (in red), however there is also the presence of folded conformation (in blue), the salt form tyrammonium *m*-toluate (MTOL/MEDCUV) with both extended α and folded conformations and salt forms with both extended α and β conformations (2OXA and HIP, in orange). When increasing the cluster size to three there are another twenty-nine salt forms that do not have any further similarity with the others. At this low level of structural similarity there are numerous small structural groups containing

most of the cations with the less common conformations. Only one non-red (extended α) group matches more than 3 fragments. This is the folded conformation group, containing the samples OXA and HOB.

The most interesting and informative part of the diagram are the isostructural groups at the bottom. All isostructural groups with a match of 15 cations from 15 are derivatives of small structural groups with packing of 3 cations. The first three isostructural groups are related via a common root in the sample DLMAL.H2O. All structures within these three groups are anhydrous and all are compounds of benzoate or a mono-substituted benzoate: Group 1 contains five compounds that are methyl or halide derivatives of benzoates that are variously substituted in the *ortho-*, *meta-* or *para-*positions (2CB, OTOL, 3FB, 4FB and 4CB.2), Group 2 containing benzoate and *o*-fluorobenzoate (BZ and 2FB, respectively), and Group 3 containing only the *para-*substituted benzoates (4AB and PTOL). Groups 2 and 3 are unchanged from earlier analysis, but this work now adds one new structure to Group 1 when compared with the previously published work [1] the monoclinic form of the salt form of *p*-chlorobenzoate (4CB.2).

There is also the formation of two other larger isostructural groups. Group 4 is characterized by the presence of hydrated salts of tyramine with dicarboxylic acids. All have cation-anion stoichiometry of 2:1 (LTAR.2H2O, SUC.2H2O, HSUC.2H2O, 2DLMAL.H2O and FUMS.H2O). This work also adds two new structures of hydrated salts to group 4 when compared with the previously published work: FUMS.H2O and 2DLMAL.H2O. Joined to Group 4 by the small structural group containing 2AB, there is also Group 5, where the counterions are characterized as being derived from inorganic acids. Interestingly the group contains two anhydrous structures, CL and BR, and four hydrated structures, the new structure TYR.CL.H2O and PO4.H2O, CLO4.H2O and BF4.H2O. This last group raises the point that gross physical changes (here the absence or presence of water and the inclusion in one structure of a zwitterionic form of tyramine) that must lead to very different intermolecular hydrogen bonding arrangements do not necessarily lead to large changes in the packing of the organic cations. As other authors have pointed out, this highlights the large effect that molecular shape plays in governing packing and array structure [5]. Here this is true

even in ionic salts with strong hydrogen bonding interactions. A similar if somewhat more subtle change in molecular structure is also accommodated by Group 1, with its range of benzoate anions with different substitution positions.

An example of the matching packing for 15 out of 15 cations for each group can be observed in Figures 7.2 to 7.6, where Figure 7.2 (a) is the view through c axis for the packing of 2CB and OTOL samples (Group 1) and Figure 7.2 (b) is the view through c axis for the packing of 2FB and BZ samples (Group 2); Figure 7.3 is the view through c axis for the packing of 4AB and PTOL samples (Group 3); Figure 7.4 (a) is the view through a axis for the packing of SUC.2H2O and 2DLMAL.H2O samples (Group 4) and Figure 7.4 (b) is the view through c axis for the packing of PO4.2H2O and CL samples (Group 5).

Figure 7. 1. Tree diagram for tyramine salt forms, where in red compounds with extended α conformation, in blue, compounds with folded conformation, in green compounds with extended β conformation, in pink the one compound with extended α and folded conformations, the salt form of *meta*-toluate (MTOL/MEDCUV) and in orange compounds with extended α and β conformations.
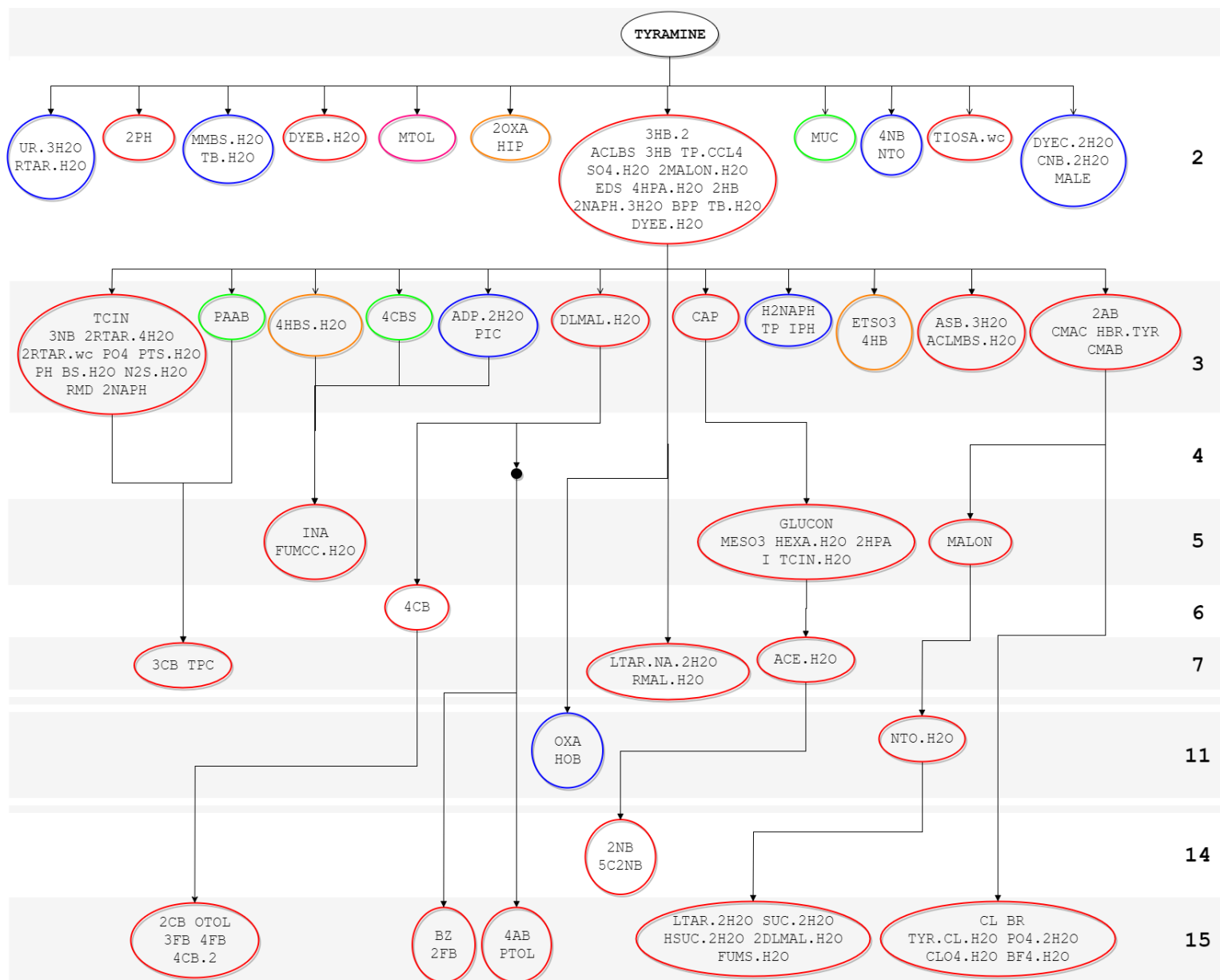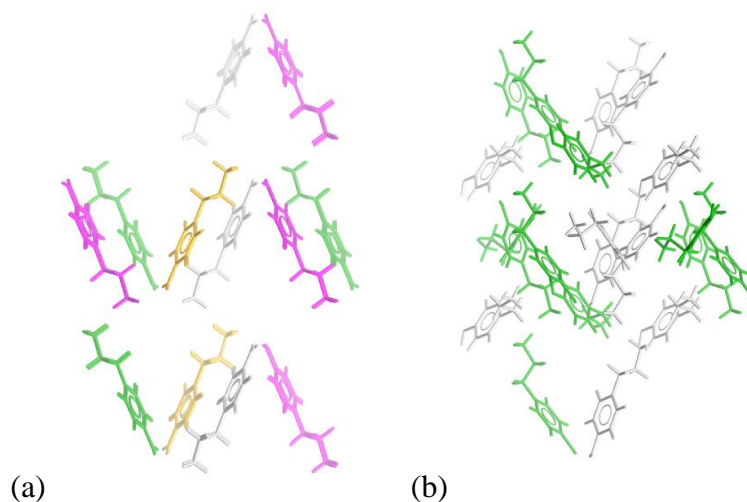
Figure 7. 2. (a) Group 1 example of packing for 15 out of 15 cations for the samples 2CB (MEDBOO) and OTOL (MEDBUU) with RMS of 0.136. View via *c* axis. (b) Group 2 example of packing for 15 out of 15 cations for the samples 2FB (MEDBII) and BZ (MEDBAA) with RMS of 0.125. View via *c* axis.
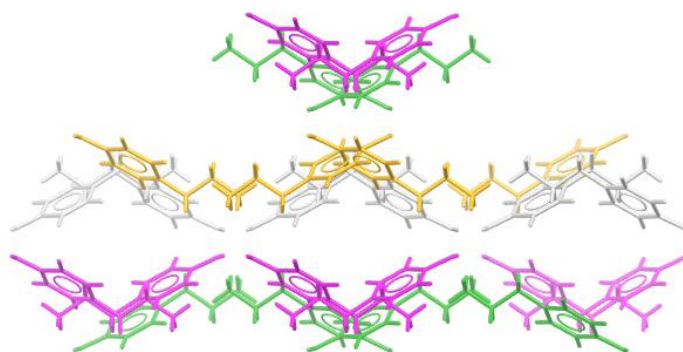
Figure 7. 3. Group 3 example of packing for 15 out of 15 cations for the samples 4AB (MEDDEG) and PTOL (MEDFEI) with RMS of 0.175. View via *c* axis.
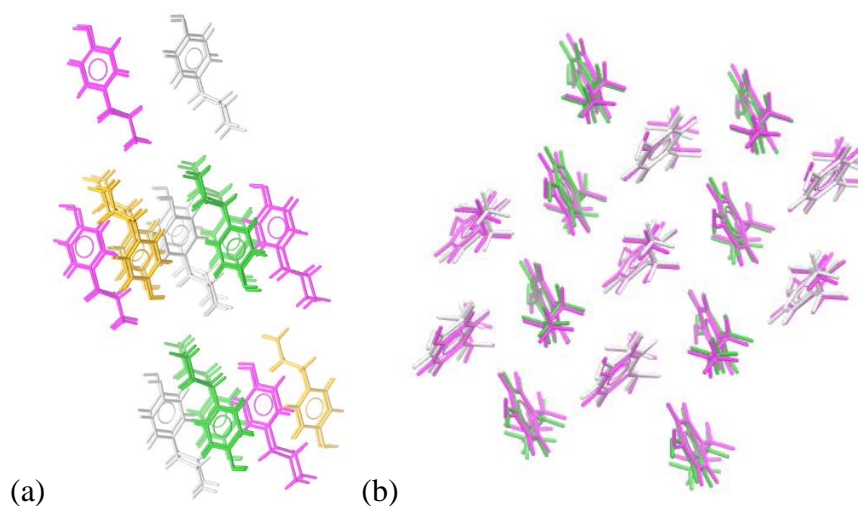
Figure 7. 4. (a) Group 4 example of packing for 15 out of 15 cations for the samples SUC.H2O (MEDGEJ)and 2DLMAL.H2O with RMS of 0.334. View via *a* axis. (b) Group 5 example of packing for 15 out of 15 cations for the samples PO4.2H2O (MECYUQ) and CL (TYRAMC11) with RMS of 0.559. View via *c* axis.

7.2. METHYLEPHEDRINE SALT FORMS

Similarity in the cation packing was analysed for all ninety-two salt forms of enantiopure and racemic methylephedrine, that is those described in Chapter 2 together with structures available from the CCDC and Morrison *et al.* [1]. Herein we are thus expanding the previously calculated tree diagram of Kennedy *et al.* [2] from thirty-five structures to ninety-one structures. We also add the new conformational descriptions now available. An earlier version of this updated analysis was published as Moraes *et al.* [6]. To facilitate visualisation, the tree diagram was developed naming only the counter-ion present in the structure, where the letter "*e*" before the label represents enantiopure compounds and the letter "*r*" before the label represents racemic compounds, see Figure 7.6.

The first result observed is an increase in the number of isostructural groups identified. Kennedy *et al.* [2] presented 6 isostructural groups with a match of 15 cations from 15. Here this is expanded to ten groups. Of the six original isostructural groups, three remain the same. These are: Group 1, containing both enantiopure salt forms of halides bromine and chlorine, *e*BR (ZZZQOS01) and *e*CL (ZZZQSE01) where all cations have conformation (γ), Group 2 containing a polymorph of racemic methylephedrine and methanesulfonate and the racemic hydrogensulfonate, *r*MESO3.2 (IVUNIX) and *r*SO4.H2O (IVUNUJ) all cations with conformation (α) and Group 3 containing two *ortho*-substituted benzoates of racemic methylephedrine, *r*2CB (IVUKOA) and *r*OTOL (IVUMES) where all cations have conformation (γ). The remaining three original groups each now have the addition of one or more new structures: Group 4, which originally contained salt forms of racemic methylephedrine with the *meta*-substituted benzoates, *r*3FB (IVULIV) and *r*3CB (IVUQUM), had added two other salt forms of racemic methylephedrine and *meta*-substituted benzoates, *r*MTOL (VAVLUC) and *r*3NB (VAVKOV), all cations with conformation (γ); Group 5 which originally contained two enantiopure methylephedrine salts with *ortho*- and *meta*-substituted benzoates, *e*2NB.H2O (IVUKUG) and *e*3FB (IVULER), had added another *meta*-substituted benzoate, *e*3AB (VAVJAG), all cations with conformation (γ); and Group 6 which originally contained three enantiopure methylephedrine salts with *ortho*- and *para*-substituted benzoates, the samples *e*OTOL (IVUMAO), *e*4CB

(IVUSIC) and *e*PTOL (IVUSOI), had added two salt forms of enantiopure methylephedrine again with *ortho-* and *para*-substituted benzoates, *e*4FB and *e*2FB (VAVHOS). This is an interesting group as it contains cations with both (α) and (β) conformations. Of the five members, the structures with only cations with conformation (α) are *e*4CB (IVUSIC) and *e*PTOL (IVUSOI). The structures *e*OTOL (IVUMAO) and 4FB have only conformation (β) and structure *e*2FB (VAVHOS) has one cation with conformation (α) and one cation with conformation (β).

There was also the formation of four new isostructural groups: Group 7 containing the sulfonates of racemic methylephedrine, *r*MESO3 and *r*EDS (IVUNAP), all cations with conformation (α); Group 8 containing both naphthalates of enantiopure methylephedrine, *e*H2NAPH [conformation (α)] and *e*2NAPH [conformation (β)]; Group 9 containing salt forms of racemic methylephedrine and a wide variety of counterions, including dicarboxylates [*r*MUC, *r*SUC (VAVMEN), *r*RTAR (VAVMIR), *r*FUM] , one naphthalate [*r*1NAPH] , one benzoate [*r*3AB] and one halide [*r*CL (ZZZLUA01)]. All compounds in this group have conformation (γ) apart from the sample *r*CL (ZZZLUA01), with conformation (α); and Group 10 containing salt forms of enantiopure methylephedrine and carboxylates, *e*RMD (VAVJUA), *e*2HPA and *e*PA, all compounds with conformation (γ).

An example of the packing for 15 out of 15 cations for each group can be observed in Figures 7.5 and 7.7 to 7.10, where Figure 7.5 (a) is the view through *b* axis for the packing of *e*BR (ZZZQOS01) and *e*CL (ZZZQSE01) samples (Group 1) and Figure 7.5 (b) is the view through *a* axis for the packing of *e*MESO3.2 (IVUNIX) and *r*SO4.H2O (IVUNUJ) samples (Group 2); Figure 7.7 (a) is the view through *a* axis for the packing of *r*2CB (IVUKOA) and *r*OTOL (IVUMES) samples (Group 3); Figure 7.7 (b) is the view through *c* axis for the packing of *r*3FB (IVULIV) and *r*3CB (IVUQUM) samples (Group 4); Figure 7.8 (a) is the view through *a* axis for the packing of *e*3AB (VAVJAG) and *e*3FB (IVULER) samples (Group 5); Figure 7.8 (b) is the view through *c* axis for the packing of samples *e*4CB (IVUSIC) and *e*PTOL (IVUSOI) samples (Group 6); Figure 7.9 (a) is the view through *c* axis for the packing of samples *r*MESO3 and *r*EDS (IVUNAP) samples (Group 7); Figure 7.9 (b) is the view through *c* axis for the packing of samples *e*H2NAPH and *e*2NAPH samples

(Group 8); Figure 7.10 (a) is the view through *c* axis for the packing of samples *r*MUC and *r*SUC samples (Group 9); and Figure 7.10 (b) is the view through *c* axis for the packing of samples *e*RMD (VAVJUA) and *e*2HPA samples (Group 10).

(a)   (b)
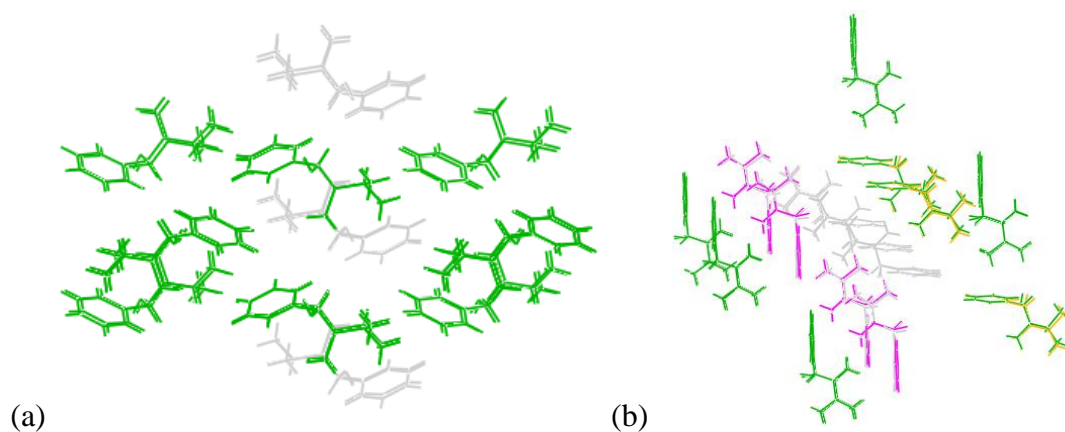
Figure 7. 5. (a) Group 1 example of packing for 15 out of 15 cations for the samples *e*BR (ZZZQOS01) and *e*CL (ZZZQSE01) with RMS of 0.181. View via *b* axis. (b) Group 2 example of packing for 15 out of 15 cations for the samples *r*MESO3.2 (IVUNIX) and *r*SO4.H2O (IVUNUJ) with RMS of 0.201. View via *a* axis.

(a)   (b)
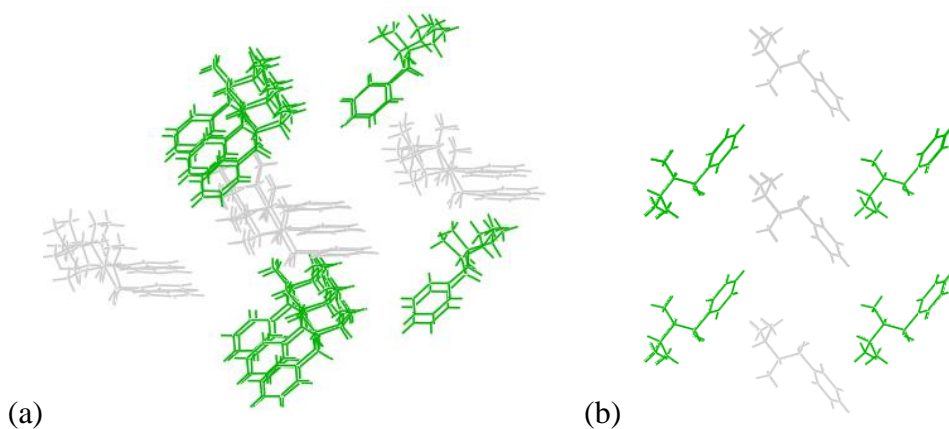
Figure 7. 6. (a) Group 5 example of packing for 15 out of 15 cations for the samples *e*3AB (VAVJAG) and *e*3FB (IVULER) with RMS of 0.470. View via *a* axis. (b) Group 6 example of packing for 15 out of 15 cations for the samples *e*4CB (IVUSIC) and *e*PTOL (IVUSOI) with RMS of 0.106. View via *a* axis.

Figure 7. 7. Tree diagram for methylephedrine salt forms, where in red compounds with conformation (α), in blue compounds with conformation (β), in green compounds with conformation (γ). More than one coloured circle in a group represents the presence of more than one cation conformation.

152
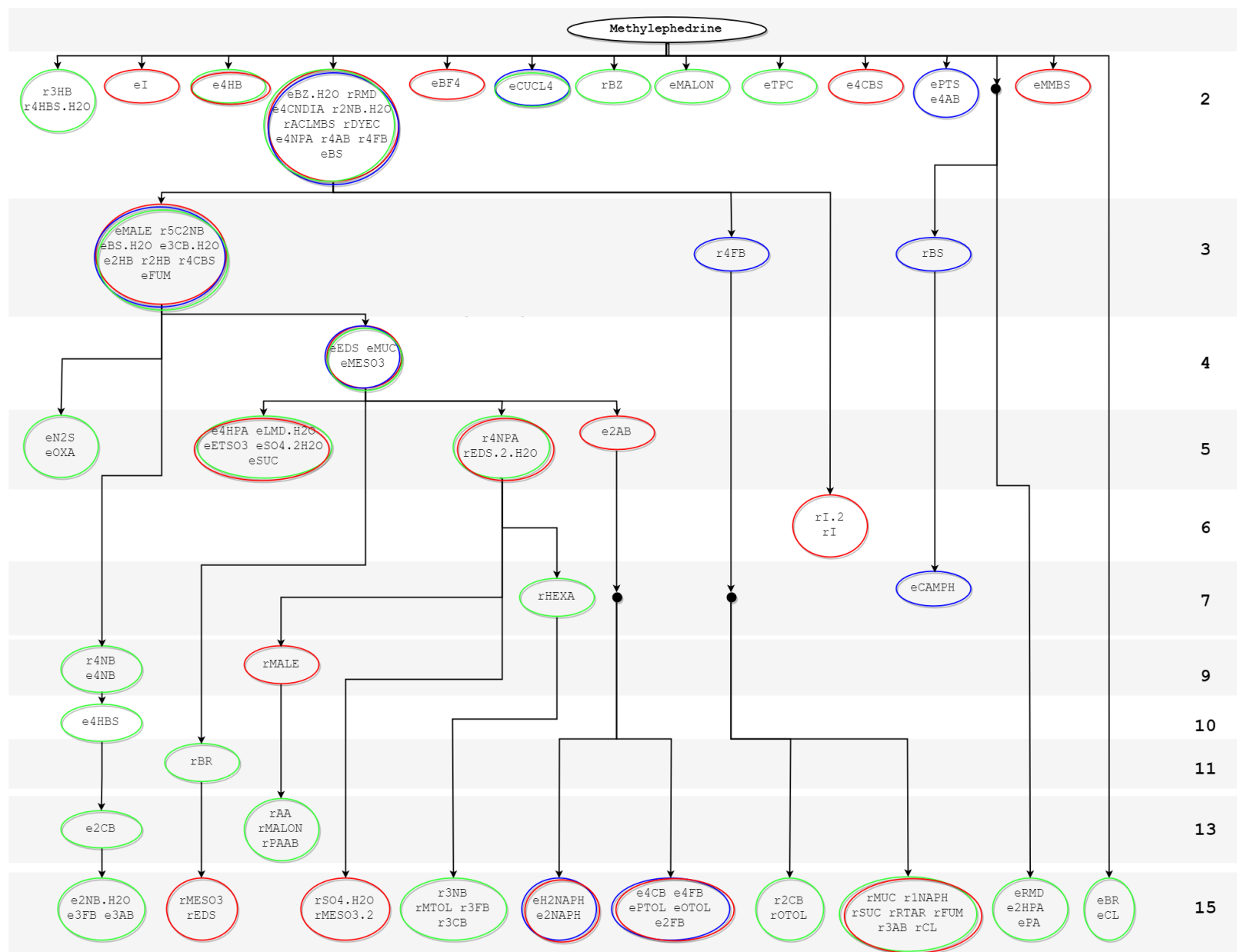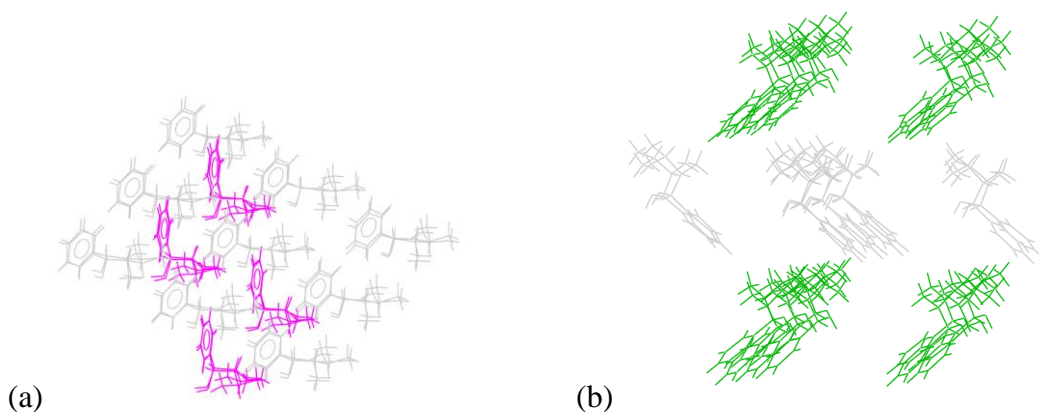
Figure 7. 8. (a) Group 7 example of packing for 15 out of 15 cations for the samples *r*MESO3 and *r*EDS (IVUNAP) with RMS of 0.284. View via *a* axis. (b) Group 8 example of packing for 15 out of 15 cations for the samples *e*H2NAPH and *e*2NAPH with RMS of 0.591. View via *a* axis.
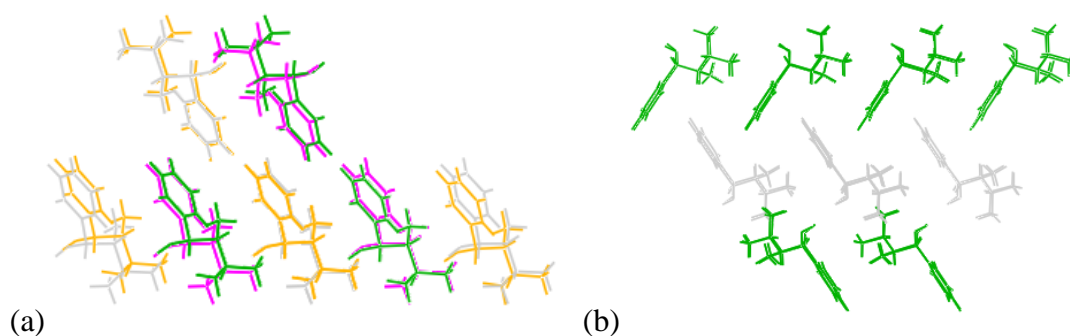
Figure 7. 9. (a) Group 9 example of packing for 15 out of 15 cations for the samples *r*MUC and *r*SUC (VAVMEN) with RMS of 0.608. View via *c* axis. (b) Group 10 example of packing for 15 out of 15 cations for the samples *e*RMD (VAVJUA) and *e*2HPA with RMS of 0.170. View via *b* axis.

7.3. EPHEDRINE SALT FORMS

Cation packing similarity analysis for salt forms of ephedrine was made for eighty-seven salt forms obtained from Chapter 2.4 or available from CCDC database. Although there are various publications regarding ephedrine salt forms in the literature [3,4], there was no mention of cation packing for these structures in the original publication. However, these structures were used in a case study for Crystal Form Analysis published by CCDC [9]. Thus, this work will expend this tree diagram considering all these samples presented in this work and obtained by CCDC database. Again, to facilitate visualisation, the tree diagram was developed naming only the

counter-ion present in the structure, as it can be observed in Figure 7.11. Information on the cation conformation, as described in Chapter 5.3, is also observed in the tree diagram. The colour code for the circles in the tree diagram is: Circles in red represents extended conformation; circles in orange represents cations with conformation extended α_1; circles in yellow represents conformation extended α_2; circles in dark brown represents conformation extended β; circles in blue represents the folded conformation; circles in light blue represents conformation folded α_1; circles in dark blue represents conformation folded α_2; circles in purple represents conformation folded β; and circles in green represents the compound with conformation γ. When the circle is filled with colour, there is more than one cation conformation observed.

As it can be observed in Figure 7.11, eight of nine isostructural group have only the standard extended conformation: Group 1 includes the phosphorinates OPH (FILGAI) and OPH.3 (FIMVEC); Group 2 includes the phosphorinates OPH.1 (FIMTUQ) and OPH.8 (SUMWEC); Group 3 includes the *meta*-substituted benzoates 3CB and MTOL; Group 4 includes the hydrogenphosphate and methanesulfonate salt forms of ephedrine, H2PO4 (EPHDHP) and MESO3 (GEHKUA), respectively. The packing of these two structures were also observed in the case study published in CCDC website [9]; Group 5 includes the samples the dicarboxylates MALON (GEHKOU) and OXA (ZEXQIF); Group 6 includes the halides CL (ZEXLAS/EPHECL02) and BR (ZZZLBU01); Group 7 is larger and more diverse and includes two monocarboxylates, 4APA and 4HPA, one *ortho*-substituted benzoate, AA, and one dicarboxylate, HEXA (GEHJEJ); and Group 9 including the sulfonates BROPH.1 (TAPNED) and BROPH.2 (TAPNIH). There is also one group containing only standard folded conformation cations and a wide variety of counterion. This is Group 8 which includes the sulfonates N2S, 4CBS, PTS (GEHLOV) and EDS (GEHJOT), one salt form of ephedrine and the nitrate, NO3 (GEHLAH), and the monoclinic form of ephedrine iodide, I.2 (ZZZSDC02). The samples PTS (GEHLOV), EDS (GEHJOT) and NO3 (GEHLAH) were also presented as the folded group in the analysis done by CCDC [9]. Thus, this work includes 3 new folded structures in this group.

An example of the packing for 15 out of 15 cations for each group can be observed in Figures 7.12 to 7.15, where Figure 7.12 (a) is the view through *b* axis for the packing

of OPH (FILGAI) and OPH.3 (FIMVEC) samples (Group 1) and Figure 7.12 (b) is the view through *b* axis for the packing of OPH.1 (FIMTUQ) and OPH.8 (SUMWEC) samples (Group 2); Figure 7.13 (a) is the view through *b* axis for the packing of 3CB and MTOL samples (Group 3); Figure 7.13 (b) is the view through *b* axis for the packing of H2PO4 (EPHDHP) and MESO3 samples (Group 4); Figure 7.14 (a) is the view through *b* axis for the packing of MALON (GEHKOU) and OXA (ZEXQIF) samples (Group 5); Figure 7.14 (b) is the view through *b* axis for the packing of CL (ZEXLAS/EPHECL02) and BR (ZZZLBU01) samples (Group 6); Figure 7.14 (c) is the *a-b* view for the packing of HEXA (GEHJEJ) and AA samples (Group 7); Figure 7.15 (a) is the view through *c* axis for the packing of NO3 (GEHLAH) and N2S samples (Group 8); and Figure 7.15 (b) is the view through *b* axis for the packing of BROPH.1 (TAPNED) and BROPH.2 (TAPNIH) samples (Group 9).

(a)　　　　　　　　　　　　　　　　　　(b)
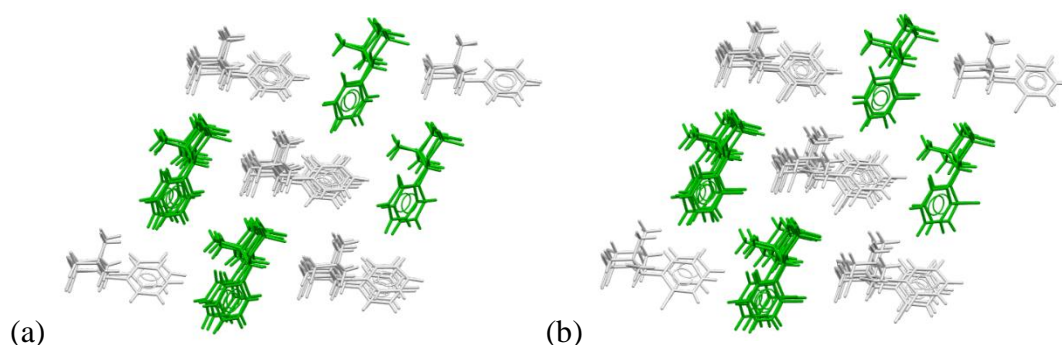
Figure 7. 10. (a) Group 1 example of packing for 15 out of 15 cations for the samples OPH (FILGAI) and OPH.3 (FIMVEC) with RMS of 0.741. View via *b* axis. (b) Group 2 example of packing for 15 out of 15 cations for the samples OPH.1 (FIMTUQ) and OPH.8 (SUMWEC) with RMS of 0.883. View via *b* axis.

Figure 7. 11. Tree diagram for ephedrine salt forms, where in red compounds with standard extended conformation, in orange is conformation extended α1, in yellow is is conformation extended α2, in dark brown conformation extended β, in blue compounds with standard folded conformation, in light blue is conformation folded α1, in dark blue s conformation folded α2, in puple is conformation folded β and in green compounds with conformation γ. More than one coloured circle in a group represents the presence of more than one cation conformation.

156

(a)   (b)
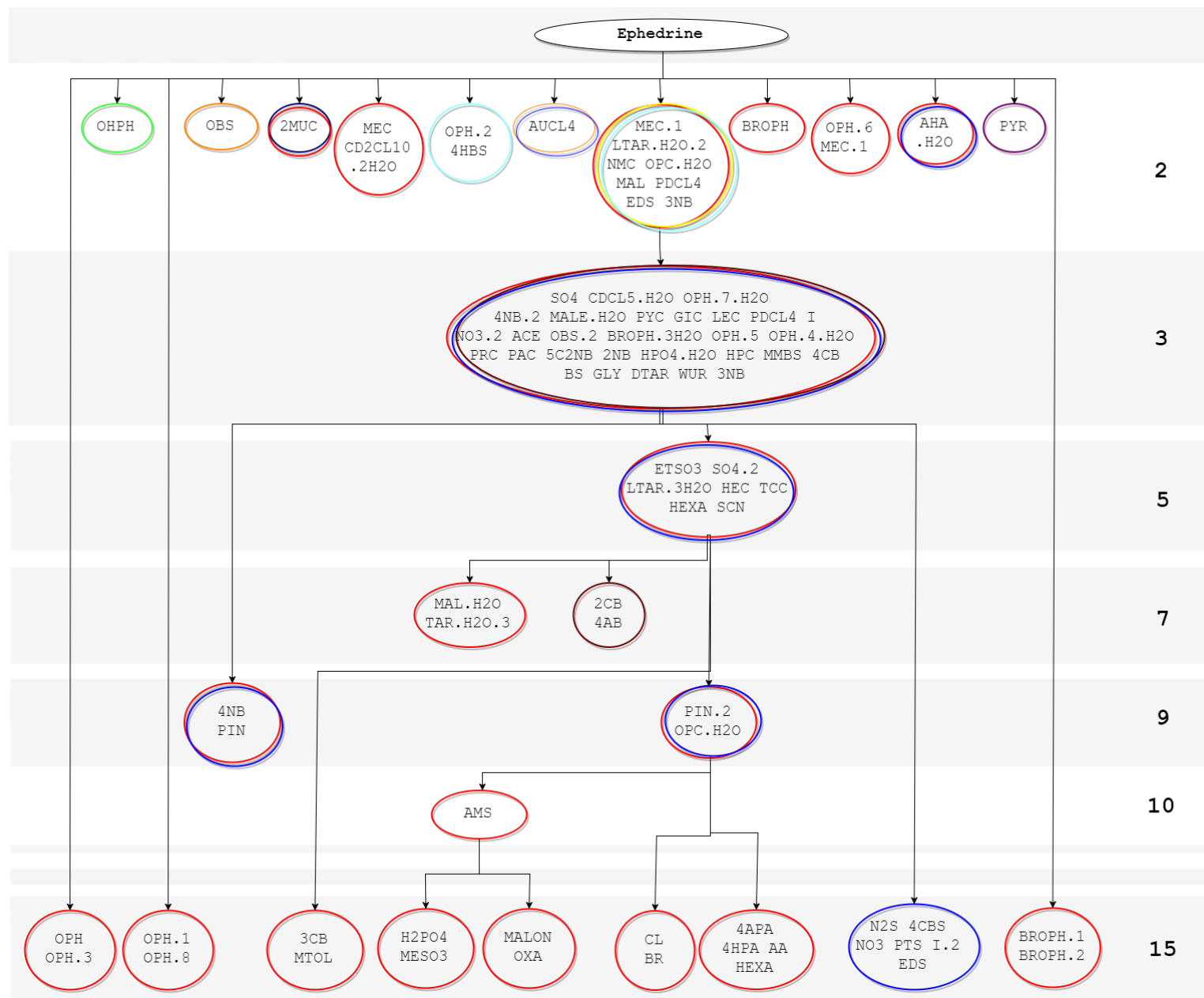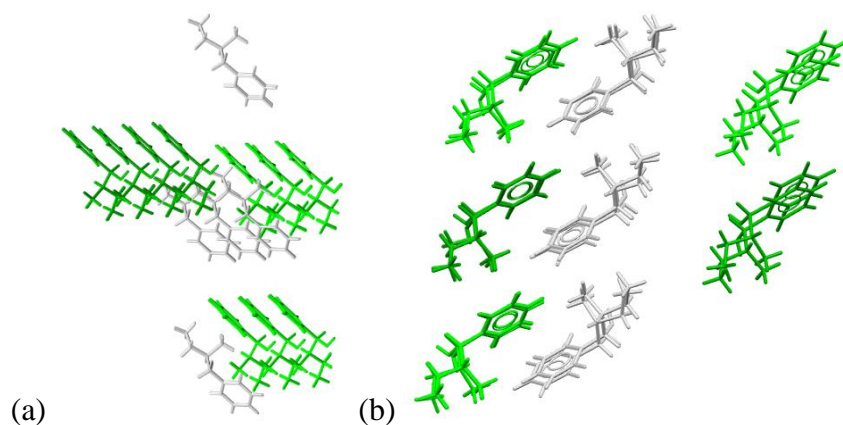
Figure 7. 12. (a) Group 3 example of packing for 15 out of 15 cations for the samples 3CB and MTOL with RMS of 0.071. View via *b* axis. (b) Group 4 example of packing for 15 out of 15 cations for the samples H2PO4 (EPHDHP) and MESO3 (GEHKUA) with RMS of 0.544. View via *b* axis.

(a)   (b)   (c)
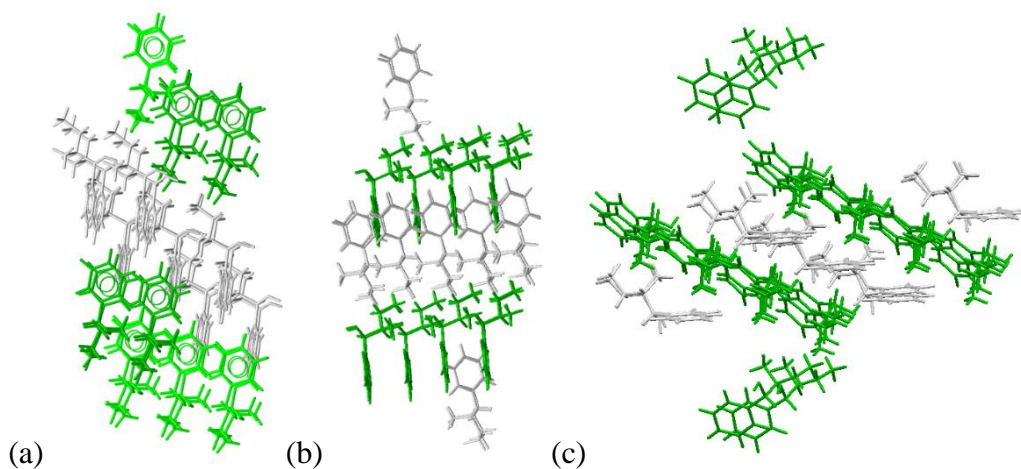
Figure 7. 13 (a) Group 5 example of packing for 15 out of 15 cations for the samples MALON (GEHKOU) and OXA (ZEXQIF) with RMS of 0.608. View via *b* axis. (b) Group 6 example of packing for 15 out of 15 cations for the samples CL (ZEXLAS/EPHECL02) and BR (ZZZLBU01) with RMS of 0.157. View via *b* axis. (c) Group 7 example of packing for 15 out of 15 cations for the samples HEXA (GEHJEJ) and AA with RMS of 0.910. View via *ab* plane.

(a)   (b)
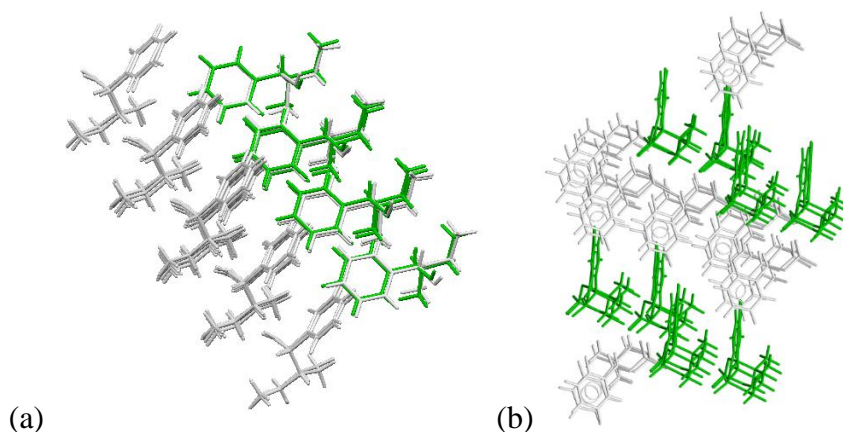
Figure 7. 14. (a) Group 8 example of packing for 15 out of 15 cations for the samples NO3 (GEHLAH) and N2S with RMS of 0.292. View via *c* axis. (b) Group 9 example of packing for 15 out of 15 cations for the samples BROPH.1 (TAPNED) and BROPH.2 (TAPNIH) with RMS of 0.689. View via *b* axis.

157

7.4. CONCLUSION

The cation packing similarity tool of the Mercury [7,8] suite was used to analyse the crystal structures of ninety-seven salt forms of tyramine, ninety-two salt forms of enantiopure and racemic methylephedrine and eighty-seven salt forms of ephedrine. These structures were described in APPENDIX 3.1 for tyramine compounds, APPENDIX 3.2 for methylephedrine compounds and APPENDIX 3.3 for ephedrine compounds.

Tyramine salts forms have five isostructural groups that can be described according to the composition of the counterion. Including new salt forms in the analysis increased the number of structures in three of these isostructural groups: In Group 1 there was the addition of the monoclinic form of the salt form of p-chlorobenzoate (4CB.2); In Group 4 there was the addition of two dicarboxylates, FUMS.H2O and 2DLMAL.H2O; and in Group 5 there was the addition of the new structure TYR.CL.H2O.

This work also increased the number of known isostructural groups for enantiopure and racemic methylephedrine salt forms from six to ten groups. Of the six original isostructural groups, the three groups have the addition of one or more structures: Group 4, had added two other salt forms of racemic methylephedrine and *meta*-substituted benzoates, *r*MTOL (VAVLUC) and *r*3NB (VAVKOV); Group 5 had added another *meta*-substituted benzoate, *e*3AB (VAVJAG); and Group 6 had added the two salt forms of enantiopure methylephedrine with benzoates *ortho-* and *para*-substituted benzoate, *e*4FB and *e*2FB (VAVHOS). The four new isostructural groups for these bases contained sulfonates of racemic methylephedrine (Group 7), naphthalates of enantiopure methylephedrine (Group 8), salt forms of racemic methylephedrine and a variety of counterions, including dicarboxylates, naphthalate, benzoates and halide (Group 9) and containing salt forms of enantiopure methylephedrine and monocarboxylates (Group 10).

In the case of ephedrine salt forms, analysis generated nine new isostructural groups. Again, these groups are divided according to the composition of the counterion and conformation of the cation. Groups 1, 2 and 9 includes two compounds each with

counterions derivatives of phosphates, Group 3 including the *meta*-substituted benzoates; Group 4 includes only the hydrogenphosphate and methanesulfonate salt forms of ephedrine, Group 5 includes dicarboxylates; Group 6 including only halides; Group 7 including monocarboxylates, *ortho*-substituted benzoate and dicarboxylate; and Group 8 including the sulfonates, nitrate and one halide.

It is interesting to note that salt forms of the halides chlorine and bromine are isostructural for tyramine, enantiopure methylephedrine and ephedrine. However, for racemic methylephedrine these salt forms have cations with different conformations [*r*CL (ZZZLUA01) conformation (a) and *r*BR (ZZZFCS02) conformation (c)] and do not pack similarly. This may suggest that there exist unknown but accessible new polymorphs of *r*MEPD chloride or bromide. Although some of the structural groups contain only structures with obvious similarities, many groups are highly varied. Isostructural groups are identified where a single group contains highly variable anion types, or both hydrated and anhydrous structures, or different cation conformations, or cocrystal structures with extra neutral organic molecules present in some members. The only structural feature not found to mix within a single isostructural group is that all racemic and enantiopure methylephedrine structures are found to pack differently from each other. This is not surprising as the enantiopure structures cannot utilise the same symmetry elements as the racemic ones can. The wide variety of coformer species found within isostructural groups leads to very different hydrogen bonding interactions. That isostructurality is maintained despite this, highlights the importance of molecular and/or ionic shape in the packing of organic materials.

7.5. REFERENCES

[1]   Briggs, N., Kennedy, A., & Morrison, C. (2012). Acta Crystallographica Section B, 68(4), 453-464.

[2]   Kennedy, A. R., Morrison, C. A., Briggs, N. E., & Arbuckle, W. (2011). Crystal Growth and Design, 11(5), 1821-1834.

[3]   Collier, E., Davey, R., Black, S., & Roberts, R. (2006). Acta Crystallographica Section B, 62(3), 498-505.

[4]   Black, S., Collier, E., Davey, R., & Roberts, R. (2007). Journal of Pharmaceutical Sciences, 96(5), 1053-1068.

[5]   Gelbrich, T. B., & Hursthouse, M. (2006). CrystEngComm, 8(6), 448-460.

[6]   De Moraes, S.L., Edwards, D., Florence, A.J., Johnston, A., Johnston, B.F., Morrison, C.A., & Kennedy, A.R. (2017). Crystal Growth and Design, 17(6), 3277-3286.

[7]   Macrae, C.F., Bruno, I.J., Chisholm, J.A., Edgington, P.R., McCabe, P., Pidcock, E., Rodriguez-Monge, L., Taylor, R., van de Streek, J. & Wood, P. A. (2008). J. Appl. Cryst., 41, 466-470.

[8]   Macrae, C.F., Edgington, P. R., McCabe, P., Pidcock, E., Shields, G. P., Taylor, R., Towler M. & van de Streek, J. (2006), J. Appl. Cryst., 39, 453-457.

[9] CCDC. Crystal Form Similarity < https://www.ccdc.cam.ac.uk/Community/ crystalformconsortium/casestudies/crystalformsimilarity/ >. Accessed on 20/07/2019

8. NANOINDENTATION RESULTS FOR ACTIVE PHARMACEUTICAL INGREDIENTS

8.1. TYRAMINE SALT FORMS

Of the twenty-nine salt forms of tyramine measured using nanoindentation, eleven were synthesized by Morrison *et al.* [1] while the syntheses for other eighteen compounds are described in chapter 2.4. The composition of the counterion selection used in this work is divided as follows. Four inorganic salt forms (chloride, bromide, iodide and tetrafluoroborate), seven di-substituted benzoates, eleven carboxylates (four monocarboxylates, seven dicarboxylates) and three sulfonates. There are also structures labelled as the group "Others" that do not belong in the more uniform categories. These are two naphthalates (2NAPH and 2NAPH.H2O), one poly-substituted benzoate (5C2NB) and the structure of TIOSA.3H2O where the anion is a sulphur-sulphur bonded dimer of the thiosalicylic acid used during synthesis. Figure 8.1 shows the percentage distribution of the counterions used in this experiment. Details about the crystal structures of the salt forms can be obtained in APPENDIX 3.1.
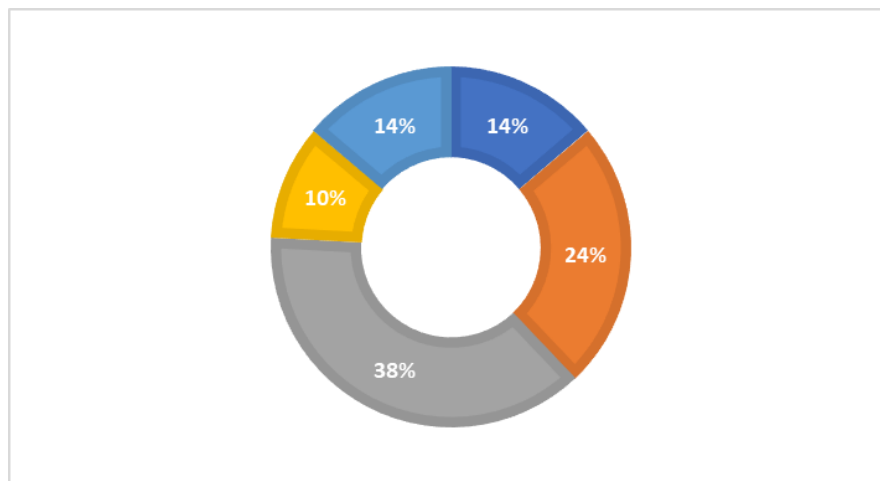
Figure 8. 1 Distribution of the salt selection by composition of counterion where in blue represents percentage of inorganic compounds, in orange represents percentage of benzoates, in grey represents percentage of carboxylates, in yellow percentage of sulfonates and in dark blue represents the percentage of salt forms characterised as other.

All compounds were analysed using the technique described in Chapter 2.7, where the gradient hardness (H_G), the intercept, the regression coefficient (R^2) and Young's Modulus were obtained. Complete details about nanoindentation measurements can be observed in APPENDIX 8.1. However, a summary of these values is detailed in Table 8.1. The selection of salt forms was not only done to present a range of counterion types but also to give a range of other features in the crystal structure, for example, presence of water in the structure, presence of an extra cation per asymmetric unit ($Z' > 1$) and presence of an neutral acid in the unit cell along with the ionised form. The distribution of compounds according to these structural features can be observed in Figure 8.2 where the blue box represents anhydrous compounds and the orange box represents hydrated compounds.
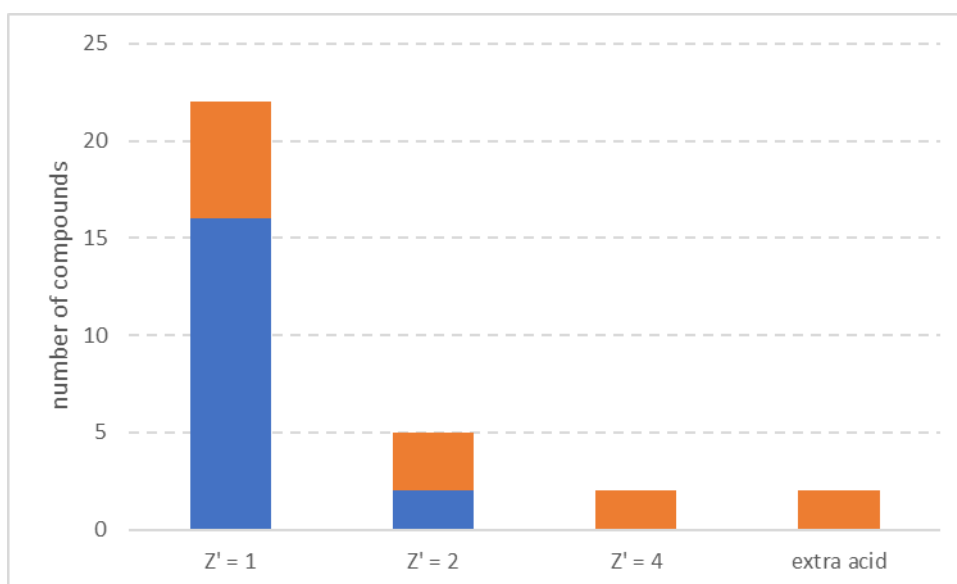
Figure 8. 2. Distribution of structural features of the 18 anhydrous compounds (in blue) and 11 hydrated compounds (in orange) analysed in this work.

Table 8. 1. Results for tyrammonium salt forms where n_m is the number of measurements in each sample, H_G is the gradient hardness, E_G is the gradient Young's Modulus and σ represents the errors in each measurement. There is also structural information about the presence of water molecules (.H2O), presence of a free acid in the structure (*), and otherwise specified, presence of another cation per asymmetric unit ([a] represents Z' = 2 and [b] represents Z' = 4)

Sample	n_m	H_G	σH_G	Intercept	$\sigma_{Intercept}$	R^2	E_G	σ_{EG}	Intercept	$\sigma_{Intercept}$	R^2
2CB [2]	18	2.28	0.09	-0.29	0.37	0.9763	24.99	1.17	-0.63	0.46	0.9659
2FB [2]	18	0.66	0.03	0.85	0.45	0.9668	4.98	0.21	1.18	0.41	0.9713
2HB	18	0.97	0.11	1.86	0.85	0.8237	11.36	1.10	1.30	0.76	0.8705
2MALON.H2O [a]	13	0.49	0.04	2.71	0.44	0.9253	4.37	0.48	2.84	0.55	0.8840
2NAPH	9	2.22	0.26	-6.21	2.36	0.9125	25.05	3.29	-6.59	2.70	0.8924
2NAPH.3H2O	9	2.90	0.69	-6.5	4.81	0.7156	26.01	5.21	-5.11	3.78	0.7808
2OXA [b]	9	2.36	0.17	1.18	0.42	0.9664	27.44	1.68	0.63	0.40	0.9743
2RMAL.H2O	9	0.66	0.19	1.97	1.64	0.6406	7.17	1.94	1.82	1.60	0.6622
3HB	9	1.03	0.13	1.89	0.65	0.8998	12.54	1.34	1.41	0.60	0.9264
4CB	9	0.86	0.11	-2.88	2.12	0.8985	6.15	0.61	-1.22	1.49	0.9360
4CBS	9	2.32	0.89	1.90	2.92	0.4905	25.06	10.88	1.99	3.25	0.4308
4FB [2]	18	0.73	0.04	1.20	0.73	0.9503	5.89	0.27	1.57	0.58	0.9663
5C2NB [a]	18	0.51	0.02	2.52	0.55	0.9651	4.49	0.18	2.64	0.45	0.9757
ASB.3H2O [a]	18	0.61	0.02	3.28	0.31	0.9870	5.87	0.17	3.22	0.31	0.9872
BF4.H2O [2]	18	0.45	0.02	0.34	0.33	0.9823	4.22	0.11	0.60	0.25	0.9889
BR [2]	9	1.39	0.10	1.39	1.96	0.9663	15.52	0.76	0.12	1.42	0.9834
CAP [a]	18	0.14	0.01	1.09	0.65	0.9491	1.41	0.07	0.89	0.59	0.9595
CL [4]	27	2.33	0.08	0.23	0.31	0.9706	25.73	0.92	-0.03	0.33	0.9690
FUMCC.H2O * [2]	36	1.75	0.04	0.49	0.20	0.9815	18.52	0.45	0.33	0.21	0.9806
FUMS.H2O	18	2.95	0.16	-0.05	0.50	0.9537	32.87	1.77	-0.39	0.51	0.9555

HIP	9	0.82	0.06	2.42	0.8	0.9679	6.83	0.44	2.50	0.74	0.9718
I [3]	18	0.57	0.07	4.79	1.01	0.8247	4.60	0.45	4.48	0.90	0.8649
LTAR.3H2O [b]	18	0.76	0.07	4.56	0.92	0.8717	7.27	0.47	4.02	0.65	0.9375
MMBS.H2O	9	0.78	0.09	3.45	1.18	0.9216	6.81	0.63	3.40	1.00	0.9427
OTOL [2]	18	1.82	0.09	0.13	0.47	0.9582	19.08	1.06	-0.05	0.51	0.9529
OXA	9	2.28	0.09	1.26	0.24	0.9886	26.68	1.06	0.83	0.25	0.9890
TCIN	18	1.24	0.13	0.84	1.51	0.8555	8.81	0.59	0.90	0.99	0.9324
TCIN.H2O *	9	1.51	0.21	-8.28	3.05	0.8795	9.10	0.74	-3.71	1.42	0.9556
TIOSA.3H2O [a]	18	1.04	0.08	-0.32	1.08	0.9185	10.61	0.73	-0.71	1.03	0.9288

Of the twenty-nine compounds measured, three sets of measurements were excluded from any further analysis as they gave coefficient of determination lower than 80 %: These were the anhydrous compound 4CBS (R^2 = 0.4905) and the hydrated compounds 2NAPH.H2O (R^2 = 0.7156) and 2RMAL.H2O (R^2 = 0.6406). A scatter plot of the gradient hardness (H_G) versus gradient Young's Modulus (E_G) for the remaining compounds, considering the standard deviation of both measurements, can be observed in Figure 8.3. There is a linear relationship between Hardness and Young's Modulus for this set of samples which fits the trendline with equation H_G = $(0.092 \pm 0.003) \cdot E + (0.05 \pm 0.02)$ with R^2 equal to 0.9766. In other words, for tyrammonium salt forms hardness values measured using DNISP probe will be around 0.09 times the values of gradient Young's Modulus. This value is also related to what we will define as elasticity Index (I_E) of the tyrammonium salt forms, meaning that salt forms using tyramine as the base will constrain 9.2 %.
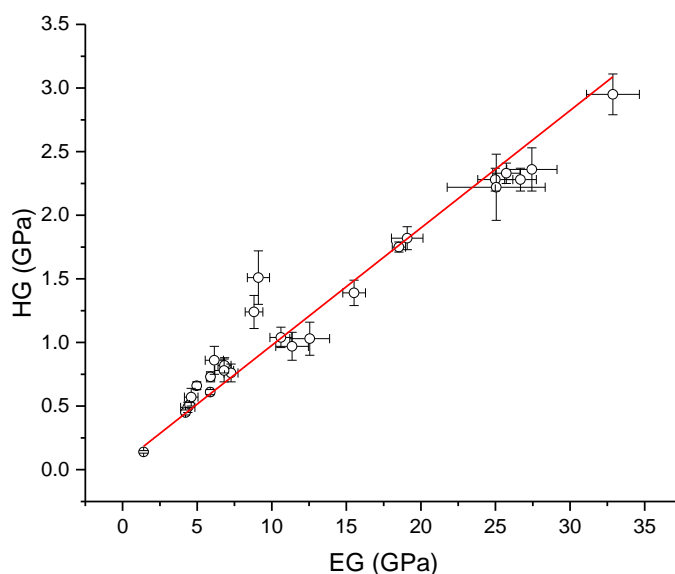
Figure 8. 3. Scatter plot of gradient hardness (H_G) versus Young's Modulus (E_G) for tyrammonium salt forms including standard deviation of the measurements.

8.1.1. GENERAL TRENDS IN HARDNESS

An arbitrary scale of hardness was used to classify the compounds in different categories: Soft compounds are thus here defined as those that have hardness lower than 1.0 GPa. Medium hardness compounds will have hardness between 1.0 and 2.0 GPa and hard materials will have hardness higher than 2.0 GPa. Considering these categories, 50 % of tyrammonium salt forms are soft materials, 26.9 % of the compounds have medium hardness and 23.1 % are hard compounds. Figure 8.4 shows the distribution of hardness values for all twenty-six compounds, where light grey represents soft materials, grey represents medium hardness and dark grey represents hard materials. There is no obvious trending of hardness according to the composition of the counterion where, for example, halides can be hard (CL), medium hard (BR) and soft (I). There were also not obvious trends comparing features in the crystal structure, for example, hydrated compounds can be hard (FUMS.H2O), medium hard (TCIN.H2O) and soft (MMBS.H2O). Statistical analysis showed no preference for the hardest or softest materials to be hydrates, to have a particular class of anion, or to have Z' >1. As for the isostructural groups identified in the packing analysis above, these also seem to have no effect. Thus CL (hard), BR (medium) and BF4 (soft) are all in the same isostructural group. Similarly, FUMS.H2O is the hardest material present, but it is in the same isostructural group as the soft LTAR.3H2O.
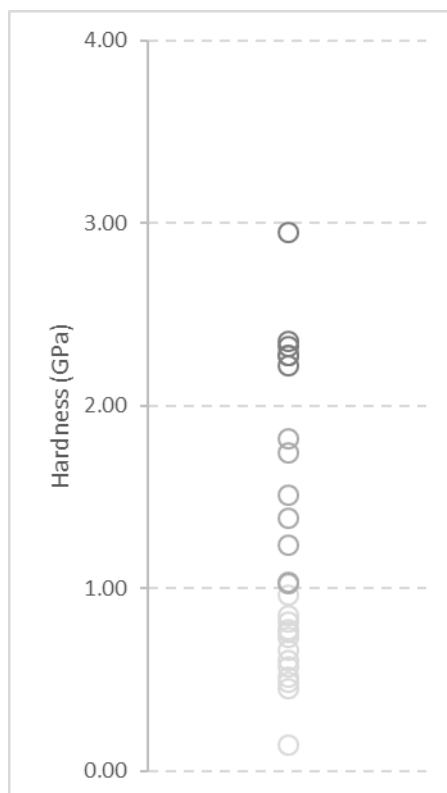
Figure 8. 4. Hardness scale for all salt forms of tyramine where light grey represents soft materials, grey represents medium hardness and dark grey represents hard materials.

8.1.2. TRENDS IN HARDNESS ACCORDING TO FEATURES IN THE UNIT CELL

The found relationship between H_G and E_G was used in an attempt to find structural features that may affect it. Considering only compounds with coefficients of regression higher than 80 %, data was analysed according to features in the crystal structure, such as presence or absence of water molecules in the structure, presence of an extra cation per asymmetric unit ($Z' > 1$) and presence of an extra neutral acid in the unit cell. Interestingly, as can be observed in Table 8.2 and Figure 8.5, even when separating all compounds according to these features in the unit cell, the elasticity index, I_E, is similar for all compound types (black trend line) to within standard deviation. The separate trend lines for the different groups are given as anhydrous compounds (red line), hydrated compounds (blue line) and compounds with only one cation per asymmetric unit ($Z' = 1$) (green line). The largest difference from average, is for the group with

167

two cations per asymmetric unit (Z' = 2) (line in purple). There is a 28.6 % difference between the trendlines when condirering only compounds with Z' = 1 and Z' = 2. These have elasticity index around 17.4 % higher than other compounds, but even this is a statistically insignificant difference. Compounds with four cations per asymmetric unit (Z' = 4) and with one free acid present in the unit cell were not considered in these analyses as they only have two samples of each to analyse, however they are represented in Figure 8.5 as beige and light blue dots representing Z' = 4 and extra acid in the unit cell, respectively.

Table 8. 2. TYR compounds separated by composition of the crystal structure where n is the number of compounds used in the analysis, I_E is the elasticity index and R^2 is the regression coefficient.

	n	$\mathbf{I_E \pm \sigma_{IE}}$	**Intercept $\pm \sigma_{Intercept}$**	$\mathbf{R^2}$
All data	26	0.092 ± 0.003	0.05 ± 0.02	0.9766
Anhydrous	17	0.092 ± 0.004	0.05 ± 0.03	0.9700
Hydrate	9	0.090 ± 0.003	0.08 ± 0.03	0.9909
Z' = 1	19	0.084 ± 0.003	0.16 ± 0.03	0.9780
Z' = 2	5	0.108 ± 0.006	-0.01 ± 0.02	0.9923
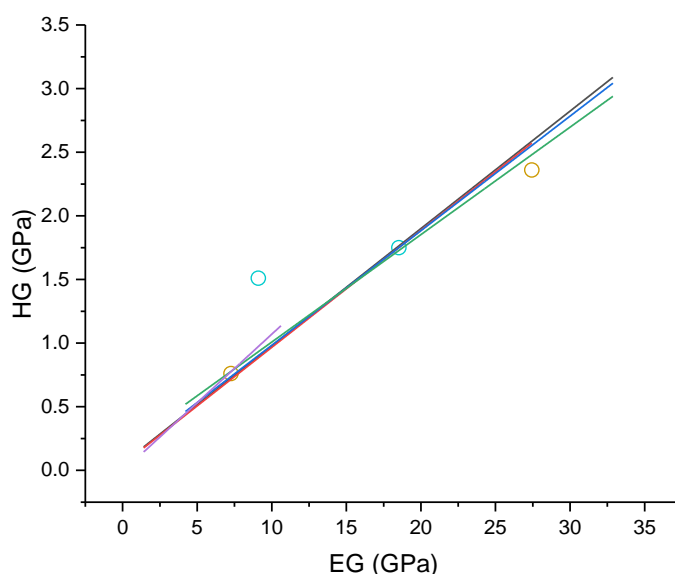
Figure 8. 5. Line in black represents all TYR compounds, line in red represents only anhydrous compounds, line in dark blue represent only hydrate compounds, line in green represents compounds with Z' = 1, line in purple represents compounds with Z' = 2, beige dots show the position of both compounds with Z' = 4 and light blue dots show the position of compounds with an extra acid in the unit cell. The circles representing the data and standard deviation were omitted for clarity.

8.1.3. TRENDS IN HARDNESS ACCORDING TO THE COMPOSITION OF THE COUNTERION

Again, no deviation from the same linear relationship between hardness and Young's Modulus was found when separating the salt forms according to the composition of the counterion, as it can be observed in Table 8.3 and Figure 8.6. Within standard deviation, inorganic compounds (red line), benzoates (green line) and carboxylates (blue line) behave the same as the trendline for all compounds with elasticity index varying from (7.9 ± 0.3) % for benzoates to (9.2 ± 0.4) % for carboxylates. Figure 8.6 also show the position of sulfonates (light blue dots) and the Others group (pink dots). However, they were excluded from this analysis as there is too little data for analysis.
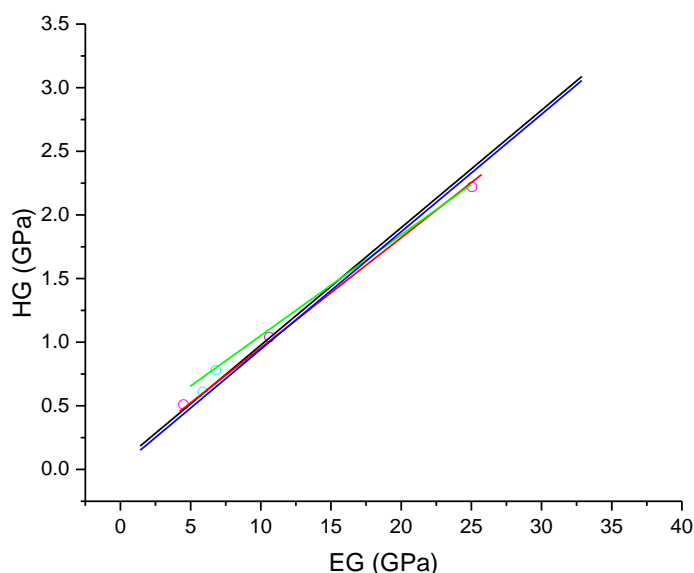
Figure 8. 6. Line in black represents all TYR compounds, line in red represents only inorganic compounds, line in green represent only benzoate compounds, line in blue represents carboxylate, light blue dots show the position of both sulfonate compounds and pink dots show the position of compounds classified as others. The circles representing the data and standard deviation were omitted for clarity.

Table 8. 3. TYR compounds separated by composition of the counterion where n is the number of compounds used in the analysis, I_E is the elasticity index and R^2 is the regression coefficient.

	n	$I_E \pm \sigma_S$	Intercept $\pm \sigma_{Intercept}$	R^2
All	26	0.092 ± 0.003	0.05 ± 0.02	0.9766
Inorganic	4	0.087 ± 0.003	0.09 ± 0.03	0.9972
Benzoates	7	0.079 ± 0.005	0.26 ± 0.05	0.9821
Carboxylates	10	0.092 ± 0.004	0.02 ± 0.02	0.9855

A hardness scale for compounds according to the composition of the counterion was also constructed, as it can be observed in Figure 8.7, where blue circles represent inorganic counterions, orange circle represents monocarboxylates, grey circles represent dicarboxylates, yellow circles represent *ortho*-substituted benzoates, light blue circle shows the only measurement on *meta*-substituted benzoate, green circles represent *para*-substituted benzoates, brown circles represent sulfonates and grey circle shows the Others group, containing data that does not fit in these categories. This figure also illustrates structural information about hydrated samples (.H2O), presence of a free acid in the structure (*), and presence of another cation per asymmetric unit ([a] represents Z' = 2 and [b] represents Z' = 4).

Using hardness scale in Figure 8.7 it is easier to analyse how hardness behaves according to the composition of the crystal structure. The first interesting result obtained from this data is regarding the two isostructural groups present in this data, as observed in Chapter 7: Group 1 including the samples CL ($H_G = 2.33 \pm 0.08$ GPa), BR ($H_G = 1.39 \pm 0.10$ GPa), and BF4.H2O ($H_G = 0.45 \pm 0.02$ GPa) and Group 2 containing the samples 2CB ($H_G = 2.28 \pm 0.09$ GPa), 4FB ($H_G = 0.73 \pm 0.04$ GPa), OTOL ($H_G = 1.82 \pm 0.09$ GPa) and 4CB ($H_G = 0.86 \pm 0.11$ GPa). As it can be observed in Figure 8.7, these isostructural cation packing groups have different values of hardness for each compound. Of special interest is the CL and BR pair which are strictly isostructural and isomorphous. This pair suggests that hardness values will not depend simply on the crystal lattice parameters of the unit cell or the position of the atom in the unit cell (as used in theoretical calculations). The cation packing similarities also mean that the wide range of cation to cation interactions are similar throughout the larger group. It would thus seem that the strength of each individual intermolecular contact must be important.
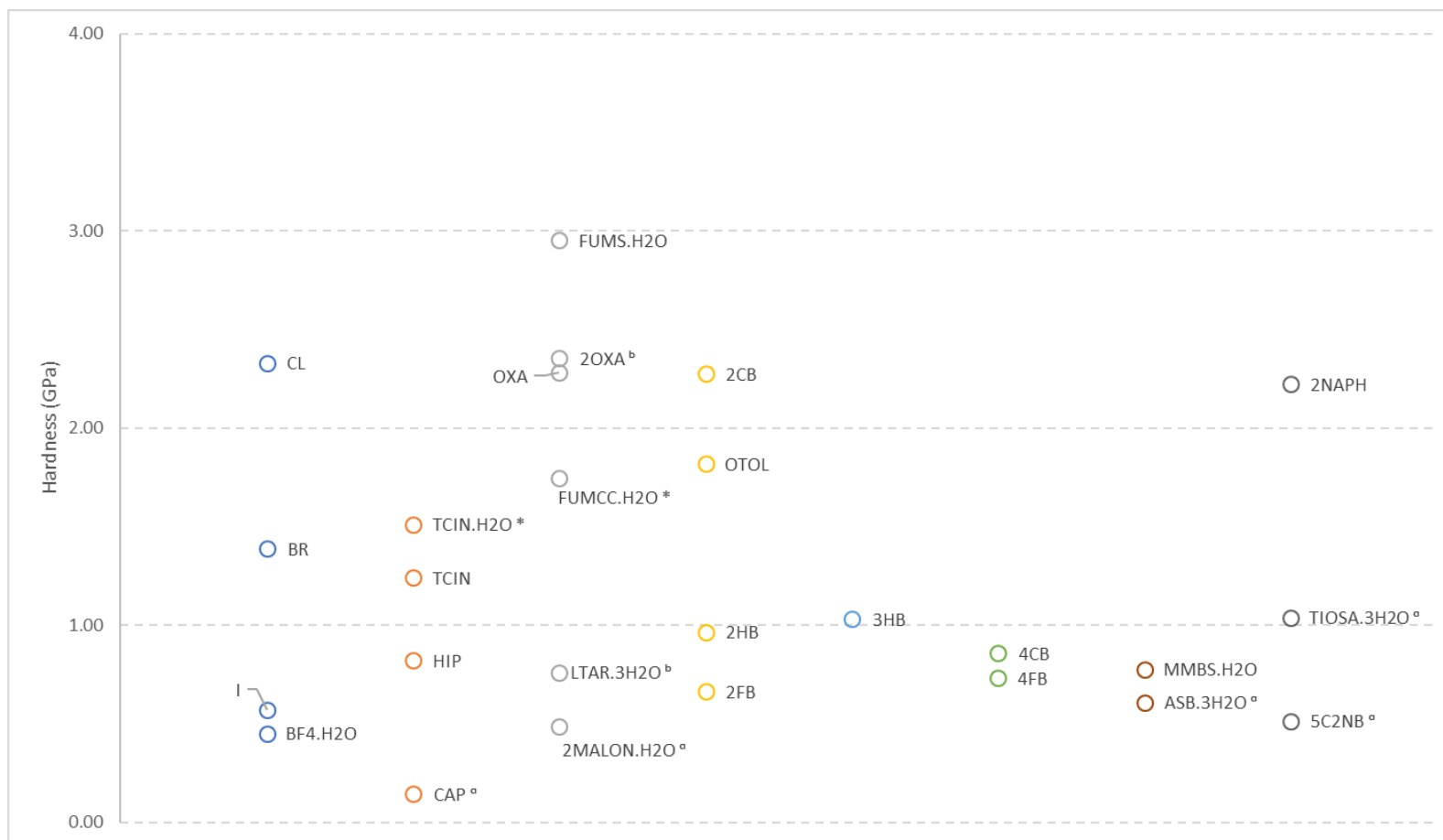
Figure 8. 7. Hardness scale according to the composition of the counterion in TYR salts. Blue circles represent inorganic counterions, orange circle represents monocarboxylates, grey circles represent dicarboxylates, yellow circles represent *ortho*-substituted benzoates, light blue circle shows the only measurement on *meta*-substituted benzoate, green circles represent *para*-substituted benzoates, brown circles represent sulfonates and grey circle show data that does not fit in these categories. There is also structural information about the presence of water molecules (.H2O), presence of a free acid in the structure (*), and otherwise specified, presence of another cation per asymmetric unit ([a] represents Z' = 2 and [b] represents Z' = 4)

As an example, we were able to compare with methods developed by Roberts and Rowe [8], which predicts hardness from the crystal structure of the molecular compound and cohesive energy density as described in Chapter 2.8. Results for all calculated hardness values using S_r equals to 0.707 can be observed in Table 8.4. For isostructural Group 1 the correct rank order was found for calculated results obtained with the method developed by Roberts & Rowe [8], when compared with experimental results. Though the spread of the theoretical results was very small as compared to experimental results. On the other hand, when comparing isostructural Group 2, the opposite rank order is found, with values of gradient hardness (H_G) decreasing as the calculated hardness increases, this is illustrated by Figure 8.8.
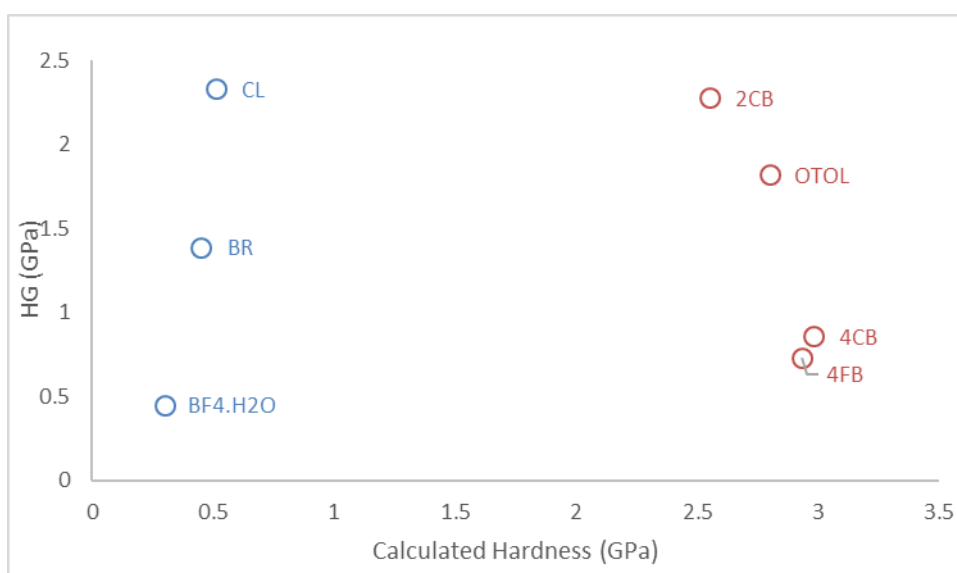
Figure 8. 8. Comparison between calculated hardness and experimental hardness (H_G). In blue are the samples from isostructural Group 1 and in red are the samples in isostructural Group 2.

Table 8. 4. Hardness results from calculated values obtained using the method described by Roberts & Rowe [8] for Sr equals to 0.707. As discussed in Chapter 2.8 only the smaller values of calculated hardness were considered.

Sample		Calculated hardness (GPa)		
		a	b	c
Group 1	BF4.H2O	2.63	12.03	0.30
	BR	0.45	2.77	6.44
	CL	0.51	3.23	7.20
Group 2	2CB	3.44	2.55	3.12
	4FB	2.93	3.48	4.07
	OTOL	3.42	2.80	3.28
	4CB	2.98	3.46	3.48

When considering only inorganic salt forms where the counterion is a halogen, these compounds have experimental hardness decreasing as the size of the anion increases (CL with hardness of 2.33 (8) GPa, BR with hardness of 1.39 (10) GPa and I with hardness of 0.57 (7)) as can be observed in Figure 8.9 which compares gradient hardness (H_G) with the molecular weight (MW) of the halide atom for each halogen (trendline in black). The equation for the trendline is $H_G = (-0.0192 \pm 0.0009) \cdot MW + (3.0 \pm 0.08)$ with R^2 equals to 0.9980. Another indication that size of the counterion influences the hardness of the compounds can be done comparing compounds with similar structural features. For example, when comparing anhydrous *ortho*-substituted benzoates 2FB [0.66 (3) GPa], OTOL [1.82 (9) GPa] and 2HB [0.97 (11) GPa], all with stoichiometry of one cation to one anion with the substited atom varying in the same period, hardness decreases when the molecular weight (MW) increases. The equation for the trendline is $H_G = (-0.27 \pm 0.05) \cdot MW + (76 \pm 14)$ with R^2 equals to 0.9667. Details of the relationship between gradient hardness for *ortho*-benzoates and the molecular weight of the compound can also be observed in Figure 8.9, trendline in red. Properties such as electronegativity and hence strength of non-covalent intermolecular interactions also trend with halide size, and thus here the observed trend may reflect these properties.

Hardness values will also have a similar behaviour when comparing positional isomers of mono-substituted benzoates. The fluorobenzoates (2FB with hardness equals to 0.66 (3) GPa and 4FB with hardness equals to 0.73 (4) GPa) are very soft materials with

similar hardness values independent of the position of the fluoro atom on the aromatic ring. The same applies to the medium-hard hydroxy benzoates (2HB with hardness of 0.97 (11) GPa and 3HB with hardness of 1.03 (13) GPa) where the position of the hydroxyl group does not seem to give any change in values of hardness. However, for the anhydrous isostructural chlorobenzoates, 2CB with hardness 2.28 (9) GPa and 4CB with hardness of 0.86 (11) GPa there is an increase of 2.75 times the values of hardness when changing from the *para-* to the *ortho-* position. Thus, the potential connection between similar size and similar chemical composition giving similar hardness breaks down here. It is not possible to make the same comparison with compounds that have the presence of water or another cation or free acid within the unit cell as these extra components in the unit cell will alter intermolecular interactions which may increase or decrease hardness.
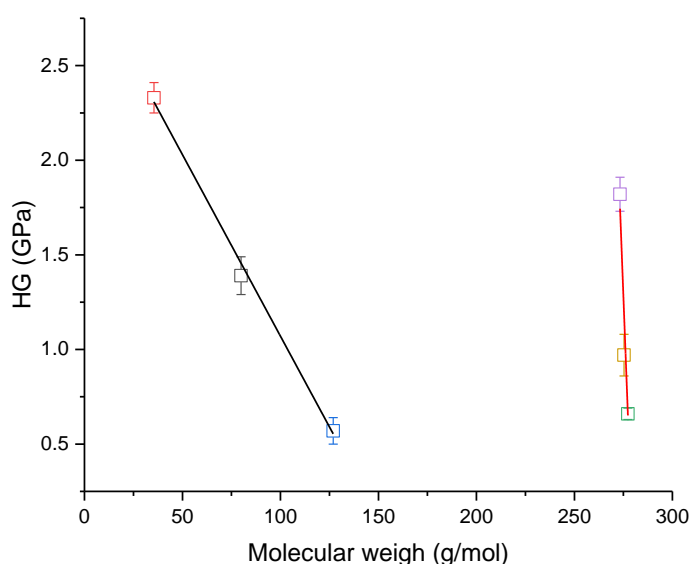
Figure 8. 9. Plot of gradient hardness (H$_G$) versus the molecular weight for halides (trendline in black) and *ortho-*benzoates (trendline in red) where the red square represents CL, the grey square represents BR, the blue square represents I, the purple square represents OTOL, the yellow square represents 2HB and the green square represents 2FB.

8.2. METHYLEPHEDRINE SALT FORMS

In this work, there were twenty-eight salt forms of enantiopure and racemic methylephedrine measured by nanoindentation. Of these salt forms measured, twelve were synthesized by Morrison *et al.* [1] (six enantiopure salt forms and six racemic salt forms) while the synthesis for other sixteen compounds is described in chapter 2.4 (eight enantiopure salt forms and eight racemic salt forms). The composition of the counterion selection used in this work for the 14 enantiopure methylephedrine salt forms is divided as follows. One inorganic salt form (mono-hydrogen sulphate), three *ortho*-substituted benzoates, one benzoate, five carboxylates (two monocarboxylates, three dicarboxylates), three sulfonates and one naphthalate. In the case of the 12 racemic compounds, the distribution of counterions is: Two inorganic salt forms (mono-hydrogen sulphate and chlorate), four di-substituted benzoates, one benzoate, and one tri-substituted benzoate, three carboxylates (two dicarboxylates, one monocarboxylates) and one di-substituted benzoate. Two racemic salt forms crystallised as conglomerates: (1R,2S)-methylephedrinium hydroxy-2-naphthalate (*r*H2NAPH) and (1R,2S)-methylephedrinium *para*-toluenesulfonate (*r*PTS). The single crystal structures and physical data of these conglomerates will be included with those of the enantiopure compounds but described with suffix ".*cong*". Figure 8.10 shows the percentage distribution of the counterions used in this experiment for enantiopure salt forms of methylephedrine (on the left) and racemic salt forms of methylephedrine (on the right). Details about the crystal structures of the salt forms can be obtained in the APPENDIX 3.2.

All compounds were analysed using the technique described in Chapter 2.2.2, where the gradient hardness (H_G), the intercept, the regression coefficient (R^2) and Young's Modulus were obtained. In these sets of data, the letter "*e"* before each compound indicate they are salt forms of enantiopure methylephedrine while "r" before each compound indicate they are salt forms of racemic methylephedrine. Complete details about nanoindentation measurements can be observed in APPENDIX 8.2. However, a summary of these values is detailed in Table 8.5.
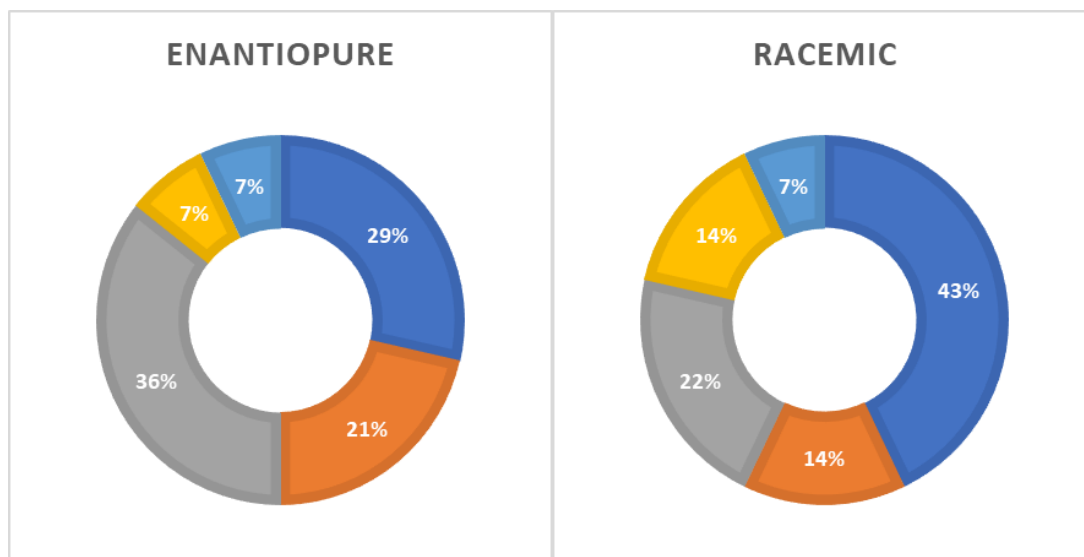
Figure 8. 10. Distribution of the salt selection by composition of counterion for enantiopure salt forms of methylephedrine (on the left) and racemic compounds of methylephedrine (on the right) where in blue represents percentage of benzoates, in orange represents percentage of sulfonates, in grey represents percentage of carboxylates, in yellow inorganic salt form and in light blue represents the only naphthalate salt form.

With respect to structural variation, of the total of salt forms measured with nanoindentation, 67.9 % were anhydrous while 32.1 % were hydrates. Unlike the tyramine samples, apart from hydration there was no other chemical species present in any of the structures beyond the expected cations and anions. There are three structures of enantiopure methylephedrine and one structure of racemic methylephedrine with two cations per asymmetric unit (Z' = 2): The anhydrous and disordered salt form of methylephedrine and fumaric acid (*e*FUM) and the di-hydrated salt form of methylephedrine and mucic acid (*e*MUC.2H2O) and the disordered and anhydrous salt form of d-tartaric acid (*r*RTAR). All the other structures had only one cation per asymmetric unit (Z' = 1). The distribution of compounds according to these structural features can be observed in Figure 8.11 where the blue box represents anhydrous compounds and the orange box represents hydrated compounds.

Of the twenty-nine compounds measured, two sets of measurements were excluded from any further analysis as they gave coefficient of determination lower than 80 %: These were the anhydrous compound *e*2CB ($R^2 = 0.7705$) and the hydrated compound *e*BZ.H2O ($R^2 = 0.6054$), as observed in Table 1, in pink. A scatter plot of the gradient hardness (H_G) versus Young's Modulus (E_G) for the remaining compounds,

considering the standard deviation for measurements with enantiopure and racemic methylephedrine, can be observed in Figure 8.12.
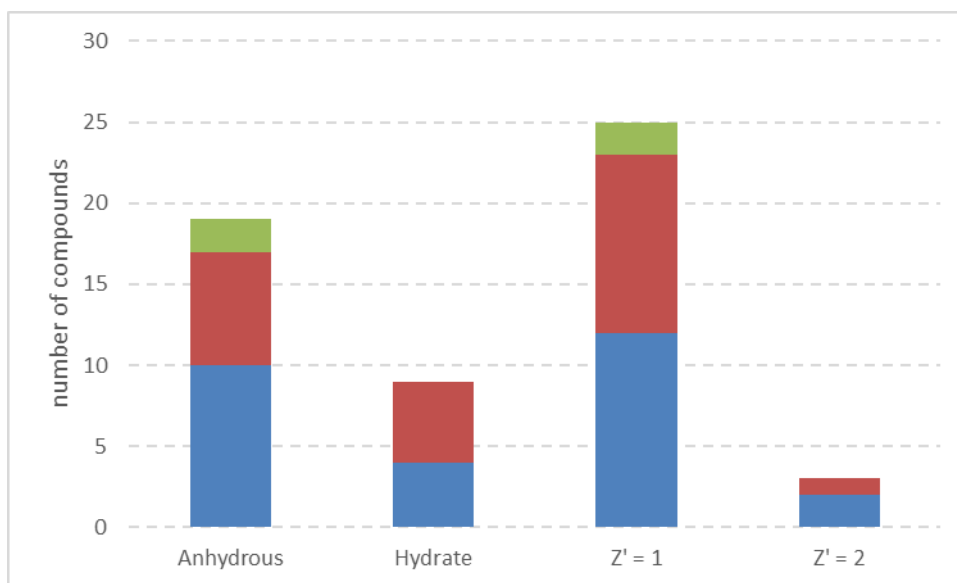
Figure 8. 11. Distribution of structural features of the total of 14 enantiopure methylephedrine compounds (in blue), 12 racemic methylephedrine compounds (in red) and two conglomerates (in green).

Table 8. 5. Results for methylephedrininum salt forms where n_m is the number of measurements in each sample, H_G is the gradient hardness, E is the Young's Modulus and σ represents the errors in each measurement. The letter "*e*" before the label of the compound indicates it is from enantiopure methylephedrine while the letter "*r*" before the compounds indicates they are from racemic methylephedrine. There is also structural information about the presence of water molecules (.H2O), crystallisation of a conglomerate (.cong) presence of a free acid in the structure (*), and otherwise specified, presence of another cation per asymmetric unit ([α] represents Z' = 2)

Enantiopure Methylephedrine											
Sample	n_m	H_G	σH_G	**Intercept**	σIntercept	R^2	E_G	σEG	**Intercept**	σIntercept	R^2
*e*2CB	9	2.08	0.43	-1.91	3.58	0.7707	15.38	2.19	0.12	2.18	0.8761
*e*2FB	18	0.72	0.05	1.99	0.76	0.9215	7.01	0.47	1.60	0.74	0.9315
*e*2HB	7	1.18	0.22	-1.93	3.63	0.8537	12.35	1.34	-3.70	2.32	0.9444
*e*2NAPH	18	0.71	0.03	1.99	0.54	0.9690	6.87	0.21	1.65	0.39	0.9846
*e*4CBS	27	1.30	0.08	0.87	0.99	0.9112	14.20	0.95	-0.29	1.13	0.8989
*e*4HPA	15	0.53	0.07	7.73	1.62	0.8186	4.40	0.35	6.97	1.04	0.9254
*e*BZ.H2O	9	3.64	1.11	3.23	4.74	0.6054	29.17	6.14	2.90	3.36	0.7635
*e*CAMPH	18	0.61	0.03	3.06	0.65	0.9662	5.08	0.20	3.22	0.54	0.9758
*e*FUM * [α]	5	1.37	0.21	-4.36	4.78	0.9338	12.10	1.18	-2.22	2.84	0.9721
*e*LMD	5	0.28	0.06	5.75	4.19	0.8915	2.67	0.36	5.51	2.82	0.9488
*e*LTAR.H2O	7	0.99	0.15	1.76	0.69	0.8934	5.95	0.93	2.42	0.61	0.8906
*e*MMBS	14	0.97	0.08	4.93	1.51	0.9161	8.18	0.49	4.93	1.03	0.9591
*e*MUC.2H2O [α]	18	1.11	0.06	1.95	0.59	0.9532	9.31	0.45	2.48	0.49	0.9637
*e*SO4.H2O	15	1.56	0.07	9.33	0.97	0.9750	13.48	0.45	9.82	0.72	0.9857
Racemic Methylephedrine											
Sample	n_m	H_G	σH_G	**Intercept**	σIntercept	R^2	E_G	σEG	**Intercept**	σIntercept	R^2
*r*2HB	16	0.73	0.05	3.02	0.62	0.9460	7.07	0.43	2.75	0.60	0.9517
*r*2NB.H2O	7	0.47	0.03	2.93	0.42	0.9784	4.02	0.21	2.88	0.39	0.9821

*r*3CB	15	1.96	0.20	-3.63	2.23	0.8752	16.22	1.48	-2.08	1.80	0.9026
*r*4CBS.H2O	18	0.49	0.04	0.80	0.87	0.9187	4.91	0.46	0.64	1.10	0.8788
*r*5C2NB	18	0.70	0.02	1.29	0.39	0.9849	5.92	0.16	1.47	0.33	0.9891
*r*BZ	13	0.54	0.02	4.71	0.23	0.9814	4.49	0.29	4.92	0.33	0.9599
*r*CL	9	1.09	0.07	3.21	0.86	0.9714	9.74	0.46	3.02	0.64	0.9845
*r*RTAR * [a]	7	1.18	0.10	3.33	1.23	0.9634	11.46	0.70	2.04	0.94	0.9817
*r*FUM	6	0.44	0.06	5.54	0.53	0.9243	2.68	0.25	5.97	0.31	0.9666
*r*H2NAPH.*cong*	13	1.79	0.27	0.58	1.69	0.8032	14.68	1.52	0.49	1.19	0.8940
*r*MUC.H2O	9	1.17	0.12	2.83	0.85	0.9418	10.73	1.05	2.87	0.81	0.9461
*r*PAAB.H2O	9	1.87	0.33	2.18	2.37	0.8225	14.46	1.47	2.45	1.35	0.9326
*r*PTS.*cong*	6	0.72	0.08	1.80	0.52	0.9572	5.18	0.56	1.56	0.56	0.9547
*r*SO4.H2O	14	1.11	0.09	2.36	1.15	0.9292	9.99	0.76	2.07	1.12	0.9353

There is a linear relationship between Hardness and Young's Modulus for the set of samples including all racemic and enantiopure compounds fits the trendline with equation $H_G = (0.102 \pm 0.005) \cdot E_G + (0.07 \pm 0.03)$ with R^2 equals to 0.9390 (Figure 8.12 – trendline in black). When considering only enantiopure compounds, including conglomerates, the trendline is the same as observed with all compounds with equation $H_G = (0.101 \pm 0.008) \cdot E_G + (0.08 \pm 0.06)$ and $R^2 = 0.9612$ (Figure 8.12 – dots and trendline in blue). However, when plotting hardness versus Young's Modulus for only racemic compounds, the gradient of the curve increases, and equation becomes $H_G = (0.119 \pm 0.007) \cdot E_G + (-0.03 \pm 0.07)$ with $R^2 = 0.9650$. In other words, enantiopure methylephedrine salt forms hardness values measured using DNISP probe will be around 0.10 times the values of gradient Young's Modulus and racemic compounds will be 0.12 times. The difference observed is small and probably have no significance. This value is also related to what we will define as "elasticity index" (I_E) meaning that salt forms using enantiopure methylephedrine as the base will constrain 10.1 % while salt forms of racemic methylephedrine will constrain 11.9 %.
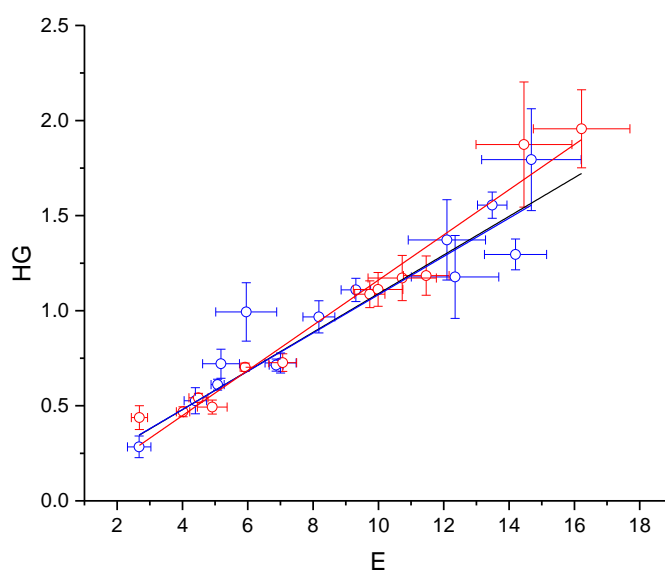
Figure 8. 12. Scatter plot of gradient hardness (H_G) versus gradient Young's Modulus (E_G) for all MEPD compounds (trend line in black), enantiopure (in blue) and racemic (in red) methylephedrinnium salt forms including standard deviation of the measurements.

8.2.1. GENERAL TRENDS IN HARDNESS

The same arbitrary scale of hardness used for tyrammonium salt forms was used to classify enantiopure methylephedrine compounds in different categories: Soft compounds are thus here defined as those that have hardness lower than 1.0 GPa. Medium hardness compounds will have hardness between 1.0 and 2.0 GPa and hard materials will have hardness higher than 2.0 GPa. Considering these categories, 57.1 % of enantiopure methylephedrine and 50 % of racemic methylephedrine salt forms are soft materials while the other 42.9 % of the enantiopure compounds and 50 % of the racemic compounds have medium hardness. Unlike tyramine, none of the compounds investigated were classified as hard materials. Again, there is no obvious trending of hardness according to the composition of the counterion where, for example, benzoates can have medium hardness (*r*3CB and *e*2HB) or be soft (*r*2NB and *e*2FB). There were also no obvious trends observed on comparing structural features in the crystal. Figure 8.13 shows the distribution of hardness values for all enantiopure and racemic compounds where in light blue are the enantiopure metyhlephedrinium soft materials, in dark blue are the enantiopure methylephedrinium compounds with medium hardness, light red are the racemic metyhlephedrinium soft materials and in dark red are the racemic methylephedrinium compounds with medium hardness.

Figure 8. 13. Hardness scale for salt forms of enantiopure methylephedrine (in blue) and racemic methylephedrine (in red) where light grey represents soft materials, grey represents medium hardness and dark grey represents hard materials.

8.2.2. TRENDS IN HARDNESS ACCORDING TO FEATURES IN THE UNIT CELL

Considering only compounds with coefficient of regression higher than 80 %, there were only three compounds with more than one cation per asymmetric unit (Z' > 1): *e*FUM, *e*MUC.2H2O and *r*RTAR. The inexpressive number of compounds with Z' = 2, all carboxylates, restrict any further analysis only considering structures with Z' >1. However, there were eight crystal structures with presence of water in the unit cell considering enantiopure and racemic methylephedrine salt forms and comparison between anhydrous and hydrated compounds can be observed in Figure 8.14. Interestingly, when separating hydrated and anhydrous compounds, the compounds behave slightly differently than the original trendline (Figure 8.14 – black trendline).

Hydrated compounds are harder than anhydrous compounds for the same stiffness (Young's Modulus) in the case of methylephedrine compounds, however this was not observed for tyramine compounds. The elasticity index (I_E) for anhydrous compounds show they will constrain 9.1 % while for hydrated compounds they will constrain 11.7 %. Table 8.6 shows the resultant gradient and intercept of the trendlines in Figure 8.14.

Table 8. 6. MEPD compounds separated by composition of the crystal structure where n is the number of compounds used in the analysis, I_E is the elasticity index and R^2 is the regression coefficient.

	n	$I_E \pm \sigma_{IE}$	Intercept $\pm \sigma_{Intercept}$	R^2
All data	26	0.102 ± 0.005	0.07 ± 0.03	0.9390
Anhydrous	18	0.091 ± 0.006	0.14 ± 0.04	0.9310
Hydrate	8	0.117 ± 0.008	-0.02 ± 0.05	0.9753
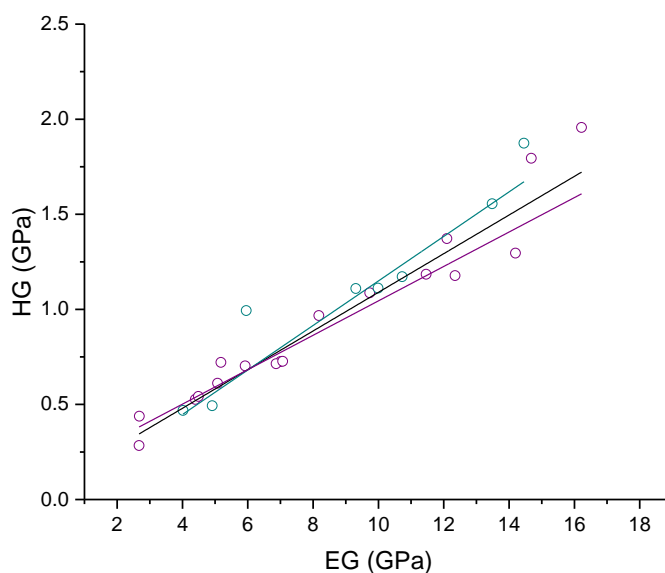
Figure 8. 14. Line in black represents all MEPD compounds, line in ciano blue represents all hydrated compounds and line in purple represents all anhydrous compounds. Standard deviation was omitted for clarity.

8.2.3. TRENDS IN HARDNESS ACCORDING TO THE COMPOSITION OF THE COUNTERION

When analysing the relationship between hardness and Young's Modulus according to the composition of the counterion, no deviation from the linear relationship containing all compounds was found for benzoates and carboxylates within the standard deviation, as it can be observed in Table 8.7 and Figure 8.15. However, considering only the five enantiopure and racemic sulfonates, there is a decrease in the elasticity index to (8.3 ± 1.7) %. Figure 8.15 also show the position of inorganic counterions (green dots) and the naphthalates (purple dots) however they were excluded from this analysis as there is not enough data for analysis.

Table 8. 7. MEPD compounds separated by composition of the counterion where n is the number of compounds used in the analysis, I_E is the elasticity index and R^2 is the regression coefficient.

	n	$I_E \pm \sigma_S$	Intercept $\pm \sigma_{Intercept}$	R^2
All	26	0.102 ± 0.005	0.07 ± 0.03	0.9390
Benzoates	7	0.101 ± 0.012	0.08 ± 0.06	0.9385
Carboxylates	9	0.107 ± 0.009	0.08 ± 0.06	0.9506
Sulfonates	5	0.083 ± 0.017	0.17 ± 0.10	0.8922

As values of gradient hardness and gradient Young's Modulus have a linear relationship further analysis will be only done for hardness values. A hardness scale for compounds according to the composition of the counterion was also constructed, as it can be observed in Figure 8.16, where blue circles represent benzoates counterions, red circle represents mono and di-carboxylates, green circles represent inorganic counterions, grey circles represent naphthalates and light blue circles represents sulfonates. containing data that does not fit in these categories. This figure also illustrates structural information about the presence of water molecules (.H2O), presence of a free acid in the structure (*), and otherwise specified, presence of another cation per asymmetric unit ($^\alpha$ represents Z' = 2).
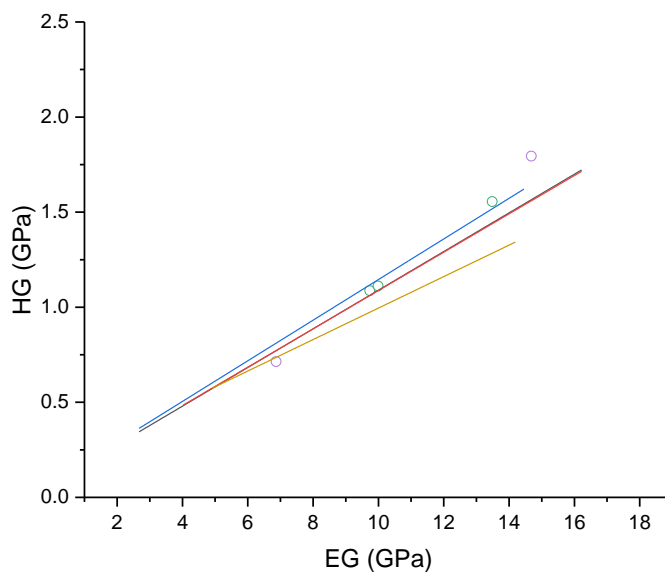
Figure 8. 15. Hardness versus Young's Modulus for methylephedrine samples according to the counterion composition. Trendline in black represents all compounds, in red represents only benzoates, in blue represents carboxylates, in beige represents sulfonates. The dots in green represents inorganic compounds and in purple represents naphthalates. The other circles representing the data and standard deviation were omitted for clarity.

Using hardness scale in Figure 8.16 it is easier to analyse how hardness behaves according to the composition of the crystal structure. Unfortunately, there were not enough halide and halobenzoates available for isostructural analysis as observed in the tyramine chapter. However, when considering only pairs of benzoates substituted in the same position in the ring, it was found to relationship between the molecular weight of the counterion and the hardness also observed for tyramine salt forms. When comparing chlorobenzoates and fluorobenzoates, hardness increases as the molecular weight of the compound increases, this trend occurs for the *ortho*-substituted benzoates (2CB and 2FB) of tyramine and enantiopure methylephedrine and for *para*-substituted benzoates (4CB and 4FB) of tyramine.
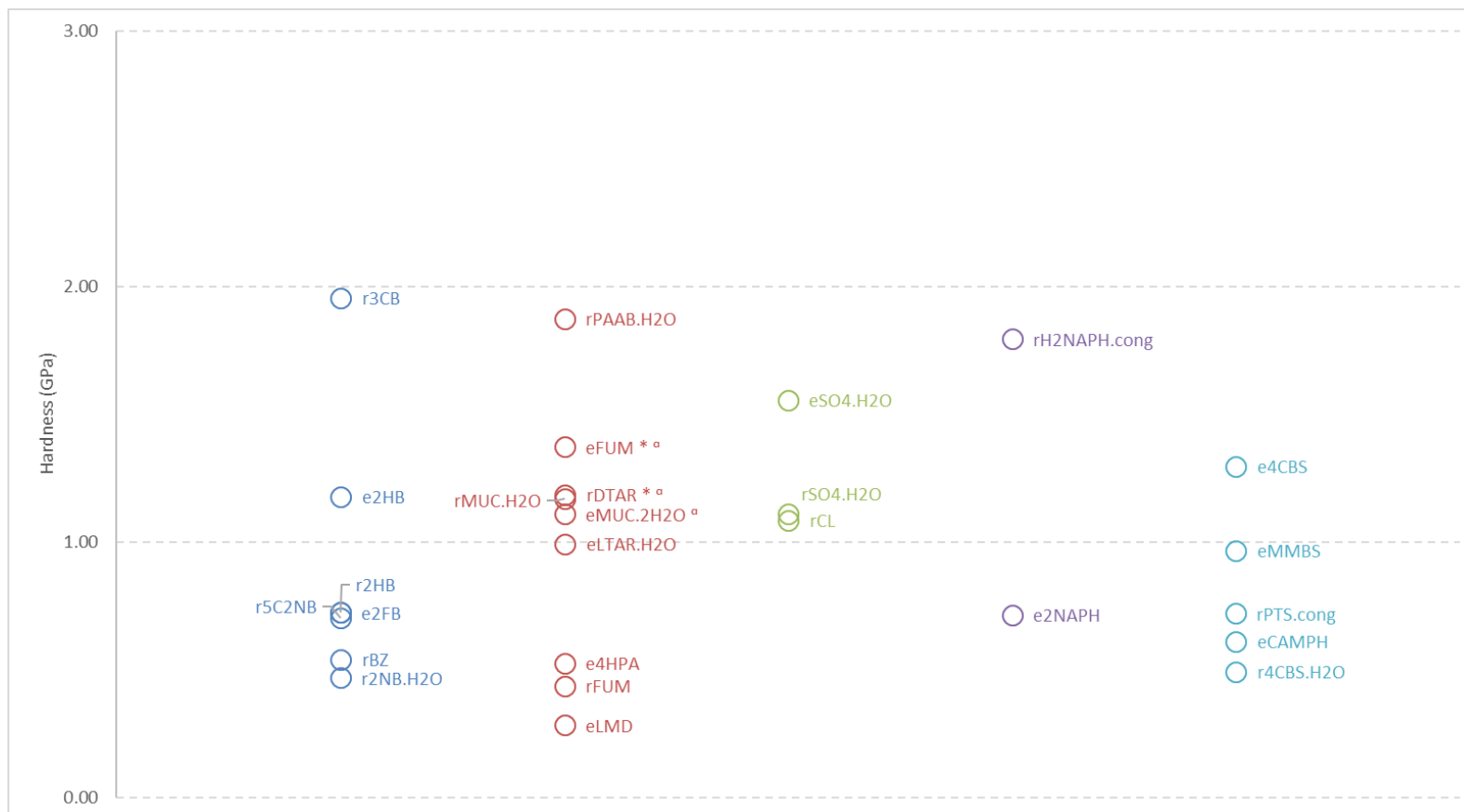
Figure 8. 16. Hardness scale according to the composition of the counterion. Blue circles represent benzoates counterions, red circle represents mono and di-carboxylates, green circles represent inorganic counterions, grey circles represent naphthalates and light blue circles represents sulfonates. There is also structural information about the presence of water molecules (.H2O), presence of a free acid in the structure (*), and otherwise specified, presence of another cation per asymmetric unit ($^\alpha$ represents Z' = 2)

The first interesting result obtained from this data is regarding to the six pairs of enantiopure and racemic compounds. This analysis is somewhat complicated as of all the pairs analysed, only two pairs have exactly the same composition within the unit cell when they were racemic and enantiopure: the anhydrous structures with one cation per asymmetric unit 2-hydroxybenzoate (2HB) and the hydrate structures with one cation per asymmetric unit hydrogen-sulfonate (SO4). The other pairs have different compositions when they are enantiopure and racemic and it is thus harder to make simple comparisons: These differences are, the racemic salt form of 4-chlorobezensesulfonate (r4CBS.H2O) has a water molecule present in the structure when compared with the enantiopure and anhydrous one (e4CBS) and enantiopure fumarate have the presence of an extra cation in the unit cell (eFUM) in opposition to the racemic fumarate (rFUM) that only have one cation per asymmetric unit; the racemic salt form of the meso chiral compound MUC is a mono-hydrate while the enantiopure have the presence of an extra cation and an extra molecule of water. Another pair of structures analysed are the enantiopure salt form monohydrated (1R,2S) methylephedrinium L-tartarate and the anhydrous racemic salt form (+/-) methylephedrinium R-tartarate. As it can be observed in Figure 8.17, for four of the six pairs, the enantiopure salt forms are harder than racemic salts. For the remaining two salt form pairs, those with mucic and tartaric acids as counterion, formers, the differences in hardness are statistically insignificant within standard deviation. It is interesting that this split 4 to 2 split corresponds to the 4 achiral salt formers and the 2 salt formers with stereocentres.

There were no large cation packing isostructural groups found among these samples. The two isostructural groups identified contained only two structures in each group: There is no evidence that belonging to an isostructural group leads to similarity in hardness. Group 1 containing e2NAPH ($H_G = 0.71$ (3) GPa) and rH2NAPH.cong (HG = 1.79 (27) GPa); and Group 2 containing rFUM ($H_G = 0.44$ (6) GPa) and rMUC.H2O ($H_G = 1.17$ (12) GPa). For this reason, further comparison between isostructural structures will not be done.
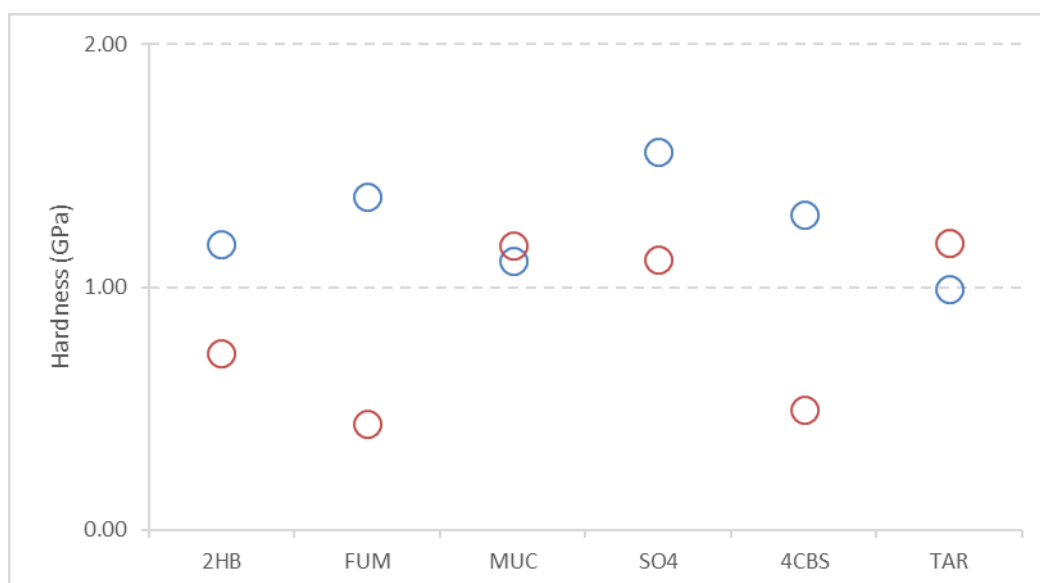
Figure 8. 17. Hardness for pairs of enantiopure (in blue) and racemic (in red) compounds.

8.3. EPHEDRINE AND PSEUDOEPHEDRINE SALT FORMS

In this work twenty-one salt forms of enantiopure ephedrine and sixteen salt forms of enantiopure pseudoephedrine were analysed. These APIs are diastereomers and this similarity means that they are herein considered together. Of these compounds measured by nanoindentation, fourteen salts of ephedrine and all salt forms of pseudoephedrine were synthesized by Morrison *et al.* [1] while the synthesis of the remaining seven compounds were described in Chapter 2.4. The composition of the counterion selection used in this work for ephedrine salt forms is divided as follows. Two inorganic salt forms (sulfate and chloride), three *ortho*-substituted benzoates, two *meta*-substituted benzoates and three *para*-substituted benzoates, five carboxylates (three monocarboxylates, two dicarboxylates) and six sulfonates. In the case of pseudoephedrine salt forms, the distribution of counterions is: One inorganic salt form (iodide), three *ortho*-substituted benzoates, two *meta*-substituted benzoates and three *para*-substituted benzoates, unsubstituted benzoate, four carboxylates (two dicarboxylates, two monocarboxylates) and two sulfonates. Figure 8.18 shows the percentage distribution of the counterions used in this experiment for ephedrine salt forms (on the left) and pseudoephedrine salt forms (on the right). Details about the crystal structures of the salt forms can be obtained in the APPENDIX 3.2.
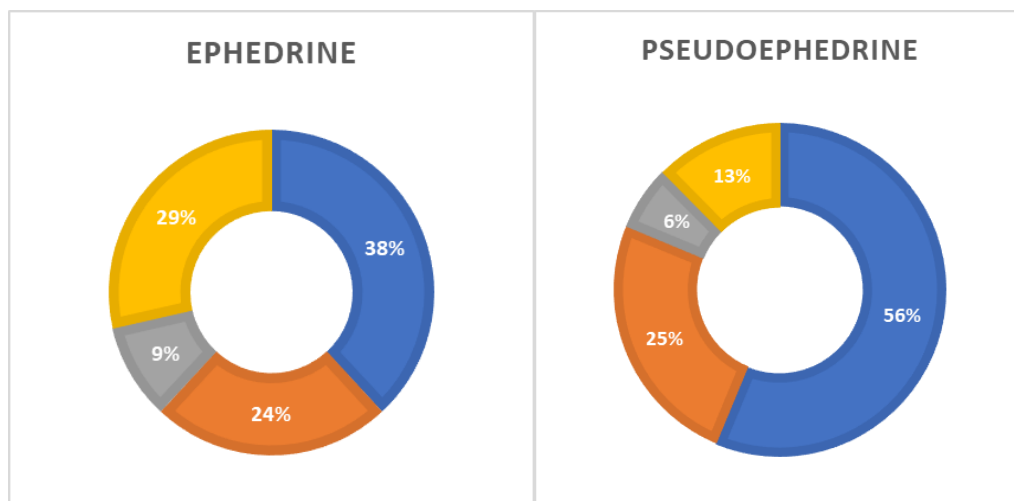
Figure 8. 18. Distribution of the salt selection by composition of counterion for enantiopure salt forms of ephedrine (left) and pseudoephedrine (right) where in blue represents percentage of benzoates, in orange represents percentage of carboxylates, in grey represents percentage inorganic and in yellow represents the percentage of sulfonates.

All compounds were analysed using the technique described in Chapter 2.7, where the gradient hardness (H_G), the intercept, the regression coefficient (R^2) and Young's Modulus were obtained. In these sets of data, the letter "*p"* before each compound indicate they are salt forms of pseudoephedrine while the letter "*e*" before each compound means they are salt forms of enantiopure ephedrine. Complete details about nanoindentation measurements can be observed in APPENDIX 8.3. However, a summary of these values is detailed in Table 8.8.

Of the total of ephedrine and pseudoephedrine salt forms measured with nanoindentation, 75.7 % were anhydrous while the remaining 24.3 % were hydrates. There are four structures of ephedrine and pseudoephedrine with two cations per asymmetric unit (Z' = 2): the monohydrated salt form of ephedrine and d-tartaric acid (*e*2DTAR.H2O), the tetra-substituted sulfonate *e*MMBS, and two anhydrous nitrobenzoates of pseudoephedrine, the *meta*-substituted *p*3NB and the *para*-substituted *p*4NB. There is also one compound with four cations per asymmetric unit (Z' = 4), the anhydrous and disordered salt form of ephedrine and naphthalene-2-sulfonate (*e*N2S). All the other structures had only one cation per asymmetric unit (Z'

= 1). The distribution of compounds according to these features within the unit cell can be observed in Figure 8.19.
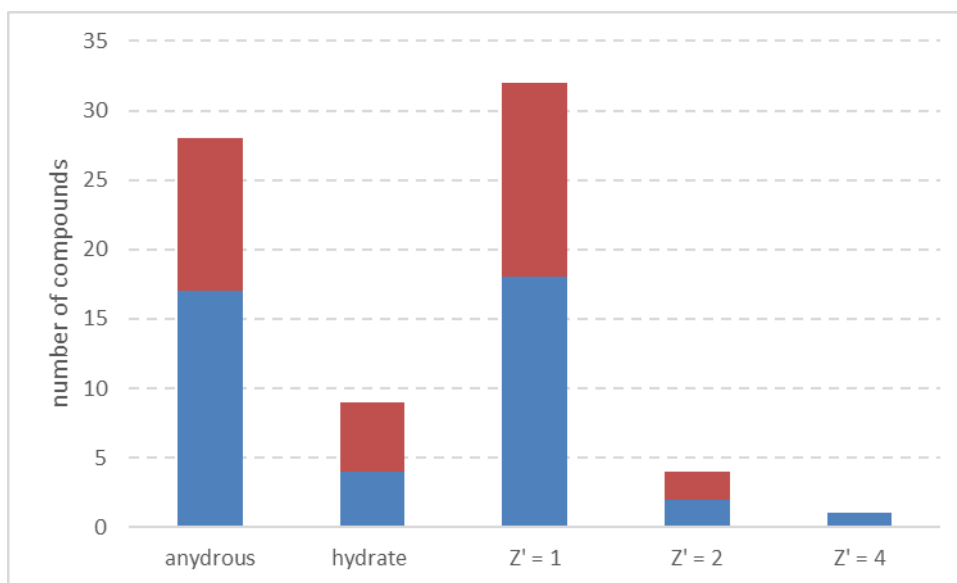
Figure 8. 19. Distribution of structural features of the total of 21 ephedrine compounds (in blue) and 16 pseudoephedrine compounds (in red).

Table 8. 8. Results for ephedrine and pseudoephedrine salt forms where n_m is the number of measurements in each sample, H_G is the gradient hardness, E_G is the Young's Modulus and σ represents the errors in each measurement. There is also structural information about the presence of water molecules (.H2O), crystallisation of a conglomerate (.cong) presence of a free acid in the structure (*), and otherwise specified, presence of another cation per asymmetric unit ([a] represents Z' = 2 and [b] represents Z' = 4)

Ephedrine											
Sample	**n_m**	**H_G**	**σH_G**	**Intercept**	**σIntercept**	**R^2**	**E_G**	**σ_{EG}**	**Intercept**	**σIntercept**	**R^2**
*e*2CB	9	1.47	0.13	3.73	0.61	0.9508	11.40	0.68	3.76	0.42	0.9757
*e*2DTAR.H2O [a]	6	0.20	0.02	0.86	0.73	0.9405	1.71	0.17	0.75	0.60	0.9607
*e*2NB	9	0.56	0.02	4.14	0.30	0.9902	4.70	0.16	4.03	0.27	0.9923
*e*3CB	9	0.54	0.05	2.37	0.51	0.9499	4.53	0.34	2.38	0.44	0.9630
*e*4AB	17	0.88	0.06	2.95	0.40	0.9423	6.17	0.52	2.99	0.52	0.9051
*e*4APA	6	0.68	0.11	3.85	1.09	0.8563	5.07	0.46	3.61	0.66	0.9448
*e*4CB	6	0.84	0.07	4.23	0.62	0.9565	6.83	0.44	4.06	0.51	0.9713
*e*4CBS	8	0.30	0.05	7.45	1.58	0.8393	0.95	0.17	7.76	1.54	0.8370
*e*4HBS.H2O	9	0.72	0.07	4.75	0.57	0.9443	5.89	0.42	5.06	0.42	0.9658
*e*4HPA	6	0.98	0.19	3.85	2.01	0.8684	6.96	0.91	4.07	1.32	0.9364
*e*4NB	5	0.13	0.03	5.63	0.93	0.8693	0.70	0.15	5.78	0.84	0.8819
*e*AA	6	0.64	0.10	0.24	1.57	0.8644	5.00	0.56	0.79	1.11	0.9199
*e*BS [5]	6	1.28	0.13	1.79	1.04	0.9162	11.01	1.25	2.04	1.14	0.8967
*e*CL [5]	12	0.56	0.04	3.35	0.41	0.9554	3.46	0.28	3.37	0.48	0.9405
*e*ETSO3 [5]	9	1.33	0.15	3.44	0.82	0.9186	11.49	1.07	2.76	0.74	0.9425
*e*LMD [5]	7	0.71	0.12	5.03	1.45	0.8816	5.90	0.75	4.80	1.16	0.9249
*e*LTAR.H2O [5]	12	1.27	0.07	0.72	0.79	0.9727	11.06	0.63	0.28	0.87	0.9685
*e*MMBS [a]	6	0.52	0.05	2.40	0.61	0.9617	3.09	0.25	2.18	0.51	0.9748
*e*MTOL	9	0.59	0.05	4.34	0.55	0.9536	4.95	0.39	4.14	0.53	0.9583
*e*N2S [b]	6	0.67	0.02	2.66	0.20	0.9916	5.57	0.20	2.47	0.21	0.9908
*e*SO4.H2O [5]	8	0.48	0.03	4.16	0.51	0.9690	4.03	0.25	4.29	0.42	0.9782

Pseudoephedrine										
Sample	n_m	H_G	σH_G	**Intercept**	$\sigma_{Intercept}$	R^2	E_G	σ_{EG}	**Intercept**	$\sigma_{Intercept}$	R^2
p2CB.H2O	9	3.47	0.28	0.43	0.85	0.9739	34.08	4.01	-0.16	1.28	0.9118
p2HB	9	1.20	0.11	2.72	0.77	0.9425	10.70	0.72	2.84	0.55	0.9695
p3HB.3H2O	18	0.46	0.04	1.96	1.12	0.8971	2.97	0.18	2.59	0.78	0.9428
p3NB [a]	9	0.81	0.09	2.89	0.88	0.9205	6.57	0.54	2.43	0.69	0.9546
p4AB.2H2O	9	0.27	0.03	4.39	0.68	0.9321	2.63	0.24	4.31	0.62	0.9442
p4CB	9	0.64	0.10	4.00	1.02	0.8650	5.08	0.51	3.73	0.71	0.9349
p4HBS	9	0.78	0.06	4.81	0.46	0.9701	7.24	0.40	4.56	0.37	0.9818
p4NB [a]	9	0.16	0.02	6.78	0.58	0.8800	1.27	0.15	6.53	0.52	0.9119
pBS	9	0.21	0.02	5.03	0.44	0.9652	1.80	0.07	5.07	0.25	0.9882
pBZ	9	1.20	0.06	2.91	0.42	0.9814	10.94	0.61	2.89	0.45	0.9789
pI	9	0.51	0.04	3.72	0.60	0.9530	4.11	0.29	3.94	0.49	0.9672
pLMD	9	0.36	0.02	3.74	0.47	0.9707	2.90	0.15	3.93	0.36	0.9818
pLTAR.H2O	9	0.91	0.10	4.37	0.73	0.9196	7.44	0.70	4.48	0.61	0.9414
pMALE	9	1.42	0.22	3.68	1.10	0.8604	14.95	1.92	2.74	1.05	0.8967
pOTOL.H2O	9	0.53	0.08	3.61	1.09	0.8659	4.89	0.58	3.41	0.89	0.9104
pRMAL	18	2.00	0.12	3.72	0.71	0.9439	15.90	0.78	3.43	0.59	0.9626

Of all thirty-seven compounds of ephedrine and pseudoephedrine measured by nanoindentation, no set of measurement was excluded from analysis as all compounds obtained regression coefficient higher than 80 %. A scatter plot of the gradient hardness (H_G) versus Young's Modulus (E_G) for the compounds, considering the standard deviation, can be observed in Figure 8.20. There is a linear relationship between Hardness and Young's Modulus for the set of samples including all ephedrine and pseudoephedrine compounds, which fits the trendline with equation $H_G = (0.114 \pm 0.004) \cdot E_G + (0.03 \pm 0.02)$ with R^2 equals to 0.9648 (Figure 8.20 – trendline in black). When considering only ephedrine salt forms the trendline is the same as observed with all compounds within standard deviation with equation $H_G = (0.113 \pm 0.006) \cdot E_G + (0.06 \pm 0.03)$ and $R^2 = 0.9541$ (Figure 8.20 – dots and trendline in red). The same occur when it is considered only pseudoephedrine salt forms, with equation $H_G = (0.111 \pm 0.005) \cdot E_G + (0.03 \pm 0.02)$ with $R^2 = 0.9766$ (Figure 8.20 – dots and trendline in blue). For this reason, ephedrine and pseudoephedrine will be compared together in further analysis. Ephedrine and pseudoephedrine will have hardness values around 0.114 times the values of gradient Young's Modulus, constraining 11.4 %.
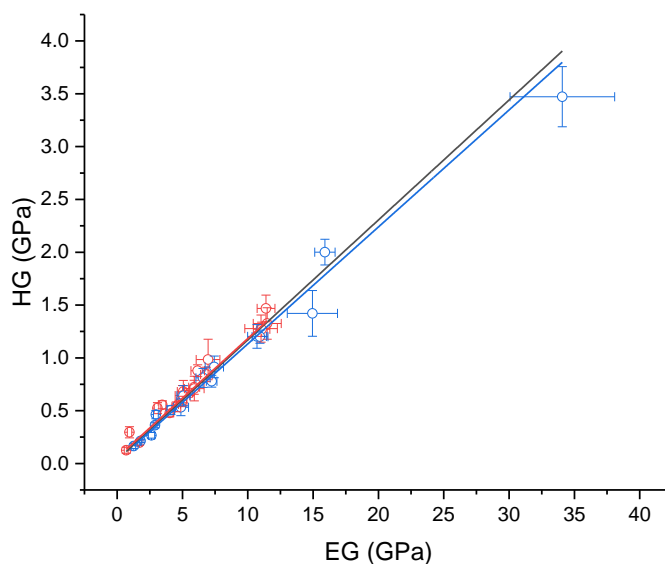
Figure 8. 20. Scatter plot of gradient hardness (H_G) versus gradient Young's Modulus (E_G) for all compounds (trend line in black), ephedrine (in red) and pseudoephedrine (in blue) salt forms, including standard deviation of the measurements.

8.3.1. GENERAL TRENDS IN HARDNESS

The same arbitrary scale of hardness used for tyrammonium and methylephedrinium salt forms was used to classify enantiopure ephedrine and pseudoephedrine compounds into different categories: Soft compounds are thus here defined as those that have hardness lower than 1.0 GPa. Medium hardness compounds will have hardness between 1.0 and 2.0 GPa and hard materials will have hardness higher than 2.0 GPa. Considering these categories, 76.1 % of ephedrine and 68.8 % of pseudoephedrine salt forms are soft materials while 23.8 % of the ephedrine compounds and 18.8 % of the pseudoephedrine compounds have medium hardness. While there were no very hard ephedrine salt forms, 12.5 % of pseudoephedrine compounds were very hard. The 2CB salt forms of both bases gave the hardest materials. 2CB salts, where measured, give consistently relatively hard forms for the other bases. Again, there is no obvious trending of hardness according to the composition of the counterion or features in the crystal structure. Figure 8.21 shows the distribution of hardness values for all ephedrine (in blue) and pseudoephedrine (in red).
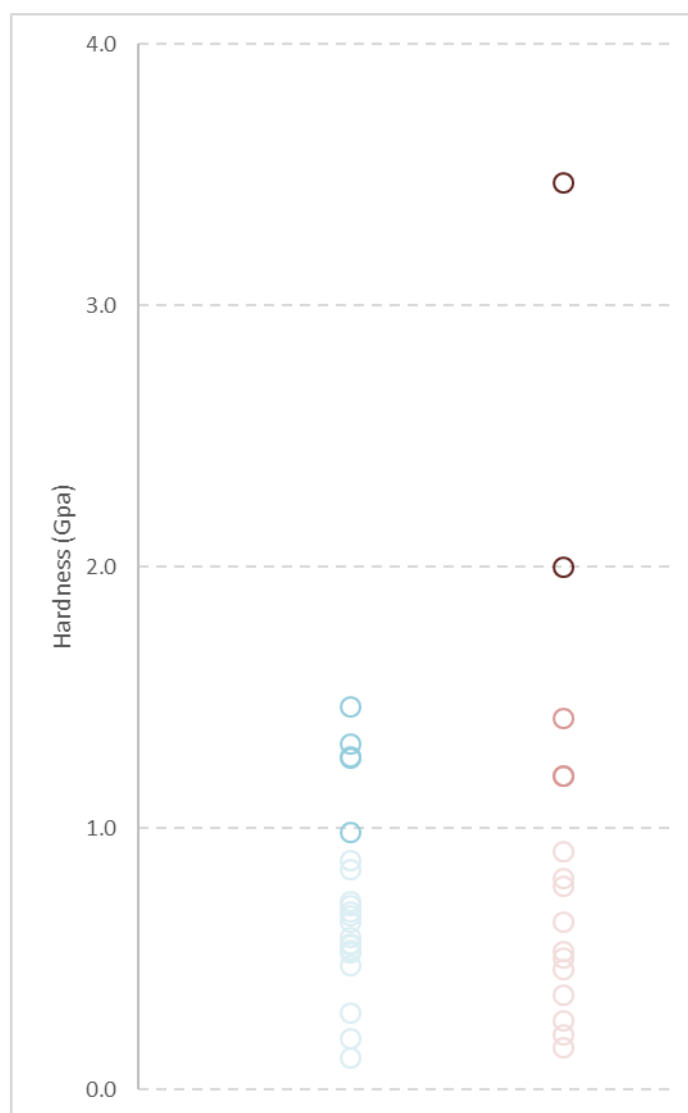
Figure 8. 21. Hardness scale for salt forms of ephedrine (in blue) and pseudoephedrine (in red) where light colour represents soft materials, medium colour represents medium hardness and dark colour represents hard materials.

8.3.2. TRENDS IN HARDNESS ACCORDING TO FEATURES IN THE UNIT CELL

There were only five compounds with more than one cation per asymmetric unit (Z' > 1): *e*2DTAR.H2O, *e*MMBS, *p*3NB and *p*4NB (with Z' = 2) and *e*N2S (with Z' = 4). The inexpressive number of compounds with Z' > 1 restrict any further analysis for this set of data. However, there were nine crystal structures with presence of water in the unit cell considering both ephedrine (four) and pseudoephedrine (five) salt forms and comparison between anhydrous and hydrated compounds can be observed in

Figure 8.22. Interestingly, in this case, when separating hydrated (Figure 8.22 – blue trendline) and anhydrous compounds (Figure 8.22 – red trendline), the compounds behave the same as the original trendline (Figure 8.22 – black trendline) within standard deviation. Table 8.9 have a summary of the equations for anhydrous and hydrated compounds of ephedrine and pseudoephedrine.

Table 8. 9, Compounds separated by composition of the crystal structure where n is the number of compounds used in the analysis, I_E is the elasticity index and R^2 is the regression coefficient.

	n	$I_E \pm \sigma_{IE}$	Intercept ± $\sigma_{Intercept}$	R^2
All data	37	0.114 ± 0.004	0.03 ± 0.02	0.9648
Anhydrous	28	0.114 ± 0.004	0.04 ± 0.02	0.9658
Hydrate	9	0.111 ± 0.008	0.02 ± 0.03	0.9676
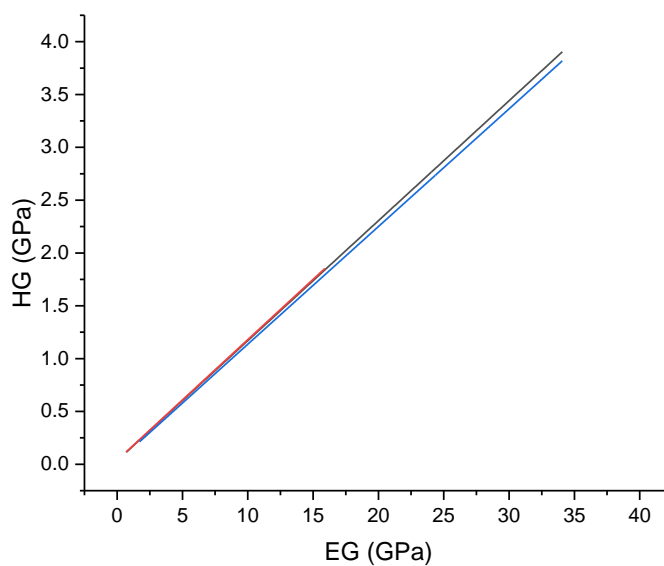
Figure 8. 22. Line in black represents all compounds, line in red all anhydrous compounds and line in blue all hydrated compounds.

8.3.3. TRENDS IN HARDNESS ACCORDING TO THE COMPOSITION OF THE COUNTERION

When analysing the relationship between hardness and Young's Modulus according to the composition of the counterion, no deviation from the linear relationship containing all compounds was found for benzoates, carboxylates and sulfonates within the standard deviation, as it can be observed in Table 8.10 and Figure 8.23. There were only three compounds with inorganic counterions, and these compounds were taken off the analysis, as shown in Figure 8.23 as the green dots.

Table 8. 10. Compounds separated by composition of the counterion where n is the number of compounds used in the analysis, I_E is the elasticity index and R^2 is the regression coefficient.

	n	$I_E \pm \sigma_S$	Intercept $\pm \sigma_{Intercept}$	R^2
All	37	0.114 ± 0.004	0.03 ± 0.02	0.9648
Benzoates	17	0.112 ± 0.005	0.04 ± 0.02	0.9710
Carboxylates	9	0.118 ± 0.005	0.09 ± 0.02	0.9888
Sulfonates	8	0.111 ± 0.010	0.04 ± 0.04	0.9553
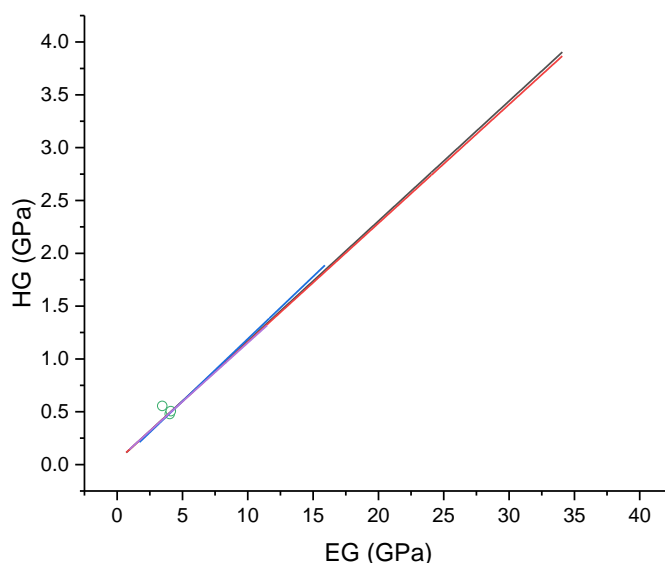
Figure 8. 23. Hardness versus Young's Modulus for methylephedrine samples according to the counterion composition. Trendline in black represents all compounds, in red represents only benzoates, in blue represents carboxylates and in purple represents sulfonates. The dots in green represents inorganic compounds. The other circles representing the data and standard deviation were omitted for clarity.

Again, as values of gradient hardness and gradient Young's Modulus have a linear relationship further analysis will be only done for hardness values. A hardness scale for compounds according to the composition of the counterion was also constructed, as it can be observed in Figure 8.24. This is a more detailed version of the hardness scale according to the composition of the counterion, where blue circles represent *ortho*-substituted benzoates, orange circles represent *meta*-substituted benzoates, grey circles represent *para*-substituted benzoates, yellow circles represent mono-substituted benzoate and sulfonate, light blue circles represent mono-carboxylates, green circles represents dicarboxylates, dark blue circles represent sulfonates and dark red circles represent inorganic counterions. This figure also illustrates structural information about the presence of water molecules (.H2O), presence of a free acid in the structure (*), and otherwise specified, presence of another cation per asymmetric unit ([a] represents Z' = 2 and [b] represents Z' = 4).

The first result which can be obtained from this data is related to the isostructural groups present in this data, as observed in Chapter 7. There are three isostructural groups of ephedrine salt forms: Group 1 including the samples *e*4APA ($H_G = 0.68$ (11) GPa), *e*4HPA ($H_G = 0.98$ (19) GPa) and *e*AA ($H_G = 0.64$ (10) GPa); Group 2 containing the samples *e*3CB ($H_G = 0.54$ (5) GPa) and *e*MTOL ($H_G = 0.59$ (5) GPa) and Group 3 containing the samples *e*N2S ($H_G = 0.67$ (2) GPa) and *e*4CBS ($H_G = 0.30$ (5) GPa). In the case of pseudoephedrine salt forms, there are four isostructural groups in this data set: Group 4 containing the samples *p*BZ ($H_G = 1.20$ (6) GPa), *p*4CB ($H_G = 0.64$ (10) GPa) and *p*2HB ($H_G = 1.20$ (11) GPa); Group 5 with the samples *p*3NB ($H_G = 0.81$ (9) GPa) and *p*4NB ($H_G = 0.16$ (2) GPa); Group 6 with the samples *p*2CB.H2O ($H_G = 3.47$ (28) GPa) and *p*OTOL.H2O ($H_G = 0.53$ (8) GPa); and Group 7 containing the samples *p*4HBS ($H_G = 0.78$ (6) GPa) and *p*LMD ($H_G = 0.36$ (2) GPa). As it can be observed in Figure 8.25, apart from Group 2, the structure of all the other isostructural groups have different values of hardness from their isostructural matches. This difference of hardness can be illustrated by two groups: In isostructural Group 2, which contains enantiopure ephedrine salt forms with *meta*-chlorobenzoate and with *meta*-toluate, the two structures have the same value of hardness. Isostructural Group 6 contains salt forms of pseudoephedrine with position isomers of the Group 2 anions, namely *ortho*-chlorobenzoate and *ortho*-toluate. Despite these similarities to Group 2,

the hardness of the two members of Group 6 differs by the large amount of 2.94 GPa. Another interesting isostructural group is Group 5, containing *meta-* and *para-* substituted nitrobenzoate. Both these structures are Z' > 1 (they contain an "extra" cation per asymmetric unit) and have different values of hardness.

Such differences between similar sized and functionalised groups which even adopt isostructural packing modes for the API cations again suggests that hardness values depend not only on the composition and size of the counterions but must be related to individual structural features such as the strength of each individual intermolecular contact. The last result observed for isostructural groups includes the two bigger groups: Group 1 contains ephedrine salts of two monocarboxylates (*e*4HPA and *e*4APA) and an *ortho*-substituted benzoate (*e*AA). Group 4 contains pseudoephedrine salts of benzoate (*p*BZ) and the substituted benzoates (*p*2HB and *p*4CB). These isostructural groups contain three samples and, interestingly, there are two samples samples with the same value of hardness within standard deviation (Group 1: *e*AA, *e*4HPA and *e*4APA; Group 4: *p*BZ and *p*2HB).
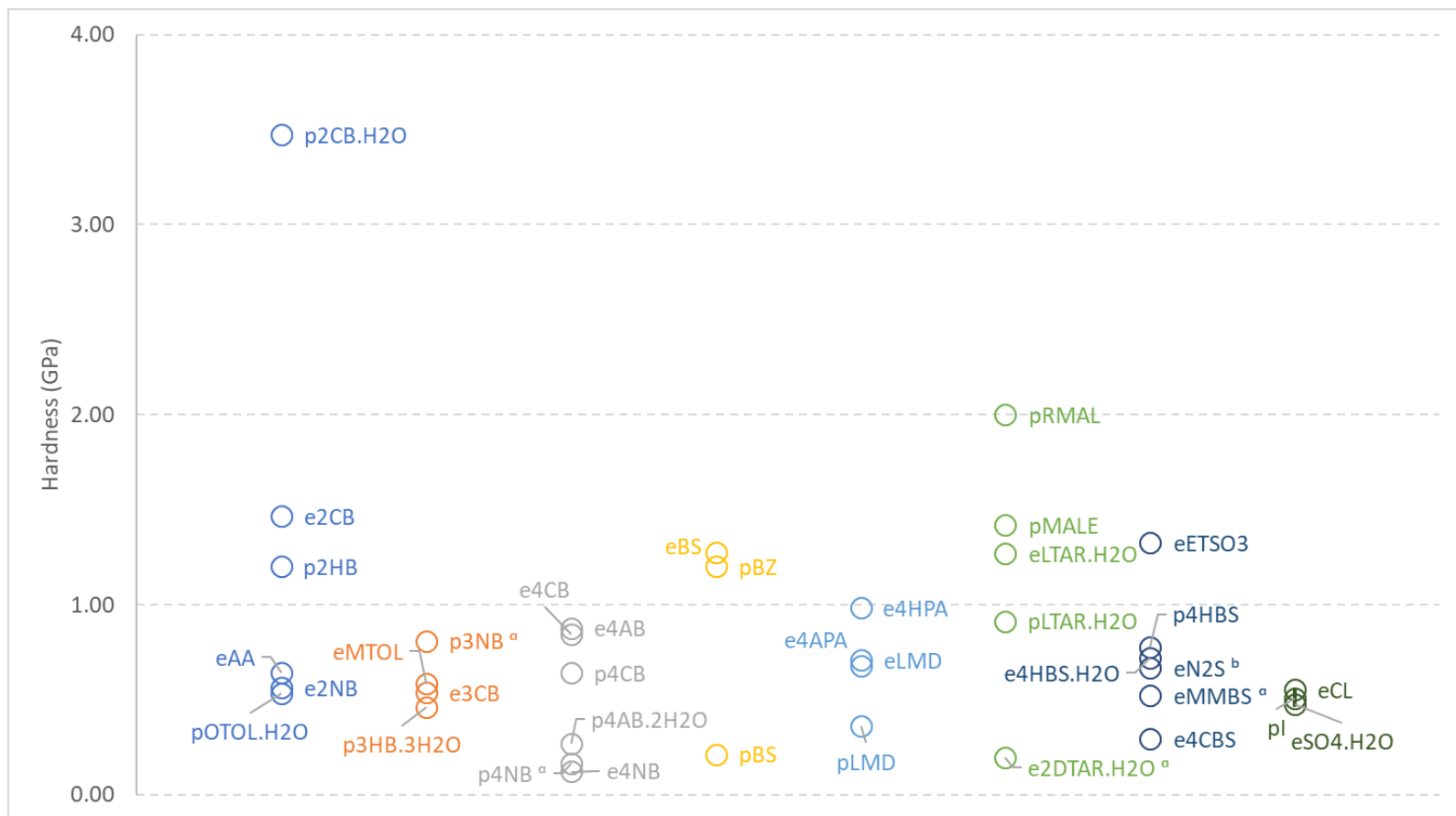
Figure 8. 24. Hardness scale according to the composition of the counterion. Blue circles represent *ortho*-substituted benzoates, orange circles represent *meta*-substituted benzoates, grey circles represent *para*-substituted benzoates, yellow circles represent benzoate and benzenesulfonate, light blue circles represent mono-carboxylates, green circles represent dicarboxylates, dark blue circles represent sulfonates and dark green circles represent inorganic counterions. There is also structural information about the presence of water molecules (.H2O), presence of a free acid in the structure (*), and otherwise specified, presence of another cation per asymmetric unit (ᵃ represents Z' = 2 and ᵇ represents Z' = 4)
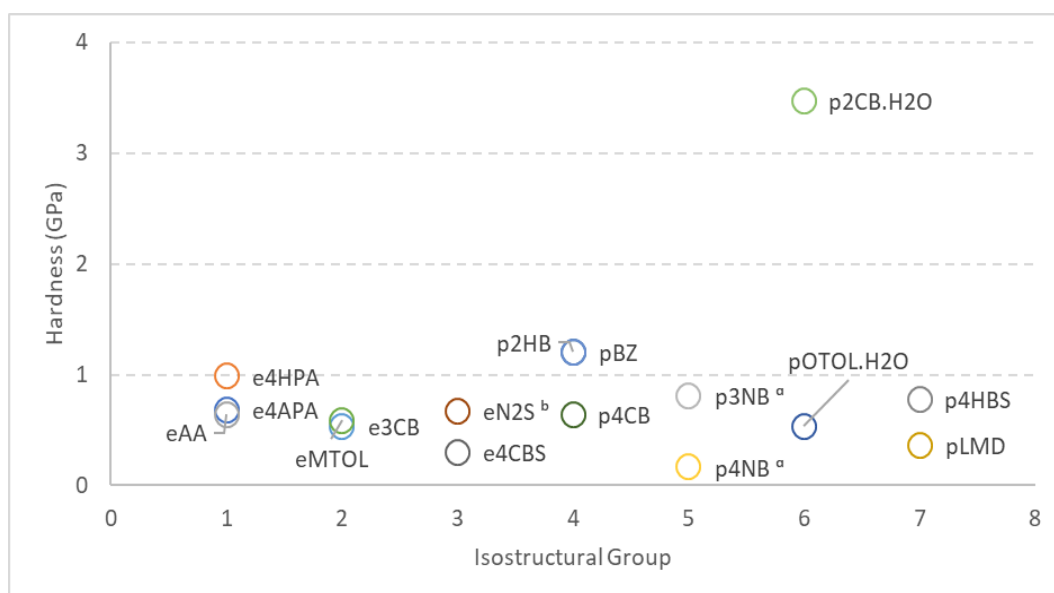
Figure 8. 25. Hardness for isostructural groups of ephedrine and pseudoephedrine salt forms.

There are eight pairs of compounds of ephedrine and pseudoephedrine with the same counterion. Of those pairs, four sets have pairs with the same Z' value and the same chemical composition, differing only by the stereocentre of the API. These are: three anhydrous structural pairs with one cation per asymmetric unit, 4-chlorobenzoate (4CB), benzenesulfonate (BS) and enantiopure mandelate (LMD); and one hydrate pair again with one cation per asymmetric unit of, namely enantiopure tartarate (LTAR). The other four pairs have different compositions when they crystallised with ephedrine or pseudoephedrine: ephedrine 2-chlorobenzoate (*e*2CB) has a water molecule present in the structure while the pseudoephedrine 2-chlorobenzoate (*p*2CB) is anhydrous; The same profile of crystallisation also occurs with salt forms of 4-hydrozybenzenesulfonate (4HBS) where the salt form of ephedrine is hydrated while the salt form of pseudoephedrine is anhydrous. The opposite profile applies to the 4-aminobenzoate (4AB) where the salt form of ephedrine is anhydrous, and the salt form of pseudoephedrine is a hydrate. Finally, chemically equivalent but having a different composition in the asymmetric unit cell is 4-nitrobenzoate (4NB) where the salt form of pseudoephedrine has two cations per asymmetric unit while the salt form of ephedrine has only one cation per asymmetric unit. Pairs of hardness values for these compounds can observed in Figure 8.26. In 50 % of these pairs, salt forms of ephedrine

were harder than salt forms of pseudoephedrine: 4AB, BS, LMD and LTAR. Interestingly, the difference between hardness for the pairs of ephedrine and pseudoephedrine of the carboxylates LMD and LTAR are the same, 0.355 (5) GPa. Of the eight pairs, three contain the same hardness within standard deviation, the *para*-substituted compounds 4CB, 4NB and 4HBS. The only pair of these compounds have hardness higher for pseudoephedrine salt than ephedrine salt (2CB) where the ephedrine salt is a hydrate and the pseudoephedrine salt is anhydrous. This shows that it might have a relationship between the anhydrous and hydrated form of benzoates, which will influence intermolecular interactions between the molecules and consequently the hardness of these compounds.
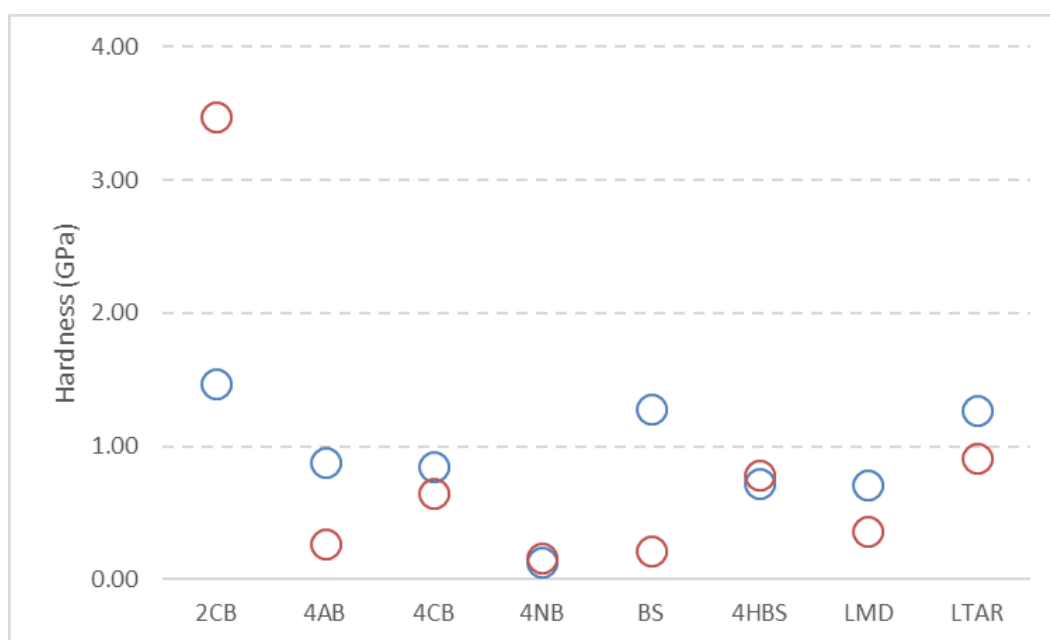
Figure 8. 26. Hardness for pairs of ephedrine (in blue) and pseudoephedrine (in red).

8.4. PHENYLETHYLAMINE AND METHYL DERIVATIVES SALT FORMS

The last group of cations analysed by nanoindentation is related to 2-phenylethylamine (PEA) and two derivatives of phenylethylamine: 2-methylphenylethylamine (MPEA) and 2-dimethylphenylethylamine (DMPEA). All salt forms in this chapter were synthesized by Morrison *et al.* [1]. In this chapter, the selection of salt forms is divided as twenty-four salt forms of PEA, ten salt forms of MPEA and four salt forms of DMPEA. The composition of the counterion selection for PEA salts forms is divided as follows: Four inorganic salt forms (chloride, bromide, sulfate and hexafluorosilicate), two monocarboxylates and seven di-carboxylates, eight substituted benzoates and three sulfonates. In the case of MPEA salt forms, the selection is divided as two inorganic salt forms (bromide and iodine), three di-carboxylates, four substituted benzoates and one sulfonate. For the four salt forms of DMPEA is separated as two benzoates, one di-carboxylate and one sulfonate. Figure 8.27 shows the percentage distribution of the counterions used in this experiment, where in blue represents percentage of benzoates, in orange represents percentage of carboxylates, in grey represents percentage of sulfonates and in yellow percentage of inorganic compounds. Details about the crystal structures of the salt forms can be obtained in the APPENDIX 8.4.
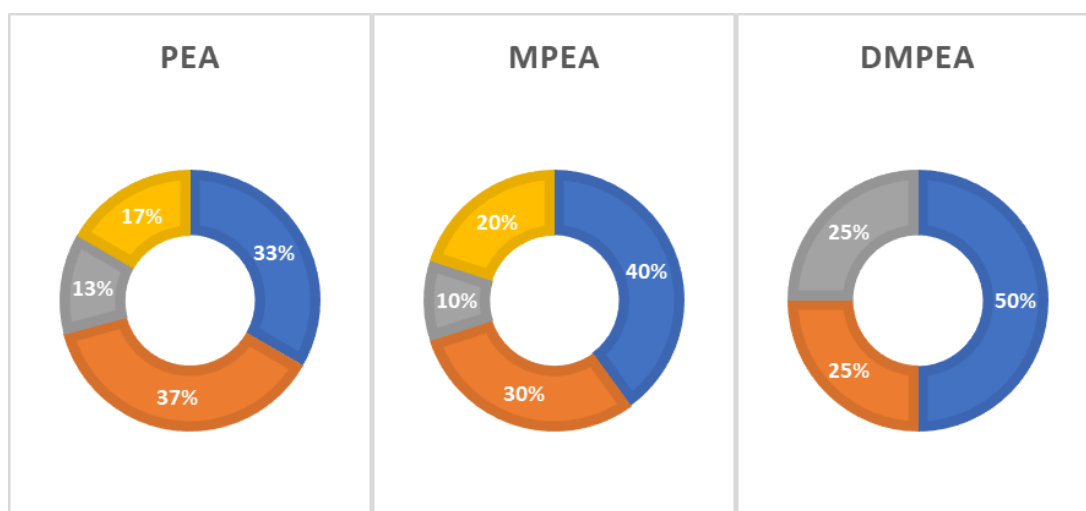
Figure 8. 27. Distribution of the salt selection by composition of counterion where in blue represents percentage of benzoates, in orange represents percentage of carboxylates, in grey represents percentage of sulfonates and in yellow percentage of inorganic compounds.

These salt forms were selected because of the diversity of features in the crystal structure, for example, presence of water in the structure, presence of an extra cation per asymmetric unit (Z' > 1) and presence of a neutral acid in the unit cell along with the ionised form. While all salt forms of MPEA analysed were anhydrous, 87.5 % of PEA salts were anhydrous and 12.5 % of PEA salt forms were hydrated and 75 % of DMPEA salt forms were anhydrous and 25 % of salt forms hydrated. Most compounds had only one cation per asymmetric unit however there was a presence of five salt forms of PEA and two compounds of DMPEA with two cations per asymmetric unit (Z' = 2) and both PEA and MPEA had one structure with four cations per asymmetric unit (Z' = 4) and one with the presence of a free acid in the unit cell. The distribution of compounds according to these structural features can be observed in Figure 8.28 where the blue boxes represent PEA salt forms, orange boxes represent MPEA salt forms and grey boxes represent DMPEA salt forms.
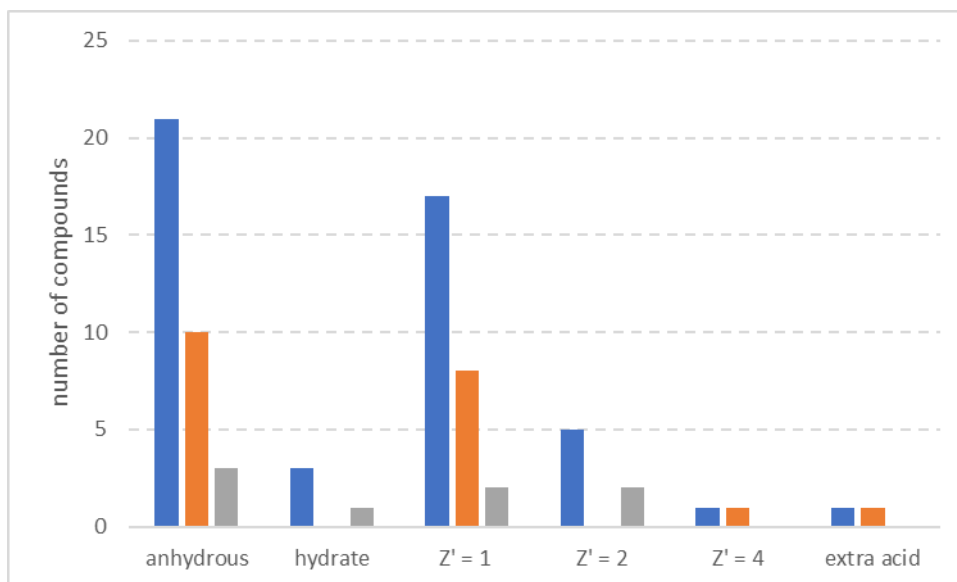
Figure 8. 28. Distribution of structural features of the PEA compounds (in blue) and MPEA compounds (in orange) and DMPEA compounds (in grey) analysed in this work.

All compounds were analysed using the technique described in Chapter 2.2.2, where the gradient hardness (H_G), the intercept, the regression coefficient (R^2) and gradient Young's Modulus (E_G) were obtained. Complete details about nanoindentation measurements can be observed in APPENDIX 8.4. However, a summary of these values is detailed in Table 8.11 where the presence of a "*m*" before the labels represent salt forms of MPEA and presence of "*dm*" before the labels represent salt forms of DMPEA.

There were no set of data analysed in this work with coefficient of determination lower than 80 % however two salt forms of PEA were excluded from any analysis as they obtained bad imaging before and / or after nanoindentation. The scatter plot of the gradient hardness (H_G) versus gradient Young's Modulus (E_G), considering the standard deviation of both measurements, for PEA compounds (in black), for MPEA compounds (in red) and for DMPEA (in blue) can be observed in Figure 8.29. There is a similar relationship between Hardness and Young's Modulus for this set of samples which fits the linear trendline with equation $H_G = (0.106 \pm 0.002) \cdot E_G + (0.022 \pm 0.005)$ with R^2 equal to 0.9921 for PEA, equation $H_G = (0.111 \pm 0.003) \cdot E_G + (0.0031 \pm 0.009)$ with R^2 equal to 0.9928 for MPEA and equation $H_G = (0.099 \pm 0.005) \cdot E_G +$

(0.02 ± 0.02) with R^2 equal to 0.9948 for DMPEA. Although there are not enough measurements of DMPEA compounds (only 4 nanoindentation measurements) both PEA and MPEA have very similar trendlines.
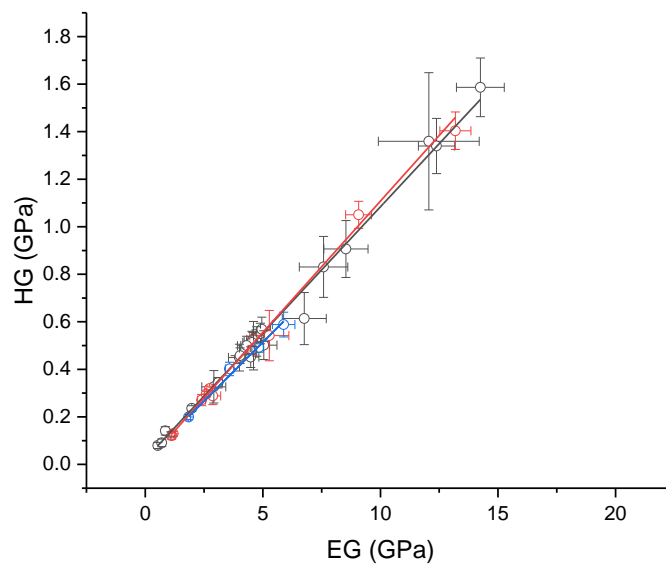
Figure 8. 29. Scatter plot of gradient hardness (H_G) versus Young's Modulus (E_G) for PEA salt forms (in black), MPEA salt forms (in red) and DMPEA salt forms (in blue) including standard deviation of the measurements.

Table 8. 11. Results for phenylethylamine and derivatives salt forms where n_m is the number of measurements in each sample, H_G is the gradient hardness, E_G is the gradient Young's Modulus and σ represents the errors in each measurement. In this table, the presence of a "*m*" before the labels represent salt forms of MPEA and presence of "*dm*" before the labels represent salt forms of DMPEA. There is also structural information about the presence of water molecules (.H2O), presence of a free acid in the structure (*), and otherwise specified, presence of another cation per asymmetric unit ([a] represents Z' = 2 and [b] represents Z' = 4)

2-Phenylethylamine Salt Forms (PEA)											
Sample	n_m	H_G	σH_G	**Intercept**	σIntercept	R^2	E_G	σEG	**Intercept**	σIntercept	R^2
3FB *	9	0.52	0.06	6.47	1.36	0.9090	4.74	0.54	6.41	1.29	0.9178
3HB	9	0.53	0.03	4.50	0.37	0.9781	4.58	0.26	4.60	0.36	0.9785
3NB	9	0.45	0.06	5.64	0.65	0.9002	4.01	0.47	5.61	0.61	0.9119
4AB	9	1.59	0.12	4.35	0.51	0.9594	14.25	1.02	3.78	0.51	0.9656
4FB	9	0.83	0.13	3.99	1.04	0.8571	7.58	1.03	3.32	1.00	0.8856
4HB [b]	9	0.13	0.01	5.67	0.67	0.9518	1.09	0.07	5.52	0.51	0.9725
4HBS.H2O	9	0.55	0.04	5.12	0.47	0.9586	4.90	0.35	5.11	0.44	0.9649
4NB [a]	9	0.33	0.07	6.53	0.92	0.7655	2.92	0.51	6.21	0.82	0.8235
ADP	9	0.57	0.05	2.54	0.74	0.9467	4.96	0.36	2.71	0.59	0.9641
BR	9	0.24	0.01	3.54	0.36	0.9837	1.98	0.06	3.76	0.22	0.9931
CL	9	0.34	0.02	3.65	0.46	0.9722	3.10	0.18	3.74	0.42	0.9768
EDS	6	0.50	0.10	5.96	1.51	0.8574	4.60	0.68	5.31	1.19	0.9191
ETSO3	9	0.45	0.04	4.74	0.61	0.9390	4.48	0.35	4.40	0.52	0.9594
FUM [a]	9	0.08	0.01	18.73	1.72	0.8575	0.54	0.06	18.45	1.31	0.9151
LMD	9	0.50	0.06	5.00	0.72	0.9077	5.04	0.56	4.75	0.69	0.9200
MALE	9	0.46	0.03	2.34	0.62	0.9643	4.04	0.21	2.42	0.45	0.9806
MALON	16	0.91	0.12	6.93	1.02	0.8039	8.53	0.94	6.36	0.91	0.8548
PTOL	9	0.51	0.05	4.82	0.58	0.9437	4.53	0.38	4.92	0.52	0.9520
RMAL [a]	9	1.34	0.12	4.65	0.55	0.9500	12.39	0.77	4.34	0.41	0.9735
RMD	9	0.61	0.11	5.94	0.92	0.8176	6.76	0.93	4.99	0.84	0.8823

Sample	n_m	H_G	σH_G	Intercept	$\sigma_{Intercept}$	R^2	E_G	σ_{EG}	Intercept	$\sigma_{Intercept}$	R^2
RTAR.H2O	7	1.36	0.29	4.71	1.30	0.8158	12.06	2.14	4.25	1.17	0.8634
SIF6 [a]	9	0.14	0.02	5.48	1.00	0.9034	0.86	0.09	6.17	0.75	0.9336
SO4.H2O	6	0.09	0.02	6.49	0.78	0.8918	0.70	0.11	6.32	0.71	0.9150
SUC [a]	9	0.50	0.04	3.88	0.54	0.9590	4.31	0.25	3.47	0.43	0.9772
2-Methylphenylethylamine Salt Forms (MPEA)											
Sample	**n_m**	**H_G**	**σH_G**	**Intercept**	**$\sigma_{Intercept}$**	**R^2**	**E_G**	**σ_{EG}**	**Intercept**	**$\sigma_{Intercept}$**	**R^2**
m 2CB	9	0.13	0.01	2.63	0.26	0.9629	1.19	0.09	2.61	0.25	0.9654
m 2HB	7	0.54	0.11	0.49	1.22	0.8399	5.28	0.83	0.83	0.93	0.8891
m 4HB	9	0.32	0.01	5.67	0.17	0.9930	2.73	0.11	5.68	0.23	0.9881
m 4HBS	9	0.12	0.02	6.79	1.01	0.9004	1.12	0.12	6.64	0.85	0.9294
m 4NB *	9	0.27	0.02	4.77	0.56	0.9490	2.40	0.17	4.86	0.44	0.9664
m BR	9	0.48	0.02	4.44	0.26	0.9890	4.54	0.13	4.27	0.19	0.9943
m I	9	0.29	0.04	5.04	0.74	0.8987	2.87	0.34	4.86	0.71	0.9102
m LMAL	9	1.05	0.06	3.93	0.39	0.9799	9.07	0.55	4.21	0.42	0.9750
m LTAR	9	1.40	0.08	4.36	0.38	0.9783	13.19	0.66	4.05	0.35	0.9828
m MALE [b]	9	0.30	0.01	5.03	0.24	0.9893	2.60	0.09	5.14	0.21	0.9915
2-Dimethylphenylethylamine Salt Forms (DMPEA)											
Sample	**n_m**	**H_G**	**σH_G**	**Intercept**	**$\sigma_{Intercept}$**	**R^2**	**E_G**	**σ_{EG}**	**Intercept**	**$\sigma_{Intercept}$**	**R^2**
dm 2HB [a]	9	0.20	0.01	4.80	0.33	0.9811	1.85	0.07	4.89	0.25	0.9891
dm 3HB	9	0.49	0.02	2.20	0.15	0.9882	4.84	0.18	2.16	0.14	0.9903
dm BS.H2O	9	0.59	0.05	3.75	0.63	0.9479	5.89	0.48	3.95	0.56	0.9557
dm MALE [a]	9	0.40	0.03	5.61	0.93	0.9666	3.59	0.18	6.42	0.61	0.9832

8.4.1. GENERAL TRENDS IN HARDNESS

Using the same arbitrary scale of hardness as used in the previous chapters, where soft compounds are thus here defined as those that have hardness lower than 1.0 GPa, medium hardness compounds will have hardness between 1.0 and 2.0 GPa and hard materials will have hardness higher than 2.0 GPa, all four DMPEA compounds were soft. In the case of PEA compounds, 87.5 % of were soft and the remaining 12.5 % of the PEA compounds have medium hardness. These three compounds with medium hardness are anhydrous dicarboxylate RMAL (H_G = 1.34 (12) GPa) and the hydrated dicarboxylate RTAR.H2O (H_G = 1.36 (29) GPa), and p-aminobenzoate 4AB (H_G = 1.59 (12) GPa). In the case of MPEA, 80.0 % of the salt forms are soft and the remaining 20 % have medium hardness. The two compounds with medium hardness are both anhydrous and enantiopure dicarboxylates, mLMAL (H_G = 1.05 (6) GPa) and mLTAR (H_G = 1.40 (8) GPa). This is consistent with salt forms of tartaric acid and malic acid for other APIs presents in this work, with these counterions being harder than benzoates or sulfonates.

8.4.2. TRENDS IN HARDNESS ACCORDING TO FEATURES IN THE UNIT CELL

Of the three bases used in this chapter, 2-phenylethylamine (PEA), 2-methylphenylethylamine (MPEA) and 2-dimethylphenylethylamine (DMPEA), only PEA had a good range of different features in the crystal structure to be compared. All the compounds analysed of the base MPEA were anhydrous and only one had four cations per asymmetric unit (Z' = 4), the sample mMALE, and only one sample had the presence of a free acid in the unit cell, the sample m4NB. Although there were different features in the unit cell for DMPEA compounds, the limited number of samples also made difficult any further analysis for this base.

Considering only PEA salt forms, the same profile is observed for this sample as was observed in analysis for tyramine compounds, when separating all compounds according to these features in the unit cell, the index of elasticity (I_E) is the same for

all compound types within standard deviation. As there were only three hydrated compounds, Figure 8.30 shows only the behaviour of the anhydrous compounds (red line) in comparison with the line for all PEA salt forms (black trend line). Hydrated salts are represented in Figure 4 as blue dots. The same occurs when comparing the number of cations per asymmetric unit, as can be observed in Figure 8.31 where compounds with only one cation per asymmetric unit (Z' = 1) are represented by the red line and the group with two cations per asymmetric unit (Z' = 2) is represented by the blue line. Compounds with four cations per asymmetric unit (Z' = 4) and with one free acid present in the unit cell were not considered in these analysis as they only have one samples of each to analyse, however they are represented in Figure 8.31 as green and purple dots representing Z' = 4 and extra acid in the unit cell, respectively.
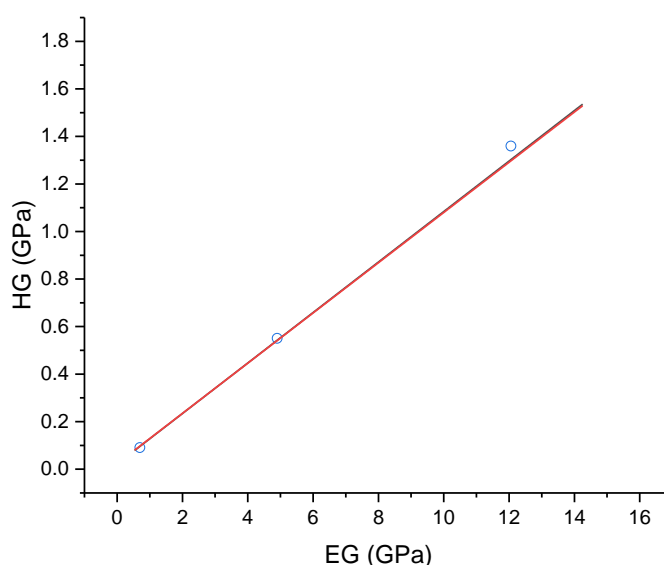
Figure 8. 30. Hardness (H_G) versus Elastic Modulus (E_G) for PEA salt forms. Line in black represents all compounds, line in red represents only anhydrous compounds and dots in blue represents only hydrate compounds. The circles representing the other data points and standard deviation were omitted for clarity.

Table 8. 12. Compounds separated by composition of the crystal structure where n is the number of compounds used in the analysis, I_E is the elasticity index and R^2 is the regression coefficient.

	n	$I_E \pm \sigma_{IE}$	Intercept $\pm \sigma_{Intercept}$	R^2
All data	24	0.106 ± 0.002	0.022 ± 0.005	0.9921
Anhydrous	21	0.106 ± 0.002	0.023 ± 0.006	0.9912
Hydrate	3	0.1098 ± 0.0008	0.014 ± 0.001	0.9999
Z' = 1	17	0.106 ± 0.002	0.021 ± 0.008	0.9922
Z' = 2	5	0.108 ± 0.006	0.031 ± 0.009	0.9922
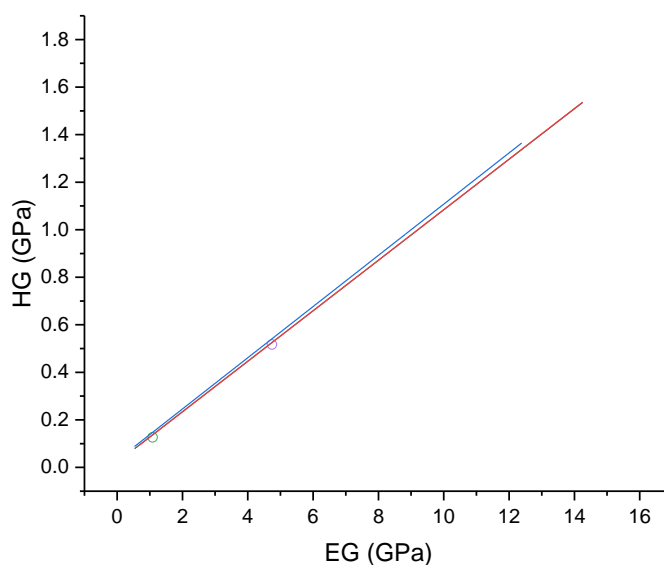
Figure 8. 31. Hardness (H_G) versus Elastic Modulus (E_G) for PEA salt forms. Line in red represents compounds with Z' = 1, line in blue represents compounds with Z' = 2, green dot shows the position of both compounds with Z' = 4 and purple dot shows the position of compounds with an extra acid in the unit cell. The circles representing the other data points and standard deviation were omitted for clarity.

8.4.3. TRENDS IN HARDNESS ACCORDING TO THE COMPOSITION OF THE COUNTERION

Again, the limited number of samples of MPEA and DMPEA limits any further analysis according to counterion for these samples. The analysis in this chapter will be done only for PEA salt forms. No deviation from the same linear relationship between hardness and Young's Modulus was found when separating the salt forms according to the composition of the counterion, as it can be observed in Table 8.13 and Figure 8.32. Within standard deviation, inorganic compounds (purple line), benzoates (red

line) and carboxylates (blue line) behave the same as the trendline for all compounds with elasticity index varying from 10.5 (3) % for carboxylates to 11.2 (1) % for benzoates. Figure 6 also show the position of sulfonates (green dots) which were excluded from this analysis as there is not enough data for analysis.

Table 8. 13. Compounds separated by composition of the counterion where n is the number of compounds used in the analysis, I_E is the elasticity index and R^2 is the regression coefficient.

	n	$\mathbf{I_E \pm \sigma_{IE}}$	**Intercept $\pm \sigma_{Intercept}$**	$\mathbf{R^2}$
All data	24	0.106 ± 0.002	0.022 ± 0.005	0.9921
Benzoate	8	0.112 ± 0.001	0.005 ± 0.003	0.9995
Carboxylates	9	0.105 ± 0.003	0.024 ± 0.008	0.9942
Inorganic	4	0.10 ± 0.01	0.04 ± 0.02	0.9806
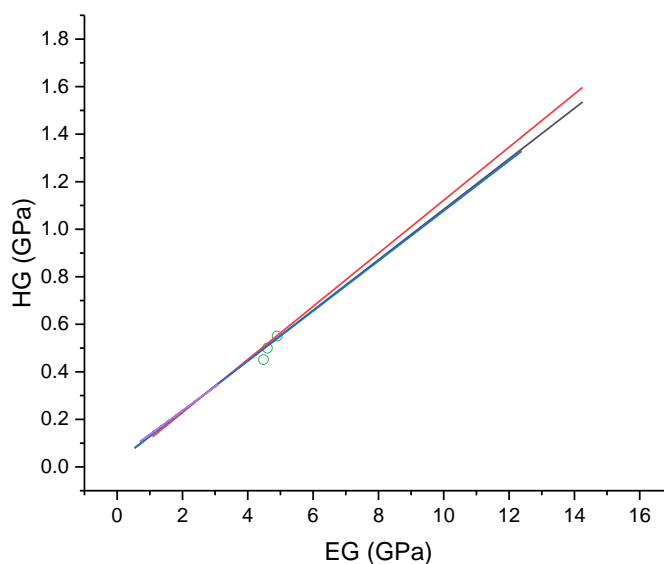
Figure 8. 32. Hardness (H_G) versus Elastic Modulus (E_G) according to the composition of the counterion. Line in black represents all compounds, line in red represents only benzoates, line in blue represents carboxylate, line in purple represents inorganic compounds and green dots show the position of three sulfonate. The circles representing the other data points and standard deviation were omitted for clarity.

The hardness scale for compounds according to the composition of the counterion was also constructed, as it can be observed in Figure 8.33, where blue circles represent benzoate counterions, orange circles represents sulfonates, green circles represent carboxylates and yellow circles represent inorganic counterions. The scale is also

separated according to the base used, where "*m*" before the label represents MPEA and "*dm*" before the label represents DMPEA. This figure also illustrates structural information about the presence of water molecules (.H2O), presence of a free acid in the structure (*), and otherwise specified, presence of another cation per asymmetric unit (^{α} represents Z' = 2 and ^{b} represents Z' = 4).

The first interesting result obtained from this data is regarding the three anhydrous *meta*-substituted benzoates from PEA which have the same indentation hardness within standard deviation: 3FB with $H_G = 0.52$ (6) GPa, 3HB with $H_G = 0.53$ (3) GPa and 3NB with $H_G = 0.45$ (6) GPa. The sample *dm*3HB, from DMPEA, also have the same value of hardness, with $H_G = 0.49$ (2) GPa. Interestingly the same behaviour was not present when comparing *ortho-* and *para*-substituted benzoates, with hardness range 0.13 (1) GPa for the sample *m*2CB to 0.54 (11) GPa for the sample *m*2HB for *ortho*-benzoates and from 0.13 (1) GPa for the sample 4HB to 1.59 (12) GPa for the sample 4AB for *para*-benzoates.

As mentioned before, salts formed using as counterions malic (MAL) and tartaric (TAR) acids, whether as enantiopure compounds or racemic mixtures, tend to be harder than other carboxylates for both PEA and MPEA bases. Other dicarboxylate acids used do not have the hydroxyl substituents that MAL and TAR do and tend to be softer. Here the FUM salt of PEA is the extreme example with a hardness of 0.08(1) GPa. As observed for *meta*-benzoates, when the counterion was maleic acid (MALE), hardness values are similar across the PEA derived bases and range from 0.30 (1) GPa (for MPEA base) to 0.46 (3) GPa (for PEA base). There is also an interesting result observed when comparing the only pair of enantiopure and racemic compound with the same base: the racemic salt form of 2-phenylethylamine and mandelic acid (RMD) with hardness equals to 0.61 (11) GPa and the enantiopure salt form of 2-phenylethylamine and mandelic acid (LMD) with hardness equals to 0.50 (6) GPa. These values being the same within standard deviation are consistent with results obtained in Chapter 8.2.3, where enantiopure salts of methylephedrine had the same hardness as racemic salt forms of the same base for compounds with a chiral centre.
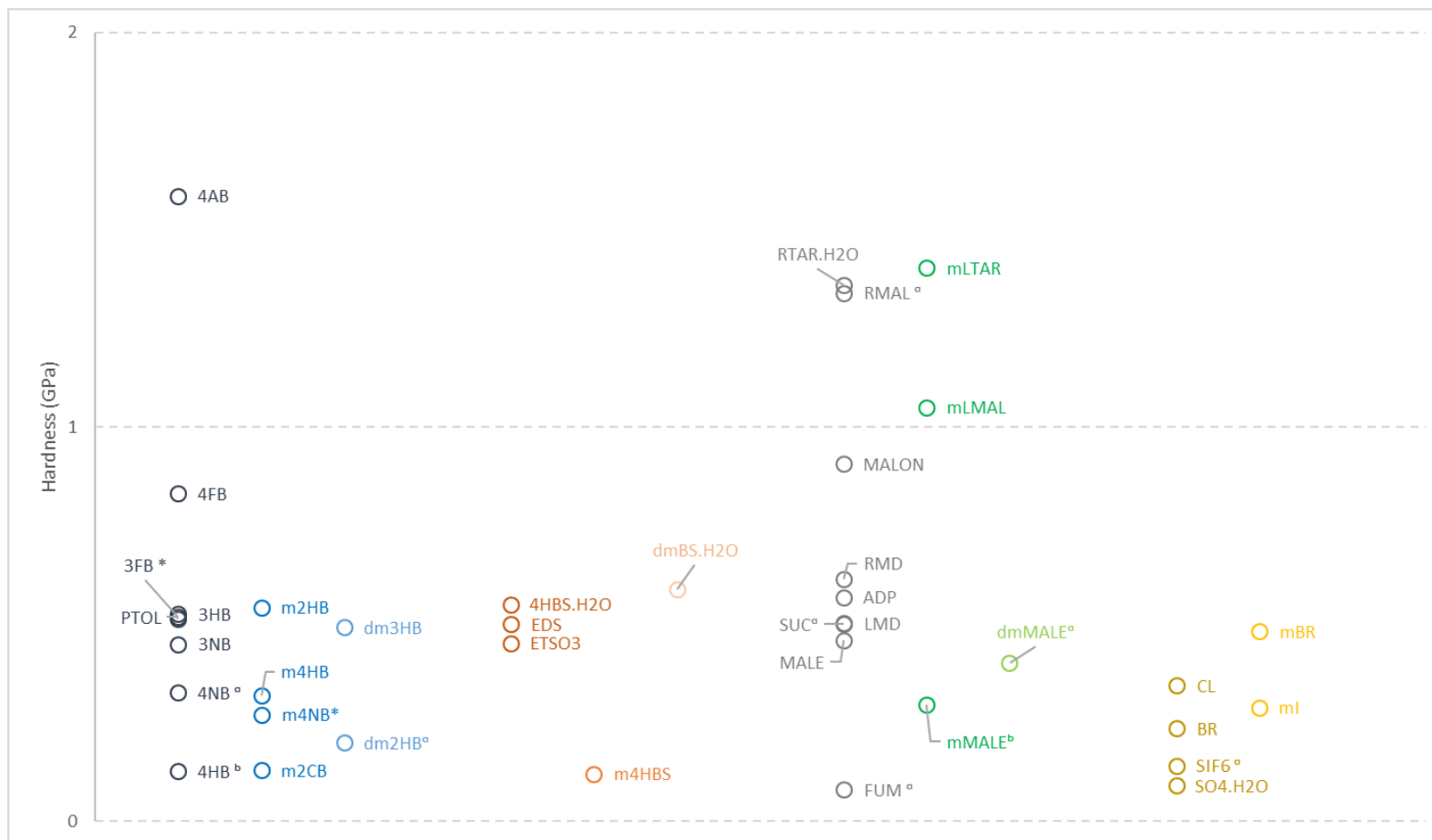
Figure 8. 33. Hardness scale according to the composition of the counterion. Blue circles represent benzoates counterions, orange circle represents sulfonates, green circles represent carboxylates, yellow circles represent inorganic counterions. The scale is also separated according to the base used, where "*m*" before the label represents MPEA and "*dm*" before the label represents DMPEA. There is also structural information about the presence of water molecules (.H2O), presence of a free acid in the structure (*), and otherwise specified, presence of another cation per asymmetric unit ([a] represents Z' = 2 and [b] represents Z' = 4)

When considering only inorganic salt forms, these compounds have hardness decreasing as the size of the anion increases, strictly so where the halide salts are concerned. This is consistent with the same comparison made for tyrammonium salt forms. For PEA salt forms, CL has hardness of 0.34 (2) GPa, BR has hardness of 0.24 (2) GPa, SIF6 has hardness of 0.14 (2) GPa and the hydrated SO4 has hardness of 0.09 (2) GPa. Note that the large dianions are softer than the halides. For MPEA salt forms, with mBR the hardness is 0.48 (2) GPa and with mI the hardness is 0.29 (4) GPa. These can be observed in Figure 8.34. It is important to note that the number of compounds with similar composition (*e.g.* anhydrous compounds with 1:1 cation – anion ratio in the unit cell) limits any further analysis regarding to the relationship between size of counterion and hardness of the crystal structure. However, would it be possible to predict hardness for the missing halogen salt forms with PEA and MPEA from the molecular weight of the salt form? Using the linear regression from the experimental results, the estimation of hardness for the salt form PEAI (Figure 8.34, blue full circle) is 0.13 GPa and the salt form MPEA (Figure 8.34, red full circle) should have hardness of 0.64 GPa.
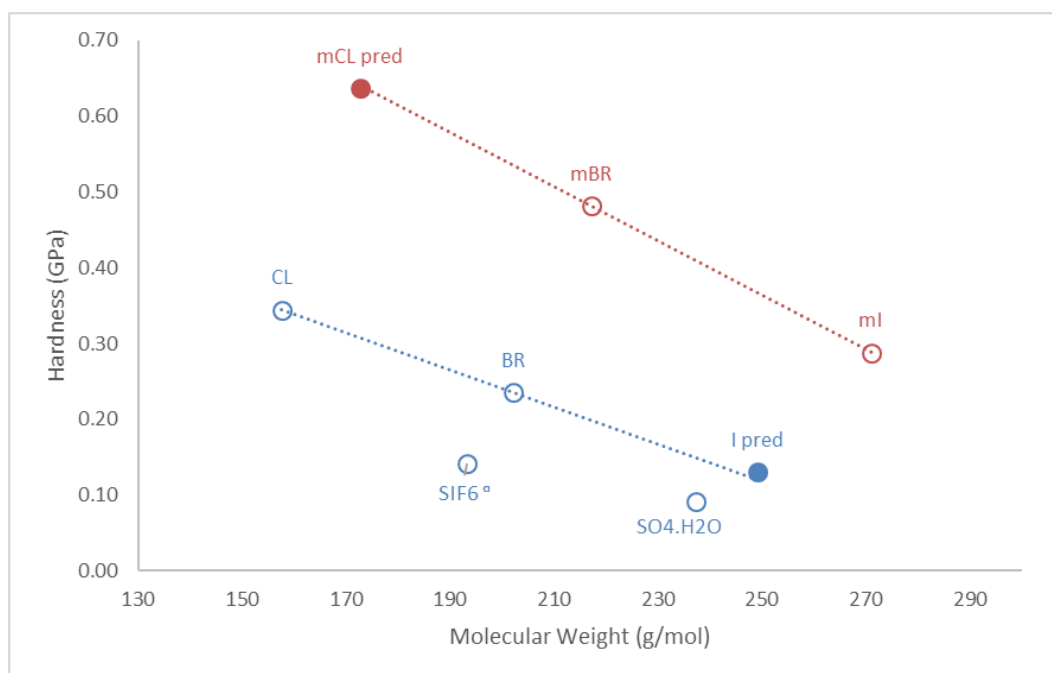
Figure 8. 34. Plot of gradient hardness (H_G) versus the molecular weight for inorganic salts where the blue dots represent PEA salt forms and the red dots represents MPEA salt forms. The empty circles represent experimental values and the full circles represents predicted values.

8.5. COMPARISON BETWEEN ALL PHARMACEUTICAL INGREDIENTS

There were eight bases analysed by nanoindentation, twenty-six salts of tyramine (TYR), sixteen salts of enantiopure methylephedrine (MEPD), twelve salts of racemic methylephedrine (RMEPD), twenty-one salts of enantiopure ephedrine (EPD), sixteen salts of pseudoephedrine (PEPD), twenty-four salt forms of 2-phenylethylamine (PEA), ten salt forms of 2-methylphenylethylamine (MPEA) and four salt forms of 2-dimethylphenylethylamine (DMPEA). It is interesting to note that all salt forms had a linear relationship between gradient hardness (H_G) and gradient Young's Modulus (E_G) as observed in Figure 8.35. Table 8.14 summarises the elasticity index, intercept of the line and regression coefficient for all the APIs.
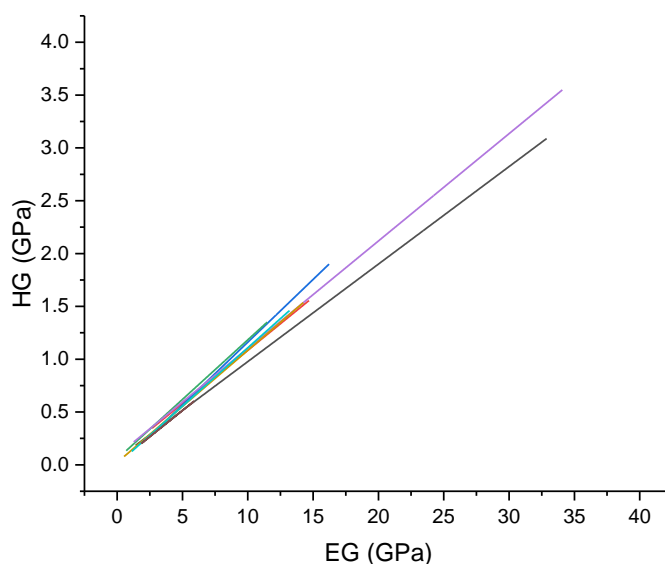
Figure 8. 35. Distribution of the relationship between gradient hardness (H_G) and gradient Young's Modulus (E_G) by composition of API where the trendline in black represents TYR salts, the trendline in red represents MEPD salts, the trendline in blue represents RMEPD salts, the trendline in green represents EPD salts, the trendline in purple represents PEPD salts, the trendline in beige represents PEA salts, the trendline in light blue represents MPEA salts and the trendline in brown represents MPEA salts. Dots and standard deviation were omitted for clarity.

Table 8. 14. Compounds separated by composition of the crystal structure where n is the number of compounds used in the analysis, I_E is the index of elasticity and R^2 is the regression coefficient.

	n	$I_E \pm \sigma_{IE}$	Intercept $\pm$ $\sigma_{Intercept}$	R^2
TYR	26	0.092 (3)	0.054 (19)	0.9766
MEPD	16	0.101 (8)	0.078 (61)	0.9239
RMEPD	12	0.119 (7)	-0.027 (67)	0.9650
EPD	21	0.113 (6)	0.055 (26)	0.9541
PEPD	16	0.102 (3)	0.087 (39)	0.9845
PEA	24	0.106 (2)	0.022 (5)	0.9921
MPEA	10	0.111 (3)	0.003 (9)	0.9928
DMPEA	4	0.099 (5)	0.017 (15)	0.9948

Although the values of elasticity index (Table 8.14) are very similar for measurements using the different salt forms of APIs, an interesting rank order for this value can be observed, as illustrated in Figure 8.36. The value of I_E for RMEPD is consistent with the relationship observed in Chapter 8.2.3 where enantiopure compounds were harder than racemic compounds. The higher value of I_E for RMEPD indicates that in general, racemic compounds will observe reversible deformation of the indentation, recovering 11.9 (7) % of the indentation in comparison with enantiopure methylephedrine (I_E = 10.1 (8) %). On the other side of the scale are tyramine salt forms, with lowest value of I_E equals to 9.2 (3) % which is also a high value for reversible deformation of the indentation.
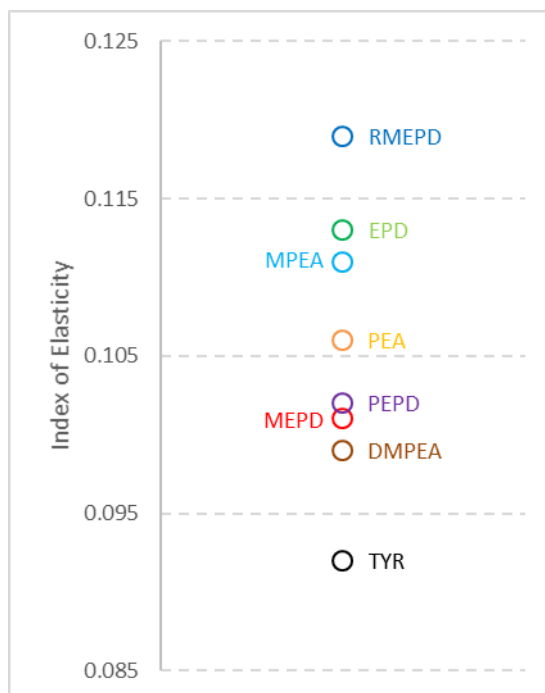
Figure 8. 36. Elasticity index (I_E) scale for all seven bases derivative of phenylethylamine.

8.6. COMPARISON BETWEEN GRADIENT AND PUNCTUAL HARDNESS AND YOUNG'S MODULUS

As observed in the previous chapters, gradient hardness (H_G) and gradient Young's Modulus (E_G) were chosen to analyse experimental data as the linear relationship between load applied and indented area results in smaller standard deviations. Traditionally, indentation hardness is calculated using Oliver and Pharra's [6] method, as described in Chapter 2.7.4 , where hardness is measured for each load applied and the final hardness will be the average of all punctual hardness (which is labelled in this work as H_P). In the case of Young's Modulus, Sneddon's model for elasticity [7] is used by the software Nanoscope Analysis to obtain each value of Young's Modulus for each load applied. Again, the average punctual Young's Modulus is related to the average of all these values. In this work, both gradient and punctual methods were used for calculating hardness and Young's Modulus for all compounds. Thus, a comparison between both methods can be made. In this chapter, relationship between hardness and Young's Modulus using both methods will be shown. First, all results of punctual hardness (H_P) and punctual Young's Modulus (E_P) are shown in Tables 8.15 to 8.22,

218

where Table 8.15 summarises the data of H_P and E_P twenty-six salt forms of tyramine (TYR) used in Chapter 8.1, Table 8.16 shows data for fourteen enantiopure methylephedrine compounds (MEPD) used in Chapter 8.2, Table 8.17 shows data for twelve racemic methylephedrine salt forms (RMEPD) used in Chapter 8.2, Table 8.18 shows data for twenty-one salts of ephedrine (EPD) used in Chapter 8.3, Table 8.19 shows data for sixteen pseudoephedrine salt forms (PEPD) used in Chapter 8.3, Table 8.20 shows data for twenty-four compounds of 2-phenylethylamine (PEA) used in Chapter 8.4, Table 8.21 shows data for ten salt forms of 2-methylphenylethylamine (MPEA) used in Chapter 8.4 and Table 8.22 shows data for four salts of 2-dimethylphenylethylamine (DMPEA) used in Chapter 8.4.

Table 8. 15. Results for tyramine salt forms where n_m is the number of measurements in each sample, H_P is the punctual hardness, E_P is the punctual Young's Modulus and σ represents the errors in each measurement. There is also structural information about the presence of water molecules (.H2O), presence of a free acid in the structure (*), and otherwise specified, presence of another cation per asymmetric unit ([a] represents Z' = 2 and [b] represents Z' = 4)

	H_P (GPa)	σ_{HP} (GPa)	E_P (GPa)	σ_{EP} (GPa)
TYR CL	2.49	0.35	17.78	3.44
TYR BR	1.48	0.14	12.39	1.36
TYR FUMCC.H2O *	1.99	0.33	12.97	3.14
TYR FUMS.H2O	2.96	0.36	20.27	9.02
TYR OTOL	1.93	0.25	13.06	3.50
TYR 2HB	1.36	0.31	9.38	2.00
TYR 2CB	2.20	0.20	17.25	6.51
TYR I	1.29	0.55	5.80	2.25
TYR 4CB	0.69	0.09	4.74	1.08
TYR 4FB	0.82	0.07	4.84	0.71
TYR 2FB	0.79	0.17	4.08	1.05
TYR BF4.H2O	0.49	0.06	3.51	0.96
TYR 3HB	1.49	0.22	11.91	3.38
TYR TCIN.H2O *	0.90	0.16	8.00	3.45
TYR TCIN	1.33	0.27	9.92	2.88
TYR 2NAPH	1.49	0.22	22.89	14.06
TYR OXA	2.95	0.41	17.88	3.52
TYR 2OXA [b]	2.97	0.38	17.53	4.11
TYR TIOSA.3H2O [a]	1.02	0.13	9.95	2.85
TYR LTAR.3H2O [b]	1.28	0.33	8.08	2.71
TYR CAP [a]	0.16	0.01	1.14	0.23

	H$_P$ (GPa)	σ$_{HP}$ (GPa)	E$_P$ (GPa)	σ$_{EP}$ (GPa)
TYR 5C2NB [α]	0.66	0.07	4.07	0.36
TYR MMBS.H2O	1.14	0.28	6.58	0.76
TYR ASB.3H2O [α]	0.85	0.11	5.17	0.57
TYR HIP	1.04	0.11	6.54	3.25
TYR 2MALON.H2O [α]	0.83	0.18	3.30	0.81

Table 8. 16. Results for enantiopure methylephedrine salt forms where n$_m$ is the number of measurements in each sample, H$_P$ is the punctual hardness, E$_P$ is the punctual Young's Modulus and σ represents the errors in each measurement. In this table, the presence of the label and ".cong" after the label indicates the salt crystallised as a conglomerate. There is also structural information about the presence of water molecules (.H2O), presence of a free acid in the structure (*), and otherwise specified, presence of another cation per asymmetric unit (Z' = 2)

	H$_P$ (GPa)	σ$_{HP}$ (GPa)	E$_P$ (GPa)	σ$_{EP}$ (GPa)
MEPD 2FB	0.89	0.10	5.84	1.34
MEPD 2HB	1.05	0.10	6.58	1.19
MEPD 2NAPH	0.86	0.08	4.97	0.33
MEPD 4CBS	1.42	0.28	9.44	2.53
MEPD 4HPA	0.90	0.12	3.64	0.43
MEPD CAMPH	0.79	0.10	4.82	0.99
MEPD FUM * [α]	1.18	0.03	7.37	0.59
MEPD LTAR.H2O	1.58	0.45	6.82	1.95
MEPD MMBS	1.29	0.13	6.98	0.59
MEPD MUC.2H2O [α]	1.37	0.17	7.65	1.06
MEPD LMD	0.37	0.02	2.57	0.35
MEPD SO4.H2O	2.38	0.31	10.81	1.39
MEPD H2NAPH.cong	1.89	0.18	8.25	2.41
MEPD PTS.cong	1.02	0.10	3.82	0.33

Table 8. 17. Results for racemic methylephedrine salt forms where n$_m$ is the number of measurements in each sample, H$_P$ is the punctual hardness, E$_P$ is the punctual Young's Modulus and σ represents the errors in each measurement. There is also structural information about the presence of water molecules (.H2O), presence of a free acid in the structure (*), and otherwise specified, presence of another cation per asymmetric unit ([α] represents Z' = 2 and [b] represents Z' = 4)

	H$_P$ (GPa)	σ$_{HP}$ (GPa)	E$_P$ (GPa)	σ$_{EP}$ (GPa)
RMEPD 2HB	1.09	0.21	5.80	1.54
RMEPD 2NB.H2O	0.76	0.18	3.15	0.71
RMEPD 3CB	1.61	0.14	11.21	3.16
RMEPD 4CBS.H2O	0.53	0.05	3.43	0.78
RMEPD 5C2NB	0.79	0.05	4.52	0.56
RMEPD BZ	1.11	0.20	3.80	0.67
RMEPD CL	1.41	0.16	7.08	1.07
RMEPD RTAR * [α]	1.49	0.10	7.24	0.51

RMEPD FUM	1.22	0.28	5.01	1.63
RMEPD MUC.H2O	1.60	0.12	9.04	0.96
RMEPD PAAB.H2O	2.19	0.16	8.67	0.64
RMEPD SO4.H2O	1.35	0.17	7.22	1.20

Table 8. 18. Results for enantiopure ephedrine salt forms where n_m is the number of measurements in each sample, H_P is the punctual hardness, E_P is the punctual Young's Modulus and σ represents the errors in each measurement There is also structural information about the presence of water molecules (.H2O), presence of a free acid in the structure (*), and otherwise specified, presence of another cation per asymmetric unit ([a] represents Z' = 2 and [b] represents Z' = 4)

	H_P (GPa)	$σ_{HP}$ (GPa)	E_P (GPa)	$σ_{EP}$ (GPa)
EPD 2CB	2.35	0.27	8.13	1.33
EPD 2DTAR.H2O [a]	0.23	0.01	1.12	0.04
EPD 2NB	0.95	0.15	3.97	0.92
EPD 3CB	0.81	0.12	3.22	0.48
EPD 4AB	1.44	0.29	4.58	1.07
EPD 4APA	1.10	0.14	4.14	0.63
EPD 4CB	1.42	0.25	5.36	0.86
EPD 4CBS	0.57	0.08	0.84	0.12
EPD 4HBS.H2O	1.38	0.23	5.31	1.05
EPD 4HPA	1.37	0.09	5.45	0.29
EPD 4NB	0.33	0.09	0.91	0.28
EPD AA	0.66	0.04	3.01	0.46
EPD BS	1.53	0.15	7.55	2.09
EPD CL	1.05	0.32	3.32	1.06
EPD ETSO3	1.19	0.16	5.61	0.73
EPD LMD	1.14	0.10	4.53	0.22
EPD LTAR.H2O	1.35	0.09	4.86	0.49
EPD MMBS [a]	0.82	0.18	1.95	0.35
EPD MTOL	1.05	0.16	4.44	1.07
EPD N2S [b]	1.07	0.17	4.43	0.77
EPD SO4.H2O	0.81	0.13	3.35	0.56

Table 8. 19. Results for pseudoephedrine salt forms where n_m is the number of measurements in each sample, H_P is the punctual hardness, E_P is the punctual Young's Modulus and σ represents the errors in each measurement. There is also structural information about the presence of water molecules (.H2O), presence of a free acid in the structure (*), and otherwise specified, presence of another cation per asymmetric unit ([a] represents Z' = 2 and [b] represents Z' = 4)

	H_P (GPa)	$σ_{HP}$ (GPa)	E_P (GPa)	$σ_{EP}$ (GPa)
PEPD 2CB.H2O	3.79	0.28	20.88	7.28
PEPD 2HB	1.65	0.17	6.23	0.72

PEPD 3HB.3H2O	0.55	0.08	2.36	0.58
PEPD 3NB [a]	1.15	0.14	4.17	0.31
PEPD 4AB.2H2O	0.48	0.08	2.15	0.54
PEPD 4CB	1.07	0.14	4.07	0.52
PEPD 4HBS	1.49	0.30	6.45	1.52
PEPD 4NB [a]	0.54	0.16	1.61	0.37
PEPD BS	0.43	0.08	1.45	0.23
PEPD BZ	1.69	0.16	6.80	0.80
PEPD I	0.81	0.09	3.37	0.48
PEPD LMD	0.58	0.09	2.10	0.48
PEPD LTAR.H2O	1.65	0.36	5.79	1.31
PEPD MALE	2.26	0.41	9.58	1.97
PEPD OTOL.H2O	0.83	0.09	4.66	0.76
PEPD RMAL	2.85	0.58	10.23	1.50

Table 8. 20. Results for 2-phenylethylamine salt forms where n_m is the number of measurements in each sample, H_P is the punctual hardness, E_P is the punctual Young's Modulus and σ represents the errors in each measurement. There is also structural information about the presence of water molecules (.H2O), presence of a free acid in the structure (*), and otherwise specified, presence of another cation per asymmetric unit ([a] represents Z' = 2 and [b] represents Z' = 4)

	H_P (GPa)	$σ_{HP}$ (GPa)	E_P (GPa)	$σ_{EP}$ (GPa)
PEA 3FB	1.12	0.40	4.94	2.19
PEA 3HB	0.95	0.14	3.88	0.60
PEA 3NB	1.04	0.20	3.89	1.03
PEA 4AB	2.86	0.50	10.31	1.67
PEA 4FB	1.39	0.21	6.03	0.80
PEA 4HB [b]	0.23	0.03	0.69	0.07
PEA 4HBS.H2O	1.14	0.25	4.52	0.99
PEA 4NB [a]	0.98	0.27	3.45	0.92
PEA ADP	0.76	0.07	3.23	0.24
PEA BR	0.37	0.05	1.28	0.21
PEA CL	0.55	0.07	2.10	0.26
PEA EDS	0.96	0.16	4.99	0.67
PEA ETSO3	0.86	0.16	4.29	0.62
PEA FUM [a]	0.22	0.02	0.62	0.08
PEA LMD	1.01	0.17	4.55	0.87
PEA MALE	0.60	0.04	2.45	0.17
PEA MALON	2.07	0.45	9.56	2.02
PEA PTOL	1.01	0.22	3.64	0.62
PEA RMAL [a]	2.55	0.48	9.01	1.49
PEA RMD	1.54	0.45	5.50	1.39

PEA RTAR.H2O	2.65	0.57	9.51	1.67
PEA SIF6 [ɑ]	0.25	0.04	0.83	0.19
PEA SO4.H2O	0.30	0.13	0.83	0.25
PEA SUC [ɑ]	0.82	0.10	3.75	0.23

Table 8. 21. Results for 2-methylphenylethylamine salt forms where n_m is the number of measurements in each sample, H_P is the punctual hardness, E_P is the punctual Young's Modulus and σ represents the errors in each measurement. There is also structural information about the presence of water molecules (.H2O), presence of a free acid in the structure (*), and otherwise specified, presence of another cation per asymmetric unit ([ɑ] represents Z' = 2 and [b] represents Z' = 4)

	H_P (GPa)	$σ_{HP}$ (GPa)	E_P (GPa)	$σ_{EP}$ (GPa)
MPEA I	0.61	0.14	2.67	0.48
MPEA BR	0.88	0.18	3.73	0.59
MPEA 4HB	0.76	0.21	2.78	0.89
MPEA LTAR	2.51	0.40	10.25	1.40
MPEA MALE [b]	0.61	0.14	2.27	0.58
MPEA 4NB *	0.52	0.09	2.17	0.40
MPEA 2CB	0.48	0.35	1.57	1.17
MPEA 2HB	0.59	0.04	2.86	0.65
MPEA LMAL	1.73	0.22	6.94	1.06
MPEA 4HBS	0.23	0.01	0.86	0.10

Table 8. 22. Results for 2-dimethylphenylethylamine forms where n_m is the number of measurements in each sample, H_P is the punctual hardness, E_P is the punctual Young's Modulus and σ represents the errors in each measurement. There is also structural information about the presence of water molecules (.H2O), presence of a free acid in the structure (*), and otherwise specified, presence of another cation per asymmetric unit ([ɑ] represents Z' = 2 and [b] represents Z' = 4)

	H_P (GPa)	$σ_{HP}$ (GPa)	E_P (GPa)	$σ_{EP}$ (GPa)
DMPEA 2HB [ɑ]	0.39	0.08	1.62	0.34
DMPEA BS.H2O	0.95	0.12	5.46	0.76
DMPEA 3HB	1.34	0.78	5.16	3.14
DMPEA MALE [ɑ]	0.58	0.03	3.61	0.17

The initial and obvious result is regarding to the difference of the standard deviation in both punctual measurements of hardness (H_P) and Young's Modulus (E_P) in comparison with the gradient hardness (H_G) and Young's Modulus (E_G). The average of the errors for each sample according to the base used is shown in Table 8.23, where "n" represents the number of compounds used. Using Table 8.23, it is easier to observe that the error in hardness decreased at least 1.4 % for MEPD samples and the error in

Young's Modulus decreased at least 8.0 % for EPD samples. In all cases, obtaining the average of each punctual measurement implies in a higher error in comparison with the gradient hardness or Young's Modulus value.

Table 8. 23. Average percentual error for all the bases where n is the number of samples of each base, H_P is the punctual hardness, E_P is the punctual Young's Modulus, H_G is the gradient hardness and E_G is the gradient Young's Modulus.

API	n	Error (%)			
		H_P	E_P	H_G	E_G
TYR	26	15.9	27.2	7.4	6.5
MEPD	14	12.1	16.4	10.7	8.1
RMEPD	12	12.9	18.3	8.6	7.2
EPD	21	14.8	17.2	10.8	9.2
PEPD	16	15.6	18.9	9.9	8.1
PEA	24	18.9	18.1	11.8	9.8
MPEA	10	22.5	24.8	8.3	7.4
DMPEA	4	24.0	25.2	6.3	5.2

Another interesting comparison is regarding to the elasticity index of each API. When plotting the values of average punctual hardness (H_P) versus average punctual Young's Modulus (E_P) for all compounds according to the base used, as it can be observed in Figure 8.37, a similar profile to the graph observed in Chapter 8.4 where the relationship between hardness and Young's Modulus are linear was observed however, with a higher error and lower coefficient of regression. Details of values of elasticity coefficient (I_E), intercept and regression coefficient (R^2) are observed in Table 8.24.
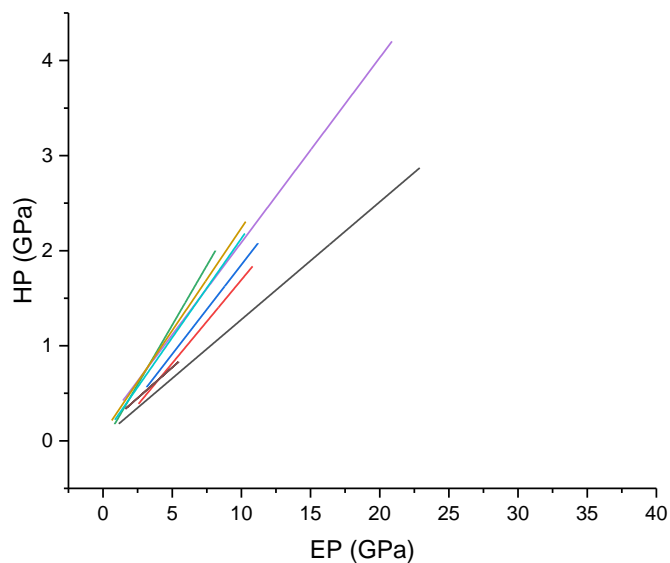
Figure 8. 37. Distribution of the relationship between punctual hardness (H_P) and punctual Young's Modulus (E_P) by composition of API where the trendline in black represents TYR salts, the trendline in red represents MEPD salts, the trendline in blue represents RMEPD salts, the trendline in green represents EPD salts, the trendline in purple represents PEPD salts, the trendline in beige represents PEA salts, the trendline in light blue represents MPEA salts and the trendline in brown represents MPEA salts. Dots and standard deviation were omitted for clarity.

Table 8. 24. Compounds separated by the active pharmaceutical ingredient where n is the number of compounds used in the analysis, I_E is the index of elasticity and R^2 is the regression coefficient.

	n	$\mathbf{I_E \pm \sigma_{IE}}$	**Intercept $\pm \sigma_{Intercept}$**	$\mathbf{R^2}$
TYR	26	0.124 (8)	0.04 (3)	0.9038
MEPD	14	0.175 (14)	-0.06 (7)	0.9297
RMEPD	12	0.188 (27)	-0.03 (15)	0.8340
EPD	21	0.250 (15)	-0.04 (3)	0.9375
PEPD	16	0.194 (15)	0.14 (6)	0.9237
PEA	24	0.216 (7)	0.08 (1)	0.9769
MPEA	10	0.209 (12)	0.04 (2)	0.9745
DMPEA	4	0.129 (35)	0.13 (13)	0.8697

There is a higher discrepancy between values of elasticity index when using punctual hardness and Young's Modulus instead of the gradient data analysis. These values range from 12.4 (8) % for TYR samples to 25.0 (15) % for EPD samples. In contrast using the gradient method gave 9.2 (3) % for TYR samples to 11.3 (6) % for EPD

samples. The same rank order of elasticity indexes was not found for the two methods, although the difference largely involves only an eccentric position for the RMEPD sample. However, values of I_E have a fair rank order when measuring with punctual ($I_{E,P}$) or gradient ($I_{E,G}$) methods, as illustrated in Figure 8.38, with equation $I_{E,G} = [0.150\ (4)]\cdot I_{E,P} + 7.5\ (8)$ and regression coefficient of 0.6914. In more detail, note that two sets of measurements deviate from the trendline in Figure 8.38: The first set of data to deviate is that for DMPEA, which only contain four salt forms, not enough data compared to the other APIs. The other set of data contain the twelve salt forms of racemic methylephedrine (RMEPD), which is the only racemic set of data in this group. Interestingly, when comparing gradient hardness (H_G) and punctual hardness (H_P) for this set of data, as observed in Figure 8.39 (line in blue), this trendline does not behave as the trendline for other active pharmaceutical ingredients, with a higher intercept on the y axis and low regression coefficient ($R^2 = 0.2799$). Similarly, RMEDP is eccentric when plotting the graph of gradient Young's Modulus (E_G) and punctual hardness (E_P), as observed in Figure 8.40 (line in blue). Here the trendline for RMEPD is like the other active pharmaceutical ingredients, the regression coefficient is very low ($R^2 = 0.5596$). Details about all the bases used in this work can be observed in Table 8.25, for H_G versus H_P and Table 8.26, for E_G versus E_P.

Table 8. 25. Compounds separated by composition of the base where n is the number of compounds used in the analysis, gradient is the gradient of the trendline between H_G and H_P and R^2 is the regression coefficient.

	n	Gradient ± $\sigma_{Gradient}$	Intercept ± $\sigma_{Intercept}$	R^2
TYR	26	0.83 ± 0.04	-0.0004 ± 0.0279	0.9470
MEPD	14	0.68 ± 0.07	0.0977 ± 0.0709	0.8939
RMEPD	12	0.41 ± 0.21	0.2466 ± 0.1973	0.2799
EPD	21	0.63 ± 0.06	-0.0150 ± 0.0516	0.8684
PEPD	16	0.73 ± 0.06	-0.1033 ± 0.0438	0.9083
PEA	24	0.54 ± 0.04	-0.0013 ± 0.0181	0.9083
MPEA	10	0.58 ± 0.08	-0.0890 ± 0.0520	0.8659
DMPEA	4	0.32 ± 0.10	0.0910 ± 0.0720	0.8309
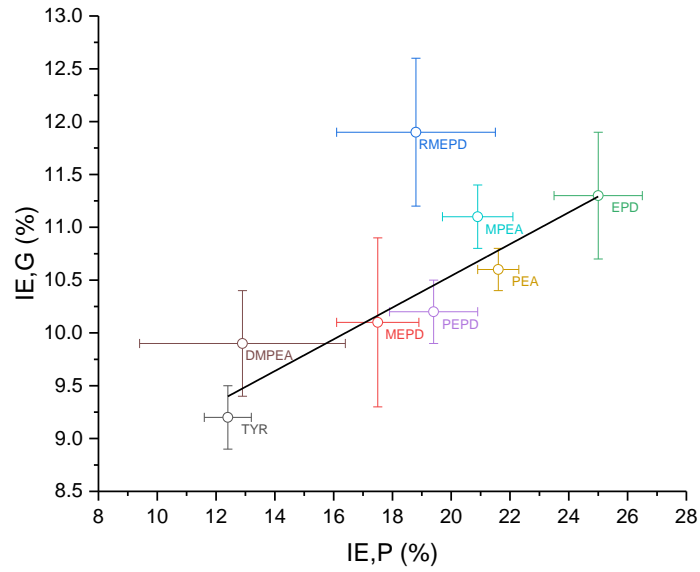
Figure 8. 38. Relationship between both nanoindentation methods used where $I_{E,G}$ is the gradient index of elasticity and $I_{E,P}$ is the punctual index of elasticity. In this graph, the dot in black represents TYR salts, the dot in red represents MEPD salts, the dot in blue represents RMEPD salts, the dot in green represents EPD salts, the dot in purple represents PEPD salts, the dot in beige represents PEA salts, the dot in light blue represents MPEA salts and the dot in brown represents MPEA salts.
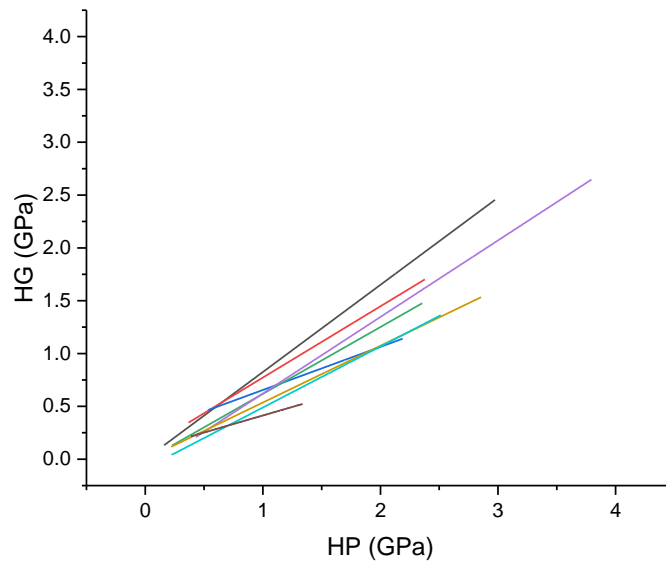
Figure 8. 39. Relationship between gradient hardness (H_G) and punctual hardness (H_P). In this graph, the dot in black represents TYR salts, the dot in red represents MEPD salts, the dot in blue represents RMEPD salts, the dot in green represents EPD salts, the dot in purple represents PEPD salts, the dot in beige represents PEA salts, the dot in light blue represents MPEA salts and the dot in brown represents MPEA salts

227
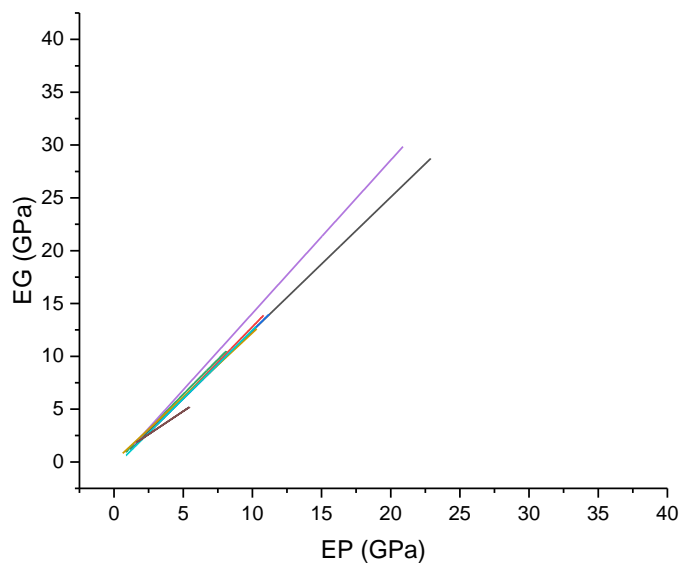
Figure 8. 40. Relationship between gradient Young's Modulus (E_G) and punctual Young's Modulus (E_P). In this graph, the dot in black represents TYR salts, the dot in red represents MEPD salts, the dot in blue represents RMEPD salts, the dot in green represents EPD salts, the dot in purple represents PEPD salts, the dot in beige represents PEA salts, the dot in light blue represents MPEA salts and the dot in brown represents MPEA salts.

Table 8. 26. Compounds separated by composition of the base where n is the number of compounds used in the analysis, gradient is the gradient of the trendline between E_G and E_P and R^2 is the regression coefficient.

	n	Gradient ± $\sigma_{Gradient}$	Intercept ± $\sigma_{Intercept}$	R^2
TYR	26	1.27 ± 0.03	-0.25 ± 0.24	0.9528
MEPD	14	1.34 ± 0.14	-0.63 ± 0.76	0.8904
RMEPD	12	1.29 ± 0.36	-0.46 ± 1.70	0.5596
EPD	21	1.31 ± 0.09	-0.18 ± 0.30	0.9114
PEPD	16	1.45 ± 0.10	-0.43 ± 0.24	0.9381
PEA	24	1.22 ± 0.08	0.06 ± 0.13	0.9126
MPEA	10	1.30 ± 0.11	-0.51 ± 0.27	0.9432
DMPEA	4	0.88 ± 0.05	0.43 ± 0.14	0.9930

8.7. CONCLUSIONS

Measurement of nanoindentation were made for one hundred and thirty-four salt forms of tyramine (TYR), enantiopure methylephedrine (MEPD), racemic methylephedrine (RMEPD), ephedrine (EPD), pseudo ephedrine (PEPD), 2-phenylethylamine (PEA),

2-methylphenylethylamine (MPEA) and 2-dimethylphenylethylamine (DMPEA). Data collection was made for these salt forms obtaining the indentation profile in least three different loads and the methodology used for data analysis involved the linear relationship between the applied force and the resultant indentation size. Values of hardness and Young's Modulus obtained using this method were labelled as gradient hardness (H_G) and gradient Young's Modulus (E_G). In a comparison between the "traditional" method described by Oliver and Pharra [6] for hardness and the "traditional" Sneddon model [7] for elasticity with the "gradient" methods, which obtain values of hardness and Young's Modulus from the linear relationship between force and the area. Using values of gradient hardness and Young's Modulus, instead of the traditional method with the average of various punctual measurements, the error in the measurements decreases at least 1.4 % in hardness and 8.0 % in Young's Modulus. Both methods have a similar rank order of elasticity index (I_E), except for the sample RMEPD, containing only racemic salts of methylephedrine. Further analysis shown that both "gradient" models for hardness and Young's Modulus do not fit with punctual values of hardness and Young's Modulus for this set of samples. This contrasts to values found for enantiopure and achiral compounds, where the traditional and new methods give the same rank order.

Of the twenty-nine salt forms of tyramine measured using nanoindentation, twenty-six compounds were successfully measured with a regression of coefficient higher than 80 %. There is a linear relationship between hardness and Young's Modulus which is characterised by the gradient of the trendline. The selection of salt forms measured was deliberately chosen to give ranges in the composition of the counterion and features in the crystal structure. However, these classifications did not show any difference between one another in the elasticity index when the graph of hardness versus Young's Modulus was obtained. When considering only halide salts there is a relationship between the hardness of the compounds and the size of the anion. Another indication that size of the counterion influences the hardness of the compounds was made comparing di-substituted benzoates with the same composition but different position of the substitute in the ring. These comparison shows that independent of the position of the halogen atom in the aromatic ring, the hardness will be similar if these compounds have stoichiometry 1:1 and are anhydrous

Regarding to the twenty-eight salt forms of methylephedrine measured using nanoindentation, twelve compounds of enantiopure methylephedrine and fourteen compounds of racemic methylephedrine (including two conglomerates), the relationship between gradient hardness (H_G) and gradient Young's Modulus (E_G) obtained for the selection of salt forms measured obtained the gradient of the trendline of 10.2 (5) %. The same value was obtained when considering only enantiopure compounds (10.1 (8) %) while when considering only racemic compounds, the value of elasticity index increases to 11.9 (7) %. When comparing hardness of pairs of enantiopure and racemic compounds with the same counterion it was observed that, apart from compounds with an anion with a chiral centre, all enantiopure compounds were harder than racemic compounds. For methylephedrine compounds, presence of water in the crystal structure seem also to slightly affect the value of I_E, where anhydrous compounds will have value of elasticity index equals to 9.1 (6) % and hydrates will have value of elasticity index equals to 11.7 (8) %.

For the thirty-seven salt forms of ephedrine and pseudoephedrine measured using nanoindentation, twenty-one compounds of ephedrine and sixteen compounds of methylephedrine were successfully measured. There is a linear relationship between gradient hardness (H_G) and gradient Young's Modulus (E_G) obtained for the selection of salt forms measured obtained the gradient of the trendline of 11.4 (4) %. The same value was obtained when considering only ephedrine (11.3 (6) %) and pseudoephedrine (11.1 (5) %) compounds. The same gradient was found when separating these compounds according to features in the crystal structure and according to the composition of the counterion. As much as the elasticity index (I_E) for these compounds have the same value, when comparing pairs of ephedrine and pseudoephedrine with the same counterion, there is a discrepancy between gradient hardness for most of the pairs, which shows that individually compounds will have different hardness.

The selection of salt forms in Chapter 8.4 were related to phenylethylamine and its methyl derivatives. There were twenty-four salt forms of PEA, ten salt forms of MPEA and four salt forms of DMPEA. All salt forms shown a linear relationship between hardness and Young's Modulus when measured by nanoindentation, where the

elasticity index for these bases were 10.6 (2) % for PEA, 11.1 (3) % for MPEA and 9.9 (5) % for DMPEA salt forms, however, the limited number of salt forms of DMPEA reduced the any further analysis for this base. The selection of salt forms measured was deliberately chosen to give ranges in the composition of the counterion and features in the crystal structure. However, these classifications did not show any difference between one another in the elasticity index when the graph of hardness versus Young's Modulus was obtained. When considering only halide salts there is a relationship between the hardness of the compounds and the size of the anion. It may be possible to estimate the value of hardness for halides by linear regression. For these samples, all halides and hydroxy-benzoates, independent of the position of the hydroxyl group in the ring, will be soft compounds and racemic and enantiopure compounds with a chiral centred cation will have the same hardness values.

8.8. REFERENCES

[1]   Morrison, C.A. (2012). Salt selection for pharmaceutical use University of Strathclyde. Dept. of Pure and Applied Chemistry. Thesis [Ph. D] - University of Strathclyde.

[2]   Briggs, N., Kennedy, A., & Morrison, C. (2012). Acta Crystallographica Section B, 68(4), 453-464.

[3]   Ivanova, B. & Spiteller, M. (2010). Spectrochimica Acta Part A: Molecular and Biomolecular Spectroscopy, 77(4), 849-855.

[4]   Podder, A., Dattagupta, J.K., Saha, N.N. & Saenger, W. (1979). Acta Cryst. B35, 649-652

[5]   Collier, E., Davey, R., Black, S., & Roberts, R. (2006). Acta Crystallographica Section B, 62(3), 498-505.

[6]   Oliver, W.C. & Pharra, G.M. (2004). J. Mater. Res., 19 (10), pp. 3-20.

[7]   Sneddon, I. N. (1965). Int. J. Engng. Sci., 3, 47-57.

[8]   Roberts, R.J.; Rowe, R.C. & York, P. (1994). J. Mater. Sci., 29, 2289–2296.

9. RELATIONSHIP BETWEEN SOLUBILITY AND MELTING POINT FOR SALT FORMS OF ACTIVE PHARMACEUTICAL INGREDIENTS.

In order to be able to predict physicochemical properties of salt forms of active pharmaceutical ingredients, this work also analysed the relationship between aqueous solubility and melting point for compounds synthesised and analysed by Morrison *et al.* [1] thus, the current work involves only data analysis and comparison. All experimental data in this work was obtained by Morrison and both raw data and experimental details used in this work were presented in Reference 1, and part of this comparison between aqueous solubility and melting point, for fifty-one salt forms of enantiopure and racemic methylephedrine, has been published [2].

In total, there were eleven bases used in this analysis, all derivatives of phenylethylamine, as can be observed in Figure 9.1. Solubility measurements were available for two-hundred and fifty-five different salt forms of these bases while melting point measurements were available for two-hundred and sixteen compounds. The given melting point measurements were average values from three measurements, but standard deviation for these values were not available.
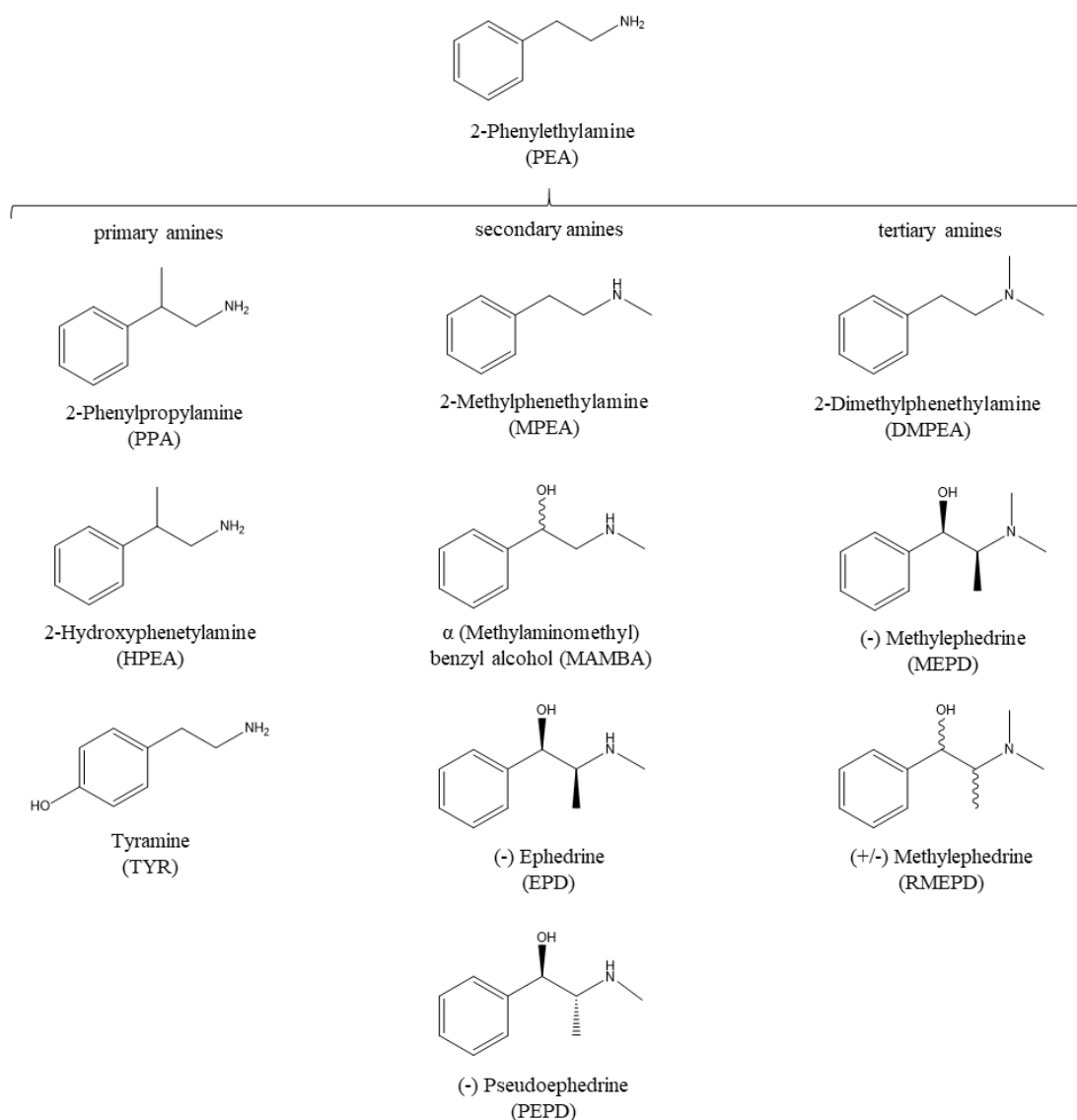
Figure 9. 1. Selection of eleven bases derivatives of phenylethylamine.

9.1. RELATIONSHIP BETWEEN SOLUBILITY AND MELTING POINT FOR ALL SALT FORMS.

Considering all data generated by Morrison *et al.* [1] there were two-hundred and sixteen compounds with melting point measured distributed as fifteen salt forms of MAMBA, thirty salt forms of MEPD, thirty-two salt forms of RMEPD, twenty-eight salt forms of PEA, twelve salt forms of MPEA, eight salt forms of DMPEA, twelve salts of PPA, eight salts of HPEA, thirty-four salts of TYR, eighteen salts of EPD and nineteen salts of PEPD. Regarding to the aqueous solubility measurements, there were

solubility analysis of two-hundred and fifty-five compounds, distributed as nineteen salts of MAMBA, thirty-two salts of MEPD, thirty-three salts of RMEPD, thirty-two salts of PEA, sixteen salts of MPEA, thirteen salts of DMPEA, twelve salts of PPA, fourteen salt forms of HPEA, thirty-nine salts of TYR, twenty-three salts of EPD and twenty-two salts of PEPD. The distribution of all values of solubility and melting point, according to the base, can be observed in Figure 9.2 and Figure 9.3, respectively.

As it can observed in Figure 9.2, there are some outliers to the boxplots of four bases: DMPEA, MAMBA, RMEPD and TYR. The outliers for the base DMPEA have relatively low solubility when compared with other salt forms of this base and are salt forms of benzenesulfonate (BS) with solubility 0.348 (21) mol/L and l-tartarate (LTAR) with solubility 1.428 (43) mol/L. In the other cases, all outliers have high solubility compared to the average of all compounds: For MAMBA salt forms the outliers are the halides bromide (BR) with solubility 6.084 (202) mol/L and iodine (I) with solubility 6.906 (278) mol/L; For RMEPD salt forms, the outliers are malonate (MALON) with solubility 3.623 (198) mol/L, methanesulfonate (MESO3) with solubility 3.982 (6) mol/L, (+/-)-mandelate (RMD) with solubility 4.132 (72) mol/L and (+/-)-tartarate (RTAR) with solubility 3.774 (308) mol/L. For TYR, there are three outliers with high solubility: hydrogensulfate (SO4) with solubility 5.641 (12) mol/L, perchlorate (CLO4) with solubility 4.767 (137) mol/L and iodine (I) with solubility 3.186 (70) mol/L.

Whilst there is much overlap between the solubilities of the bases, it is interesting that the generally most soluble is DMPEA. Free base DMPEA is the only base selected with no OH or NH substituent. As such it would appear to be the least polar species and an unlikely choice to show high aqueous solubility. A general comment is that polar OH functionalities do not seem to cause greater solubility. Four of the eleven selected bases have no OH group and these rank 1st, 3rd, 4th and 6th for overall solubility.
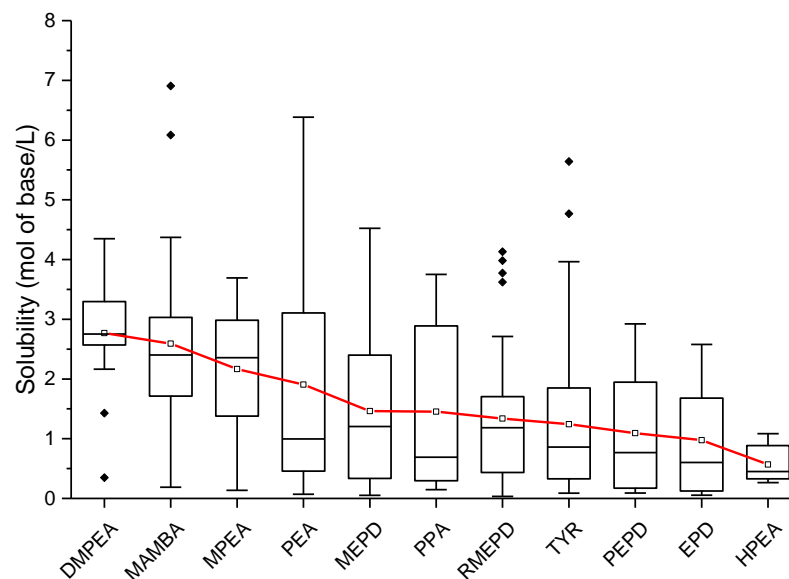
Figure 9. 2. Distribution of solubility for all two-hundred and fifty-five compounds according to the base.

The presence of outliers can also be observed when plotting the boxplots for all values of melting point, as it can be observed in Figure 9.3. Again, there are four bases with outliers in this sample: HPEA, TYR, PEA and RMEPD. The samples TYR and HPEA have outliers in both extremes of the boxplot. in the case of tyramine (TYR), the lower melting point are the salt form of ethanesulfonate (ETSO3) with melting point of 9.0 °C and RMAL, the salt of tyramine and malic acid, with melting point of 68.9 °C. The sample ETSO3 was hydroscopic and thus, excluded from any further analysis. The higher melting points for this sample are ethanedisulfonate (EDS) with melting point 295.3 °C, chlorine (CL) with melting point 276.6 °C and bromine (BR) with melting point 249.4 °C. In the case of HPEA the outlier with low melting point is the salt form of *ortho*-toluate (OTOL, 48.0 °C) and the outlier with higher melting point is, again, ethanedisulfonate (EDS, 359.4 °C). For PEA salts, the two melting point outliers are, again, ethanedisulfonate (EDS, 373.9 °C) and tetrafluoroborate (BF4, 257.6 °C). Finally, the last compound with the presence of outliers is RMEPD, with two outliers around 200 °C, the salt of chlorine (CL, 211.8 °C) and ethanesulfonate (ETSO3, 208.2 °C). The average of all these results can be observed in Table 9.1.
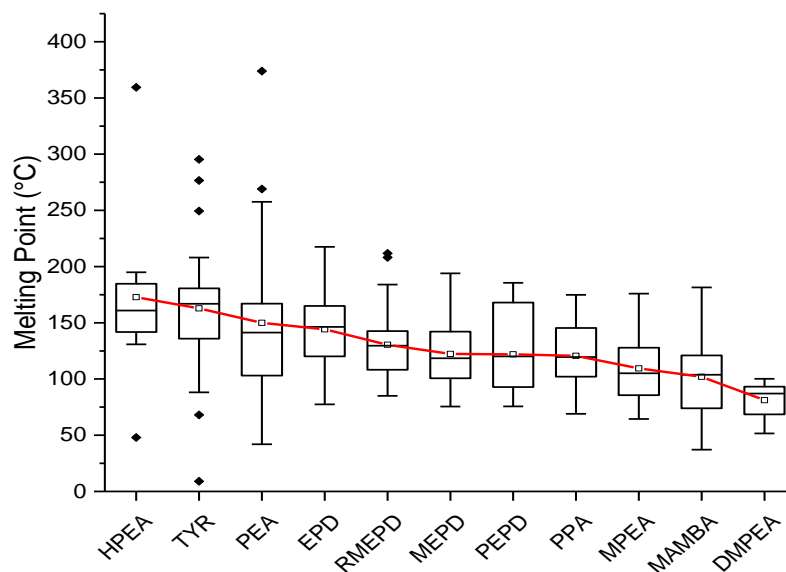
Figure 9. 3. Distribution of melting point for all two-hundred and sixteen compounds according to the base.

When plotting the average values of solubility (SOL) versus the average values of melting point (MP) for all salt forms used according to the base, there is a general trend between both physicochemical properties, with equation $SOL = -(0.022 \pm 0.003) \cdot MP + (4.3 \pm 0.4)$ and $R^2 = 0.8702$. As it can be observed in Figure 9.4, the average of solubility and melting point have an inverse rank order: compounds with higher solubility have a low melting point, for example salt forms of DMPEA (Figure 9.4, in black), and compounds with a high melting point have low solubility, for example HPEA (Figure 9.4, in cyan blue). Indeed the 3 bases with the lowest average melting points are the three with the highest average solubilities. Conversely, HPEA with the highest melting point has the lowest solubility value.

Table 9. 1. Average of values of melting point and solubility according to the base used.

.	n	Melting Point ± σ_{MP} (°C)	ns	Solubility ± σ_{Sol} (mol/L of base)
MAMBA	15	102 ± 37	19	2.6 ± 1.7
MEPD	30	122 ± 32	32	1.5 ± 1.3
RMEPD	32	130 ± 31	33	1.3 ± 1.2
PEA	28	150 ± 71	32	1.9 ± 1.8
MPEA	12	109 ± 30	16	2.2 ± 1.1
DMPEA	8	81 ± 18	13	2.8 ± 1.1
PPA	12	121 ± 31	12	1.5 ± 1.4
HPEA	8	173 ± 87	14	0.6 ± 0.3
TYR	34	163 ± 53	39	1.2 ± 1.3
EPD	18	144 ± 36	23	1.0 ± 0.9
PEPD	19	122 ± 39	22	1.1 ± 1.0
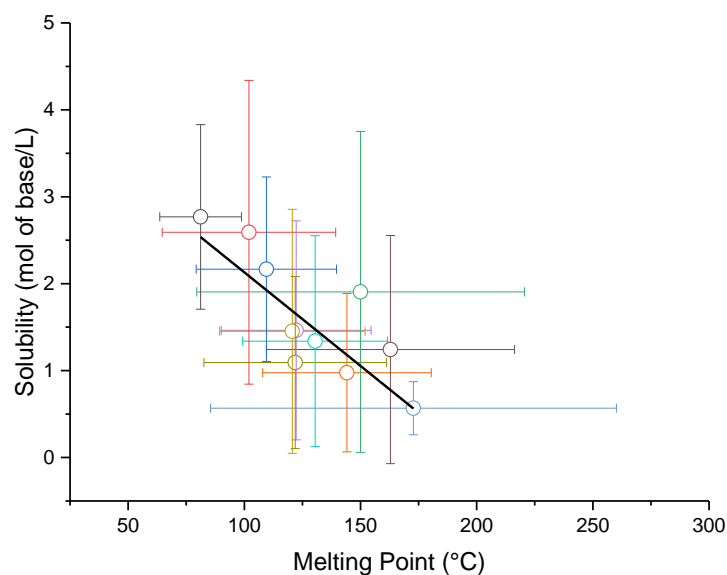
Figure 9. 4. Solubility versus melting point averages for all compounds according to the base used. The dot in black represents the average of DMPEA values, in red represents MAMBA, in blue represents MPEA, in green represents PEA, in orange represents EPD, in brown represents TYR, in light blue represents RMEPD, in purple represents MEPD, in light orange represents PPA, in beige represents PEPD and in cyan blue represents HPEA.

Of these samples, there are two-hundred and five anhydrous compounds with melting point data and one-hundred and seventy-two anhydrous compounds with solubility data. The remaining values are compounds that have the presence of one or more water molecules in the structure. Details of average values can be observed for anhydrous

compounds in Table 9.2 and for hydrated compounds in Table 9.3. As it can be observed in Figure 9.5, separating anhydrous compounds from hydrated compounds, gives a trendline for anhydrous compound (Figure 9.5, in grey) that is equivalent to that for all compounds. The equation for anhydrous compounds is SOL = (− 0.021 ± 0.002)·MP + (4.6 ± 0.4) with R^2 = 0.9072. There was no relationship found for the hydrated compounds (in blue), with best found R^2 = 0.0102. Note that the hydrated compounds tend to have lower solubility and lower MP than the anhydrous compounds. That hydrated compounds have lower aqueous solubility values than the equivalent anhydrous compounds are a well know phenomenon [3,4].

Table 9. 2. Average values of solubility and melting point for all anhydrous compounds where n is the number of compounds.

		Anhydrous		
	n	**Melting Point ± σ_{MP} (°C)**	**n**	**Solubility ± σ_{Sol} (mol/L of base)**
MAMBA	17	109 ± 34	13	2.8 ± 1.7
MEPD	27	131 ± 29	25	1.6 ± 1.3
RMEPD	26	137 ± 30	26	1.2 ± 1.2
PEA	29	156 ± 70	25	1.8 ± 1.8
MPEA	14	109 ± 30	12	2.1 ± 1.1
DMPEA	9	91 ± 9	5	3.0 ± 0.6
PPA	10	121 ± 29	10	1.5 ± 1.5
HPEA	12	197 ± 83	6	0.6 ± 0.3
TYR	28	173 ± 53	25	0.9 ± 0.8
EPD	19	153 ± 31	15	0.9 ± 0.9
PEPD	14	142 ± 35	10	1.3 ± 1.1

Table 9. 3. Average values of solubility and melting point for all hydrated compounds where n is the number of compounds.

		Hydrates		
	n	**Melting Point ± σ_{MP} (°C)**	**n**	**Solubility ± σ_{Sol} (mol/L of base)**
MAMBA	2	56 ± 26	2	1.0 ± 0.9
MEPD	5	81 ± 3	5	0.9 ± 1.0
RMEPD	6	101 ± 12	7	1.8 ± 1.4
PEA	3	98 ± 62	3	2.5 ± 3.0
MPEA	0		2	2.3 ± 0.5
DMPEA	3	66 ± 19	4	2.2 ± 1.7
PPA	2	118 ± 55	2	1.1 ± 1.0
HPEA	2	101 ± 75	2	0.6 ± 0.4
TYR	9	136 ± 45	11	2.1 ± 2.0
EPD	3	98 ± 23	4	1.6 ± 1.0
PEPD	9	100 ± 32	8	0.7 ± 0.8

Figure 9. 5. Trendline for average MP and average SOL data for anhydrous compounds (in black) and scatterplot for hydrated compounds (in blue). Standard deviations were omitted for clarity.

9.2. RELATIONSHIP BETWEEN SOLUBILITY AND MELTING POINT USING ONLY PAIRED DATA.

There are two-hundred and fifteen compounds with data for both solubility and melting point, this excludes one value of melting point, the sample MEPD ADP, and forty solubility values. The solubility data excluded in this chapter was: Four samples of MAMBA (CL, EDS, I and MESO3), three samples of MEPD (CLO4, ETSO3 and MESO3), one sample of RMEPD (MESO3), four samples of PEA (4CB, 4FB, CLO4 and I), four samples of MPEA (BR, EDS, I and PO4), five samples of DMPEA (3HB, CL, CLO4, MALE and SUC), six samples of HPEA (2NB, 3NB, MALE, PO4, PTOL and RMAL), five samples of TYR (BF4, CLO4, I, PO4 and RMD), five samples of EPD (2HB, 3NB, I, MESO3 and SO4) and three samples of PEPD (ADP, CLO4 and I). The average of the remaining values of melting point and solubility can be observed in Table 9.4.

Table 9. 4. Average of values of melting point and solubility for samples containing both data according to the base used.

	n	Melting Point ± σ_{MP} (°C)	n	Solubility ± σ_{Sol} (mol/L of base)
MAMBA	15	102 ± 37	15	2.3 ± 1.6
MEPD	29	123 ± 32	29	1.4 ± 1.3
RMEPD	32	130 ± 31	32	1.3 ± 1.1
PEA	28	150 ± 71	28	1.8 ± 1.9
MPEA	12	109 ± 30	12	2.0 ± 1.1
DMPEA	8	81 ± 18	8	2.4 ± 1.0
PPA	12	121 ± 31	12	1.5 ± 1.4
HPEA	8	173 ± 87	8	0.5 ± 0.3
TYR	34	163 ± 53	34	1.0 ± 1.1
EPD	18	144 ± 36	18	0.8 ± 0.8
PEPD	19	122 ± 39	19	1.0 ± 1.0

Using this data, the linear equation for solubility as a function of the melting point becomes: $SOL = - (0.019 \pm 0.003) \cdot MP + (3.8 \pm 0.4)$ with $R^2 = 0.8599$, as it can be observed in Figure 9.6. Although there is a decrease in solubility for DMPEA sample,

the same rank order for average solubility versus melting point is observed for all compounds. Interestingly, excluding this data did not change the trend line of anhydrous compounds. This can be observed in Figure 9.7 for anhydrous compounds (in grey) and hydrated compounds (in blue). The equation for anhydrous compounds is $Sol = (-0.022 \pm 0.002) \cdot MP + (4.7 \pm 0.3)$ with $R^2 = 0.9343$.
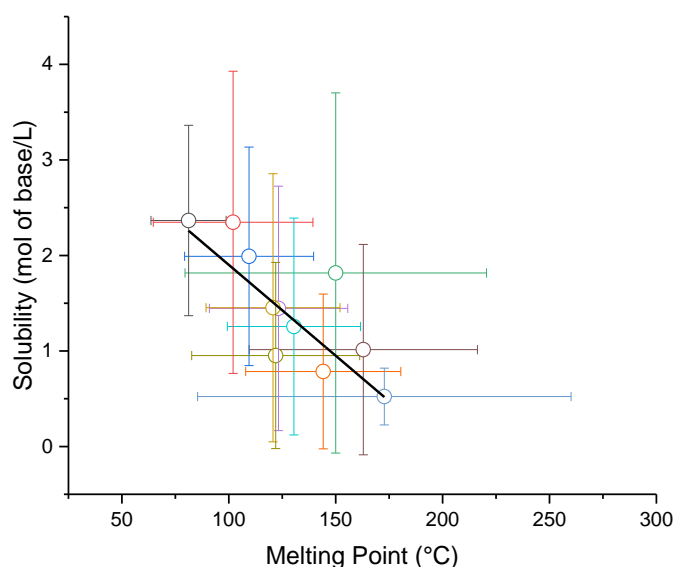
Figure 9. 6. Solubility versus melting point averages for all compounds with both values according to the base used. The dot in black represents the average of DMPEA values, in red represents MAMBA, in blue represents MPEA, in green represents PEA, in orange represents EPD, in brown represents TYR, in light blue represents RMEPD, in purple represents MEPD, in light orange represents PPA, in beige represents PEPD and in cyan blue represents HPEA.

It is also interesting to observe the distribution of hydrated compounds according to the base. For compounds with both values of solubility and melting point, there were no hydrated salt formed with the base MPEA and DMPEA is the compounds with the higher percentage of hydrates, 42.1 %. Then, the rank order for hydrate formation is: PEA (10.7 %), MAMBA (13.3 %), PPA (16.7 %), EPD (16.7 %), MEPD (17.2 %), RMEPD (18.8 %), HPEA (25.0 %), TYR (26.5 %) and DMPEA (37.5 %). The distribution of hydrated and anhydrous compounds can be observed in Figure 9.8 where, in red are the number of anhydrous compounds while in blue are the number of hydrated compounds.

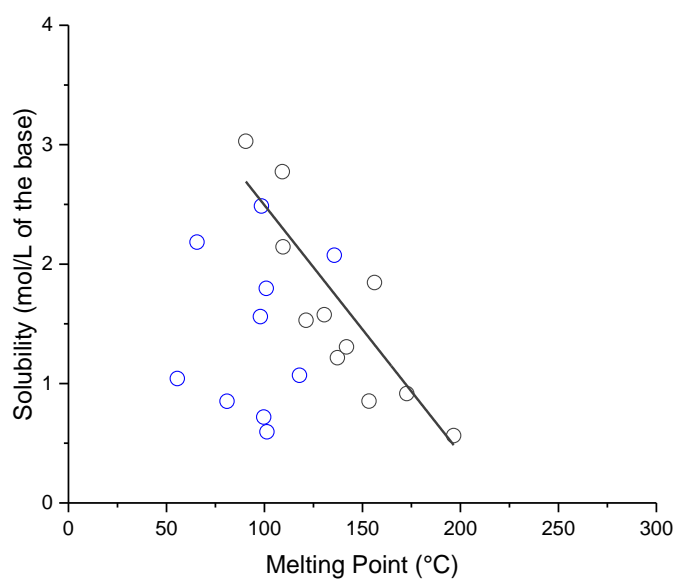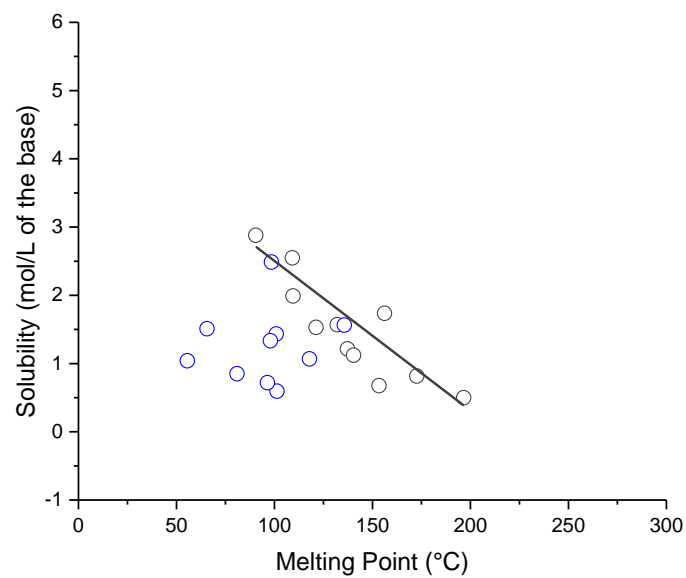**Figure 9. 7.** Trendline for all anhydrous compounds (in black) and scatterplot for hydrated compounds (in blue). Standard deviations were omitted for clarity.
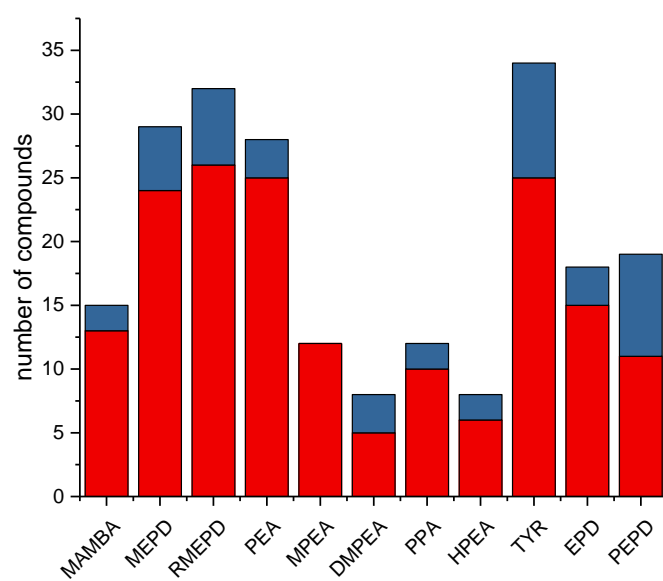
Figure 9. 8. Distribution of anhydrous (in red) and hydrated (in blue) compounds according to the composition of the cation for all compounds with pairs of solubility and melting point.

9.3. RELATIONSHIP BETWEEN SOLUBILITY AND MELTING POINT FOR COMPOUNDS WITH PXRD CHECKED.

To ensure that pairs of solubility and MP data were both for the same crystalline phase, the analysis was repeated only with compounds where the phase of the salt form was checked by powder x-ray diffraction before and after solubility measurements. There remained one-hundred and seventy-four salt forms with the same phase before and after solubility measurements. Thus, there were forty-one samples that had a phase change during solubility measurements or did not have powder diffraction patterns measured for the sample. The average of the remaining values of melting point and solubility can be observed in Table 9.5.

Table 9. 5. Average of values of melting point and solubility for samples containing both data and checked by PXRD according to the base used.

	n	Melting Point $\pm \sigma_{MP}$ (°C)	Solubility $\pm \sigma_{Sol}$ (mol/L of base)
MAMBA	9	109 ± 39	2.6 ± 1.7
MEPD	26	125 ± 33	1.4 ± 1.2
RMEPD	26	134 ± 27	1.2 ± 1.2
PEA	23	161 ± 71	1.9 ± 2.0
MPEA	8	117 ± 35	1.9 ± 1.1
DMPEA	6	85 ± 18	2.3 ± 1.2
PPA	8	128 ± 33	1.3 ± 1.4
HPEA	7	174 ± 94	0.6 ± 0.3
TYR	29	164 ± 57	1.0 ± 1.2
EPD	16	150 ± 34	0.7 ± 0.8
PEPD	16	124 ± 41	1.1 ± 1.0

It important to point that although excluding values without powder x-ray diffraction checked did not change the trendline for the solubility versus melting point scatterplot [equation: $SOL = - (0.019 \pm 0.003) \cdot MP + (3.8 \pm 0.5)$] the fitting of the remaining data is not as good as observed in Chapter 9.2, with regression coefficient decreasing from 0.9343 to 0.7942. The scatterplot for this set of data can be observed in Figure 9.9.

Again, separation of anhydrous and hydrated compounds did not affect the equation for anhydrous compounds [SOL = – 0.022 (2)·MP + 4.8 (4) and R^2 = 0.9035].
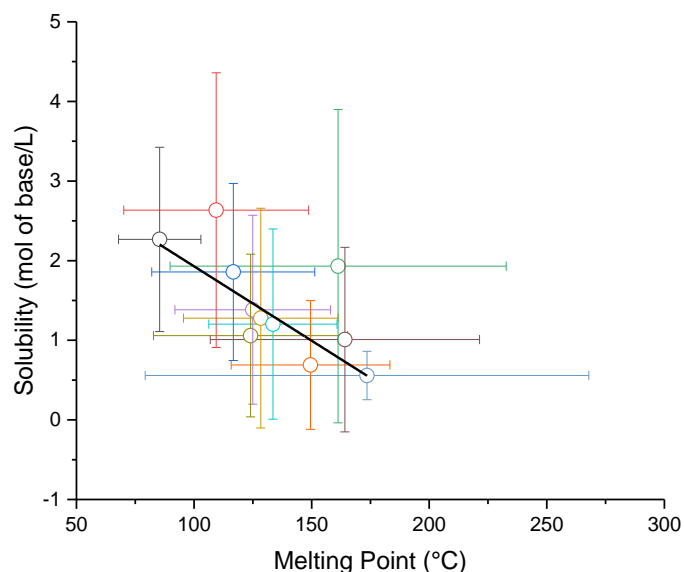
Figure 9. 9. Solubility versus melting point averages for all compounds with both values and phase checked according to the base used. The dot in black represents the average of DMPEA values, in red represents MAMBA, in blue represents MPEA, in green represents PEA, in orange represents EPD, in brown represents TYR, in light blue represents RMEPD, in purple represents MEPD, in light orange represents PPA, in beige represents PEPD and in cyan blue represents HPEA.

9.4. RELATIONSHIP BETWEEN SOLUBILITY AND MELTING POINT FOR INDIVIDUAL GROUPS OF COUNTERIONS.

For the eleven bases analysed in this work, there are seventeen counterions with four or more anhydrous structures and pairs of solubility (checked by powder x-ray diffraction) and melting point available. The list of counterions and bases used in this analysis can be observed in Table 9.6. These counterions used are classified as eight benzoates (2CB, 2HB, 3CB, 3FB, 4AB, 4CB, 4HB and 4NB), two sulfonates (4HBS and EDS), two halides (CL and BR), two monocarboxylates (LMD and RMD) and three dicarboxylates (MALE, MALON and SUC). Further analysis will be made according to the composition of the counterion.

Table 9. 6. Samples used in the analyses of salt forms with both solubility and melting point data checked with PXRD. Each compound used is marked with a check symbol.

	MAMBA	MEPD	RMEPD	PEA	MPEA	DMPEA	PPA	HPEA	TYR	EPD	PEPD
2CB			✓		✓				✓	✓	
2HB		✓			✓	✓					✓
3CB	✓		✓	✓				✓	✓	✓	
3FB		✓	✓	✓					✓		
4AB		✓	✓	✓				✓		✓	
4CB		✓	✓						✓	✓	
4HB	✓	✓	✓	✓	✓	✓		✓	✓		
4NB		✓	✓	✓	✓					✓	✓
4HBS	✓	✓			✓		✓				✓
EDS		✓		✓				✓	✓	✓	
BR		✓	✓	✓					✓	✓	✓
CL		✓	✓	✓					✓	✓	✓
LMD		✓		✓				✓	✓	✓	
MALE		✓	✓	✓	✓				✓		✓
MALON	✓	✓	✓	✓		✓	✓				
RMD		✓	✓	✓			✓			✓	
SUC	✓	✓	✓	✓							

9.4.1. BENZOATES

In the analysis of solubility versus melting point for benzoates, in all cases, when the melting point increases the solubility decreases. This is represented by a negative gradient in the trendlines. Results for the eight benzoates can be observed in Table 9.7. Three compounds have a linear fitting of solubility and melting point, as defined by a regression coefficient higher than 80 %: 2HB [SOL = (-0.055 ± 0.009)·MP + (7.4 ± 1.0), R^2 = 0.9479], 4AB [SOL = (-0.027 ± 0.005)·MP + 5.2 ± 0.7), R^2 = 0.9166] and 4NB [SOL = (-0.051 ± 0.010)·MP + 8.6 ± 1.6), R^2 = 0.8683]. Interestingly, although this analysis was made for salt forms of different bases and the samples 2HB and 4NB, the trendline for these counterions is parallel within standard deviation. Figure 9.10 illustrates the analysis for benzoates.

Figure 9. 10. Solubility versus melting point according to the composition of the counterion for benzoates where 2CB is represented by the dots in black, 2HB is represented by the line in red, 3CB is represented by the dots in blue, 3FB is represented by the dots in green, 4AB is represented by the line in purple, 4CB is represented by the dots in beige, 4HB is represented by the dots in light blue and 4NB is represented by the line in brown.

Table 9. 7. Gradient (B_1), intercept and regression coefficient (R^2) for all trendlines obtained for benzoates.

	n	B_1 (mol·°C·L^{-1})	Intercept (C)	R^2
2CB	4	-0.016 ± 0.012	2.9 ± 1.8	0.4781
2HB	4	-0.055 ± 0.009	7.4 ± 1.0	0.9479
3CB	6	-0.039 ± 0.012	5.8 ± 1.5	0.7248
3FB	4	-0.040 ± 0.025	6.3 ± 3.5	0.5708
4AB	5	-0.027 ± 0.005	5.2 ± 0.7	0.9166
4CB	4	-0.011 ± 0.006	2.0 ± 1.0	0.6163
4HB	8	-0.015 ± 0.008	3.2 ± 1.3	0.3807
4NB	6	-0.051 ± 0.010	8.6 ± 1.6	0.8683

9.4.2. SULFONATES AND HALIDES

For this analysis, the melting point and solubility data for halide counterions, CL and BR, was only considered for the salt forms they had base in common: MEPD, RMEPD, PEA, TYR, EPD and PEPD. Whilst the chlorides have no linear relationship between solubility and melting point for these compounds (Figure 9.11), an interesting result is the positive gradient for the bromide samples, with equation [SOL = (0.024 ± 0.006)·MP + (-4 ± 1), R^2 = 0.8016]. That means that solubility for these compounds have a direct proportional relationship to the melting point, when the solubility increases, the melting point also increases. We have earlier shown that halide salts of methylephedrine have a direct relationship between MP and aqueous solubility, whilst all other salt forms of methylephedrine adopt the expected inverse relationship [2]. Although the remaining samples analysed in this section (4HBS, EDS and CL) have a poor fit of the data, all of them have a negative gradient (B_1), as it can be observed in Table 9.8.

Table 9. 8. Gradient (B_1), intercept and regression coefficient (R^2) for all trendlines obtained for sulfonates and halides.

	n	B_1 (mol·°C·L^{-1})	Intercept (C)	R2
4HBS	5	-0.019 ± 0.021	4 ± 3	0.2026
EDS	5	-0.007 ± 0.005	3 ± 1	0.3951
BR	6	0.024 ± 0.006	-4 ± 1	0.8016
CL	6	-0.016 ± 0.014	6 ± 3	0.2543
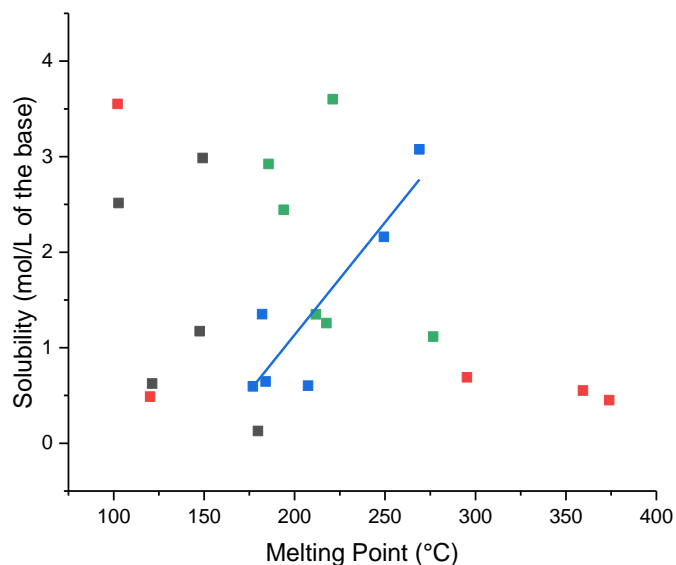
Figure 9. 11. Solubility versus melting point according to the composition of the counterion for sulfonates and halides where 4HBS is represented by dots in black, EDS is represented by dots in red, BR is represented by line in blue and CL is represented by dots in green.

9.4.3. CARBOXYLATES

The compound with best fit between the data when analysing carboxylates was MALE, with equation [SOL = (-0.030 ± 0.010)·MP + (5.1 ± 1.2), R2 = 0.7091], and it have the same gradient as the benzoate 4AB within standard deviation [B_1 = -0.027 (5) mol·°C·L^{-1}]. Unfortunately, for this set of samples, there was no significant linear fitting for the other monocarboxylate and dicarboxylates. It is also important to note that all compounds have a negative gradient (B_1), as it can be observed in Table 9.9. Figure 9.12 illustrate the position of the salt forms according to the composition of the counterion, where LMD is represented by the dots in black, MALE is represented by the dots and line in red, MALON is represented by the dots in blue, RMD is represented by the dots in green and SUC is represented by the dots in purple.
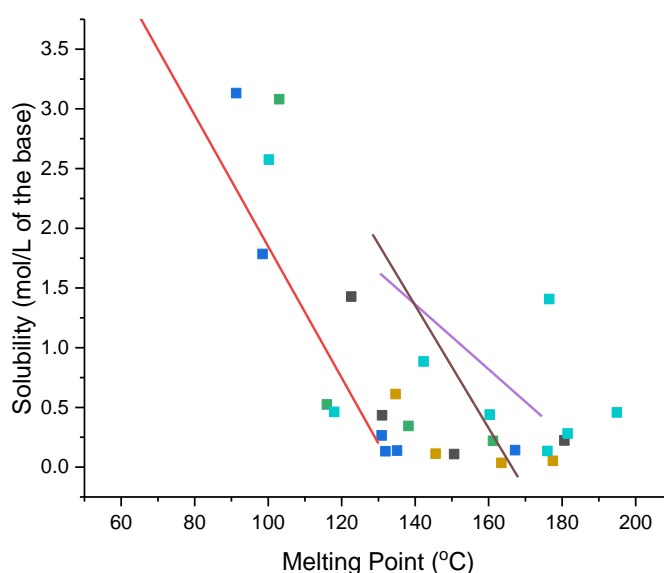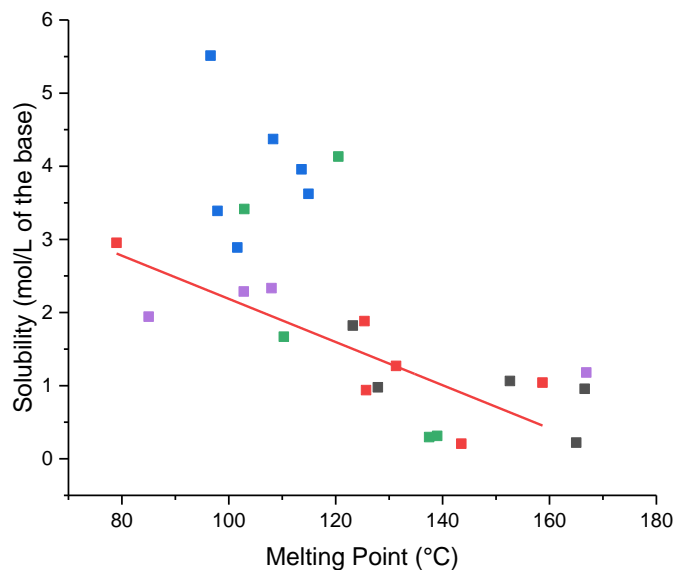
Figure 9. 12. Solubility versus melting point according to the composition of the counterion for carboxylates where LMD is represented by the dots in black, MALE is represented by the dots and line in red, MALON is represented by the dots in blue, RMD is represented by the dots in green and SUC is represented by the dots in purple.

Table 9. 9. Gradient (B_1), intercept and regression coefficient (R^2) for all trendlines obtained for carboxylates.

	n	B_1 (mol·°C·L^{-1})	Intercept (C)	R^2
LMD	5	-0.020 ± 0.011	4.0 ± 1.6	0.5262
MALE	6	-0.030 ± 0.010	5.1 ± 1.2	0.7091
MALON	6	-0.023 ± 0.056	6.4 ± 6.0	0.0413
RMD	5	-0.079 ± 0.044	11.6 ± 5.4	0.5177
SUC	4	-0.012 ± 0.006	3.4 ± 0.7	0.6695

9.5. CONCLUSIONS

This work started the analysis for two-hundred and sixteen compounds with melting point and two-hundred and fifty-five salt forms of eleven phenylethylamine derivatives. The first result observed is the linear relationship between solubility and melting point when comparing salt forms according to the type of active pharmaceutical ingredient used, with equation SOL = − (0.022 ± 0.003)·MP + (4.3 ± 0.4). Polishing the data by considering only compounds with pairs of solubility and melting point and considering only phase matched pairs gave essentially no change in

this equation. However, it was shown that hydrated compounds did not follow the same trends as anhydrous compounds. Contrary to the wide-spread belief that more polar compounds should give higher aqueous solubility, the most soluble base was the only one with no OH or NH groups. This may be because although such polar groups increase hydration energy by encouraging interactions with water, they also encourage intermolecular hydrogen bonding in the solid – thus increasing lattice energy and the stability of the solid [5].

When plotting solubility versus melting point for individual counterions, most of the compounds had no significant fitting of the data. However, five counterions had interesting results: The samples 2HB (Figure 9.13, in blue) and 4NB (Figure 9.13, in purple) had the gradient of the trendline equals to -0.055 (9) mol·°C·L^{-1} and -0.051(10) mol·°C·L^{-1}, respectively. An interesting result for these linear equations, with the shape of SOL = B_1·MP + C, is that when the solubility tends to zero (SOL → 0), the value of the x axis for the samples 2HB and 4NB tends to the molecular weightt of the free acid (138.12 g/mol for 2HB and 167.12 g/mol for 4NB) with a discrepancy in modulus of 2.6 % for 2HB and 0.9 % for 4NB. This behaviour was not found analysing the samples MALE (Figure 9.13, in black) and 4AB (Figure 9.13, in green), with the gradient of the trendline equals to -0.030 (10) mol·°C·L^{-1} and -0.027 (5) mol·°C·L^{-1}, respectively. In this case, when SOL → 0, x axis does not tend to the molecular weightt of the free acid (137.14 g/mol for 4AB and 116.07 g/mol for MALE). Instead, it tends to higher values (192.6 u for 4AB and 170.0 u for MALE). Interestingly, when the value of C is corrected by the density of the free acid (1.37 g/L for 4AB and 1.59 g/L for MALE), when SOL → 0, x axis tends, again, to the value of the molecular weightt of the free acid, with a discrepancy in modulus of 7.9 % for MALE and 2.5 % for 4AB. Finally, the BR trenline did not behave as any of the samples above and had solubility increasing with the melting point.
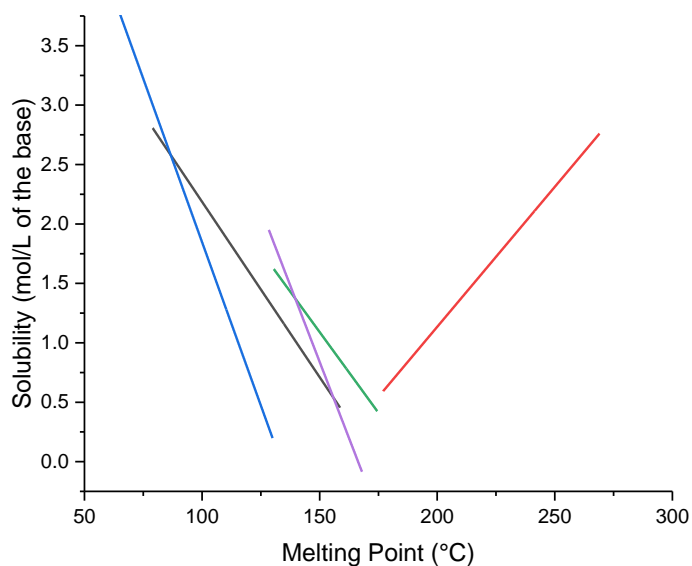
Figure 9. 13. Trendlines of solubility versus melting point for the counterions where the line in black represents MALE, in red represents BR, in blue represents 2HB, in green represents 4AB and in purple represents 4NB.

9.6. REFERENCES

[1]   Morrison, C.A. (2012). Salt selection for pharmaceutical use University of Strathclyde. Dept. of Pure and Applied Chemistry. Thesis [Ph. D] - University of Strathclyde.

[2]   De Moraes, S.L., Edwards, D., Florence, A.J., Johnston, A., Johnston, B.F., Morrison, C.A., & Kennedy, A.R. (2017). Crystal Growth and Design, 17(6), 3277-3286.

[3]   Grant, D. J. W. & Higuchi, T (1990). Solubility Behaviour of Organic Compounds' Wiley: New York.

[4]   Shefter, E. & Higuchi (1963). T. J. Pharm. Sci., 52, 781.

[5]   Agharker, S., Lindenbaum, S. & Higuchi, T. J. (1976) Pharm. Sci., 65, 747.

10. CONCLUSIONS

This work expanded the pre-existing database of crystal structures of salt forms of phenylethylamine derived active pharmaceutical ingredients (APIs) by elucidating seventy-five new structures of salt forms of four API bases, *p*-hydroxyphenylethylamine (TYR), (1R,2S)-(−)-N-methylephedrine (MEPD), (+/-) methylephedrine (RMEPD) and (1R,2S)-(−)-N-ephedrine (EPD). The selection of APIs included primary, secondary and tertiary amines while the counterion selection included first- and second-class pharmaceutical counter-ions [1]. As well as the four main bases, new single crystal structures are also presented for salt forms of the structurally related bases phenylethylamine (PEA), methylphenylethylamine (MPEA), and pseudoephedrine (PEPD). The entire structural database now consists of around 300 systematically related single crystal structures of pharmaceutically relevant species. These new compounds, with the addition of salt forms obtained from the CCDC database [2] were analysed for structural features of the crystal structure, such as occurrence of more than one cation per asymmetric unit (Z' > 1), cation conformation, presence of water in the crystal structure and crystal packing similarity. The features identified from these analyses were used in attempts to understand structure-property relationships. This is an invaluable resource for any research group attempting to understand how crystal structure effects material properties such as solubility, melting point, hardness and elasticity.

The occurrence of more than one cation per asymmetric unit for TYR, MEPD and EPD salt forms was found to be more common than the literature suggests [11] however, RMEPD did not have the same profile, showing no such deviation from the norm. This suggests that enantiopure salt forms are much more likely to form Z'> 1 structures than their racemic equivalents. There is a general formation of salt forms with multiple cations per asymmetric unit in 20.2 % of the carboxylates, 23.8 % of the benzoates, 27.7 % of the sulfonates and 19.4 % of the inorganic compounds.

To comprehensively describe the conformation of the cations, this work analysed all torsion angles involved in the aliphatic chain of the API cations, giving a total of three

torsion angles for tyramine and fourteen torsion angles for methylephedrine and ephedrine. This analysis greatly expands upon previously published studies [3-5, 12]. In the case of tyramine, there was identified a new sub-class of extended cations involving the rotation of the aromatic ring in comparison with the standard extended conformation. There was found to be no conformational difference between racemic and enantiopure methylephedrine samples, and these results matched well with smaller previously published studies [3, 13]. In the case of enantiopure ephedrine, the two major conformations observed by Collier *et al.* [5], extended and folded conformations, were also observed in this work, but the extended conformation is now identified as the more common of the two main conformations. Furthermore, these main conformations were expanded by the creation of three different sub-classes. There was also the creation of another class, conformation γ, albeit involving only one compound, which did not behave similarly to the other classifications.

When analysing hydrate formation in the samples synthesised in this work or obtained by the database, one or more water molecule was present in 27.4 % of the total of salt forms. Detailed analysed for all hydrates enable this work to expand to methylephedrine and ephedrine salt forms, the analysis published by Morrison *et al.* [4] for tyramine compounds:

(i)   There is around a 10.0 % occurrence of hydrates in halides, aliphatic sulfonates benzoates and monocarboxylates. These compounds will predominantly form anhydrous salt forms even when crystallised from water.

(ii)   There is around a 50 % occurrence of hydrates in dicarboxylates, inorganic salts with tetrahedral anions and aryl-sulfonates. Formation of hydrates for these compounds is thus relatively likely given suitable synthesis and crystallisation conditions.

Tyramine salts were found to be much more likely than salts of the other bases to form hydrates. An obvious factor here is that the tyramine RNH_3 cation has more charged hydrogen bond donor groups than the other cations. This also leads to the common observation of water molecules acting as 4-fold hydrogen bonding nodes for tyramine

salts – a feature that is largely absent from the others. Both a high total number of reliable hydrogen bonding groups and a low donor:acceptor ratio were found to favour hydrate formation. For methylephedrine and ephedrine, no hydrates were formed where there were more potential donor atoms than acceptor atoms.

Analysing all salt forms of tyramine, enantiopure methylephedrine, racemic methylephedrine and ephedrine using cation packing similarity identified several isostructural packing groups for the cations. This was an entirely new analysis for ephedrine and a large expansion on previous work for the other bases [6,7]. Four new isostructural groups of methylephedrine were identified, two new groups for racemic forms of methylephedrine and two new groups for enantiopure methylephedrine. In the case of ephedrine salt forms there was the creation of seven new isostructural groups, none of which had been identified by previous case studies [12]. Although some of the structural groups contain only structures with obvious similarities (e.g. the isostructural group of the halides chloride and bromide for tyramine, enantiopure methylephedrine and ephedrine), many groups are highly varied containing different anion types, differently hydrated structures or different cation conformations. The retention of cation packing structure despite wholescale changes to coformers and hence intermolecular interactions suggests that cation size and shape is just as important in determining packing structure as are interactions such as hydrogen bonding.

When analysing mechanical properties of materials, a new method for analysis of nanoindentation data was presented and is used in this work for one hundred and thirty-four salt forms of eight different APIs. This new methodology decreased experimental errors when interpreting force curves to obtain values of hardness and Young's Modulus in comparison with traditional methods [8,9], and also indicated outlier data and eliminated the indentation size effect (ISE), where hardness may increase or decrease according to the force applied [14]. There is a linear relationship between hardness and Young's Modulus, named elastic index [15], with a rank order according to the composition of the API [RMEPD > EPD ≈ MPEA > PEA > PEPD ≈ MEPD ≈ DMPEA > TYR]. In other words, salt forms of racemic methylephedrine will have higher strain related to the other salts, and salt forms of tyramine with have the lower

strain in general. Analysis of nanoindentation results were made according to the features in the crystal structure and the composition of the counterions. For example, when separating compounds according to the presence of one or more water molecules in the unit cell, the elasticity index for all anhydrous and hydrated compounds is the same as when considering all compounds together, apart from methylephedrine salt forms, where hydrates have elasticity index 28.6 % higher than anhydrous compounds. This difference in the elasticity index for anhydrous and hydrated compounds was only found for methylephedrine compounds. Interestingly, a similar effect was observed when analysing the elasticity index of the compounds according to the composition of the counterion. All had the same value of elasticity index, within standard deviation, except for sulfonate, salt forms of methylephedrine where the elasticity index decreased by 18.6 %. Also, a relationship was observed between the hardness / Young's Modulus of the compounds and the size of the anion for halides and *ortho*-substituted benzoates. Hardness decreased when the size of the counterion, or the substitute atom in the *ortho*-position, increased as long as these atoms were in the same group or period of the periodic table.

Finally, this work started the analysis of two-hundred and sixteen compounds with melting point values and two-hundred and fifty-five salt forms with solubility values of eleven phenylethylamine derivatives obtained from Morrison *et al.* [10]. These values were refined by considering only compounds with pairs of solubility and melting point and analysing only compounds where powder x-ray diffraction patterns obtained after solubility measurements matched well characterised, known, single phases. There is a linear relationship between solubility and melting point when comparing salt forms according to the type of active pharmaceutical ingredient used. It is interesting to point out there was also a linear relationship found when plotting solubility versus melting point, in the shape of $SOL = B_1 \cdot MP + C$, for individual counterions in five cases: 2HB, 4AB, 4NB, MALE and BR. Further study of the linear relationships showed three different types of behaviour:

(i) When the solubility tends to zero ($SOL \rightarrow 0$), the value of the x axis for the samples 2HB and 4NB tends to the molecular weight of the free acid (138.12

g/mol for 2HB and 167.12 g/mol for 4NB) with a discrepancy in modulus of 2.6 % for 2HB and 0.9 % for 4NB.

(ii) When SOL $\rightarrow$ 0, x axis does not tend to the molecular weight of the free acid (137.14 g/mol for 4AB and 116.07 g/mol for MALE). Instead, it tends to higher values: 192.6 u for 4AB and 170.0 u for MALE. In this case, correcting the value of C by the value of density of the free acid, the x axis will, again, tend to the value of the molecular weight of the free acid, with a discrepancy in modulus of 7.9 % for MALE and 2.5 % for 4AB, when solubility tends to zero.

(iii) The group of samples that does not behave as any of the samples above and had solubility increasing with the melting point, which was the case of the salt forms with bromine (BR) as counterions.

10.1.   REFERENCES

[1]   Pfannkuch, F., Rettig, H. & Stahl, P. H. (2002). Biological effects of the drug salt form. In: Stahl, P.H. & Wermuth, C.G., eds. Handbook of Pharmaceutical Salts. Zurich: Wiley-VCH.

[2]   The Cambridge Structural Database (CSD). Available at < https:// www.ccdc.cam.ac.uk/solutions/csd-system/components/csd/   >   Accessed   on 19/01/2018

[3]   De Moraes, S.L., Edwards, D., Florence, A.J., Johnston, A., Johnston, B.F., Morrison, C.A., & Kennedy, A.R. (2017). Crystal Growth and Design, 17(6), 3277-3286.

[4]   Briggs, N., Kennedy, A., & Morrison, C. (2012). Acta Crystallographica Section B, 68(4), 453-464.

[5]   Collier, E., Davey, R., Black, S., & Roberts, R. (2006). Acta Crystallographica Section B, 62(3), 498-505.

[6]   Macrae, C.F., Bruno, I.J., Chisholm, J.A., Edgington, P.R., McCabe, P., Pidcock, E., Rodriguez-Monge, L., Taylor, R., van de Streek, J. & Wood, P. A. (2008). J. Appl. Cryst., 41, 466-470.

[7]   Macrae, C.F., Edgington, P. R., McCabe, P., Pidcock, E., Shields, G. P., Taylor, R., Towler M. & van de Streek, J. (2006), J. Appl. Cryst., 39, 453-457.

[8]   Oliver, W.C. & Pharra, G.M. (2004). J. Mater. Res., 19 (10), pp. 3-20.

[9]   Sneddon, I. N. (1965). Int. J. Engng. Sci., 3, 47-57.

[10]   Morrison, C.A. (2012). Salt selection for pharmaceutical use University of Strathclyde. Dept. of Pure and Applied Chemistry. Thesis [Ph. D] - University of Strathclyde.

[11]   Steed, K.M. & Steed,J.W. (2015). Chem. Rev. 115 (8), 2895–2933

[12]   CCDC. Crystal Form Similarity < https://www.ccdc.cam.ac.uk/Community/crystalformconsortium/casestudies/crystalformsimilarity/ >. Accessed on 20/07/2019

[13]   Kennedy, A. R., Morrison, C. A., Briggs, N. E., & Arbuckle, W. (2011). Crystal Growth and Design, 11(5), 1821-1834.

[14]   Berg, G and Grau, P. (1997). Cryst. Res. Technol, 32 (1), pp. 149-154.

[15]   Cheng, Yang-Tse, & Cheng, Che-Min. (1998). Applied Physics Letters, 73(5), 614-616.

11.FURTHER WORK

Apart from the data presented in this thesis, the author also (1); measured the compression behaviour of fifteen compounds using Dynamic Mechanical Analysis (DMA) [1] and (2) eighteen compounds using INSTRON instrumentation [2] at department of Mechanical and Aerospace Engineering and EPSRC Centre for Innovative Manufacturing in Continuous Manufacturing and Crystallisation (CMAC), respectively; (3) measured powder patterns under variable pressure [3] for four salts of tyramine using synchrotron radiation at Diamond Light Source, (4) measured the bulk compression profile using the Texture Analyser (micronisation) [4] of two salt forms of tyramine at GSK and (5) made predictions of solubility and hardness using RandomForest [5] and Materials Studio software [6]. All the raw data obtained for these measurements can be observed in APPENDIX 11. All this work has been initiated but requires further work to be finished.

Various attempts were made to do compression tests (DMA and INSTRON) using single crystals of our organic materials. Problems with crystal to crystal reproducibility were encountered. The INSTRON measurements did not have a good relationship with the more reproducible nanoindentation results presented above, but the DMA results of average maximum strength (AMS) were promising and interesting. For benzoate salts of tyramine, hardness (from nanoindentation) was found to increase with the material's strength. Conversely, halide salts hardness decreased with strength, as can be observed in Figure 11.1. This methodology is promising but requires further work to improve reproducibility.

Powder patterns under variable pressure were measured for four salts of tyramine (the isostructural pair TYR BR and TYR CL as well as TYR I and TYR OXA) using synchrotron radiation at Diamond Light Source on February 2019. Although the initial results of data analysis were promising, there was not enough time to finish data analysis and include this technique in the thesis. Data analysis and possibly experimental technique need to be refined in order to produce reliable compression data for comparison with the other mechanical measurements presented herein.
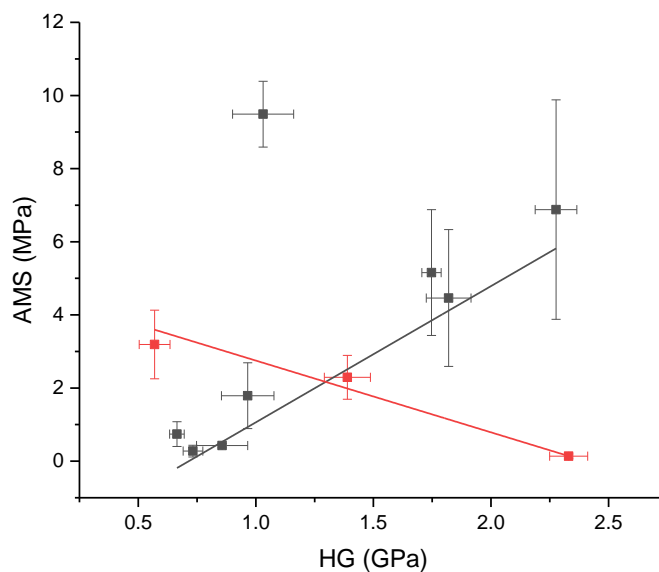
Figure 11. 1. Average Maximum Strength (AMS) versus the gradient hardness (H$_G$) for salt forms of tyramine. In black are the benzoates and in red are the halides.

RandomForest was used to predict the aqueous solubility of salt forms of both racemic and enantiopure methylephedrine and hardness of tyramine salt forms using a variety of counterions. A successful prediction method would allow the identification of what features (molecular, structural, or other property) are important to solubility or mechanical properties. There was the creation of classification and regression models for these compounds and chemometric analyses was performed. The initial work carried out showed that although the selected descriptors of methylephedrine were able to predict 70 % of solubility values, tyramine descriptors were only able to predict 50 % of hardness values

All these analyses could be expanded in further research, reproducing solubility using other methods for all salt forms in this thesis and analysing if the correlation is still valid. This work can be continued increasing the number of compounds measured using compression tests and correlating with nanoindentation results. The same is applied to results obtained using high pressure crystallography. Chemometrics can be

used to predict physicochemical properties of salt forms when the right descriptors are used; further work can be done analysing individual descriptors of each compound before running classification and prediction sets.

11.1.　REFERENCES

[1]　Perkin Elmer. Dynamic Mechanical Analysis (DMA). Available at < https://www.perkinelmer.co.uk/CMSResources/Images/44-74546GDE_IntroductionToDMA.pdf >. Accessed on 05 June 2019.

[2]　Instron Corporation. Instron Model 4400 Universal Testing System. Available at < http://fab.cba.mit.edu/content/tools/instron/M10-94400-1.pdf >. Accessed on 05 June 2019.

[3]　I15. Diamond Light Source. Available at < https://www.diamond.ac.uk/Instruments/Crystallography/I15-1.html# > . Accessed on 05 June 2019.

[4]　PharmaTech. Using Micronization to Reduce API Particle Size. Available at < http://www.pharmtech.com/using-micronization-reduce-api-particle-size　>　. Accessed on 05 June 2019.

[5]　Fortran original by Leo Breiman and Adele Cutler, R port by Andy Liaw and Matthew Wiener. Package 'randomForest'. Available at < https://cran.r-project.org/web/packages/randomForest/randomForest.pdf > . Accessed on 05 June 2019.

[6]　Biovia Material Studio 2017 R2. Available at < http://accelrys.com/products/collaborative-science/biovia-materials-studio/　　> Accessed on 19/01/2018